MANCHESTER 1824
The University of Manchester

Lateral Control of Tailless Aircraft With Reduced Directional Stability

A thesis submitted to the University of Manchester for the degree of
Doctor of Philosophy
in the Faculty of Science and Engineering

2022

Thomas R. Shearwood
Department of Mechanical Aerospace and Civil Engineering

Contents

Word Count: 47,836

List of figures

List of tables

List of publications

[1] T. R. Shearwood, M. R. A. Nabawy, and W. J. Crowther, "Modelling high angle of attack aerodynamics of lambda wing planforms," in *RAES 2018 Applied Aerodynamics Conference*, 2018, pp. 24–26.

[2] W. Crowther, I. Lunnon, T. Shearwood, *et al.*, "Flight demonstration of fluidic controls on a tailless flight vehicle – an overview of the magma programme fluidic technologies," in *RAES 2018 Applied Aerodynamics Conference*, 2018, pp. 24–26.

[3] T. R. Shearwood, M. R. A. Nabawy, W. J. Crowther, and C. Warsop, "Directional control of finless flying wing vehicles – an assessment of opportunities for fluidic actuation," in *AIAA Aviation 2019 Forum*, Dallas, TX: American Institute of Aeronautics and Astronautics, Jun. 2019, pp. 1–15, ISBN: 9781624105890. DOI: 10.2514/6.2019-3686. [Online]. Available: https://arc.aiaa.org/doi/10.2514/6.2019-3686.

[4] C. Warsop, W. J. Crowther, and T. R. Shearwood, "Nato avt-239: Flight demonstration of fluidic flight controls on the magma subscale demonstrator aircraft nato avt-239 special session," in *AIAA Scitech 2019 Forum*, 2019, pp. 1–20, ISBN: 9781624105784. DOI: 10.2514/6.2019-0282.

[5] T. R. Shearwood, M. R. A. Nabawy, W. J. Crowther, and C. Warsop, "A novel control allocation method for yaw control of tailless aircraft," *Aerospace*, vol. 7, no. 10, pp. 1–21, 2020, ISSN: 22264310. DOI: 10.3390/aerospace7100150.

[6] ——, "Yaw control of maneuvering tailless aircraft using induced drag – a control allocation method based on aerodynamic mode shapes," in *AIAA Aviation 2020 Forum*, Reno, NV, 2020. DOI: 10.2514/6.2020-2677.

[7] ——, "A control allocation method to reduce roll-yaw coupling on tailless aircraft," in *AIAA Scitech 2021 Forum*, 2021. DOI: 10.2514/6.2021-1826. [Online]. Available: http://arc.aiaa.org.

[8] ——, “Three-axis control of tailless aircraft using fluidic actuators: MAGMA case study,” in *AIAA Aviation 2021 Forum*, Virtual Event: American Institute of Aeronautics and Astronautics (AIAA), Aug. 2021, pp. 1–12. DOI: 10.2514/6.2021-2530.

Nomenclature

α	Angle of attack	rad
α_i	Induced angle of attack	rad
β	Sideslip angle	rad
Γ	Circulation	$\frac{m^2}{s}$
γ	Non-dimensional circulation (Lifting surface)	
$\Delta[X]$	Change in variable X	
δ	Control surface deflection	rad
ζ	Asymmetric control deflection	rad
	Split drag rudder deflection (Chapter 7)	rad
η	Non-dimensional spanwise location	
	Symmetric control deflection	rad
	Angle of arc segment (Chapter 9)	rad
θ	Pitch angle	rad
Λ	Sweep angle	rad
λ	Eigenvalue	
μ	Non-dimensional pitching moment (Lifting surface)	
ξ	Antisymmetric control deflection	rad
ρ	Fluid density	$\frac{kg}{m^3}$

τ	Non-dimensional time ($\frac{m}{qS}$) Time to roll to 45 degrees bank angle	 s
ϕ	Bank angle	rad
ψ	Heading angle	rad
ω	Angular velocity	$\frac{rad}{s}$
A	Control surface area	m^2
C_D	Drag coefficient 3D	
C_{D0}	Zero lift drag of airframe	
C_L	Lift coefficient (3D)	
C_μ	Momentum Coefficient	
C_d	Drag coefficient 2D	
C_{di}	Induced drag coefficient	
C_l	Lift coefficient (2D) Rolling moment coefficient	
C_m	Pitching moment coefficient	
C_n	Yawing moment coefficient	
C_p	Pressure coefficient	
D'	Drag per unit span	N
F	Force	N
$\mathbf{F_w}$	Force vector in wind axis	N

I	Mass moment of inertia	kgm^2
J	Cost Function	
L	Lift	N
	Rolling moment	Nm
L'	Lift per unit span	$\frac{N}{m}$
M	Pitching moment	Nm
$\mathbf{M_w}$	Moment vector in wind axis	Nm
N	Yawing moment	Nm
$\mathbf{R}$, $\bar{\bar{R}}$	Linear response matrix	
R	Radius of turn	m
S	Reference area	m^2
V	Velocity	$\frac{m}{s}$
X	Force in X-direction	N
	Drag metric	
$X(a\|b)$	Value of state variable X at time a, as evaluated at time b	
Y	Force in Y-direction	N
	Aggregate control deflection metric	m^2
Z	Force in Z-direction	N
b	Wing span	m
c	Chord length	m

d	Desired objective vector (Dynamic Inversion)	
e	Error vector	
g	Acceleration due to gravity	$\frac{m}{s^2}$
h	Slot height	m
$\mathbf{k}$, $\bar{k}$	Vector of mode shape gains	
k	Time step index (Chapter 9)	
m	Mass	kg
$\mathbf{n}$	Null space matrix	
p	Roll rate	$\frac{rad}{s}$
q	Pitch rate	$\frac{rad}{s}$
	Dynamic pressure	Pa
r	Yaw rate	$\frac{rad}{s}$
t	Time	s
u	Normalised velocity in X-direction Control update vector (Dynamic Inversion)	
v	Normalised velocity in Y-direction Auxiliary Input (Dynamic Inversion)	
w	Downwash	$\frac{m}{s}$
w	Normalised velocity in Z-direction	
x	Ordinate in X-Direction State Vector (Dynamic Inversion)	m

x_{ac}	Location of aerodynamic centre	m
x_{cp}	Location of centre of pressure	m
y	Ordinate in Y-direction	m
	Objective vector (Dynamic Inversion)	

Glossary

Terms

Adverse Yaw	A yawing moment which acts in the opposite sense to the rolling moment produced by a control deflection
Aggregate control deflection	The sum of all deflected control surface areas projected onto the normal plane
Canard	An aerodynamic surface which is separate from, and positioned aft of, the main wing
Circulation control	A fluidic control device which changes the local lift over an airfoil
Conformal control	A control surface which does not create a discontinuity in the surface of the aircraft when deployed
Control allocation	A method by which the positions/inputs to control actuators are specified to achieve a target force and moment set
Control Horizon	The time period over which the control inputs are evaluated in generalised predictive control
Fin	A vertical surface intended to provide directional stability for an aircraft
Finless	An aircraft without a vertical stabilising surface
Flow control	Manipulation of the freestream flow to achieve a force or moment on the aircraft
Fluidic	See *Flow control*

Fluidic thrust vectoring	A fludic control device which changes the direction of the thrust line using the injection of a secondary flow
Flying wing	An aircraft with no distinct fuselage or tail
Induced drag	The drag due to the generation of lift, only present for wings of finite span
Lateral	Concerning the roll and yawing motion The plane defined by oXY in the standard coordinate system
Mode shape	A control state which is asymmetric about the aircraft centre line but produces no change in the lift, pitching moment or rolling moment
Normal	At 90 degrees to The plane defined by oYZ in the standard coordinate system
Null space	The vectors x which are solutions to $Ax = 0$
Observability	The degree to which an aircraft can be detected
Prediction Horizon	The time period over which the state of the system is evaluated in generalised predictive control
Proverse Yaw	A yawing moment which acts in the same sense to the rolling moment produced by a control deflection
Sideslip	The angle between the oncoming flow and flight path projected in the lateral plane
Trim	A state where the moments about all axes of the aircraft sum to zero such that the attitude is at a steady state
Tail	An aerodynamic surface which is separate from, and positioned aft of, the main wing
Tailless	An aircraft which does not have a tail or canard

Abbreviations

AFC	Active Flow Control
AGL	Above Ground Level
AIC	Aerodynamic Influence Coefficients
AoA	Angle of Attack
AR	Aspect Ratio
AVT	Advance Vehicle Technology
CAD	Computer Aided Design
CC	Circulation Control
CFD	Computational Fluidic Dynamics
CG	Centre of Gravity
ESDU	European Standard Data Unit
FTV	Fluidic Thrust Vectoring
GPC	Generalised Predictive Control
ICE	Innovative Control Effectors
LE	Leading Edge
LEV	Leading Edge Vortex
LLT	Lifting Line Theory
LS	Lifting Surface
PFTV	Pitch Fluidic Thrust Vectoring

RANS	Reynolds Averaged Navier Stokes
RMS	Root Mean Square
SDR	Split Drag Rudder
TED	Trailing Edge Down
TEU	Trailing Edge Up
UAS	Unmanned Aircraft System
VLM	Vortex Lattice Method
WRJ	Wingtip Reaction Jet
YFTV	Yaw Fluidic Thrust Vectoring

Abstract

The work in this thesis aims to create and develop an improved method of lateral control for finless flying wing aircraft using only conformal control effectors. This improves on existing methods that typically use additional non-conformal aerodynamic surfaces such as spoilers and split flaps to generate yaw control primarily through modulation of profile drag. The method is based on the design and allocation of a suite of lift based aerodynamic controls to modulate the spanwise lift distribution in such a way to provide independent control of pitch, roll and yawing moment, with the yawing moment principally produced through laterally asymmetric induced drag.

Previous relevant work in the literature has mainly focussed on the development of sophisticated control allocation methods for over-actuated suites of aerodynamic controls and development of innovative non-conformal control devices. Alternative conformal yaw control schemes based on forebody flow control have shown some promise, however to-date, all known successful finless flying wing aircraft have used non-conformal surfaces, or exceedingly large deflections of conformal control surfaces as to negate the benefits of conformity, to provide closure on the yaw control problem. Initial investigations concerning the use of fluidic yaw control show that with the fins removed, the opportunities to actuate tailless aircraft at low angles of attack with no significant coupling are scarce and require large changes in pressure over the surface of the aircraft to achieve a useful authority without modifying the thrust line.

The primary contribution of this thesis is a design method based on the use of a series of control mode shapes which are defined from the response of the aircraft in lift, pitching moment and rolling moment to a given control input. By forming this response as a linear system and taking the null space, the mode shapes are defined such that they produce a yawing moment with no coupling. Mode shapes are obtained using a low order aerodynamic analysis and can be derived for a range of flying wing geometries and control layouts of practical interest.

The proposed method is evaluated through two case studies on a generic finless flying wing aircraft. One considering steady sideslip relevant to a cross wind landing case and one concerning a coordinated rolling manoeuvre to initiate a banked turn. For steady sideslip at an angle of attack of four degrees, a given yawing moment can be produced with up to a factor of 2.5 reduction in the aggregate control deflection and 10% less overall drag when compared to a comparable conventional non-conformal control solution. For the roll case,

there is at least factor 1.25 reduction in aggregate control deflection for roll rates meeting mil-spec requirements. The greatest benefit in aggregate control deflection can be up to a factor of 5 depending on the angle of attack. The method is more effective with decreasing angle of attack as the effect of adverse yaw is reduced. As part of an assessment for three-axis fluidic control, the method was also applied to an aircraft case study that used fluidic effectors in the form of circulation control actuators in place of conventional geometric flight control surfaces. In doing this, a framework was developed to assesses novel control actuators against mission requirements.

The methods developed within this thesis show that is possible to generate yawing moments sufficient for independent three axes control of tailless aircraft using only lift based controls over a useful range of angle of attack and sideslip, though the maximum authority achievable will typically be lower than that for a comparable drag-based control implementation. The benefits demonstrated include a reduced drag increment and reduced aggregate deflection when compared to conventional, non-conformal profile drag based controls. These benefits make the application of the mode shaping technique particularly useful during the cruise phase of a typical mission. Integration of the toolset with novel fluidic controls as part of the actuator suite provides new capability to designers allowing significant opportunity for improvement of future designs of finless flying wing aircraft.

Declaration of originality

I hereby confirm that no portion of the work referred to in the thesis has been submitted in support of an application for another degree or qualification of this or any other university or other institute of learning.

Copyright statement

i The author of this thesis (including any appendices and/or schedules to this thesis) owns certain copyright or related rights in it (the "Copyright") and s/he has given The University of Manchester certain rights to use such Copyright, including for administrative purposes.

ii Copies of this thesis, either in full or in extracts and whether in hard or electronic copy, may be made *only* in accordance with the Copyright, Designs and Patents Act 1988 (as amended) and regulations issued under it or, where appropriate, in accordance with licensing agreements which the University has from time to time. This page must form part of any such copies made.

iii The ownership of certain Copyright, patents, designs, trademarks and other intellectual property (the "Intellectual Property") and any reproductions of copyright works in the thesis, for example graphs and tables ("Reproductions"), which may be described in this thesis, may not be owned by the author and may be owned by third parties. Such Intellectual Property and Reproductions cannot and must not be made available for use without the prior written permission of the owner(s) of the relevant Intellectual Property and/or Reproductions.

iv Further information on the conditions under which disclosure, publication and commercialisation of this thesis, the Copyright and any Intellectual Property and/or Reproductions described in it may take place is available in the University IP Policy (see `http://documents.manchester.ac.uk/DocuInfo.aspx?DocID=24420`), in any relevant Thesis restriction declarations deposited in the University Library, The University Library's regulations (see `http://www.library.manchester.ac.uk/about/regulations/`) and in The University's policy on Presentation of Theses.

Acknowledgements

I would like to thank my supervisors for their guidance and support over the last four years. Prof. William Crowther for allowing the freedom to explore my research ideas and for his honest feedback. Dr Mostafa Nabawy for sharing his passion of aerodynamics and for pushing me to publish my work from the outset. Finally my industrial supervisor Prof. Clyde Warsop for seeing the value in changes of direction and allowing the flexibility to follow the most interesting path, even when we were unsure where it would lead.

I would also like to thank all the other students in the PhD village for making it such an entertaining place to work. The challenging times that have covered the final 18 months of this project have shown just how valuable your companionship is and what a difference it makes.

I owe a huge debt of gratitude to my parents who have supported me in pursuing many academic and not so academic interests over the years. Without this support, the interest I developed in aviation certainly would not have developed to the point that lead me here.

To all my family and friends, this last four years has been a constant juggling act of studies, work and life. Thank you for your support and patience in helping my navigate this and keeping me focused on the most important things.

Finally to my wife Ellie, without your love and support this would not have been possible. I will be forever grateful for you listening to my rants and your willingness to proofread even after long days at work and through difficult times.

Chapter 1

Introduction

1.1 Context

A key driver for survivability of military aircraft operating in threat environments is their *observablity*, that is, the extent to which they emit and/or return incident electromagnetic radiation. Designing for low observability, however, typically comes at the cost of reduced aerodynamic performance and increased systems complexity. The work in this thesis concerns the development of methods for the design and operation of suites of aerodynamic control effectors that achieve the required control authority but with: reduced penalty to observability, reduced control complexity and reduced aerodynamic performance cost. Furthermore, the nature of the design constraints drives planform designs towards low aspect ratio, swept, all flying wing configurations without separate horizontal tail surfaces, hence the design methods focus on this class of aircraft.

The requirement for reducing the radar cross section of combat aircraft first widely appeared in generation 4.5 [1] on aircraft such as F/A-18, Eurofighter Typhoon and Rafele, Fig. 1.1. This design pressure resulted in the development of a class of tailless aircraft characterised by the absence of a vertical stablising surface Fig. 1.2. Due to the control chalenges at supersonic flight speeds [2], [3], these aircraft operate in the subsonic regime only.

Figure 1.1. Generation 4.5 Aircraft. Left to Right[1]: F/A-18 Hornet, Eurofighter Typhoon, Dassult Rafale.

One of the challenges presented by these planforms is the positioning of surfaces for directional stability and control. Typically, directional stability is provided by vertical stabilising surfaces at the rear of the aircraft. However, on tailless aircraft the moment arm between

[1]Image credit: Dave Grubb, Flickr; Copyright Eurofighter; Airwolfhound, Flickr

B2 Spirit: Northrop Grumman | Taranis: BAE Systems | X-47B: Northrop Grumman

Figure 1.2. Subsonic finless flying wing aircraft [2]

the Centre of Gravity (CG) and these surfaces is much smaller necessitating relatively large surfaces to achieve the same effectiveness as conventional configurations.

Large stabilising surfaces, whilst necessary to provide directional control for the aircraft, also have a penalty in terms of observability and drag. There is therefore a large design pressure to reduce the size of, or remove these surfaces. Conventionally this is achieved by a profile drag based control method used for stability augmentation such as mid-chord spoilers. Alternatively, some concepts use a Split Drag Rudder (SDR) where the outermost conventional control surface is substituted for a split surface which opens up as a clam shell. These control options are shown on operational aircraft in, Fig. 1.3. The mechanism by which both of these alternatives work is the same; the control surfaces are deployed asymmetrically about the aircraft centerline, this causes a corresponding asymmetry in the profile drag and therefore generates a yawing moment. When used with a suitable control system, these surfaces can be used to mimic the stability and control contribution of a fin and rudder.

Mid-chord spoiler | Split Drag Rudder | Conventional Rudder

Figure 1.3. Conventional directional control methods [3]

Again, these profile drag based yaw devices have a drawback. Aside from the weight and complexity they add to the aircraft due to the need for their actuation systems and integration to the aircraft structure, these surfaces project a large cross sectional area in the flow direction when deployed. These drag based effectors for yaw control may still be preferable to the vertical surfaces as they are are only deployed intermittently. However, they are still far from an optimal solution.

Some work has been shown the possibility of using a crow-mixing effect of conventional control surfaces to act as a distributed split drag rudder [4]. In this mode, the inner and outer control surfaces are deflected in opposing directions to a large magnitude in order to

[2]Image Credit: Christopher Ebdon, Flickr, BAE Systems, Northrop Grumman
[3]Image credit: BAE Systems; Eric Prado, Flickr; fsll2, Flickr

generate asymmetric profile drag. This has been flight tested on experimental tailless aircraft but has not yet been utilised on operational aircraft [4]. Whilst this does mitigate some of the disadvantages of spoilers and SDRs (i.e. the penalty of integration into the structure and additional actuators), the requirement to deploy large surfaces into the flow to provide a yawing moment remains.

1.2 Tailless Aircraft Research at The University of Manchester

Previous research into tailless aircraft at The University of Manchester involves the design, manufacture and flight testing of the MAGMA research aircraft in partnership with BAE Systems, Fig. 1.4. The planform is based on the Boeing 1303 planform [5] and is designed to be representative of future military UAV concepts. The aircraft has a wingspan of $4m$, leading-edge sweep of 47° and a maximum take-off mass of $60kg$.

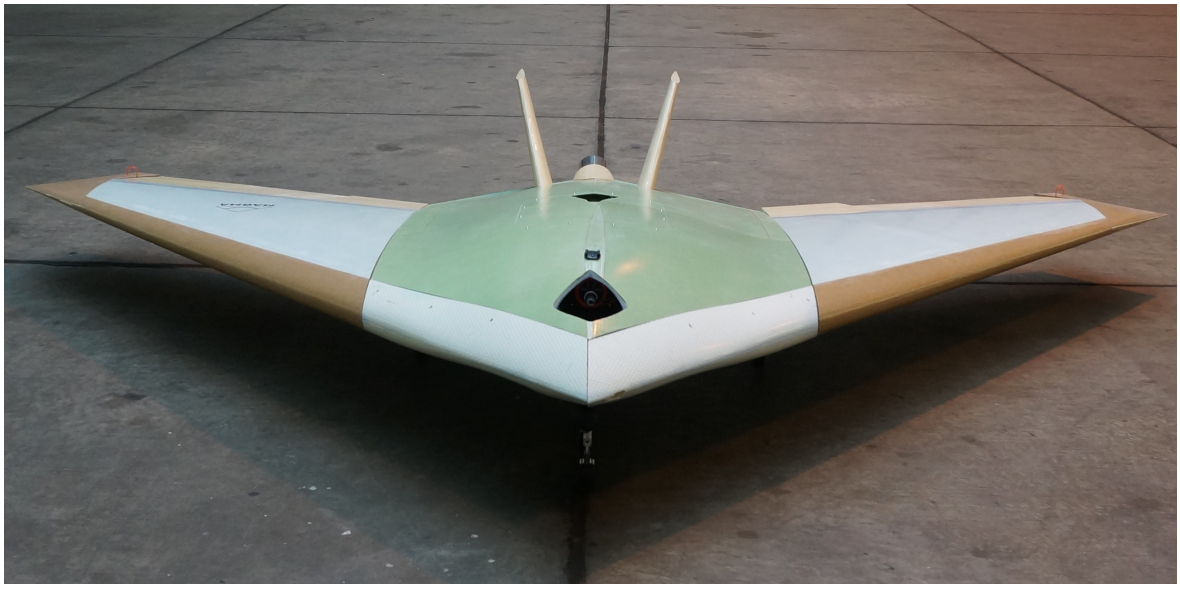

Figure 1.4. MAGMA aircraft

Two variations of the aircraft were built and tested: one conventionally controlled (i.e. with a system of trailing edge camber flaps), and a fluidically controlled variant using Circulation Control (CC) and Fluidic Thrust Vectoring (FTV), Fig. 1.5. The two variants of the aircraft demonstrated the stability of the planform and the in-flight use of novel fluidic control effectors respectively [6], [7]. It is worth noting however that whilst this aircraft is tailless, both of the variants are designed with a vertical fin but without a rudder.

In order to investigate the effect of removing the fin on this planform, the fin height was gradually reduced by halving the fin height after each successful flight on a $\frac{1}{3}$ MAGMA planform named Baboo, Fig. 1.6.

Figure 1.5. Circulation control (yellow) and fluidic thrust vectoring on the MAGMA airframe

Figure 1.6. Baboo airframe with 100%, 50% and 25% fin height.

Flights at 100% and 50% fin height were successful and showed no significant instabilities. However, at a fin height of 25% the aircraft showed a reduction in the static directional stability, yaw damping and showed significant roll-yaw coupling. These effects lead to severe excitation of a dynamic mode which was eventually recovered by the pilot. This experiment underpins the need for understanding the lateral stability and control characteristics of tailless aircraft.

1.3 Aim and Objectives

The work presented in this thesis is focused on removing or relaxing the requirement for vertical fins and profile drag based yaw control on tailless aircraft. Therefore, the aim of this thesis is:

To develop and evaluate a design toolset that enables independent directional control of finless flying wing aircraft using only conformal control effectors.

To achieve this, the following objectives are defined:

- Review the key developments in the literature surrounding tailless aircraft and in alternative methods for yaw control (Chapter 3). Identify the current state of the art and gaps in the current understanding and application of novel yaw control.
- Develop a control method which uses asymmetric induced drag to generate a yawing moment for control of tailless aircraft (Chapter 5 & 6). The method should show minimal coupling with other control axes. Compare the developed method against existing control solutions.

- Further develop the asymmetric induced drag method to alleviate adverse yaw during a rolling manoeuvre to initiate a banked turn (Chapter 7 & 8). This will minimise the sideslip of the aircraft during the roll and therefore must be capable of changing the actuation level through the manoeuvre.

- Investigate the potential for fluidic control solutions to generate a yawing moment (Chapter 4). The analysis will consider actuation of a representative tailless aircraft by changing the surface pressure over targeted regions. Specific actuation methods will not be considered.

- Develop a method for the assessment of novel fluidic control configurations on a representative tailless aircraft (Chapter 9). The method will simulate the aircraft over a representative mission and allow methods to be compared against mission performance and momentum input.

1.4 Thesis Structure

As the objectives detailed in the previous section were achieved, the outputs were disseminated through journal articles and presentation at conferences. Therefore, this work is presented as a journal format thesis. Chapter 2 presents the fundamental theory required to support the work presented in this thesis and is followed by a review of the relevant literature in Chapter 3. Both of these Chapters were developed for this thesis. The following Chapters 4 – 9 are the papers which make up the method and results sections. . Finally, the main findings are drawn together and concluding remarks made in Chapter 10. The way in which the sections are linked throughout the thesis is detailed in Fig. 1.7.

The investigation into methods of yaw control starts in Chapter 4 where the potential to generate a yawing moment using fluidic control is explored. The approach taken is agnostic of the actuator used and instead focuses on which areas of the a typical tailless aircraft geometry contribute greatest to the yawing moment. This is done with the aim of changing the surface pressure over these areas of interest in order to affect directional control. It was found that very little of the aircraft contributes to the yawing moment, and those areas which do also have a strong influence in roll. In order to achieve a yawing moment with no associated roll the changes in surface pressure were unreasonably large to achieve using current flow technology.

With the outcomes of Chapter 4 indicating that changes in surface pressure are not a feasible method of control, Chapter 5 - Chapter 8 explore the use of asymmetric induced drag to affect a yawing moment. The method developed is named mode shaping and first outlined and demonstrated in Chapter 5 for a series of trapezoidal wings generating a yawing moment to trim at angles of sideslip up to 10°. This is then demonstrated as a case study on the MAGMA aircraft in Chapter 6. The method is further developed to allow for a coordinated rolling manoeuvre in Chapter 7 and Chapter 8. The theory which allows a coordinated 3-axis

manoeuvre using the mode shaping technique superimposed on conventional control surface deflections is detailed in Chapter 7 and applied to a generic trapezoidal planform. Again, the method is demonstrated as a case study on the MAGMA aircraft in Chapter 8.

Chapter 9 returns again to the topic of fluidic control, this time using the mode shaping method developed in this thesis actuated using circulation control in addition to thrust vectoring and reaction jets. This Chapter develops a framework to allow for the assessment of fluidic control configurations against mission requirements. As part of this, a path planning algorithm is introduced to allow for the control of aircraft with limited actuation power in roll as the limited mass flow budgets for fluidic control place a limit on the agility of the aircraft. The fluidic control configurations are analysed for the MAGMA aircraft using its simplistic design philosphy and limited mass flow budget. These factors meant that the mode shaping technique using circulation control did not achieve a sufficient control authority for full 3-axis control, although other configurations using a thrust reaction could. Nevertheless, this Chapter is included to demonstrate the framework which could be used to assess the performance of any fluidic control configuration, including mode shaping using circulation control, against arbitrary mission requirements.

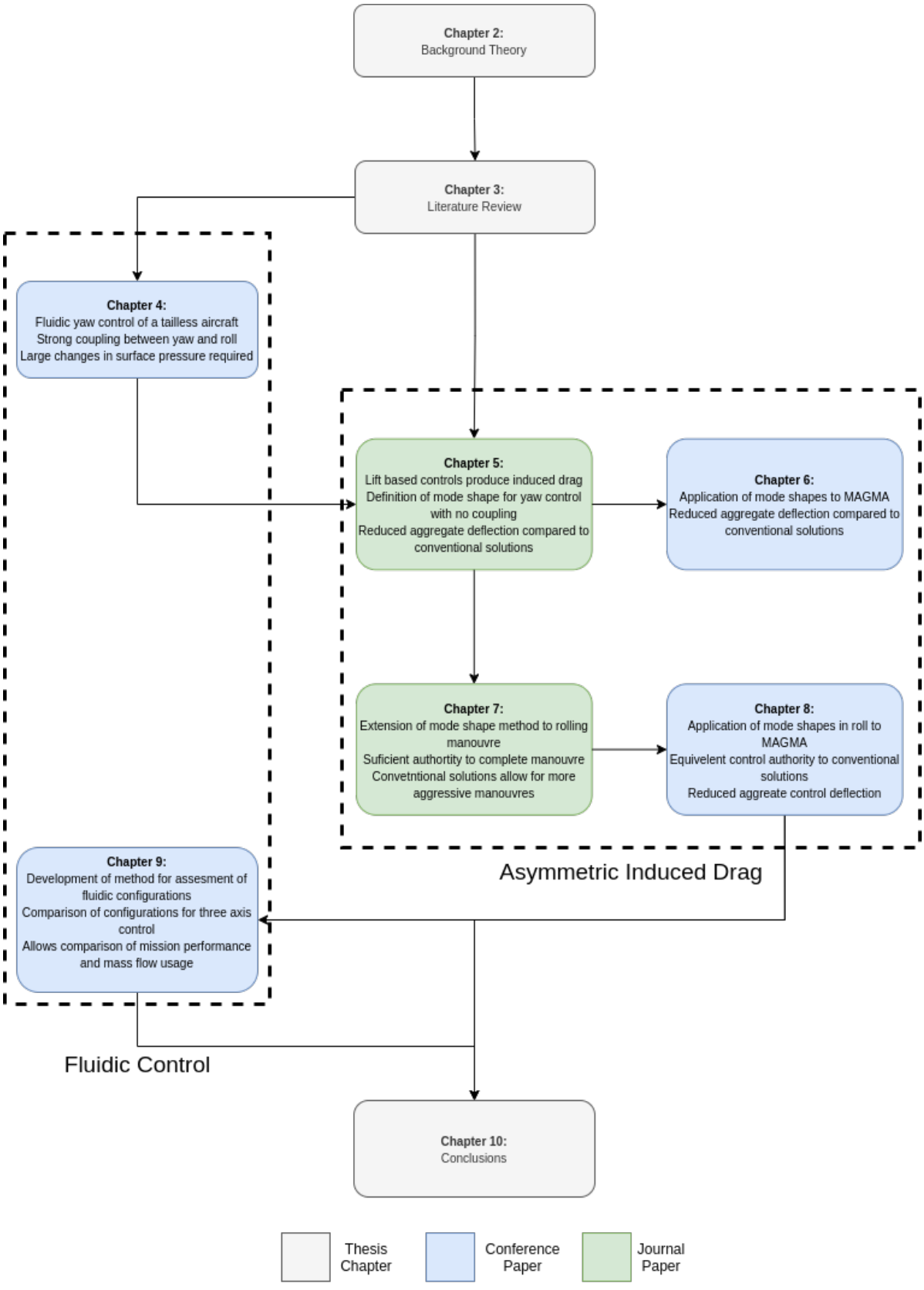

Figure 1.7. Thesis Structure

Chapter 2

Theoretical Background

2.1 Lift and Drag

2.1.1 Circulation Theory of Lift

The popular description of lift is based upon a difference in pressure due the Bernoulli principle as an aerofoil moves through the air. This description states that because the path for the air going over the airfoil is longer, it must therefore move faster than the air on the lower surface to arrive at the trailing edge at the same time. This difference in velocity gives rise to a difference in pressure and therefore a net upwards force. Though popular, this explanation for lift is flawed in that the 'equal transit time' constraint has been shown to be false [8].

A more sophisticated theory for lift can be found by using circulation theory, which provides the basis for much of the classical analysis of lifting bodies. The basis of circulation theory can be seen in Fig. 2.1 [9]. Fig. 2.1a shows a representative flowfield around a lifting airfoil, the free stream velocity is then subtracted from this to give the flowfield in Fig. 2.1b. We can approximate this flowfield by collapsing the circulating flow into a single point, shown in Fig. 2.1c. The total circulation about an airfoil can then be quantified by a single parameter, Γ. The lift generated due to this circulation for a 2D body is found using the Kutta–Joukowski theorem [9], which gives the lift per unit span as:

$$L' = \rho V \Gamma \tag{2.1}$$

Although the Kutta–Joukowski theorem gives us a way to relate circulation and lift, there are still an infinite number of solutions as we have not found a unique value for the circulation. If we impose the Kutta condition [9], which specifies that the trailing edge should either be a stagnation point (for a sharp edge) or the flow from the upper and lower surface should leave smoothly (for a cusped leading edge) a unique solution can be found.

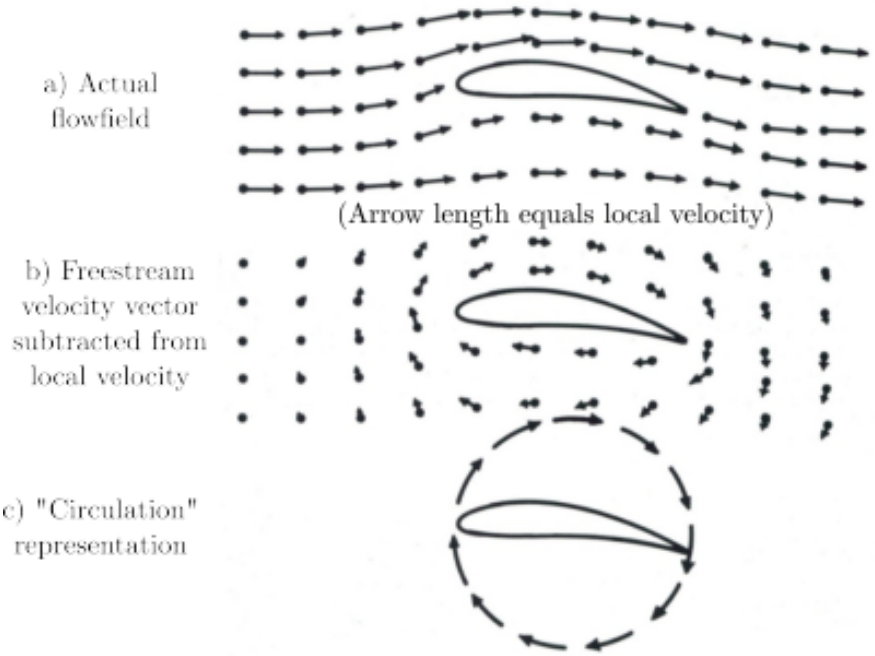

Figure 2.1. Circulation representation of flowfield around an aerofoil [10].

2.1.2 Thin Airfoil Theory

The circulation theory of lift can be further extended to find the lift and pitching moment on an arbitrary thin airfoil. It is worth noting here that this classical analysis assumes that the fluid is inviscid and therefore does not capture any drag force. This absence of drag in the classical analysis was observed by Jean le Rond d'Alembert in 1752, this contradiction between theoretical analysis and experimental observations of drag is named after him as D'Alemberts paradox [9].

For thin airfoil theory, we assume that the airfoil thickness is small relative to its chord line and therefore simplify the airfoil to only its mean camber line, Fig. 2.2a. To simplify the mathematics a sheet of vortex filaments is positioned along the airfoil chord line Fig. 2.2b. To find the strength (i.e. circulation) of each of these vortex filaments, the camber line and strength of the vortex filaments are represented as a Fourier series. The Fourier coefficients for the circulation are then found by imposing a no flow condition across the camber line. The problem is closed by imposing a condition that the circulation at the trailing edge is zero, this satisfies the Kutta condition.

By forming the problem in this way, the quantities in Table 2.1 can be found using only the first three Fourier coefficients.

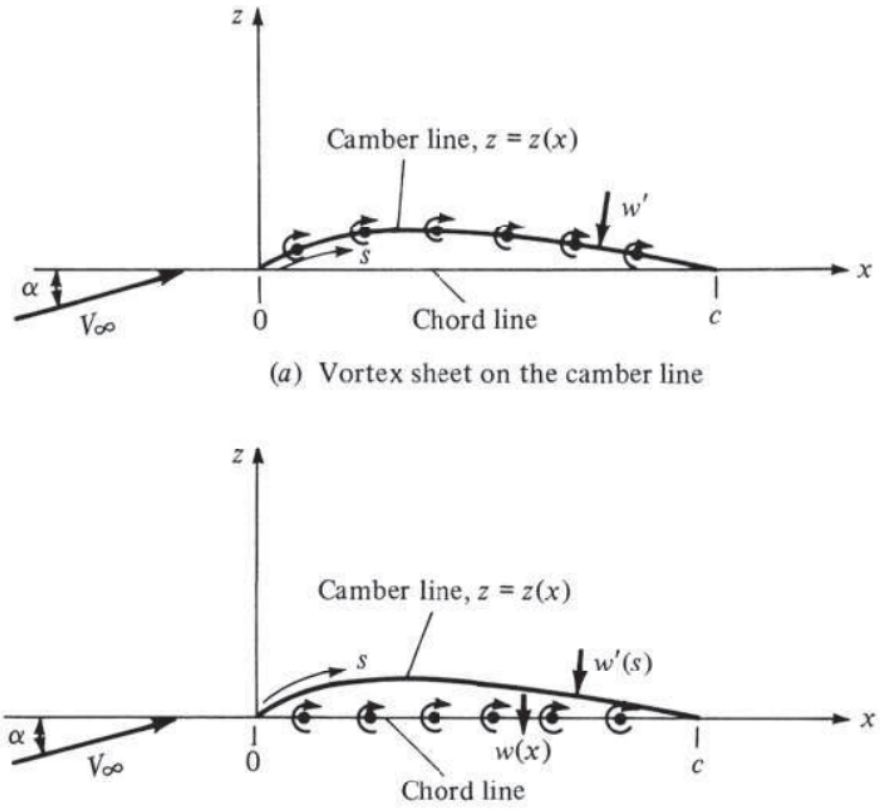

Figure 2.2. Position of vortex sheet for thin aerofoil theory [9].

Parameter	Equation
$\alpha_{L=0}$	$-\frac{1}{\pi}\int_0^{\pi}\frac{dz}{dx}(\cos\theta_0 - 1)d\theta$
$\frac{dC_l}{d\alpha}$	2π
C_l	$2\pi(\alpha - \alpha_{L=0})$
$C_{m,\frac{c}{4}}$	$\frac{\pi}{4}(A_2 - A_1)$
x_{ac}	$\frac{c}{4}$
x_{cp}	$\frac{c}{4}(1 + \frac{\pi}{C_l}(A_1 - A_2))$

Table 2.1. Airfoil parameters from thin airfoil theory

2.1.3 Prandtl's Lifting Line Theory

Whilst it is useful to predict the aerodynamic properties of airfoils, it is of much greater practical interest to calculate the forces and moments on wings of finite span. This was first achieved through the Lifting Line Theory (LLT), attributed to Ludwig Prandtl in 1918 [11].

The basis of lifting line theory involves placing a bound vortex along the quarter chord line of the wing with trailing vertices extending from the wing tips to infinity, Fig. 2.3. These trailing vertices ensure that Helmholtz vortex theorems are not broken [12]. The following sections provide an overview of the concepts found in lifting line theory which are most

relevant to the work in this thesis.

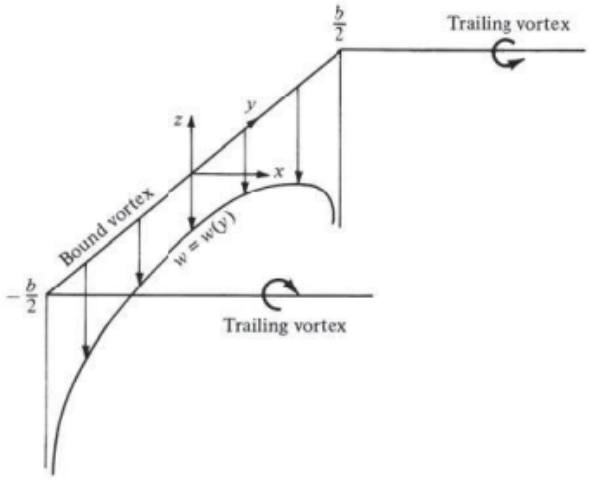

Figure 2.3. Horseshoe vortex and induced velocity [9].

Circulation

The first step in lifting line theory is to define a vortex system which can be solved to find the circulation of the bound vortex as a function of the spanwise location. As a vortex cannot change strength along its length, a trailing vortex must be present wherever the strength of the bound vortex changes. This leads to the system shown in Fig. 2.4. Each of these trailing vortices creates a down wash at the bound vortex, the strength of this downwash at any spanwised point due to all of the trailing vortices is defined by the Biot–Savart law as [ref]:

$$w(y) = -\frac{1}{4\pi}\int_{-\frac{b}{2}}^{\frac{b}{2}} \frac{\frac{d\Gamma}{dy}dy}{y_0 - y} \tag{2.2}$$

With the vortex system defined and the influence on the bound vortex quantified, it is possible to solve for the circulation along the bound vortex. The most popular method for doing so is defining the circulation distribution as a Fourier series, known as the Glauert method [13]. However other methods, developed by Prandtl's students, using quadrature (Multhop [14]) and assumed distributions (Betz [15]) are possible.

Lift

With the circulation distribution defined, finding the local lift at any spanwise station is simple using the Kutta–Joukowski theorem, Eq. (2.1). This can then be used to find the local lift coefficient:

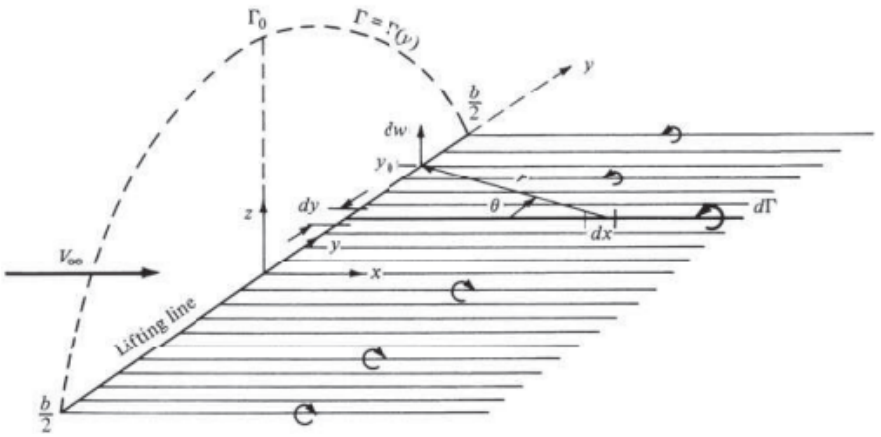

Figure 2.4. Bound and trailing vortex system in lifting line theory [9].

$$C_l(y) = \frac{2\Gamma}{Vc(y)} \tag{2.3}$$

The net lift on the aircraft can then be found by integrating the circulation distribution using the Kutta–Joukowski theorem:

$$L = \rho V \int_{-\frac{b}{2}}^{\frac{b}{2}} \Gamma(y) dy \tag{2.4}$$

The lift coefficient of the wing is found by:

$$C_L = \frac{2\int_{-\frac{b}{2}}^{\frac{b}{2}} \Gamma(y) dy}{VS} \tag{2.5}$$

Induced Drag

Unlike thin airfoil theory, LLT does predict a drag force. However, like thin airfoil theory LLT is an inviscid theory and therefore this drag cannot be due to the profile of the wing. The drag predicted by LLT is due to the downwash created by the trailing vortex system. As the strength of these trailing vortices is governed by the magnitude of the lift generated by the wing, this drag is referred to as lift induced drag (often shortened to induced drag).

The mechanism by which this drag is produced is illustrated in Fig. 2.5. The downwash on the bound vortex changes the direction of the local flow along the span of the wing. The net effect of this is that the angle of attack is increased as a function of the downwash and oncoming flow velocity ($\alpha_i = \tan(\frac{w}{V})$). Because the lift generated is perpendicular to the

local flow direction, this has the effect of tilting the lift vector rearwards. When evaluated in the global flow direction, this appears as a small drag force equal to:

$$D_i'(y) = L'(y) \sin \alpha_i(y) \tag{2.6}$$

Which, assuming that the induced angle of attack (α_i) is small, simplifies to:

$$D_i'(y) = L'(y)\alpha_i(y) \tag{2.7}$$

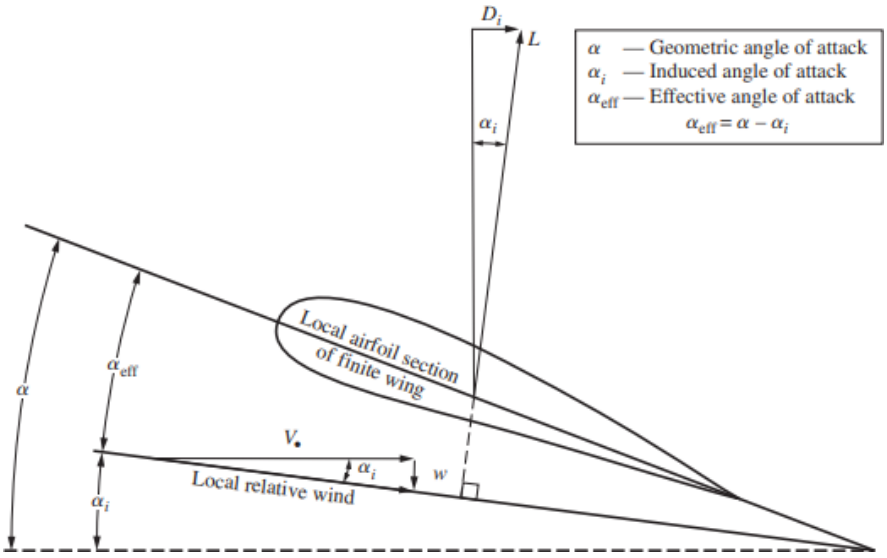

Figure 2.5. Rotation of the lift vector due to downwash responsible for the production of induced drag [9].

The induced drag coefficient at a spanwise location can then be found as:

$$C_d(y) = C_l(y)\alpha_i = \frac{2\Gamma(y)\alpha_i(y)dy}{Vc(y)} \tag{2.8}$$

And the net drag on the aircraft as:

$$C_D = \frac{2\int_{-\frac{b}{2}}^{\frac{b}{2}} \Gamma(y)\alpha_i(y)dy}{VS} \tag{2.9}$$

It is worth noting that in both Eq. (2.8) and Eq. (2.9) the magnitude of the drag coefficient is proportional to the product of the circulation and induced angle of attack ($\Gamma\alpha_i$). As stated previously, the induced angle of attack is a function of the downwash, which is a function of the spanwised derivative of circulation. Therefore, it follows that the induced drag is proportional to the product of the circulation and the spanwise derivative of the circulation distribution at any point (i.e. $C_d \propto \Gamma(y)\frac{d\Gamma(y)}{dy}$).

2.1.4 Lifting Surface Method

The insights from LLT are very useful for simple lifting surfaces. However, the assumptions in the development of LLT mean that it is unsuitable for swept wings or wings of low aspect ratio. For the work in this thesis, we are interested in the aerodynamic forces and moments on swept low aspect ratio wings LLT is clearly unsuitable. Instead the Lifting Surface (LS) methodology developed by one of Prandtl's students, Hans Multhopp, is used. This section will give an overview of the conceptual difference between LLT and LS. For a detailed description of the method, the interested reader is directed to [16].

The initial problem formulation for LS is similar to LLT, however rather than concentrating the circulation into a single bound vortex the entire lifting surface is replaced with a sheet over which the circulation can vary continuously in both the spanwise and chordwise direction. However, in this formulation the resulting integral equation is not possible to solve analytically. To overcome this, the integration is performed using interpolation functions based upon the non-dimensional circulation (γ) and non-dimensional pitching moment (μ) at carefully selected pivotal points. In doing this, the problem is reduced to a linear system of equations which can be easily solved.

2.2 Aircraft Stability

2.2.1 Aircraft Coordinate System

In order to define the aircraft equations of motion, we must first define a standard coordinate system and nomenclature. For aircraft, the standard cordinate system is with origin at the centre of gravity with the x-axis towards the nose of the aircraft or alternatively along the principle axis of inertia which passes close to the nose. The y-axis then points to starboard and the z-axis completes a right hand set, shown in Fig. 2.6.

In addition to a standard coordinate system, there must also be a standard nomenclature. This is summarised in Table 2.2, showing the notation for force, velocity, moment and angular rate about each of the axes. Note that each of these symbols are denoted by a capital letter, this denotes that the quantity is dimensional. The non-dimensionalised quantities are denoted depending on the quantity used to non-dimensionalise. For a full review of these quantities, an interested reader is directed to [17].

Throughout this thesis, the planes formed by the coordinate system defined in Fig. 2.6 are often referred to by name for convenience. The names of these planes are defined in Fig. 2.3.

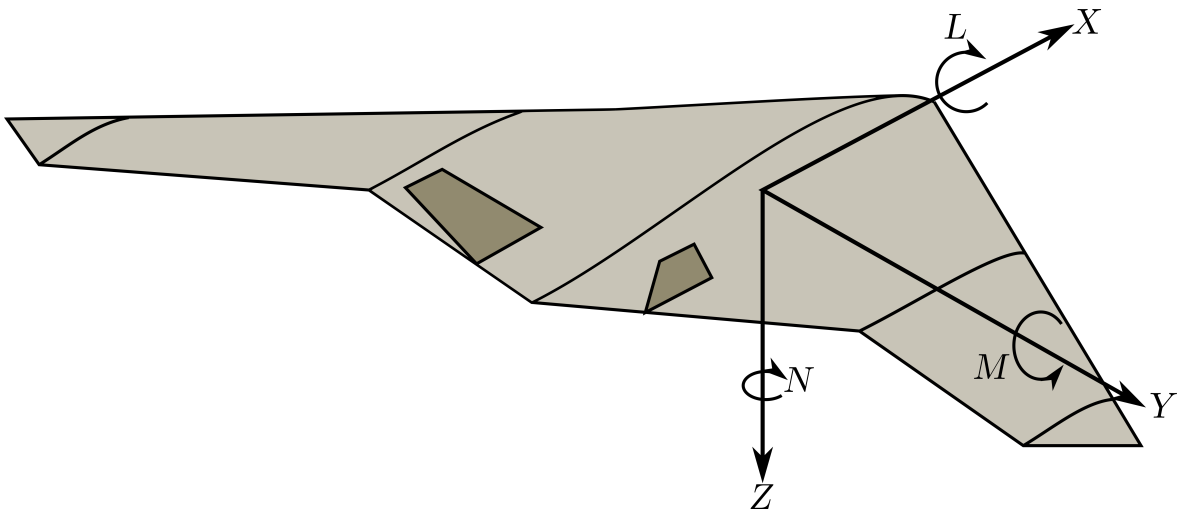

Figure 2.6. Standard aircraft coordinate system

	X-axis	Y-axis	Z-axis
Force	X	Y	Z
Velocity	U	V	W
Moment	L	M	N
Angular rate	P	Q	R

Table 2.2. Notation for aircraft forces, moments and motion.

2.2.2 Directional Stability

Much of the work in this thesis focuses on the directional stability of aircraft. This can be broken down into static and dynamic stability. The static stability is of greatest focus within this thesis and describes the aircraft's response to a sideslip. An aircraft which is directionally statically stable will yaw into any sideslip disturbance thus reducing the sideslip angle. An unstable aircraft will yaw away from any sideslip disturbance. This will lead to an increase in the sideslip angle and if not corrected quickly could lead to a departure from controlled flight.

Dynamic stability is concerned with the transient response of the aircraft following a disturbance in sideslip. An aircraft with directional static stability willA stable aircraft will eventually return to its trimmed state without pilot input whereas the motion of an unstable aircraft will become larger in amplitude until eventually the aircraft will depart from controlled flight. The two dynamic modes which may be excited in sideslip are the dutch-roll mode and spiral mode, an overview of which can be found in [17].

Plane	Defined by
Longitudinal	oXZ
Lateral	oXY
Normal	oYZ

Table 2.3. Planes defined by standard coordinate system

2.2.3 Coordinated Turns

Another key theme within the discussion in this thesis is the coordinated turn. In a coordinated turn, the aircraft flies a circular path by banking to one side, with the resultant force felt by a passenger acting through the floor. That is to say, for an observer inside the aircraft without a window, there would be no indication that the aircraft was in a turn. As this is a steady manoeuvre, an aircraft trimmed in a coordinated turn would remain in that state indefinitely.

When the aircraft is in a banked state, the lift generated is rotated by the bank angle (ϕ). This reduces the force which is counteracting weight in the vertical direction and introduces a new force in the horizontal direction, shown in Fig. 2.7.

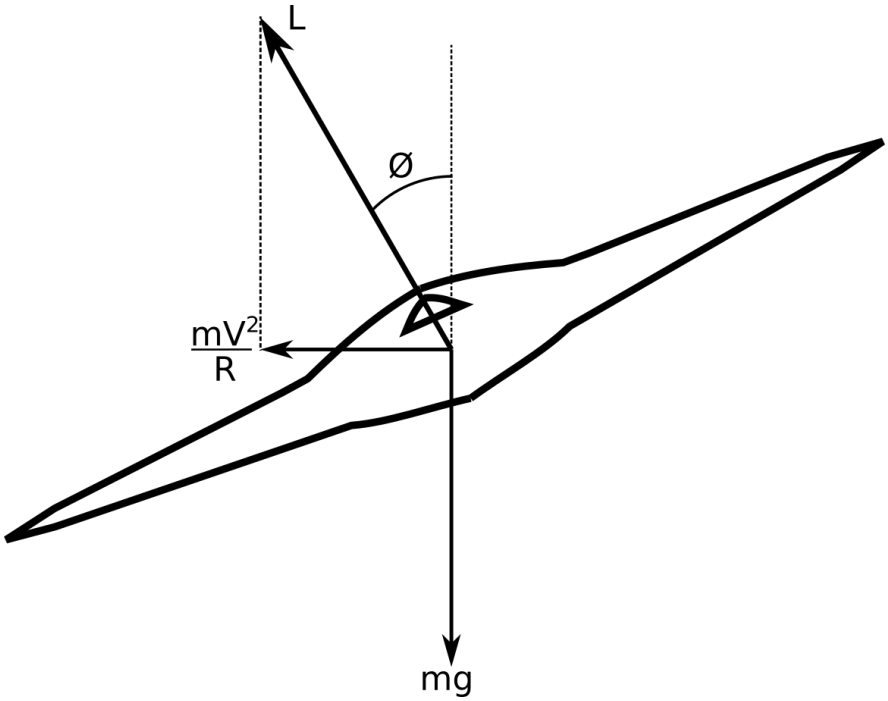

Figure 2.7. Forces on aircraft during coordinated turn

In order to maintain level flight, the amount of lift generated by the aircraft must be increased. Therefore:

$$L = \frac{mg}{\cos\phi} \tag{2.10}$$

And the force in the horizontal direction is:

$$F_h = L\sin\phi = mg\tan\phi \tag{2.11}$$

As the aircraft flies a circular path, the horizontal force directed toward the centre of the

circle is the centripetal force providing the acceleration required for circular motion. Therefore, by combining the definition of centripetal force and Eq. (2.11) we can obtain the radius of the turn:

$$R = \frac{V^2}{g \tan \phi} \tag{2.12}$$

However, simply banking the aircraft does not ensure that the path flown will be a circle. Without the aircraft also rotating about the gravity vector there will only be an acceleration in the horizontal direction meaning the aircraft will fly a curved path. To fly a circular path, the angular velocity of the aircraft about the gravity vector must equal the angular velocity of the aircraft around its circular path (i.e. $\omega = \frac{V}{R}$). This is achieved by a combination of pitch and yaw inputs in the wind axis, the relative magnitudes of each depend on the bank angle. When the aircraft is in a coordinated level turn , with the angular rates of the aircraft and the flight path are equal , therefore the sideslip angle is by definition zero throughout the manoeuvre.

2.3 Fludic Control

2.3.1 Momentum coefficient

The key parameter which governs the actuation of fluidic devices is the momentum coefficient, denoted by C_μ. It is defined as the momentum output of the fluidic device (the mass flow rate multiplied by the exit velocity for steady actuation) normalised by the product of the freestream dynamic pressure and a reference area, Eq. (2.13).

$$C_{\mu,3D} = \frac{\dot{m}_{jet} V_{jet}}{q_\infty S} \tag{2.13}$$

There are two important implications for Active Flow Control (AFC) that can be drawn from this definition. First, for a fixed momentum input, as the speed of the aircraft increases the momentum coefficient decreases. Secondly, as the momentum input is the product of the mass flow rate and jet velocity the mass flow required for a given level of actuation can be decreased by increasing the jet velocity.

The momentum coefficient definition can also be applied to a 2 dimensional airfoil section. The definition of the momentum coefficient is modified by dividing both the numerator and denominator of Eq. (2.13) by a reference length. The definition of the 2D momentum coefficient is then the momentum per unit span normalised by the product of the freestream dynamic pressure and the chord length, Eq. (2.14).

$$C_{\mu,2D} = \frac{\rho_{jet} V_{jet}^2 h}{q_\infty c} = \frac{2\rho_{jet} V_{jet}^2 h}{\rho_\infty V_\infty^2 c} \tag{2.14}$$

2.3.2 Circulation Control

One of the methods of AFC considered within this thesis is Circulation Control (CC). CC actuators use a curved surface at the trailing edge of the airfoil over which a sheet of air is blown over from a tangential slot. The jet sheet then attaches to the curved surface through a mechanism called the coanda effect [18], Fig. 2.8a. The freestream flow over the airfoil is then entrained into this jet, causing it to follow a curved path around the trailing edge. This has the effect of moving the location of the trailing edge stagnation point and therefore changes the circulation around the airfoil, hence the name of circulation control. As the circulation changes, this has the effect of changing the net lift over the airfoil section.

In order to have full control of circulation around an airfoil, i.e. to be able to increase and decrease the lift, two tangential slots are used for blowing. One on the top edge of the curved surface and another at the bottom, Fig. 2.8b. Any desired change in lift coefficient can then be achieved by blowing from either of these slots.

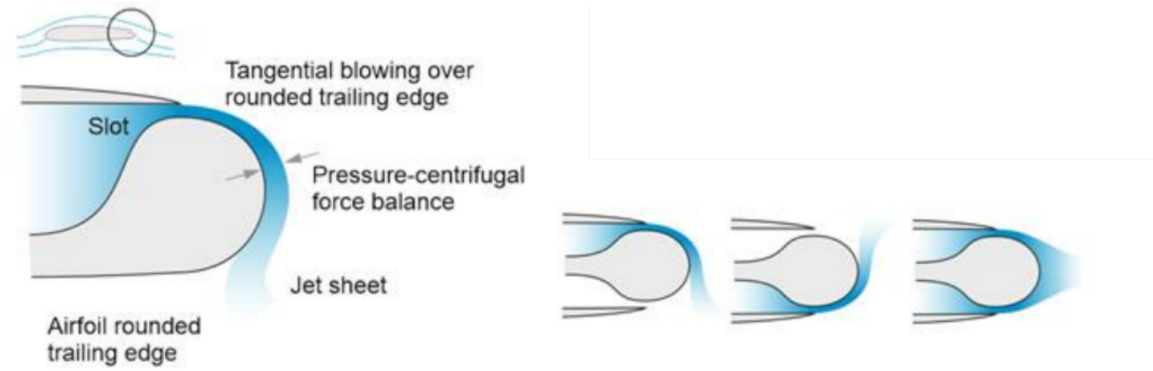

Figure 2.8. Circulation control [7].

The effectiveness of CC devices is defined by the ratio of the change in local lift coefficient to the momentum coefficient per unit span, i.e. $\frac{\partial C_l}{\partial C_{\mu,2D}}$. Therefore, it would seem possible to increase the efficiency of these devices with regards to the mass flow input by increasing the jet exit velocity. However, this is limited by two factors: Firstly the manufacturability of the slot, this will impose a minimum height of the slot and therefore a maximum velocity. Secondly, the attachment of the flow. For circular geometries, beyond a nozzle pressure ratio of approximately 6 [19] (A jet velocity of Mach 1.8) the flow will not attach to the Coanda surface leading to a stall of the CC unit. This again will limit the maximum velocity of the jet sheet.

2.3.3 Fluidic Thrust Vectoring

The other AFC technology considered in this thesis is Fluidic Thrust Vectoring (FTV). This technology changes the path of the main engine exhaust to effect a force at the aft of the aircraft, leading to a moment. Typically, this is orientated such that the force generated is vertical and therefore a pitching moment is produced.

FTV devices achieve the change in thrust angle by passing the primary (core) flow over a step to cause the flow to separate from both the upper and lower surfaces. A small secondary flow is then injected normal to the flow to encourage the flow to reattach to either the upper or lower surface and therefore vector the thrust, Fig. 2.9.

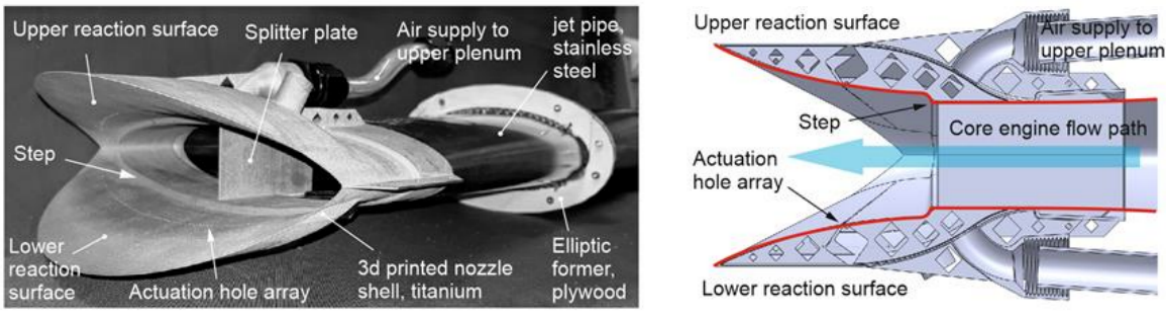

Figure 2.9. Fluidic Thrust Vectoring [7].

The mechanism for control through FTV is different to many other AFC methods as the flow being manipulated is the core engine flow and not the freestream. Therefore, it is not appropriate to normalise the effect of FTV by a momentum coefficient. Instead, the effect is normalised by the ratio of the secondary mass flow rate to the primary mass flow rate $\left(r_{\dot{m}} = \frac{\dot{m}_s}{\dot{m}_p}\right)$. The effect of the thrust vectoring is not always consistant in the literature, however it typically fits one of two categories, either: A thrust coefficient (C_F ,i.e. the vectored force normalised by the total force; or, the thrust vectoring angle (θ). Therefore, the effectiveness of the FTV device can be quantified as either $\frac{\partial C_F}{\partial r_{\dot{m}}}$ or $\frac{\partial \theta}{\partial r_{\dot{m}}}$.

Chapter 3

Literature review

3.1 Stability and Control of Tailless Aircraft

Tailless aircraft have long been considered in aircraft design with references with the literature before the first powered flight in 1903 through to the present day. The first description of a tailless aircraft was made in 1870 by Richard Harte [20]. The aircraft was a pusher configuration with a weighted beak positioned to maintain a longitudinal trim and hinged flaps connected to a stick near the pilot to effect turns. The planform and control surface are shown in Fig. 3.1 and are remarkably similar to planforms we see today. Although the design had a somewhat cumbersome fuselage section, the understanding of stability and control for these planforms discussed in the patent was significantly ahead of its time.

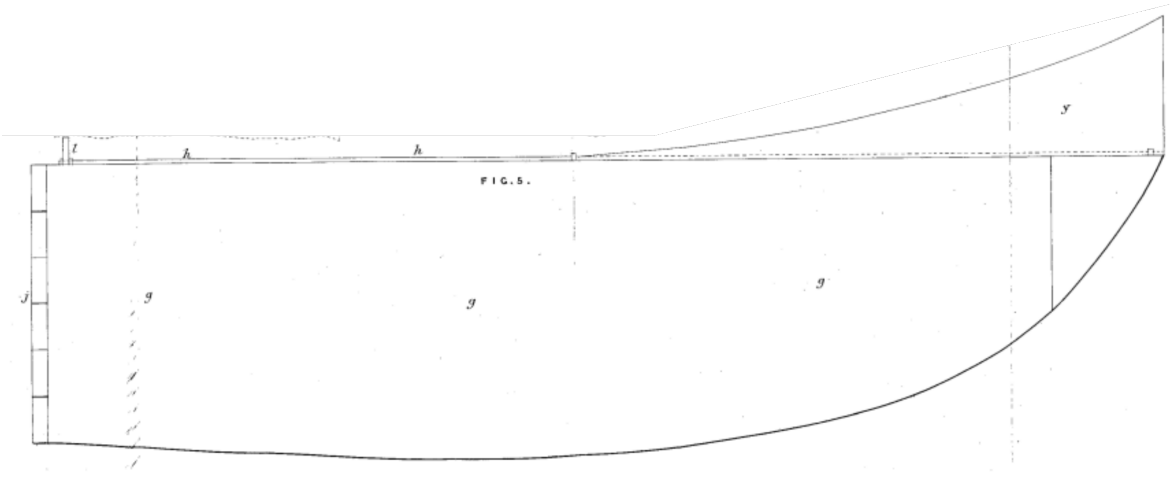

Figure 3.1. The wing planform and hinged control surface proposed by Harte [20].

It was almost 30 years following Harte's description before the first pioneers of tailless aircraft made their first flights, Fig. 3.2. An excellent review of the early work on tailless aircraft is made by Weyl [21] so will not be repeated in detail here. However, the work of Dunne on the stability of tailless aircraft bears repeating. Dunne was highly focused on the stability of tailless aircraft and was the first to demonstrate an extended period of trimmed flight by writing notes with both hands whilst the aircraft was in flight in 1910 [21]. As such

the control surfaces included on his aircraft were there for voluntary changes of direction only, with the flight path maintained by the inherent stability of the aircraft [22]. The work of Dunne set out the principles for stability and control of tailless aircraft, yet receives little credit within the literature [21].

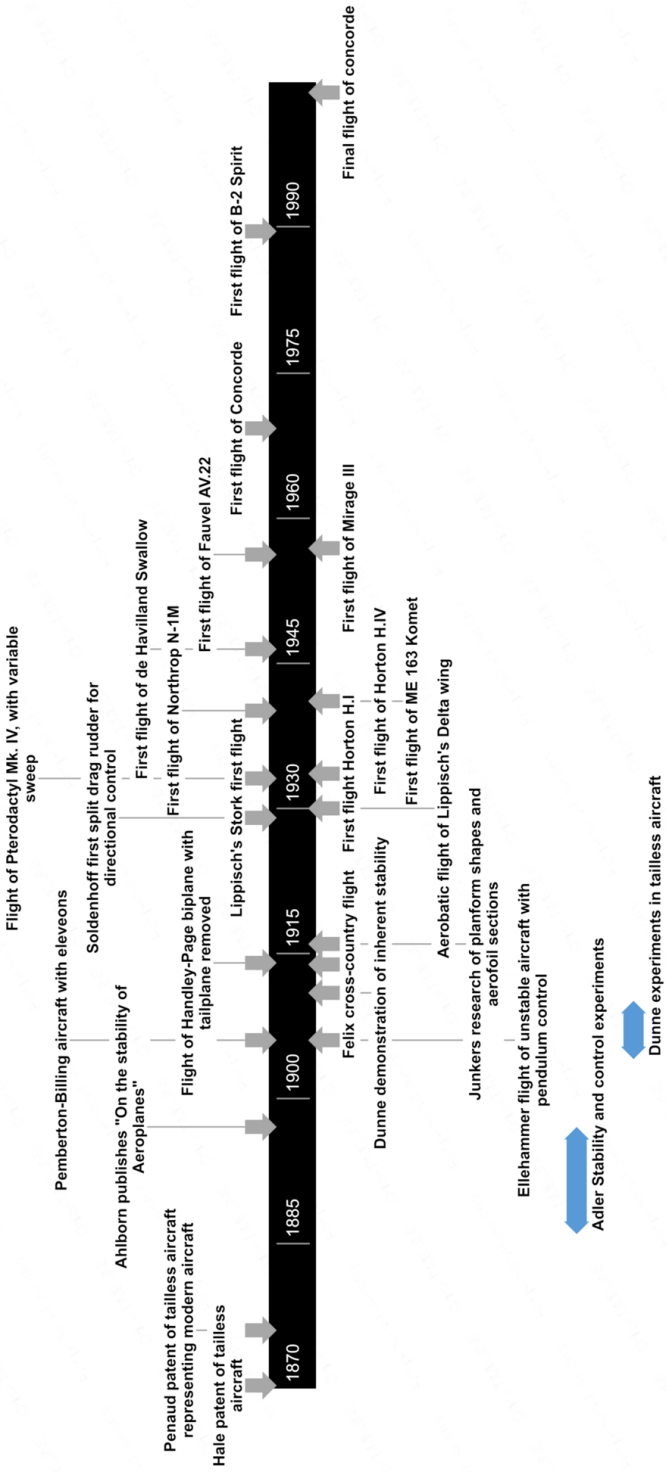

Figure 3.2. Significant events in the history of tailless aircraft.

Although there was a significant amount of early work on these tailless aircraft, the literature

output was initially sparse, Fig. 3.3. Much of the early work on these tailless aircraft was concerned with the stability of the planform [23]–[25] and justification for its use [26]–[28]. Much of this work on stability was initially concerned with the lateral stability of the aircraft due to the high roll-sideslip coupling created by the sweep and reduced effectiveness of the vertical fins [23].

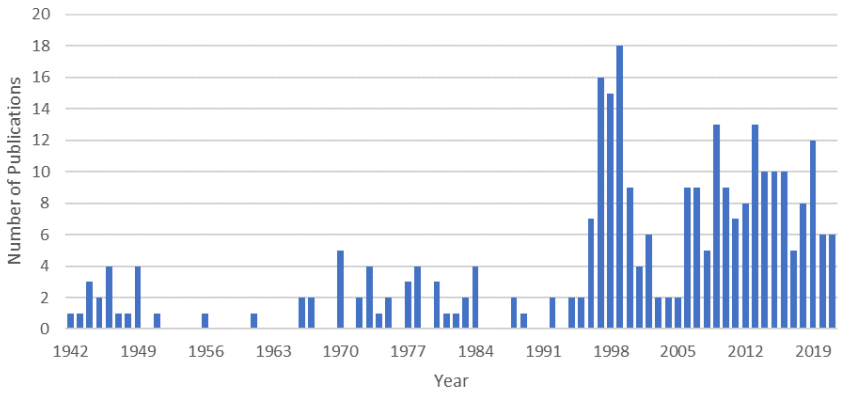

Figure 3.3. Publications with ”Tailless Aircraft” or ”Flying Wing” in title over time.

Over the next 30 years, the literature regarding tailless aircraft was focused mostly on practical aspects of the design and flight testing of specific configurations. However, it is worth noting that the number of publications on the topic was at most 4/5 per year. In the early 1990s, the interest in tailless aircraft in the literature increased dramatically, Fig. 3.3. This was during the inception of the generation 4.5 jet fighter aircraft which were begining to take a much greater interest in stealth capabilities [29]. This interest drove planforms to tailless/semi-tailless [1] aircraft with swept wings of low-aspect ratio. At this point, the planform effect on the aerodynamics was pushed lower down the priority list with the aircraft designed primarily for their mission requirements. Therefore a large body of literature appeared on how to control these aircraft, this can be seen in Fig. 3.4 which shows a breakdown of the main topics of publications on the subject of tailless aircraft. It can be seen that the vast majority of the literature (57%) is comprised of studies regarding the stability and control of these planforms.

The majority of the research in the early 1990s was focused on the Innovative Control Effectors (ICE) program, Fig. 3.5. Two aircraft were proposed with a highly swept all-flying wing configuration proposed as the land based version, and a moderately swept canard-delta planform as a carrier version. The canard configuration of the carrier based version does strictly not fit our definition of tailless aircraft as it has a somewhat separate horizontal stabilising surface in front of the main wing. Therefore, any further references to the ICE study vehicles will be to the land based (ICE-101) configuration.

[1] A semi-tailless aircraft posses a recognisable lifting surface which forms a section of a single, larger lifting surface. For example, see the F-22.

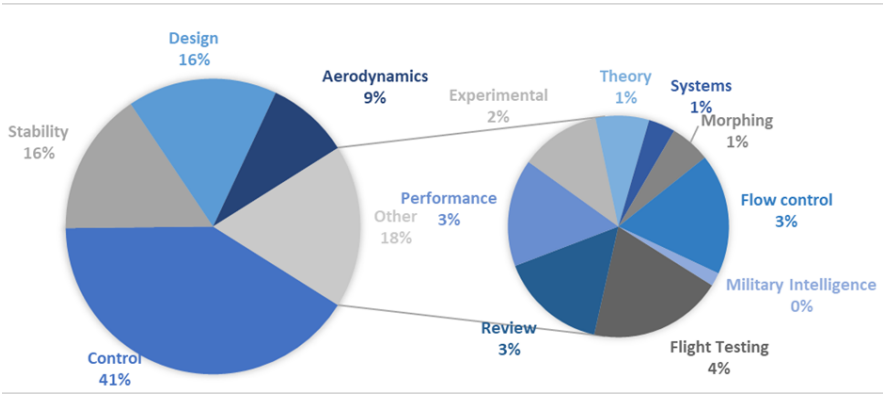

Figure 3.4. Breakdown of topic of tailless aircraft publications, 1942-2021.

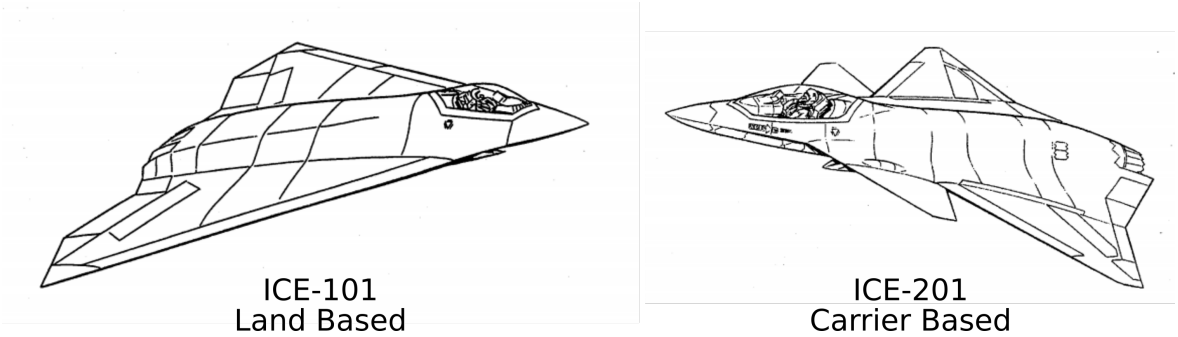

Figure 3.5. Planforms of the ICE aircraft [30].

The ICE study investigated the implementation of effectors for full 3-axis control of a tailless aircraft with no vertical fin. The aerodynamic effectors investigated included: All moving wing tips, differential leading edge flaps, deployable rudders, lower surface spoilers, spoiler-slot deflectors and split drag rudders [30]. There were two initial configurations proposed for ICE (Fig. 3.6): one with pure aerodynamic controls ICE 101, and one with thrust vectoring and aerodynamic controls ICE 101-TV.

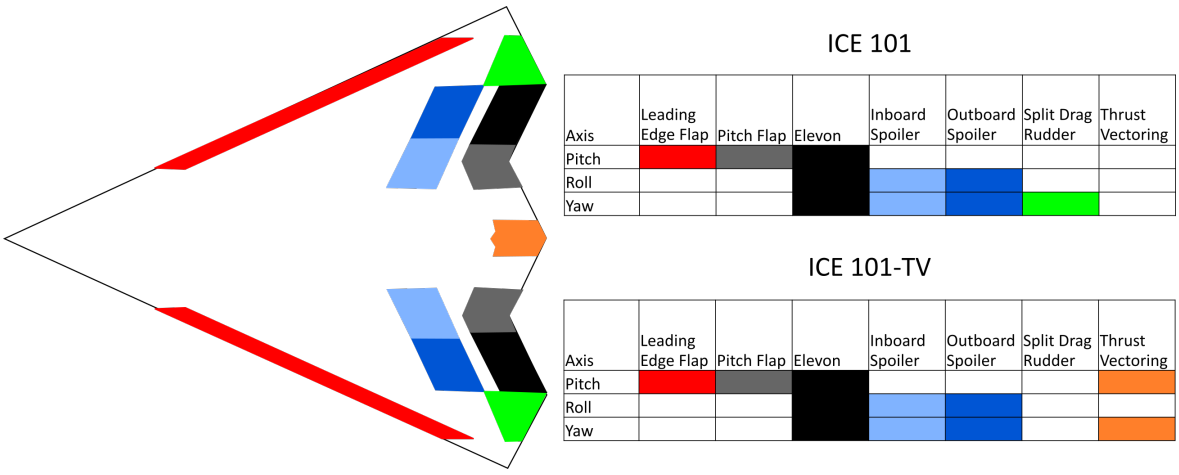

Figure 3.6. Control configurations for ICE.

The complex control suites proposed for ICE illustrate some of the problems presented

with control of tailless aircraft. The large number of actuators is required because the changing flow physics at varying angles of attack has an effect on the effectiveness of the control options, particularly the leading edge flaps [30]. Furthermore the drag based controls such as the split drag rudders and spoilers, whilst providing high authority control, generate large hinge moments and are therefore limited by the actuator power. This limits the effectiveness at high speeds and impacts the roll performance of the aircraft. It is also worth noting here that many of the controls have effectiveness in more than one axis. Whilst at first glance this may appear as a positive attribute, providing additional redundancy, this actually represents a significant coupling between axes for these control effectors.

Many studies [31]–[41] have investigated methods of control allocation using the ICE geometry and control definitions. These methods of control allocation each attempt to define an optimal allocation for the over actuated system which artificially reduces the coupling for a given control action. Whilst this achieves the goal of providing control through the aircraft's flight envelope, it comes at the expense of the weight and complexity of the associated actuation systems. Much of the literature would appear to suggest that this coupling is something to be tolerated and overcome with complex control systems. There has been little interest in approaching the control suite design from the other direction to reduce or remove the coupling through changing the planform or control surface geometry.

The most disruptive research interest for control of tailless aircraft is in Active Flow Control (AFC). This involves using a small amount of air to cause greater changes in the global flow and effect forces or moments on the aircraft. The technology has matured sufficiently in recent years to warrant a detailed study as part of a NATO Advanced Vehicle Technology (AVT) working group [7], [42]–[49]. This working group concluded that fluidic control of a representative tailless aircraft was feasible and future research should focus on the maturation of existing technology to improve reliability and integration into aircraft systems.

A well researched area of AFC is in vortex dominated flows. This is because changing the path and/or strength of the vortex can lead to large changes in forces or moments. A summary of this work on tailless aircraft can be found in Appendix A. However, these methods of AFC have two major drawbacks: first, the position, strength and, depending on the LE sweep, the formation of a LE vortex depends strongly on the angle of attack. It is therefore difficult to provide a control solution effective through the entire operational envelope of the aircraft in this way. Secondly, when the experiments reviewed in the literature are scaled to the size of operational aircraft, the volume of air required to effect the control is often unreasonably large and therefore would not be a feasible control solution.

The issue of large mass flow rates was overcome for two types of AFC, namely Circulation Control (CC) and Fluidic Thrust Vectoring (FTV), through PhD studies at the University of Manchester [50]–[52]. The CC and FTV units are able to change the local lift coefficient on the

wing and modulate the thrust line respectively. These changes can be used to impart moments in all three axes of the aircraft to achieve full fluidic control [53]. The developments in reducing the mass flow rate requirement for these devices has lead to the in-flight demonstration of integrated fluidic controls using only a small bleed off take from the compressor of the engine to supply the required fluid for control [6], [7]. Whilst the authority of these devices is still not as great as conventional controls, they nevertheless provide a feasible control solution which can minimise the negative impacts of conventional control surfaces on mission performance. Therefore, developments and improvements in these and other AFC methods represent a route by which the applicability of tailless aircraft, particularly for military applications, can be expanded.

3.2 Novel Yaw Control

Yaw control of tailless aircraft has not been extensively studied within the literature. Part of the reason for this is that aircraft are generally directionally stable [54] and very few manoeuvres require the use of yaw power alone leading to a rather prescriptive approach to yaw effector design. Typically this takes the form of a rudder which is sized to account for the yaw required to trim in the event of a single engine failure at takeoff [55]. As such, the literature on yaw control is sparse until the mid-2000s, Fig. 3.7. At this point, the interest in reducing the fin size on tailless aircraft to reduce the observability provides an impetus for development of yaw control.

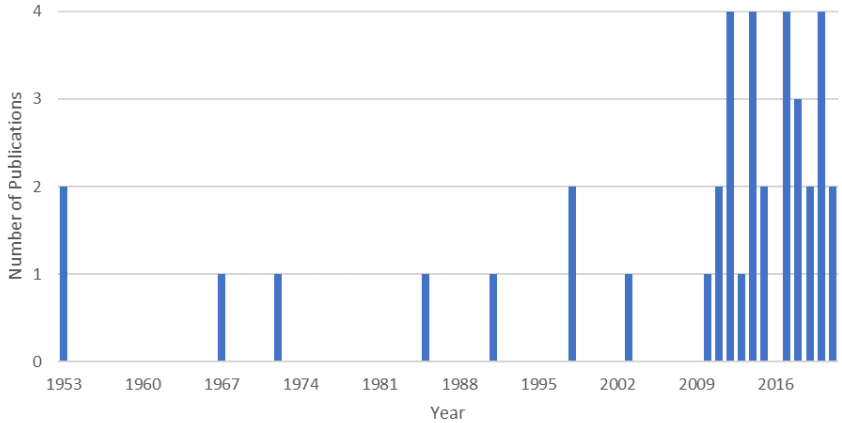

Figure 3.7. Publications on the subject of aircraft yaw control over time.

Despite this design pressure to find alternate methods of yaw control only 27% of the literature is devoted to exploring these methods, Fig. 3.8. The topic of greatest interest within the literature is control allocation, making up 42% of total publications. These publications vary in the complexity of algorithm used, however all seek to use some control algorithm with a set of previously defined control surfaces to effect three axis control of the aircraft.

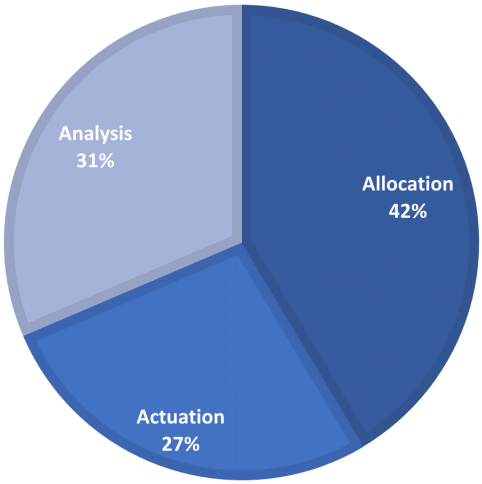

Figure 3.8. Breakdown of topic of yaw control publications (1953-2021). Literature is classified as either analysis of existing systems (Analysis), development of novel actuation techniques (Actuation) and development of control allocation algorithms (Allocation).

The remaining 31% of publications is devoted to the analysis of existing yaw control systems and their effect on the vehicle dynamics. The majority of these studies are concerned with analysis of the roll-yaw coupling during manoeuvre [56], [57] and the effects of damaged yaw dampers [58]–[61]. The former is of most interest to tailless aircraft and is addressed later in this section.

Of the publications addressing novel methods of actuating yaw control, the research can be broken down into six main groups: Lateral asymmetries in engine thrust, Forebody geometry changes, Forebody blowing, Morphing, Asymmetric control deflection, and Induced drag methods (Discussed in Section 3.3.2). The remainder of this section will address these in turn.

3.2.1 Asymmetric Thrust

The use of asymmetric thrust first appears in the literature as a method of yaw control in hover for Vertical/Short-field TakeOff and Landing (V/STOL) aircraft [62]. This used a ventral nozzle which swiveled to provide pitch control and had internal vanes to direct the flow laterally to generate a yawing moment. In forward flight the yaw control was provided by a conventional rudder mounted to a fin with the thrust vectored where there was insufficient dynamic pressure for these controls to be effective.

Asymmetric thrust has also been used on a multi-engine and over actuated tailless aircraft in order to reduce the required control deflections for a yawing moment [63]. In this work, the aircraft made use of SDRs and rudders positioned in the wiglets for yaw control in the short term. This is because the response time for the engine is far to slow to respond to pilot input or disturbances. An example case of a rudder step input is shown where over a period of 50

seconds the conventional controls are driven to zero deflection whilst the yawing moment and net thrust is maintained, thereby reducing the trim drag. This work shows that it is possible to trim out steady-state yawing moment requirements (i.e. drag from asymmetric stores or a crosswind), however for yaw control of the aircraft (i.e. response to gusts) the response times are too long to provide effective control.

3.2.2 Forebody Geometry Changes

The use of forebody strakes and porous nose cones was investigated in the NASA Langley 12 foot low-speed wind tunnel as part of the Boeing multirole fighter programme [64]. The configurations investigated are shown in Fig. 3.9 and comprise two forebody strakes and a nosecone of variable porosity. The aircraft tested in this work does have a conventional fin and rudder for yaw control. However, at the high angles of attack ($\alpha > 20^{\circ}$) which can be achieved by this aircraft, the fin is positioned in the low energy wake of the fuselage and therefore its effectiveness is reduced. This, coupled with the increased yaw requirements to manoeuvre at high angles of attack lead to the motivation of using the forebody, which is in much higher energy flow, to generate yawing moments.

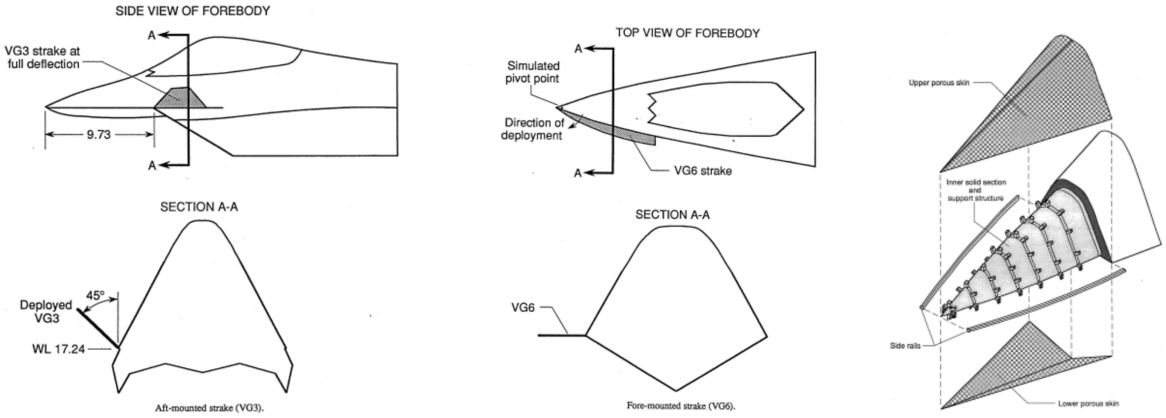

Figure 3.9. Forebody strakes and nose cone investigated [64].

The configurations shown in Fig. 3.9 generate a yawing moment by promoting an asymmetry in the leading edge vortices developed at high angles of attack. These vortices have a large impact on the drag of the aircraft therefore an asymmetric development leads to an asymmetry in drag and therefore a yawing moment. As a solution to yaw control at high angles of attack ($< 45^{\circ}$), this method is particularly effective due to the strength of the leading edge vortecies. However, as shown in Fig. 3.10 the rudder effectiveness begins to diminish at an angle of attack of approximately 30° leading to a region of reduced yaw authority between 30° and 45° angle of attack. This has the potential to limit the envelope of the aircraft.

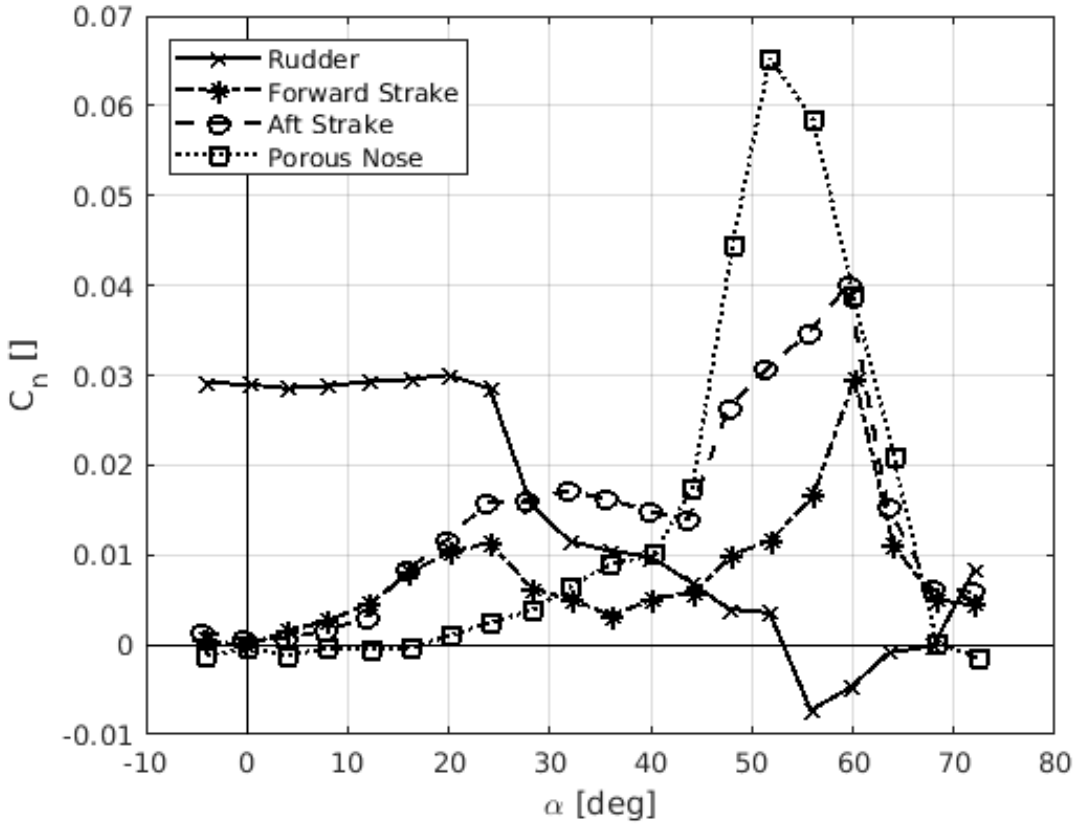

Figure 3.10. Yawing moments generated from forebody geometry changes compared to a 30° rudder deflection [64].

3.2.3 Forebody Blowing

Wood and Roberts [65] took the concept of control of the Leading Edge Vortex (LEV) and applied a flow control solution to effect their development, Fig. 3.11. Whilst the original goal of this study was to use the LEV to augment the lift on the aircraft, it was found that an asymmetry in these could be used to generate rolling moments. This methodology was later extended to forebody blowing to generate the same effect as the strakes discussed previously but without the need for external moving parts [66]–[69]. These studies show the effectiveness of forebody blowing for high angles of attack. However, they still show the same drawback as using strakes in that there will be an intermediate region where neither the rudder nor blowing is effective for yaw control. Additionally, this method does show a weak coupling with both roll and pitch meaning that pure yaw control cannot be effected by pure blowing and would require input in other axes to mitigate this coupling.

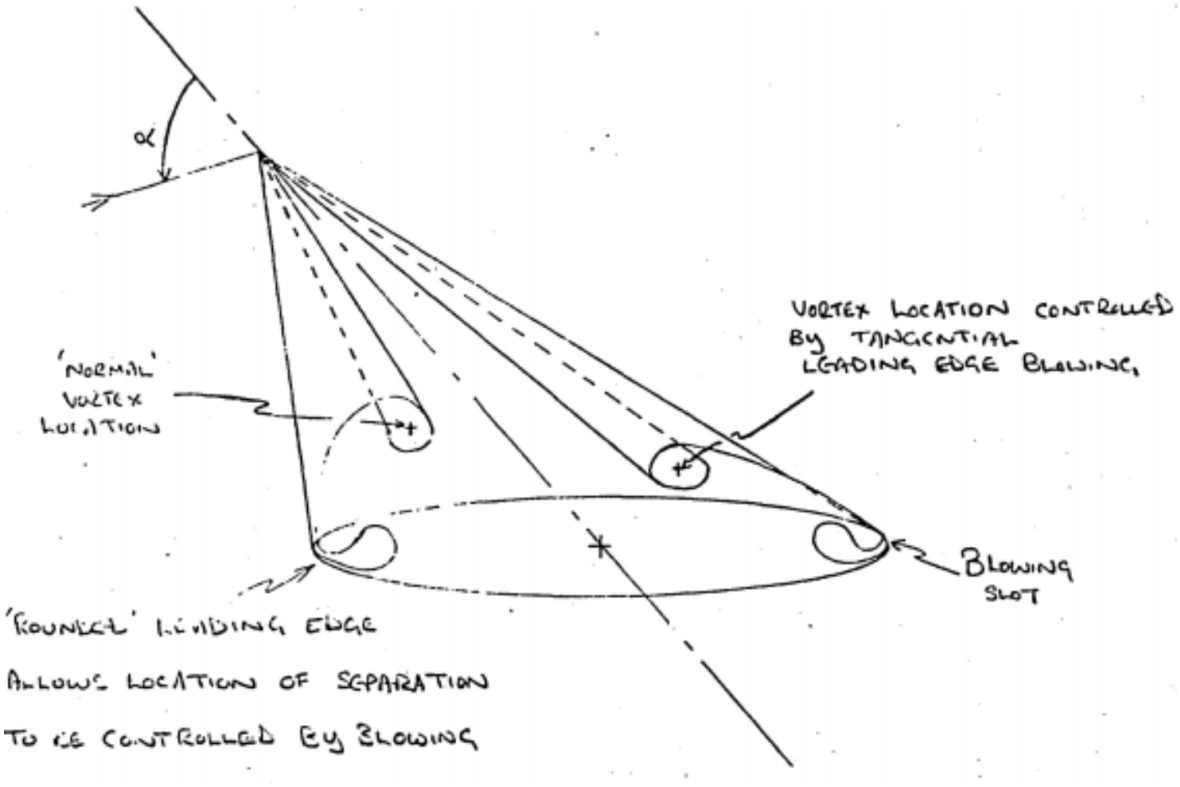

Figure 3.11. Flow control setup used by Wood and Roberts [65], the formation of leading edge vorticies was controlled by injecting momentum from slots at the leading edge of the wing.

3.2.4 Morphing

Morphing wings have been proposed in order to generate yawing moments by inducing asymmetric drag [70]–[72]. Much of the inspiration comes for this approach comes from the flight of birds, who can generate yawing moments through twisting their wings and/or tail. This approach can be highly effective in generating yawing moments. However, the practical implementation is difficult as many of these approaches use piezoelectric actuators which require complex, and often heavy [73], electrical systems to achieve small displacements [74].

Keidel et al. [71] proposed a method of morphing using compliant ribs which could be actuated with a standard electrical servo. This was investigated using a coupled aerodynamic and structural model to calculate the control inputs required for coordinated 3-axis manoeuvres. The analysis performed by Keidel et al. show the potential to not just mitigate the effect of adverse yaw, but also to control yaw throughout a rolling manoeuvre. This is shown in the lateral attainable moment subspace in Fig. 3.12. The potential is shown to achieve full lateral control up to a rolling moment coefficient of 0.35, after this point the adverse yaw becomes too strong to overcome and the yaw effectiveness begins to decrease. Nevertheless, this demonstrates a large control envelope over which a tailless aircraft can be operated with only changes in the camber distribution of the wing.

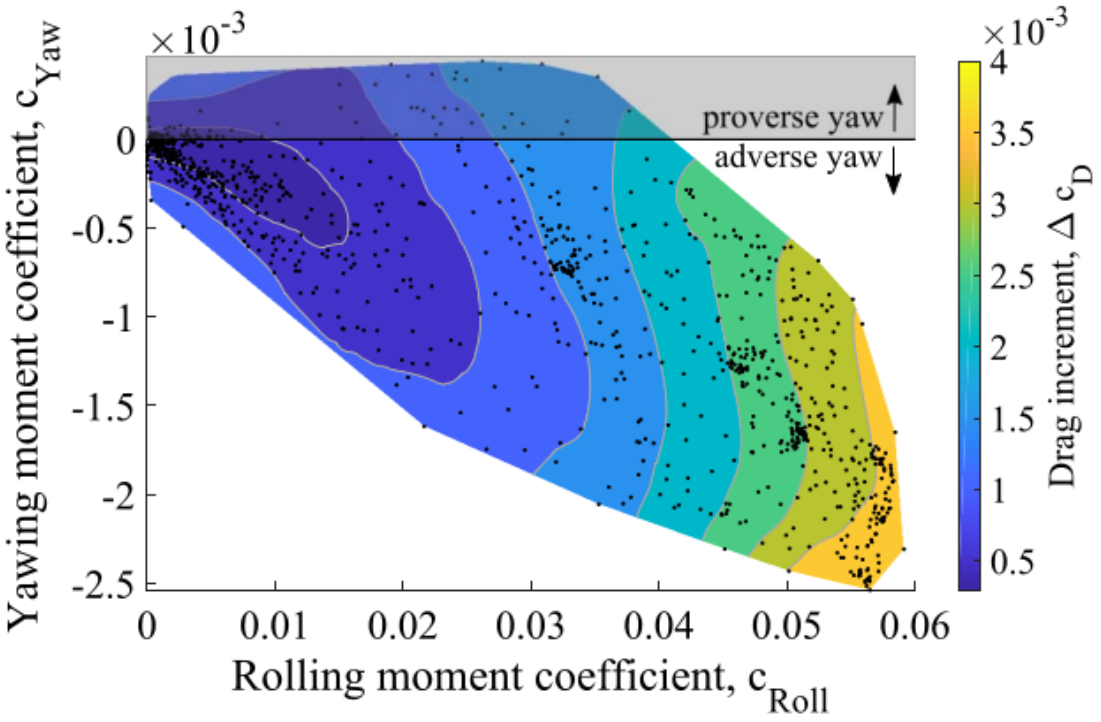

Figure 3.12. Lateral control envelope for the morphing wing defined by Keidel et al. [71].

3.2.5 Asymmetric Control Deflection

Laterally asymmetric control was proposed by Stenfelt and Ringertz in 2009 [75]–[77]. This consisted of deflecting the control surfaces on one wing only in opposing directions but with equal magnitude, shown in Fig. 3.13. The idea here being that the control deflections work as a distributed SDR, increasing the profile drag on one side of the aircraft. However, by using conventional control surfaces there is also an additional drag component from induced drag as the spanwise lift distribution will also be made asymmetric by the control surface deflection.

Figure 3.13. Wind tunnel model setup from Stenfelt and Ringertz [75].

The additional component of yawing moment can be seen in the asymmetry of the yawing

moment produced against deflection shown in Fig. 3.14. If the only source of the yawing moment generated by deflecting the control surfaces in this way was profile drag then these curves would be symmetric as the area presented to the flow would be equal in both cases. The asymmetry therefore represents this additional induced drag component.

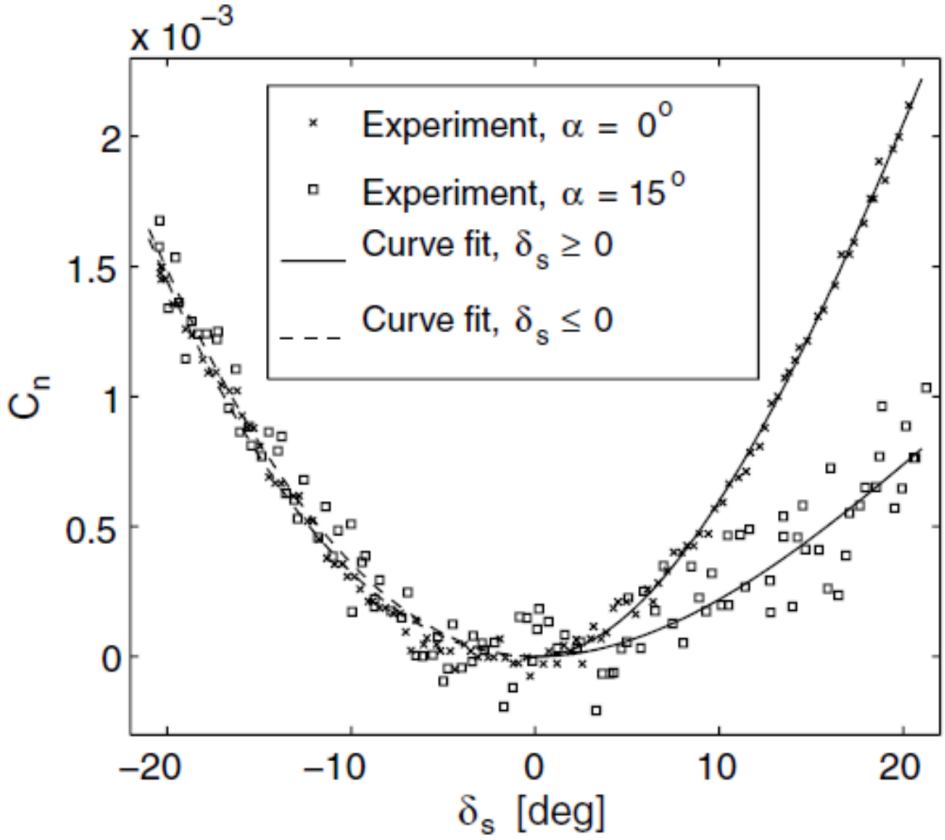

Figure 3.14. Yawing moment produced against deflection from Stenfelt and Ringertz [75]. A positive deflection is defined by deflecting the outer control surface trailing edge up and the inner control surface trailing edge down.

It is worth noting that the mechanism responsible for the induced drag in this yawing moment must come from a change in sectional lift due to the control surface deflection. We would also expect that a change in lift offset from the aircraft center line on a swept wing would create both a pitching and rolling moment. Stenfelt and Ringertz [75] argue that because the control surfaces are positioned next to each other and deflected equal magnitudes the associated rolling and pitching moments are likely to be small. This argument however has two flaws:

Firstly whilst the control surfaces are positioned adjacent to one another and cover the same spanwise extent, the taper of the wing means that the wing area influenced by each control surface is different. Therefore, the change in lift on the outer control surface will likely be less than the inner potentially leading to some degree of coupling.

Secondly, even if the coupling is weak this will still cause a perturbation in the aircraft's attitude. This perturbations would need to be corrected by adding an additional components of

symmetric and/or anti-symmetric control deflections in addition to the asymmetric deflections. Whilst on the face of it this may seem insignificant, the change in sectional lift induced by these deflections will change both the profile and induced drag contributions due to the yawing moment. Therefore, particularly for finless aircraft, it is very difficult to isolate the control effectiveness in yaw for this actuation method.

3.3 Low Order Aerodynamic Modelling

3.3.1 A Brief History

When discussing low order aerodynamic models, most peoples minds will jump immediately to Prandtl's Lifting Line Theory (LLT), developed independently by Lanchester in 1907 [78] and Prandtl in 1918 [79]. However the early developments of both authors theorised only the distribution of circulation along the span of the wing, as discussed in Section 2.1.3. The challenge of solving the circulation distribution to find the lift distribution was attempted by many of Prandtl's students. Betz first proposed a solution by assuming that the circulation distribution was elliptical, reducing the solution to finding only the peak value of circulation at the aircraft centerline [15]. This was later found to be an important reference distribution as the elliptical load leads to uniform downwash and therefore the minimum induced drag. Multhopp also proposed a solution based on gaussian quaderature [14]. By using this method the downwash could be obtained directly from a known circulation distribution, however the solution was restricted to unswept and planar wings. The popular solution used today was proposed by Glauert and involves approximating the circulation distribution as a Fourier sine series [13]. By imposing appropriate boundary conditions on the wing the Fourier coefficients can be obtained, thereby defining the circulation distribution.

There are many more low order models of varying complexity used extensively in early design studies [80]–[82]. The key developments of these models are summarised in Fig. 3.15 and will be discussed in detail through the remainder of this section. At this point, it is worth noting that as time has gone on the complexity of the low-order models has increased with the available computational power until the release of commercial CFD in 1981. However, the lower order models developed over the 80 years prior to this still find applications in early design studies [83], [84] and some flight simulation applications [85]–[87].

Following on from lifting line, Falkner proposed a method for the calculation of aerodynamic forces and moments by dividing a lifting surface into a series of trapezoidal panels in 1943 [88]. By placing a vortex line at the quater chord point, and a control point at the three quarter chord point at which the boundary conditions were applied (Known as the $\frac{1}{4}$–$\frac{3}{4}$ rule [89]) the circulation in each of the panels could be calculated. This is now known as the Vortex

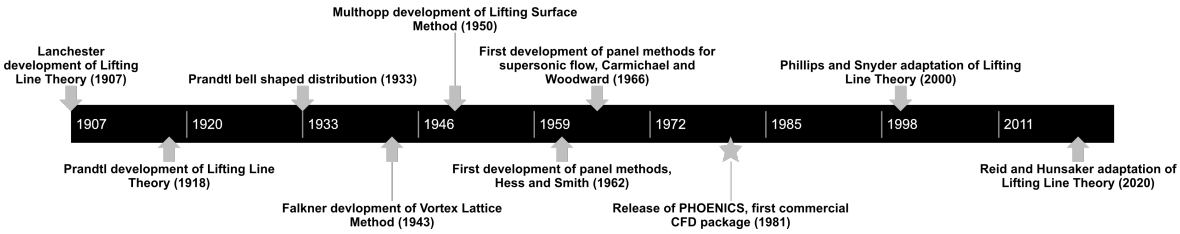

Figure 3.15. Key developments in Aerodynamic Low Order Models.

Lattice Method (VLM) This formulation allowed the calculation of wings with lower aspect ratio than the classical lifting line formulation as well as swept wings and wings in sideslip. For the interested reader, an excellent summary of the early development of the vortex lattice method is presented by DeYoung [90]. Over the years, VLM has been extended to allow for the calculation of supersonic flows in 1977 [91]. It still holds a valuable place in optimisation and design studies, conducted using open source codes such as Tornado[2] [92]–[94] and XFLR5[3] [95]–[97].

In 1950, one of Prandtl's students Multhopp proposed a Lifting Surface (LS) method in which rather than using concentrated vortex lines, the vorticity was distributed on the lifting surface and integrated in a continuous way [16]. VLM stands at a half-way step between the continuous lifting surface and LLT. Multhopp himself remarked that: *"[Falkner's] vortex lattice is not meant as a simplifying model of the actual wing but should be regarded as a rather crude method of approximate integration"* [16]. The derivation of LS is mathematically much more complex than VLM. However, the result is that LS requires far fewer control points and strips than VLM. This leads to a much simpler calculation. LS calculations require a number of control points at least three times the aspect ratio meaning that for most applications, the calculation could be performed by hand. This would be prohibitively time consuming for VLM. The applicability of LS is much the same as VLM with the ability to model swept and low aspect ratio wings. Wings in sideslip can also be modelled although the application is slightly less intuitive than in VLM. Despite its elegance, Multhopp's lifting surface does not find itself included in any commercial or open source codes to the authors knowledge.

In 1962, Hess and Smith proposed a panel method based on the superposition of potential flows [98]. The method works by distributing source and doublet panels over the surface of a body. The source panels allow a no-flow condition to be imposed on the boundary of the geometry, modelling the thickness effects, and the doublet panels impose the kutta condition, imposing the effect of circulation and therefore lift. In this way, an entire aircraft configuration can be modelled including the non-lifing surfaces such as the fuselage. Panel methods have been included in this section as they solve an aerodynamic problem using a direct analytical solution (rather than numerical solutions to the fundamental equations such

[2]http://tornado.redhammer.se/
[3]http://www.xflr5.tech/

as RANS), however it is worth noting that the computational cost of these solutions is greater than the vortex methods discussed so far in this section. Nevertheless, panel methods now play an important role in early design and optimisation studies and are the main workhorse of open source solvers such as XFLR5 [97], [99], [100]. For the interested reader, a summary of the development of panel methods and summary of the underlying theory was performed by Erickson [101].

Following the introduction of commercial CFD in 1981, much of the research effort has been concentrated on improving the fidelity of these higher order models. The models discussed so far in this section are still used in the literature, however as previously discussed are primarly used in early studies. However, there are two recent significant developments which are worthy of inclusion within this section. The first is the lifting line adaptation of Phillips and Snyder (2000) [102]. Their modification replaces the Kutta–Joukowski theorem with the more general three-dimensional vortex lifting law [12]. In doing this, the solution can no longer be analytically obtained, however the numerical scheme does converge quickly.

As shown in Appendix B, the Phillips and Snyder version of LLT agrees well with experimental data and classical LLT for straight wings. For swept wings it also calculates the net lift on the wing in good agreement with experimental data. However, in calculating the lift distribution it can be seen that this method severely over predicts the lift at the wingtips and under predicts the center line lift. This distortion of the lift distribution means that the induced drag is also over predicted by this method. As shown by Reid [103], the method of Phillips and Snyder also fails to grid converge for swept wings or wings in sideslip.

Building on the work of Phillips & Snyder [102], Reid [103] and Goats & Hunsaker [104] proposed a numerical lifting line in which the trailing vortex segment is replaced by a jointed segment perpendicular to the lifting line which then turns to a standard trailing segment some distance downstream. By formulating the problem in this way, the solution becomes grid convergent. This method still somewhat under predicts the lift at the centerline and over predicts the wing tips, however the agreement with experimental data is significantly improved compared to Phillips & Snyder [102]. From the data presented by Goats & Hunsaker [104], this method appears to under predict the drag compared to experiments [105]. However, the lifting line data does not include viscous effects so it is difficult to draw comparison with experimental data.

3.3.2 Implications for Tailless Aircraft

Despite the advances in low order methods, much of the analysis of tailless aircraft is performed using higher fidelity CFD methods [106]–[111]. However, much of the understanding of the effects of adverse yaw on the aircraft performance can be drawn from low order aerodynamic

analysis. As early as 1983, Nickel [112] used LLT to study aileron configurations which could eliminate adverse yaw and minimise the total drag produced. In this work he noted that for most aircraft configurations, adverse yaw is more of a nuisance than a problem as it can be mitigated by the pilot using the rudder. However, there are two configurations which are susceptible to problems with adverse yaw: Tailless aircraft, with reduced directional stability and no rudder to counteract with; and, High efficiency sailplanes which experience a large magnitude of adverse yaw due to their large wingspan. Here we will focus on the former, although the findings can be applied equally to both.

To calculate a lift distribution which produces a given Lift, Rolling Moment and Yawing moment, Nickel [112] assumed that the anti symmetric part of the lift distribution would be a half leminscale. The lift distribution is then described by a Fourier series neglecting the Fourier coefficients higher than a_6 and assuming $a_3 = 0$. This leads to a unique solution in which a given lift and rolling moment can be achieved with no yawing moment at the minimum induced drag.

Whilst Nickel's report does provide an elegant solution for alleviating adverse yaw, it does not provide a full control solution for tailless aircraft. The first reason for this is that the analysis does not consider the pitching moment; on tailless aircraft, the control is generally only provided by a system of trailing edge surfaces for both lateral and longitudinal control. Changing the problem to include a specified pitching moment would introduce an additional constraint into the formulation which would substantially increase the complexity.

Secondly, the output from Nickel's analysis is an optimal lift distribution. It is then left to a designer to achieve this lift distribution through a combination of planform shape, twist, camber and control surface deflection. For a tailless aircraft the planform shape is often fixed through other design pressures, leaving only twist, camber and control surface deflection. Manipulating these three factors such that the desired lift distribution can be achieved across a range of desired rolling moments is a challenge for any aircraft due to the large parameter space. Furthermore as an aircraft initiates a rolling manoeuvre, there will also be a contribution to the lift distribution from an asymmetry in angle of attack due to roll rate. Therefore either one or a combination of these factors would need to change through the manoeuvre to ensure the yawing moment is zero throughout. There is also an additional complication if conventional trailing edge control surfaces are used to modify the lift distribution, as there will be a component of profile drag introduced. This is not accounted for in Nickel's formulation and would lead to a non-zero yawing moment.

Finally, as presented Nickel's formulation presents a method to alleviate the adverse yaw due to induced drag. However aircraft which are both finless and tailless are typically at best marginally directionally stable and, particularly at low angles of attack, can become directionally unstable [54]. Therefore simply alleviating the impact of adverse yaw is not

enough to prevent the aircraft departing from controlled flight. Nickel's formulation could be easily adapted to generate the lift distribution for a specified non-zero yawing moment. However, this would be difficult to implement practically without also including the effects of profile drag and pitching moment.

Hunsaker et al. [113] through a method similar to Nickel's proposed a method of including the effects of roll rate in 2020. Their method involved using a decomposed Fourier series to include the contribution of angle of attack, twist, rolling rate and planform separately. In doing this, they define a class of optimal lift distributions for a given yaw control ratio which they define as $R_{n/l} = \frac{C_{n,\delta}/C_L}{C_l}$. By formulating the problem in this way they are able to include the asymmetry in lift induced during a steady roll within their analysis. However, the other limitations discussed of Nickel's work are still present.

Richter et al. [114] performed a parametric study of aircraft with bell shaped lift distributions, analysed using VLM modified to include viscous effects [115]. They found that placing an aileron in the upwash region created by the bell shaped distribution resulted in a favourable yawing moment when a roll is induced. This effect was exploited by increasing the wingspan to increase the yawing moment produced and increasing the washout to increase the upwash. A 10% increase in both resulted in an increase of the proverse yawing moment by 16 times. This result demonstrates the non-linear behaviours of induced drag and therefore adverse yaw which can be captured by these low-order models. Like the investigations using lifting line, this study was restricted to the lateral response of the aircraft only. It is likely that such a change in span and twist would have a large impact on the pitching moment of the aircraft, particularly for swept wings.

Aside from the analysis of adverse yaw, low order modeling techniques have also been used for the calculation of stability and control characteristics of aircraft. In 1992, Morris [116] proposed a method for simultaneous planform and control feedback design using VLM. By using this approach, part of the design process can be automated to generate a control configuration which achieves a specified level of handling qualities for the minimum trim drag. Source doublet panel methods have also been used alongside higher fidelity CFD methods for the calculation of stability derivatives of highly swept tailless aircraft [117]. For lower angles of attack the panel method shows a similar accuracy to the RANS methods, however at higher angles of attack non-linear effects such as vortex flow from the leading edge not captured by the panel method means they become less applicable. Nevertheless for low angle of attack analysis and early design studies the low order methods can provide a significant speed up in the analysis with little accuracy penalty.

3.4 Summary

Low-order aerodynamic methods have been use for the analysis of aircraft since the early 1900's. Although the early methods such as LLT are not suitable for the analysis of low aspect ratio swept wings the surface methods such as those described by Falkner and Multhopp provide a fast and suitably accurate method for the calculation of aerodynamic forces and derivatives on these planforms. In more recent years, higher fidelity CFD has provided a greater level of accuracy in calculating forces and moments on these challenging aircraft. However, for work in establishing the effectiveness of control surfaces the lower order models provide sufficient accuracy in much reduced time frames compared to CFD. Therefore, where appropriate the lifting surface methods will be used to determine control effectiveness throughout this work.

Tailless aircraft have been considered as potential configurations in design studies since before the first powered flight. However, their challenging stability and control characteristics meant that until the 1990s they were generally not chosen for production aircraft except where there was a strong aerodynamic case to do so. However, as the focus on military jet aircraft began to shift towards stealth characteristics the interest in swept tailless aircraft increased. This lead to an increase in research on these planforms, mainly focusing on the stability and control systems to mitigate the challenges presented by the complex aerodynamics. Generally, these challenges were overcome with increasingly complex control algorithms on overactuated aircraft. There has been little research on novel methods for providing this control power.

The literature surrounding generating yawing moments for tailless aircraft is primarily focused on high angle of attack. This is because at these higher angles of attack the fin effectiveness is greatly diminished and there is therefore a need for yaw control on all tailless planforms. Whilst the methods for manipulating LEVs at high angles of attack shows a high effectiveness, there is very little effect in the normal operating range of the aircraft. This being said, there has been very little research on identifying a suitable aerodynamic effect to exploit for the generation of yawing moments at low angles of attack by AFC methods. A more promising methodology for operating at low angles of attack is in generating an asymmetry in the induced drag on the aircraft by morphing or asymmetric control surface deflection.

Chapter 4

Paper 1: Directional Control of Finless Flying Wing Vehicles - An Assessment of Opportunities for Fluidic Actuation

Summary

This chapter was presented as a conference paper of the same name at the 2019 Aviation Forum[1]. It represents the start of the investigation into the feasibility of providing directional control by use of fluidic actuation. The contributions of each author are detailed in Table 4.1.

The paper takes an control effector agnostic approach to identify areas on the aircraft which contribute greatest to the yawing moment, then considering what the change in surface pressure would need to be across these to generate a required moment. To allow practical implementation of these changes in pressure, the analysis also considers how these changes in yawing moment affect the rolling moment. However, this analysis is not extended to include pitching effects. The required change in surface pressure is considered as both a function of a relative change compared to a symmetric loading due to lift and as a change in the magnitude of the pressure only.

It was found that in order to achieve a practically useful control authority in yaw, the changes in surface pressure would need to be large across multiple areas of the planform to ensure that there was no secondary effect in the rolling moment. These changes in surface pressure are sufficiently large that the required momentum input with current actuator effectiveness would be too large to find practical use. This finding provides the impetus for the induced drag approach discussed in the following chapters.

[1]From "Directional control of finless flying wing vehicles –- an assessment of opportunities for fluidic actuation" T.R.Shearwood, M.R.Nabawy, W.J.Crowther, and C.Warsop ; reprinted by permission of the American Institute of Aeronautics and Astronautics, Inc.

Task	TRS	MRAN	WJC	CW
Funding Acquisition		x	x	x
Supervision		x	x	x
Project Administration		x	x	x
Conceptualisation	x	x	x	x
Methodology	x	x	x	x
Formal Analysis	x			
Investigation	x			
Software	x	x		
Validation	x			
Visualisation	x			
Writing - original draft	x			
Writing - review and editing		x	x	x

Table 4.1. Contributor Roles Taxonomy for Chapter 4

Abstract: *This paper proposes a method for the evaluation of potential solutions for fluidic actuators to impart directional control moments. The method developed allows the requirements for the actuator of a flying wing vehicle with or without fins to be derived. This allows the calculation of the required changes in surface pressure on the aircraft to achieve the required levels of control. The research allows the suitability of proposed flow control solutions to be assessed early in the design process and provides a method of assessing their suitability against other flow control solutions.*

4.1 Introduction

Signature and aerodynamic performance requirements for low observable aircraft drive designs towards moderately swept all flying wing configurations without separate aerodynamic surfaces for longitudinal or lateral control [5], [118], [119]. The equivalent function of a horizontal tail can be attained on a tailless aircraft through camber control of the wing (elevons etc). Whilst the performance cost of achieving a given amount of control authority from a separate tailplane is less than for an integrated wing solution, the overall design benefit is clear for many mission applications.

Removal of directional stabilizing surfaces (fins) is however much more challenging. Fins provide lifting surface area projected in the longitudinal plane of the aircraft. The change in lift due to sideslip on these surfaces generate yawing moments contributing to trim and stability. For configurations without fins, the usual solution is to generate yawing moments using drag devices toward the wing tips [120]. These devices produce yaw by inducing laterally asymmetric drag on the airframe. Whilst they can achieve high effectiveness (large magnitude of yawing moment), there is usually significant cross coupling with both pitch and roll [121] which means that it may be difficult to exploit the available yawing moment without

significant deflection of other trailing edge surface controls to counteract the undesired control components. Furthermore, these deflections greatly increase the vehicle signature [122].

Several actuation methods, both using conventional control surfaces and fluidic controls, have been proposed to control the lateral response of the aircraft without the need for fins [123]–[125], examples are shown in Fig. 4.1. These studies assess the effectiveness of a given control solution on a given vehicle platform, often stating the maximum C_n attainable for the flight conditions tested. However, it is often more useful to relate this back to a vehicle design requirement; for example, a maximum sideslip angle which can be trimmed using the solution.

A directional control effector must provide sufficient control authority to manage the aircraft throughout the expected operational envelope. Authority may be defined by static constraints such as cross wind landing or coordinated turning flight, or dynamic constraints in terms of yaw rate requirements for stability augmentation. The method of analysis developed in this paper is agnostic to the method of the actuation; it identifies the areas of the geometry over which a change in the surface pressure is desirable. These data can then be interpreted to explore the potential for exploiting an aerodynamic effect to provide the required change in surface pressure.

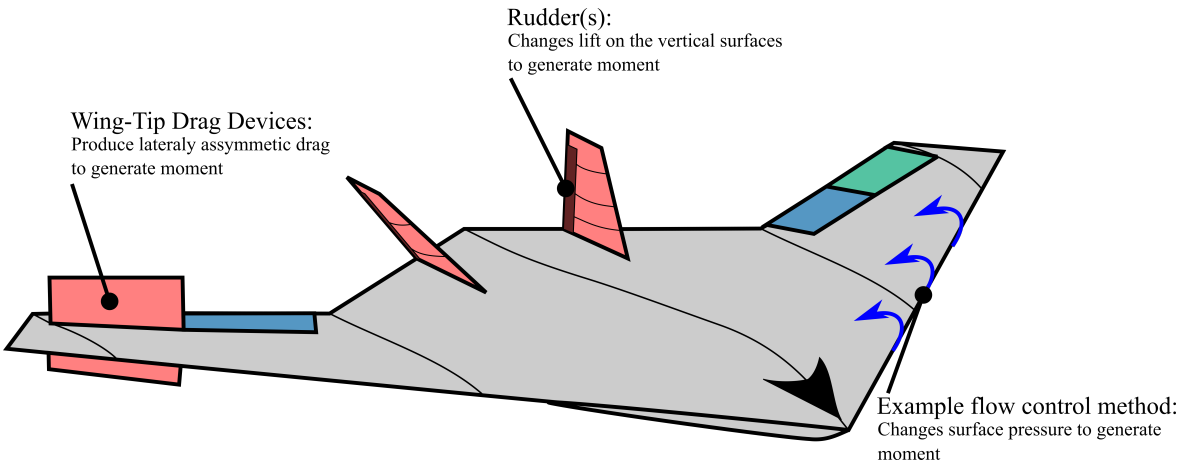

Figure 4.1. Illustration of geometric and fluidic methods for producing a yawing moment on a flying wing aircraft. Flow control methods by definition do not change the geometry of the aircraft.

In order to provide a test case for the method, it is applied to the MAGMA airframe developed at the University of Manchester, shown in Fig. 4.2. The aircraft is designed as a demonstrator for novel flight control effectors using a modified 1303 planform [5]. 16% thick sections with rounded leading edges were used in the design to improve the stability, therefore the aircraft does not possess the negative stability effects of the leading edge vortex but does provide a representative platform to examine the lateral stability of moderately swept planforms.

The method developed herein will be applied to this aircraft as a case study to assess the opportunities for fluidic directional control in the absence of a fin. Whilst the results presented

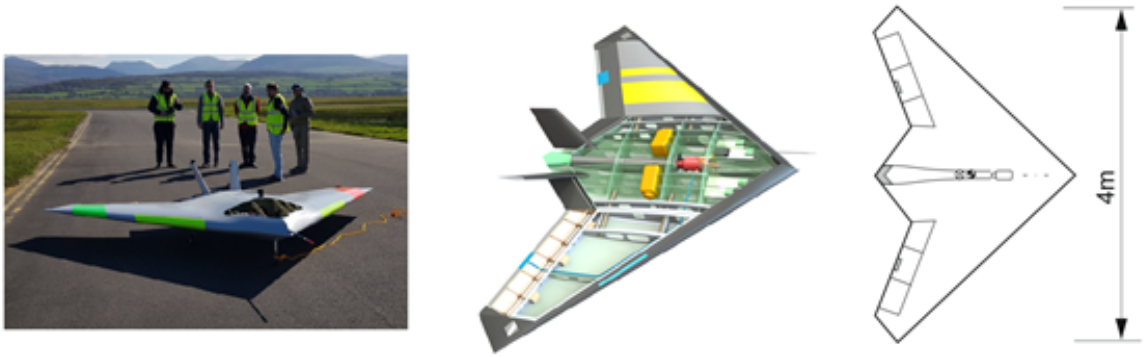

Figure 4.2. MAGMA planform. Flow control effectors comprise: Circulation control units in the central elevon and Fluidic Thrust Vectoring on the exhaust.

will be specific to this geometry the method may be applied to any flying wing geometry, with or without fins.

4.2 Theory

Throughout this paper, the forces and moments will be referred to in the standard aerodynamic body axes system summarised in Fig. 4.3. This is well defined within the literature, however it is felt that the planes through the aircraft are less well defined. Therefore, for clarity of discussion the planes are defined herein as: XZ – Longitudinal, XY – Lateral and YZ – Vertical.

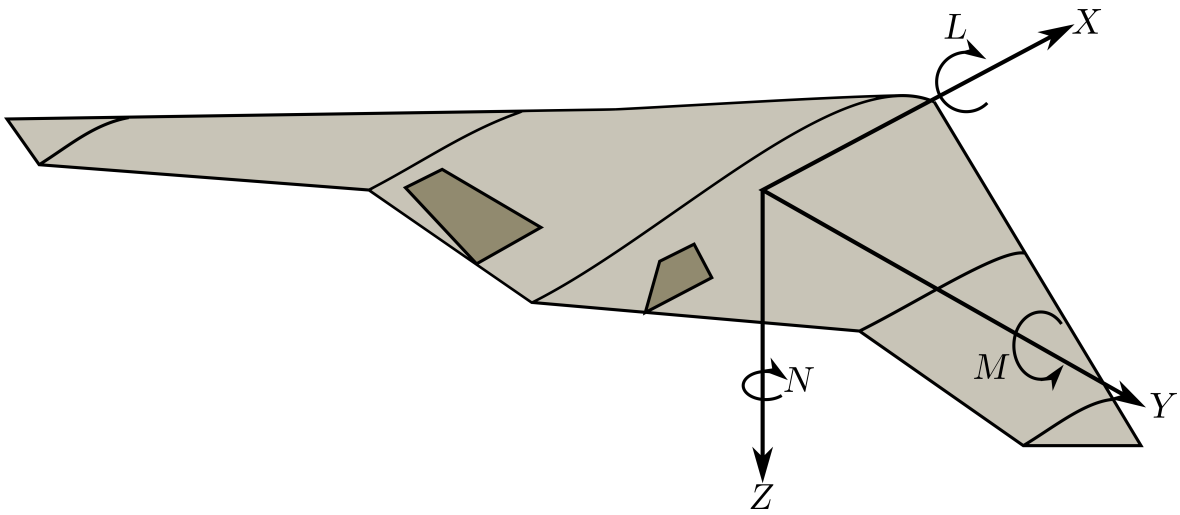

Figure 4.3. Conventional axes system and sense of rotations.

Commonly within the literature the longitudinal set of equations includes: X force and velocity; Z force and velocity; and moments about Y. The lateral set comprises: Y force and velocity; moments about X; and moments about Z. As directional control is included only in the lateral set of equations, the longitudinal set is not considered throughout this work.

The common method of maintaining directional stability is to utilise a surface with a projected area in the longitudinal plane aft of the Centre of Gravity (CG), commonly referred to as fins. These surfaces generate forces in the lateral plane in response to a lateral velocity, which cause the aircraft to yaw into the disturbance. Additionally, these surfaces create a force and therefore a moment which acts against the direction of yaw rate, referred to as yaw damping.

If the fins are removed and replaced with drag devices, the projected area of the surface is now in the vertical plane and therefore must generate drag forces to create a yawing moment. However, when closed these drag devices do not produce yaw damping.

In the absence of a fin, the lateral response of a flying wing vehicle in response to sideslip becomes strongly a function of the angle of attack [54]. This is because when the aircraft is in sideslip the effective sweep of one wing is reduced whilst the other is increased, leading to an increase in lift on wing slipping into the flow and a decrease on the opposite wing. This has two effects; the asymmetry in lift generates a restoring rolling moment away from the disturbance and also an asymmetry in induced drag, producing a yawing moment which acts to yaw the aircraft into the oncoming flow.

In the presence of a fin, the induced drag contribution to yaw is generally negligible, however on a pure flying wing planform this is the dominant contribution to the yaw response to sideslip. The other contributing factor to the yaw response is the product of the aircraft's projected area in the longitudinal plane and the longitudinal distance of each elemental area from the CG. As the aircraft's directional stability is improved by increasing the area aft of the CG, the directional stability of the aircraft is improved with increasing static margin.

As both the yaw and roll response to sideslip are functions of the change in lift, the lateral stability of the aircraft is also a function of the lift coefficient. This leads to three regions of stability throughout the angle of attack range: At low angles of attack there is a reduced roll and yaw response to sideslip and therefore potential for static instabilities; at moderate angles of attack the aircraft is inherently stable; and at high angles of attack there is a high level of static stability but the coupled nature of the response and the absence of damping from the fin leads to potential excitement of unstable dynamic modes.

In order to assess the stability using this method the full set of lateral aerodynamic derivatives as a function of angles of attack and the inertia matrix for the aircraft are required. In this work these are estimated using ESDU datasheets, however any desired method may be used for calculation or estimation of these. The relevant ESDU datasheets for wing and fin contributions are tabulated below. The inertia matrix is estimated by taking a calculated value for the structural inertia from a CAD package and combining with point masses for: the engine, fuel, landing gear and flight control systems.

	Wing	Fin
Y_v	79006	93007
Y_r	83026	82017
Y_p	81014	83006
L_v	80033	93007
L_r	72021	82107
L_p	06.01.01	83006
N_v	79006	93007
N_r	71017	82017
N_p	81014	83006

Table 4.2. ESDU data item numbers for lateral derivatives

4.3 Method

The method detailed within this section describes how from the aerodynamic derivatives, the requirements in terms of the authority required in yaw for an actuator can be derived. Unless otherwise stated, the derivatives used within this section are the aero-normalised derivatives with wingspan as the reference length.

4.3.1 Assessment of Lateral Static Stability

To assess the limits of static stability at low angles of attack once the fins are removed, one inspects the value of L_v and N_v as a function of angle of attack. The aircraft is stable where the value of $L_v < 0$ and $N_v > 0$, therefore the point at which both of these conditions are met defines the edge of the region which the aircraft will be statically unstable. It is more likely that the aircraft will be more unstable directionally than in roll with the fins removed, therefore if the aircraft is unstable the degree of instability can be assessed using the most positive root from Eq. (4.1) for the most directionally unstable Angle of Attack of interest, in Eq. (4.2). This gives the time to double amplitude from an initial disturbance in sideslip angle. This time period gives an indication of the order of magnitude of bandwidth which the actuator is required to act.

$$\lambda_{1,2} = \frac{(Y_v I_{zz} + mN_r) \pm \sqrt{(U_v I_{zz} + mN_r)^2 - 4mI_{zz}(Y_v N_r - N_v Y_r)}}{2mI_{zz}} \tag{4.1}$$

$$t_2 = \frac{\tau \ln(2)}{\lambda} \tag{4.2}$$

4.3.2 Assessment of Requirements to Trim in Sideslip

With the derivative N_v established, the yawing moment to trim at a given sideslip angle can be established by multiplying the derivative by the normalised sideslip velocity ($v = \sin(\beta)$). Ref. [126] recommends a crosswind component at landing not exceeding 25kts ($12.9m/s$), therefore the maximum required sideslip angle would be:

$$\beta = \arctan\left(\frac{12.9}{\sqrt{\frac{mg}{0.5\rho S C_{L}(\alpha)}}}\right) \tag{4.3}$$

4.3.3 Assessment of Banked Turn Requirements

Ref. [127] states that for a class II aircraft (i.e. tactical reconnaissance) must be able to complete a coordinated banked turn of up to 60° bank angle during normal flight conditions. To assess the yawing moment required to achieve this in steady state, the linearised equations of motion were simplified for a coordinated turn (i.e. zero sideslip and zero angular acceleration) Eq. (4.4).

$$C_n = -N_r \omega \tau \cos(\theta)\cos(\phi) \tag{4.4}$$

where omega is the turn rate given by:

$$\omega = \frac{mg\tan(\phi)}{mV_{\infty} - Y_r \cos(\theta)\cos^2(\phi)} \tag{4.5}$$

However, it would also be reasonable to expect that the effector would allow a coordinated turn during the banking manoeuvre. The yaw response required then becomes a function of the roll rate, the roll angle and the aircraft's moment of inertia about the z-axis given by Eq. (4.6).

$$C_n = I_{zz}\dot{r} - N_r r - N_p \dot{\phi}\tau \tag{4.6}$$

where r and $\dot{r}$ are given by:

$$r = \omega \tau \cos(\theta)\cos(\phi) \tag{4.7}$$

$$\dot{r} = \cos(\theta)\left(\frac{\partial \omega}{\partial \phi} - \omega \sin\phi\right)\dot{\phi}\tau \tag{4.8}$$

4.3.4 Assessment of Dynamic Stability

The dynamic response of the aircraft is expected to be more severe at high angles of attack. To assess whether this response becomes unstable, the linearised equations of motion are dynamically normalised and assembled into matrix form. The method by which these equations of motion are manipulated to form the characteristic equation can be found in [17].

Calculating the roots of the characteristic equation yields the response of the dynamic modes. Of particular interest for this work are the large real root and the pair of complex roots corresponding to the spiral and Dutch roll modes respectively. The small real root, corresponding to the roll subsidence mode, is driven predominantly by the wing geometry and is therefore of little significance when removing the fin [17].

Similarly to the method of assessing static stability, the degree of damping obtained from the real part of the calculated roots is examined to find the point at which the mode becomes unstable. If the sign of the real part of the root becomes positive then the oscillations induced will grow without control input. If unstable, the minimum control bandwidth and magnitude can be assessed by taking the equations of motion in frequency space for the most unstable case. The control inputs required for a marginally stable yaw oscillation with the same time period as the unstable case using Cramer's rule can then be calculated [17].

4.3.5 Assessment of Response to Turbulence

To ensure that no additional control input is required when removing the fins a transfer function fed with white noise is used to generate a turbulence spectrum of von Karman turbulence [128]. An additional set of transfer functions is computed to convert the input from the turbulence to the aircraft response using the linearised equations of motion converted to frequency space and then using Cramer's rule [17]. The RMS values of acceleration can then be calculated by transforming the spectrum back to the time domain.

It is likely that removing the fins will reduce the aircraft's response to turbulence as the sideslip-yaw and sideslip-roll cross-coupling is reduced. If the RMS levels of acceleration are still unacceptably high, the response of the aircraft will be greatest at lower frequencies. Therefore, the maximum bandwidth required is found by the cut-off frequency of a low-pass filter which brings the RMS value of acceleration below the requirement and the magnitude

found from the peak value of $I_{zz}\dot{r}$ below the cut-off frequency. This however, may not be achievable using directional control alone.

4.4 Results

Fig. 4.4 shows the static response of the aircraft in yaw and roll to a perturbation in sideslip. As would be expected, removing the fins has little effect on the roll response. The degree of stability in yaw is significantly reduced by removing the fins and becomes unstable below an angle of attack of 1.2°. However this is a very weak instability with a time to double amplitude in the order of hours and would require a yawing moment coefficient of the order 10^{-5} to counteract.

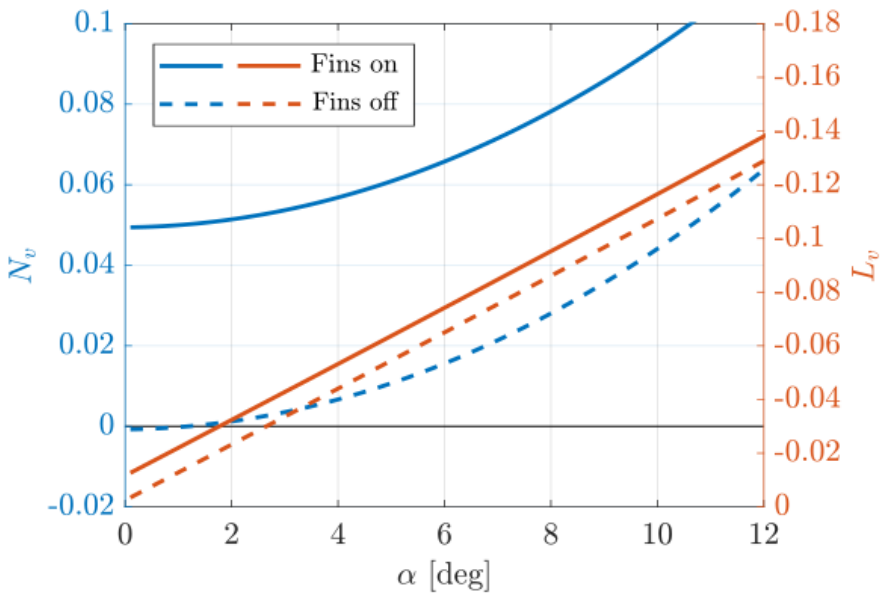

Figure 4.4. Static Lateral stability derivatives with and without fins. The limit of stability for the finless case is at 1.2° where N_v crosses 0. Note that the L_v axis is reversed (i.e. becomes increasingly negative)

The yawing moment coefficient required to trim in a 25kt crosswind is shown in Fig. 4.5 as a function of angle of attack. It can be seen that the yawing moment to trim is strongly a function of angle of attack. In the most onerous case, at $\alpha = 12^{\circ}$, the yawing moment required is reduced by 60% by removing the fins.

For a steady banked turn, the yawing moment required to maintain a coordinated turn as a function of bank angle is shown in Fig. 4.6. This is calculated for an angle of attack of 4°, however the derivatives used in this calculation are very weakly a function of angle of attack therefore this can be considered representative for the entire angle of attack range. The yawing moment required to maintain a steady banked turn is reduced when removing the fins as the

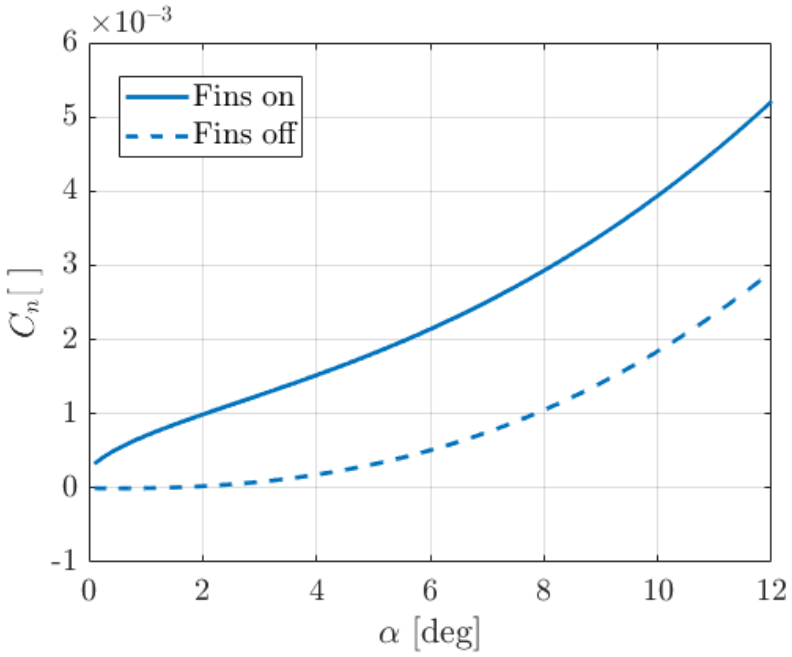

Figure 4.5. Yawing moment coefficient required to maintain trim in a 25 kt crosswind. At low angles of attack for the finless case very little input is required due to the small magnitude of the derivative N_v.

yaw damping (N_r) is reduced. This also explains why the yawing moment is such a strong function of bank angle as the body axis yaw rate is a function of the turn rate.

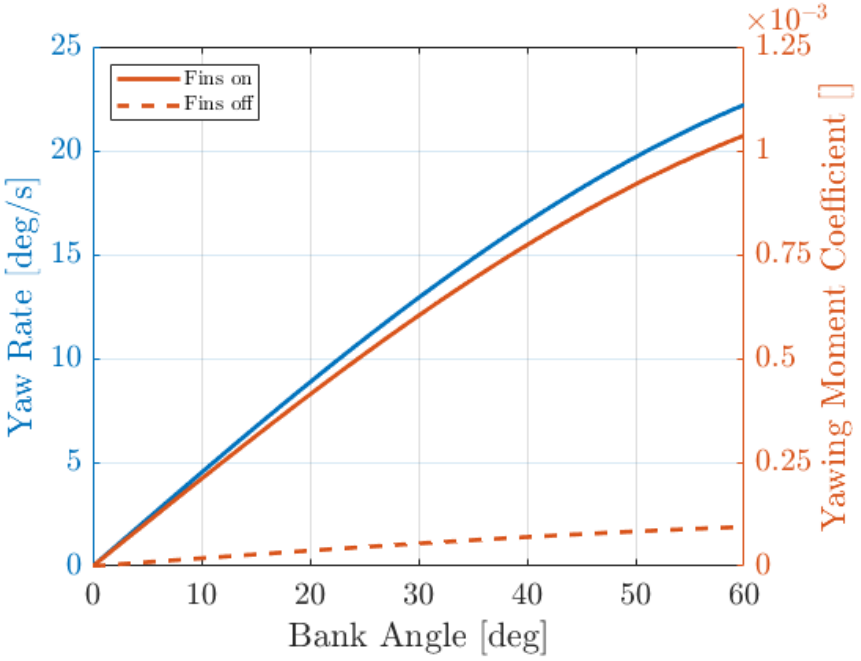

Figure 4.6. Yaw rate (left) and yawing moment coefficient (right) required with and without fins at $\alpha = 4°$ to maintain a coordinated banked turn. The yawing moment coefficient required is reduced without fins due to the reduced yaw damping.

The yawing moment required during the rolling manoeuvre to maintain a coordinated turn is shown in Fig. 4.7 as a function of bank angle and roll rate, as defined in Eq. (4.6). At the

initiation of the rolling manoeuvre the removal of fins leads to a small increase in the required yawing moment, however as the manoeuvre progresses the removal of fins again reduces the required moment. For modest roll rates of 10 deg/s the yawing moment required during the manoeuvre is approximately double the steady case.

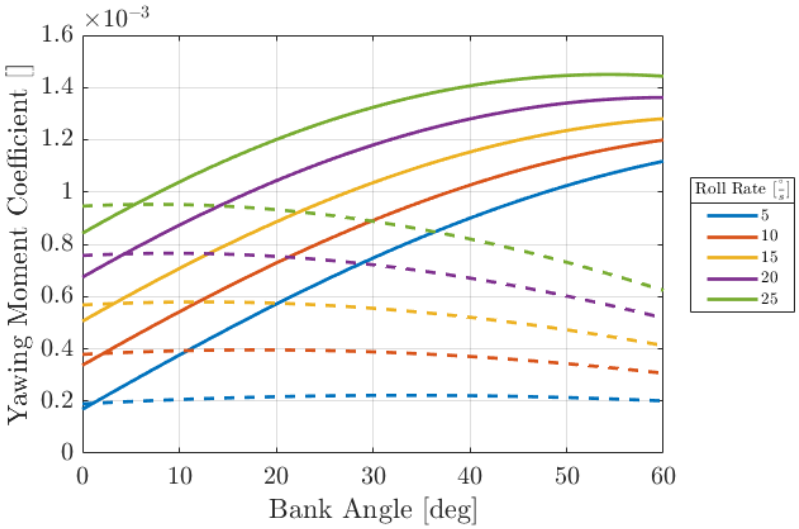

Figure 4.7. Yawing moment coefficient required to maintain a banked turn during the rolling manoeuvre. Solid lines are with fins and broken without. Removal of the fins reduces the required rolling moment due to the reduction in magnitude of the derivatives N_r and N_p.

Fig. 4.8 shows the period and damping of the Dutch roll mode. Removing the fin increases the period of the oscillation at low angles of attack with little change at higher angles. The damping with the fins removed is reduced, significantly increasing the time to half amplitude at low angles of attack and increasing the time to half amplitude at high angles of attack by approximately 30 seconds. However, in all cases this mode does not become unstable and the reduced time period means that the motion can be further reduced by pilot input.

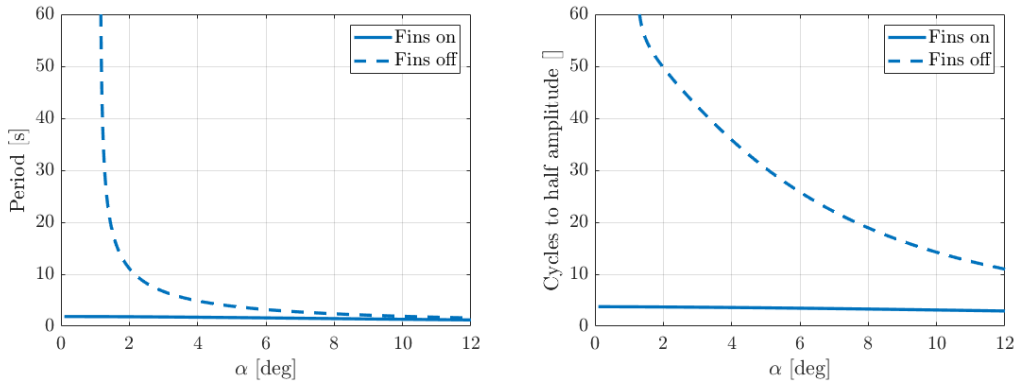

Figure 4.8. Period **(a)** and Damping **(b)** of the Dutch roll mode with and without the fins. Removing the fins significantly increases the period and reduces the damping at low angles of attack. The period tends towards that of the case with fins at higher angles of attack. At high angles of attack without fins, the damping is significantly greater than at low angles of attack but is still reduced compared to the case with fins. Although the damping is reduced, this mode does not become unstable at any point.

The time period to double amplitude of the spiral mode is shown in Fig. 4.9 and is of the order of minutes for both fins on and off cases. Removing the fins increases the time to double amplitude and therefore reduces the instability in this mode. Although unstable, it would be expected a pilot could prevent this from causing departure provided that a reasonable degree of situational awareness is maintained [129].

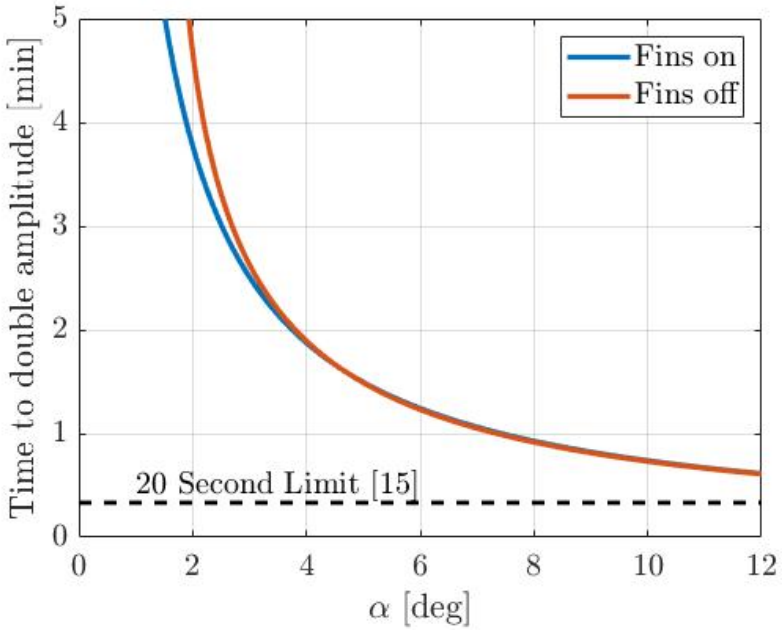

Figure 4.9. Time to double amplitude for Spiral mode with and without fins. This mode is unstable for both cases with and without fins. However, removing the fins does increase the time to double amplitude and therefore increases the stability of this mode.

To assess the aircraft's response to turbulence, the RMS accelerations are shown in Fig. 4.10 for moderate turbulence as defined by [129]. It can be seen that for angles of attack below 5°, the response to turbulence is reduced by removing the fins. However, at higher angles of attack the increased strength of the derivatives in response to the turbulence and reduced damping lead to lateral accelerations twice the level of the case with fins. Whilst these levels of acceleration seem high, this is partly due to the low wing loading and inertia of the aircraft used in this case study.

In summary for the MAGMA geometry, removing the fins creates weak instabilities at angles of attack below 1.2° with a time to double amplitude in the order of hours for the worst case. Therefore for the cases discussed above, the most onerous requirement in terms of the yawing moment required is to trim in a crosswind at high angles of attack with a required C_n of 3×10^{-3} representative of a crosswind landing approach. However it is worth noting that for the rolling manoeuvre, for roll rates of $25^{\circ}/s$ the peak C_n required is 10^{-3}. If significantly greater roll rates are required then the most onerous condition may become the rolling manoeuvre.

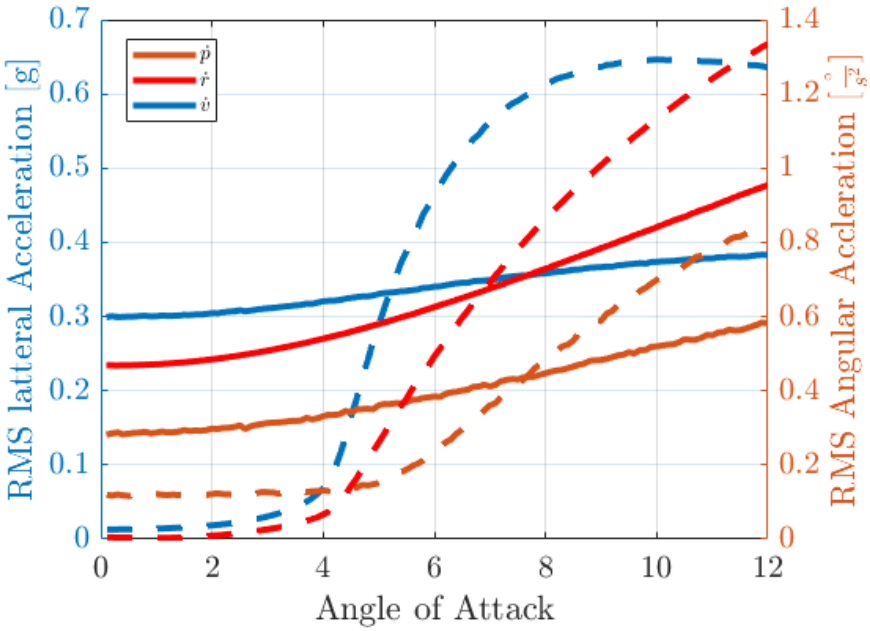

Figure 4.10. RMS accelerations due to moderate von Karman turbulence. The response is reduced at low angles of attack with the fins removed. At high angles of attack the acceleration without fins is up to twice the level with fins.

4.5 Application to Fluidic Control

In order to assess the amount of actuation required, the requirement to trim in a crosswind landing is considered. As an example of such a situation, here we consider the approach at $C_{L,max}$ ($\alpha = 8°$) with a crosswind of 25kts. The effector utilised in this case is an as yet unspecified flow control device, capable of changing the surface pressure over the airframe. As the control mechanism is unspecified, the results are presented in terms of a change in surface pressure and not an actuation level, hence allowing the assessment of any actuator. A summary of the method is provided in this section.

In order to compute the requirements for the actuator, we must first consider its placement and more specifically the area which it will influence. To aid in this, Fig. 4.11 shows the geometric contribution to the yawing moment. This is computed by breaking the geometry into small panels; the influence of each panel is then computed as the cross product of its area (outward normal) and distance from the centre of gravity. From this it can be seen that the nose and leading edges give the greatest destabilising moment whereas the greatest stabilising moment is produced at the aft sections of the centre of the body.

Combining the geometric contribution information with the surface pressure distribution at the desired flight condition (shown in Fig. 4.12) identifies which regions produce the most significant contributions to the yawing moment as shown Fig. 4.13. This process is repeated to find the areas which contribute most significantly to the rolling moment. This allows the

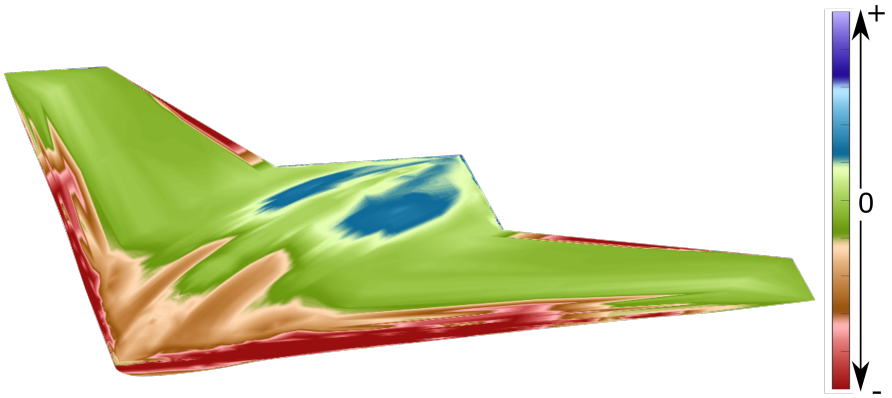

Figure 4.11. Areas which contribute the greatest geometrically to the yawing moment. This is calculated by breaking the surface into panels and taking the cross product of the normal of each panel with its distance from the CG.

assessment of what actuation is required to produce a pure body axis yawing moment, as would be required for trim on approach.

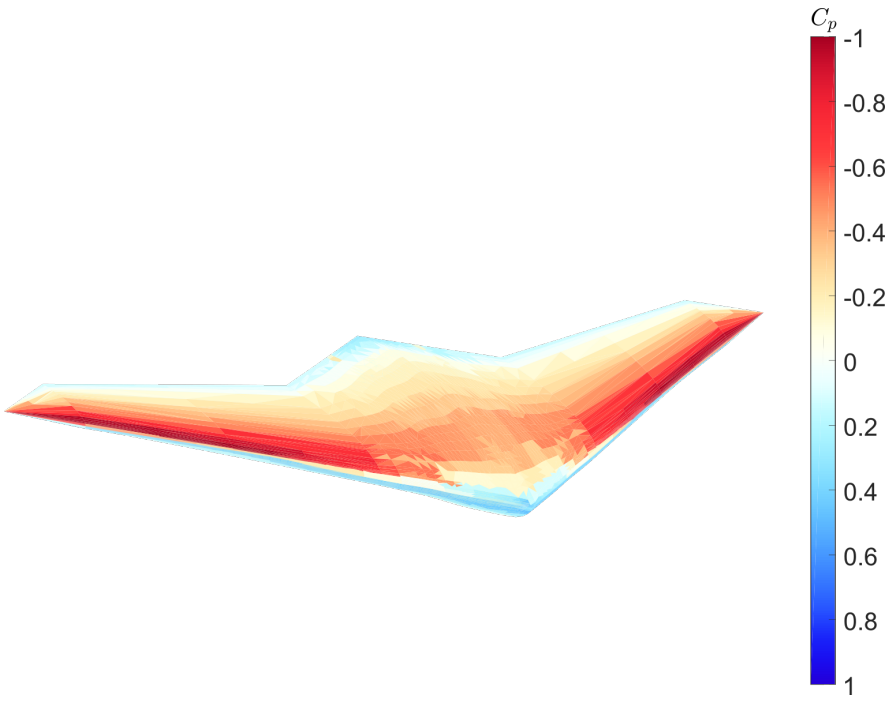

Figure 4.12. Surface pressure distribution over MAGMA geometry at $\alpha = 4°$. Pressure data from vortex panel method.

In order to assess the requirements for the fluidic actuator, the information in Fig. 4.13 is processed to identify the size and location of each of the regions which contribute most to the yawing moment, Fig. 4.14. There is only one region identified by this method, the leading edges.

To determine the required changes in surface pressure, first the response of the yawing and rolling moments to changes in the surface pressure must be determined. This is calculated by perturbing the pressure distribution and calculating the moments using the same approach

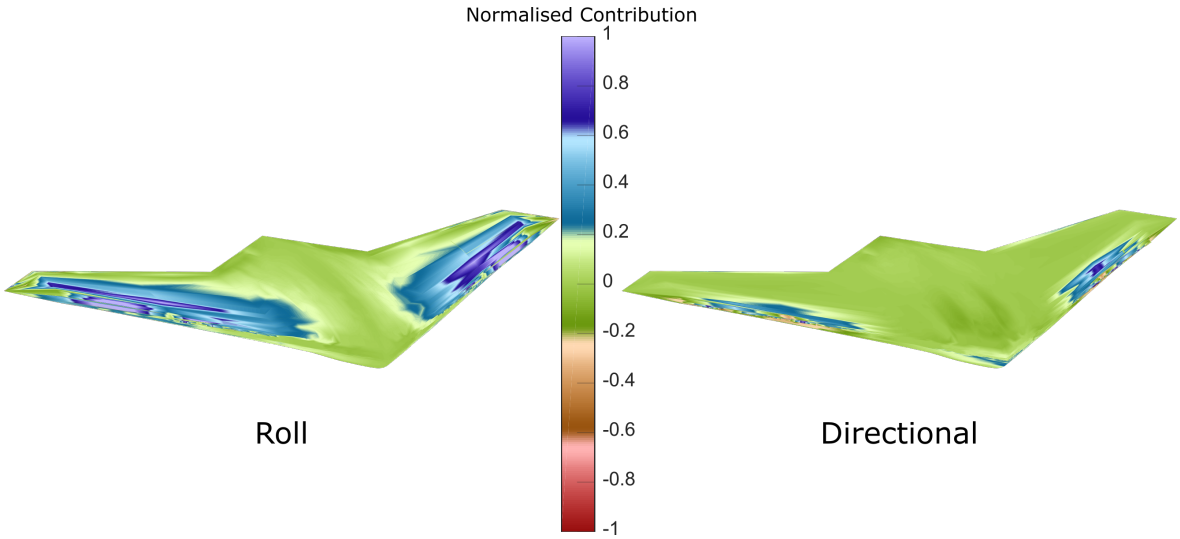

Figure 4.13. Regions which contribute greatest to the rolling and yawing moment at $\alpha = 4°$. This information is the product of the geometric contributions in Fig. 4.11 and the pressure distribution in Fig. 4.12

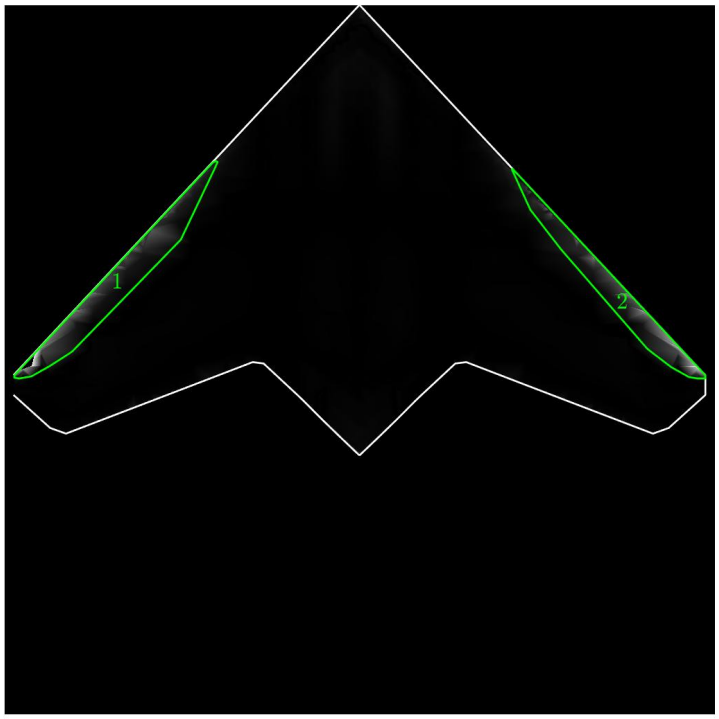

Figure 4.14. Regions which have the greatest influence on the yawing moment. This data is obtained by converting Fig. 4.13 to greyscale and passing through a thresholding algorithm.

used to produce Fig. 13. The derivatives $\frac{\partial C_n}{\partial C_p}$ and $\frac{\partial C_l}{\partial C_p}$ for each region are then calculated numerically. With the calculated derivatives, the average surface pressure for each region and the required moments for a crosswind approach ($C_n = 3 \times 10^{-3}$ and $C_l = 0$) the actuation strategy which give the least relative change in surface pressure can be found using the minimisation problem described in Eq. 4.9.

$$\text{Minimise: } \sum \frac{|\Delta C_{p,i}|}{|\overline{C_p}|}$$
$$\text{Subject to: } \begin{bmatrix} \left(\frac{\partial C_n}{\partial C_p}\right)_1 & \cdots & \left(\frac{\partial C_n}{\partial C_p}\right)_n \\ \left(\frac{\partial C_l}{\partial C_p}\right)_1 & \cdots & \left(\frac{\partial C_l}{\partial C_p}\right)_n \end{bmatrix} \begin{bmatrix} \Delta C_{p,1} \\ \vdots \\ \Delta C_{p,n} \end{bmatrix} = \begin{bmatrix} \Delta C_n \\ 0 \end{bmatrix} \tag{4.9}$$

Using this strategy it is found that it is not possible to produce a pure yawing moment without a significant secondary control effect in roll.

Using the same method described above, the analysis is repeated using just the information of the geometrical influence on the moments calculated in Fig. 4.15. The regions which give the greatest influence include the leading edge regions as previously and additionally: a trailing edge region, a forebody region and an aft region. As previous studies have shown the efficacy of forebody blowing [124] and this requires more detailed breakdown of the forebody region, hence only the leading and trailing edge regions are considered here. The minimisation problem in this case is to minimise the total magnitude in surface pressure coefficient, as shown in Eq. (4.10). Therefore, these regions represent locations where it is possible to generate a yawing moment by changing the magnitude of pressure acting over that region.

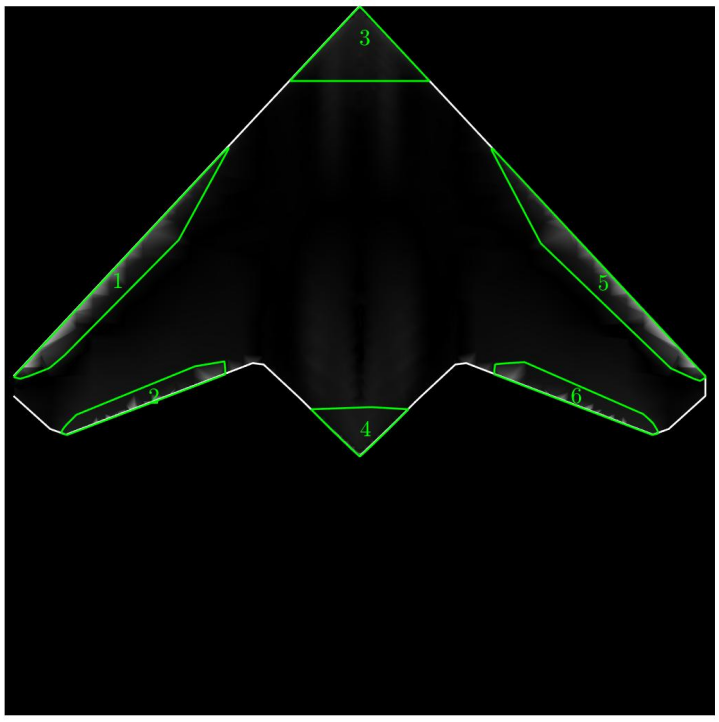

Figure 4.15. Regions which have the greatest geometric influence on the yawing moment. This data is obtained by converting Fig. 4.11 to greyscale and passing through a thresholding algorithm.

$$\begin{aligned} &\text{Minimise: } \sum \left|\Delta C_{p,i}\right| \\ &\text{Subject to: } \begin{bmatrix} \left(\frac{\partial C_n}{\partial C_p}\right)_1 & \cdots & \left(\frac{\partial C_n}{\partial C_p}\right)_n \\ \left(\frac{\partial C_l}{\partial C_p}\right)_1 & \cdots & \left(\frac{\partial C_l}{\partial C_p}\right)_n \end{bmatrix} \begin{bmatrix} \Delta C_{p,1} \\ \vdots \\ \Delta C_{p,n} \end{bmatrix} = \begin{bmatrix} \Delta C_n \\ 0 \end{bmatrix} \end{aligned} \tag{4.10}$$

This method finds that the moment can be produced most efficiently by actuating the leading edge region on one wing and the trailing edge region on the other. The total change in surface pressure using this method requires changes in C_p of ± 0.1029 and ± 0.2279 for the leading edge and trailing edge regions respectively.

It is also worth considering that rather than using a flow control device to change the surface pressures, the momentum used for flow control could be used purely as a reaction jet to produce the yawing moments required. In order for the method of changing surface pressures described above to be more effective than using a pure momentum reaction from blowing, the inequalities described in equations (4.11)&(4.12) must be satisfied.

$$\left(\frac{\partial C_p}{\partial C_\mu}\right)_{TE} \geq \frac{\Delta C_{p,TE}}{2C_n - \frac{\Delta C_{p,LE}}{\left(\frac{\partial C_p}{\partial C_\mu}\right)_{LE}}} \tag{4.11}$$

$$\left(\frac{\partial C_p}{\partial C_\mu}\right)_{LE} \geq \frac{\Delta C_{p,LE}}{2C_n} \tag{4.12}$$

These inequalities are plotted in Fig. 4.16. The efficiencies of both regions must be in the area of the plot above the line, if the efficiencies are below this line then it would be more effective to use the compressed air source for the fluidic controls as a reaction jet.

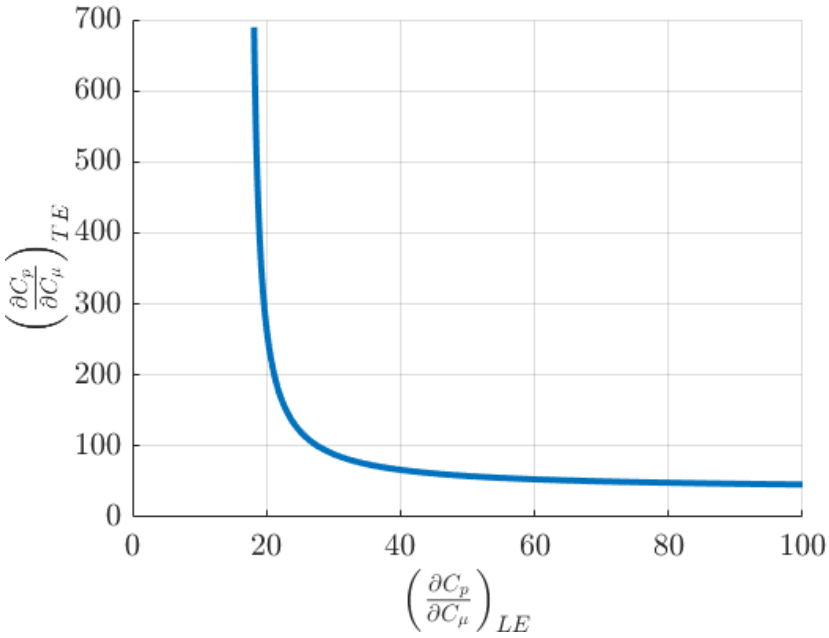

Figure 4.16. Minimum efficacy of flow control solutions at leading and trailing edge. Efficacies below this line are not worth pursuing as the required air flow would be best used as a reaction jet.

4.6 Conclusion

The method detailed in this paper predicts that whilst there is a reduction in the directional stability when removing the fins from the aircraft in this case study, in most cases this does not result in the aircraft becoming unstable. Where instabilities are created, these are very weak instabilities with time periods manageable with the aircraft's controls. The most onerous cases for directional control input were trim in a crosswind followed by maintaining a coordinated turn during a rolling manoeuvre.

By examining the areas of the aircraft geometry which most greatly contribute to the yawing moment, both as a function of area only and the force created with an unmodified pressure distribution, it is possible to identify the regions of greatest potential effectiveness for flow control. When compared against the effectiveness of using a reaction jet at the wing tips to provide a yawing moment this gives a lower bound for the efficiency of any potential flow control solution early in the design process. Whilst the changes in surface pressure calculated to trim in sideslip are moderate, a large gain in terms of the surface pressure change in response to a flow control input is required to be more effective than a reaction jet. The method has also provided an indication of the secondary (roll) effects of potential fluidic directional control methods. In the cases examined in this work, it was not always possible to produce a pure yawing moment without the secondary roll. For this reason, the analysis presented here does not guarantee that the regions identified can be actuated by a flow control solution but rather identifies potential areas of interest. Further investigation into mechanisms which may be

exploited to yield the required changes in surface pressure within the constraints of available C_μ and efficiencies would still be necessary.

Finally, it should be recognised that this analysis was limited to the lateral motion of the aircraft. Changes in surface pressure on the wing will also create both changes in lift and pitching moment which must be counteracted by other means to maintain trim. Analysis of the methods by which these changes may be counteracted is beyond the scope of this work. However, when assessing a specific effector these secondary control effects must be considered and a method of maintaining trim in other axes devised. If there is no way to maintain trim in the other axes with a yaw input, then the actuator is not suitable for flight.

Chapter 5

Paper 2: A Novel Control Allocation Method for Yaw Control of Tailless Aircraft

Summary

This chapter provides a description of the yaw control method used throughout much of the work in this thesis. It was originally presented as a Journal article in Aerospace [130]. The contributions of each author are detailed in Table 5.1.

The motivation for this work came from the finding of the previous chapter that using fluidic actuation to change surface pressures on target regions of the aircraft's surface was not a feasible method for directional control. As such, the objective of this work was to explore the opportunity to impart a yawing moment by generating a laterally asymmetric induced drag.

The paper uses trapezoidal planforms of low aspect ratio and moderate sweep to develop a general control strategy. As discussed in the literature review, previous studies have examined the generation of yawing moments by modifying the spanwise load distribution to produce asymmetries in induced drag. However, these studies have examined a continuous change in load distribution with application cited as morphing wings to achieve this. The work presented in this paper considers an aircraft with conventional trailing-edge control surfaces and examines the feasibility of using these to generate the yawing moment with no secondary control effects.

This objective is achieved by the definition of control allocation mode shapes. These mode shapes are an original contribution of this work and are defined by the null space of the matrix defining the aircraft response in lift, pitch and roll to control surface deflection. In this way, the mode shapes have no secondary control effects but are asymmetric about the aircraft center line to impart a yawing moment.

Task	TRS	MRAN	WJC	CW
Funding Acquisition		x	x	x
Supervision		x	x	x
Project Administration		x	x	x
Conceptualisation	x	x	x	x
Methodology	x	x	x	x
Formal Analysis	x			
Investigation	x			
Software	x	x		
Validation	x			
Visualisation	x			
Writing - original draft	x			
Writing - review and editing		x	x	x

Table 5.1. Contributor Roles Taxonomy for Chapter 5

Abstract: *Tailless aircraft without vertical stabilisers typically use drag effectors in the form of spoilers or split flaps to generate control moments in yaw. This paper introduces a novel control allocation method by which full three-axis control authority can be achieved by the use of conventional lift effectors only, which reduces system complexity and control deflection required to achieve a given yawing moment. The proposed method is based on synthesis of control allocation modes that generate asymmetric profile and lift induced drag whilst maintaining the lift, pitching moment and rolling moment at the trim state. The method uses low order models for aerodynamic behaviour characterisation based on thin aerofoil theory, lifting surface methodology and ESDU datasheets and is applied to trapezoidal wings of varying sweep and taper. Control allocation modes are derived using the zero-sets of surrogate models for the characterised aerodynamic behaviours. Results are presented in the form of control allocations for a range of trimmed sideslip angles up to 10 degrees optimised for either maximum aerodynamic efficiency (minimum drag for a specific yawing moment) or minimum aggregate control deflection (as a surrogate observability metric). Outcomes for the two optimisation objectives are correlated in that minimum deflection solutions are always consistent with efficient ones. A configuration with conventional drag effector is used as a reference baseline. It is shown that, through appropriate allocation of lift based control effectors, a given yawing moment can be produced with up to a factor of eight less aggregate control deflection and up to 30% less overall drag compared to use of a conventional drag effector.*

5.1 Introduction

Current performance and operational requirements for low observable aircraft drive the design towards finless low aspect ratio flying wing configurations with a leading edge sweep

between 45–60 degrees [131]–[133]. Yaw control is typically provided through laterally asymmetric deployment of drag-based aerodynamic control effectors in the form of spoilers or split elevons [134]. Whilst these devices are effective, there is a significant increase in required design effort and system complexity due to the strong pitch, roll and yaw coupling of these controls [121], [135], [136]. Furthermore, deployment of non-conformal surfaces to produce drag may have a significant impact on the observability of the platform [122], [137]. Due to the use of multiple and diverse flight control effectors for redundancy reasons, the system is overactuated and there are typically many different actuation solutions to achieve a given control effect [138]–[140]. Hence, a key design problem is assigning appropriate control allocation using some or all of these controls to meet overall performance objectives.

Several previous studies have developed control strategies for wing-tip drag devices which attempt to minimise secondary control effects. Qu et al. [141] investigated the use of drag devices that are modulated about a permanently partially open state using computational fluid dynamics (CFD) simulations. This method showed little pitch and roll coupling at low angles of attack and improved the linearity of the control. However, the use of permanently deflected controls increases signature and reduces aerodynamic performance of the aircraft. Löchert et al. [131] investigated several forms of wing-tip drag devices and tip aligned spoilers using CFD simulations and experimental testing. They showed that folding wing-tips and spoilers at the wing-tips both produce significant cross-coupling, particularly in the roll axis. For a split drag rudder design at the wing tip, the cross coupling is significantly reduced; however, control surface deflections needed to meet lateral control effectiveness requirements were large (up to 45 degrees) . Huber et al. [142] performed experimental tests on a split elevon located inboard of the wing-tip. These experiments showed a significant roll-yaw coupling with control surface deflection in contrast to results presented in [131]. It is, hence, evident that the secondary control effects of split elevons are sensitive to the spanwise location of the control surface.

There are a few studies that examine more unconventional methods for generating yawing moments on tailless aircraft. Yue et al. [143] explored the use of asymmetrically deployed telescopic wings. However, the influence on rolling moment was an order of magnitude greater than the yawing moment, limiting the usefulness of the concept. Xu et al. [144] explored the use of active flow control using synthetic jets to cause asymmetry in the leading edge vortex system. Again, the yaw control output of the method was very small compared to rolling and pitching moment.

As an alternative method of directional control, several studies have considered the use of asymmetries in induced drag to produce yawing moments [71], [114], [145], [146]. These studies have demonstrated the potential of using changes in the lift distribution to induce laterally asymmetric drag whilst simultaneously achieving requirements for pitching and

rolling moments. However, these studies have predominantly focused on identifying optimal lift distributions based upon results from lifting line analysis. Whilst useful theoretically, achieving these lift distributions in practice would require continuous spanwise control of twist or camber. Studies have demonstrated the possibility of achieving this continuous control through morphing structures [147], [148], however this method of control significantly increases the control system complexity.

The current study explores the use of drag from lift based effectors only, to provide yaw control on a finless flying wing aircraft. The limitation to lift based effectors in the form of devices that locally change the effective camber of the wing is significant. These devices are necessarily already present as primary controls for pitch and yaw, and that the observability impact of these controls can be mitigated more easily than for non-conformal controls such as split elevons and spoilers [149]. Furthermore, there is an opportunity to achieve a given level of yaw control effectiveness at a lower overall level of airframe drag. The physical premise of the approach is based primarily on the exploitation of changes in induced drag generated by the lift effector. The lift effector will also have an impact on local profile drag, but, for a well implemented design, this will be significantly smaller than the change in induced drag [150]. The problem is posed in the form of allocation of lift based effectors to achieve a given level of yawing moment with zero coupling in pitching moment and rolling moment. The yawing moment correlates directly with trimmed sideslip angle for a given level of static directional stability. A novel contribution of the work lies in the development of appropriate low order aerodynamic modelling tools and mathematical techniques to identify control allocation modes that can be used to synthesise control inputs against different performance targets.

Section 5.2 provides background aerodynamic theory to the problem. The development of the control allocation method is described in Section 5.3 and the results of example cases are presented in Section 5.4. Finally concluding comments are provided in Section 5.5.

5.2 Theoretical Background

The induced drag on a section of a finite wing is a product of the lift and induced angle of attack at that section, both of which are functions of the circulation distribution. Thus asymmetric circulation distributions will produce an asymmetric induced drag distribution and hence net yawing moment. However, modifying the circulation distribution will also have an effect on the lift, pitching moment and rolling moment. A method is, therefore, required to identify changes in the load or circulation distribution that are able to create a change in yawing moment but with negligible cross coupling with pitch and roll.

As an example, consider the simple case of a straight untapered wing with the moment

reference point at the aerodynamic centre. Since the lift acts at the moment reference, the lift is decoupled from the pitching moment and the effect of the circulation distribution on pitch can be neglected. Consider the existence of one symmetric and one asymmetric circulation distribution that both give the same overall lift and zero rolling moment. By definition, the yawing moment due to induced drag will be zero for the symmetric distribution but finite for the asymmetric distribution. An example solution of this type is shown in Fig. 5.1. The spanwise integrals of both the symmetric and the asymmetric distributions are equivalent such that the lift coefficients produced are equal, and the integral of the product of circulation and spanwise location with respect to the spanwise location ($\int \Gamma \eta d\eta$) in each case is equal to zero such that the rolling moment is zero. Note that the asymmetric circulation distribution shown is an arbitrary solution out of an infinite set of possible solutions.

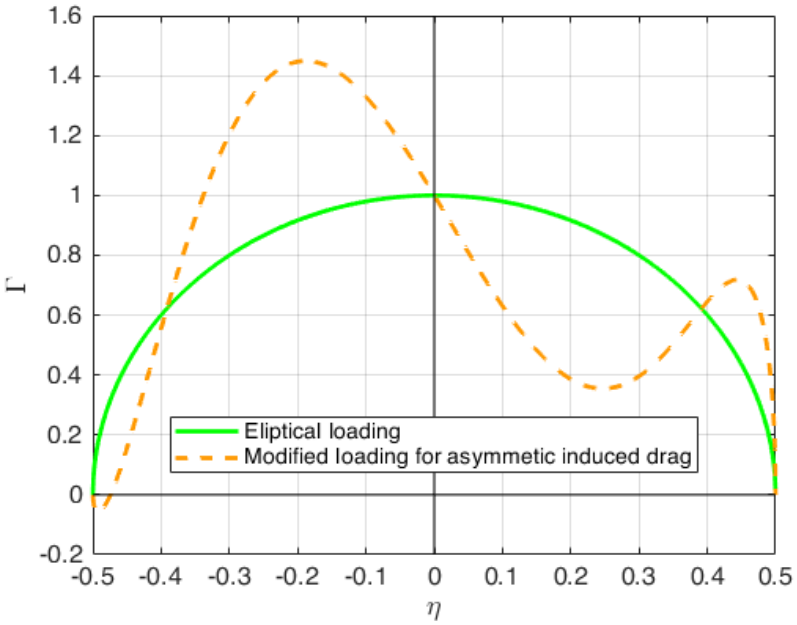

Figure 5.1. Two different load distributions that produce the same lift and no rolling moment but different levels of induced drag. Solid line, symmetric elliptical loading; dashed line, equivalent distribution tailored to produce a net yawing moment through laterally asymmetric induced drag.

Although the solution for the circulation distribution in this form may appear trivial, for swept wings and wings of low aspect ratio, evaluating the unperturbed distribution is analytically complex because simple techniques such as lifting line analysis are invalid. Furthermore, for practical cases, the circulation distribution may only be modified over discrete spanwise locations dictated by the location of control surfaces, which creates an analytical challenge.

5.3 Method

5.3.1 Wing Aerodynamic Models

To allow the control allocation studies to be undertaken as part of preliminary design studies, a computationally inexpensive method of analysing the aerodynamic effects of asymmetric control surface deflections is required. Several low-order methods were compared (see Appendix B for a detailed comparison) and from these Multhopp's Lifting Surface (LS) model [16] was selected as the most applicable.

5.3.2 Validation of Model Predictions Due to Control Surface Deflection

To validate the applicability of the selected model, model predictions were compared to experimental data from Stenfelt and Ringertz [75]. The experimental data provide information on the yawing moment due to opposing surface deflection on the same side of a tailless aircraft at zero degrees angle of attack. Whilst there is no imposed requirement to maintain trim on other axes, it provides a useful validation case nevertheless.

The yawing moment generated by the surface deflections is shown in Fig. 5.2. A positive deflection is defined as the outer control surface Trailing Edge Up (TEU) and inner surface Trailing Edge Down (TED). The solid red line on the plot shows the total drag from deflecting the control surfaces. This comprises the induced drag contribution from the LS model and the profile drag contribution modelled based on ESDU 06014 [151]. Note that throughout this paper all yawing moments are represented as an equivalent sideslip angle of trim (i.e., the ratio of yawing moment to the yawing moment with respect to sideslip derivative $\frac{C_n}{C_{n\beta}}$). The value of $C_{n\beta}$ is evaluated using the LS model with the assumption of linear aerodynamics. Wherever this metric is used, it is normalised with the yawing moment due to sideslip derivative applicable to the geometry presented.

For positive deflections, our predicted total drag agrees well with the experimental data, following the lower bound of the experimental uncertainty. However, for negative deflections, the model over predicts the yawing moment generated. This is because TED outer control surface deflections promote spanwise flow over the outer control surface, reducing the control effectiveness [142]. Despite this effect, it can be seen that for deflections less than six degrees the predicted yawing moment is within the experimental uncertainty. As the aim of the study is to minimise the control surface deflection required to generate a specific yawing moment, this is unlikely to limit the applicability of the model. However, results where the outer control surface is deflected greater than six degrees TED should be treated with caution.

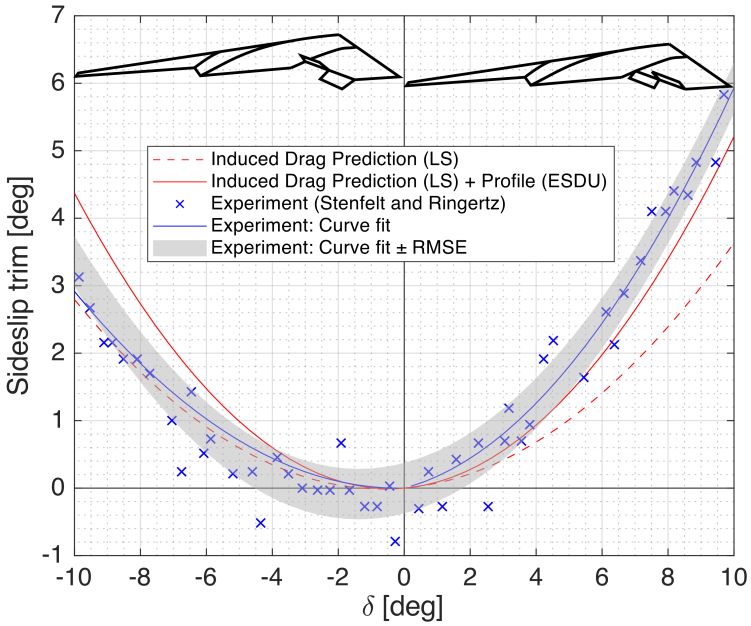

Figure 5.2. Comparison of predicted yawing moment against experimental results for opposing deflections of dual surfaces on the starboard wing. Positive deflection is outer control surface TEU and inner control surface TED (see inset). For positive deflection, the sideslip trim closely follows the lower bound on the uncertainty from the experiment. However, for negative deflections, the yawing moment is over predicted for defection greater than six degrees ($\delta > 6^{\circ}$). This is due to the reduction in effectiveness of the outer control surface due to the increasing influence of spanwise flow [1]

5.3.3 Control Allocation

The aim of the control strategy developed in this paper is to achieve a specific sideslip demand without any change in overall lift from the trim state, whilst maintaining trim in pitch and roll. Achieving such aim sounds a normal practice and indeed has been previously attempted as a pure control allocation problem (e.g., in [152]). However, to the best of our knowledge, identifying a control allocation strategy for a flying wing configuration based on a mode shaping approach has not been attempted before. As such, we here propose a novel control allocation strategy based on the calculation of a combination of control deflection mode shapes to generate a given yawing moment with zero pitch and rolling moment.

To calculate the control surfaces deflections required, a method is developed based upon the null space (zero set) of a control derivative matrix, similar to that developed by Fruchter [153]. Fruchter's method is aimed at identifying a stable gain strategy for a control system by finding the zero-set (or null space) of a linear system. Here, we extend the application of Fruchter's approach to an aerodynamic context so that the output of the null space calculation identifies aerodynamic outputs. This is a novel way of dealing with control surface effects

[1] A correction factor applied to the LS result could capture the effect of spanwise flow on the yawing moment. However, the modeling of the effects of spanwise flow are planform specific beyond the scope of this work. Instead the uncorrected result from LS is used to demonstrate the control allocation strategy within this chapter and throughout the thesis. Future work may wish to include the non-linear effects of flow breakdown within the control allocation strategy.

through allowing a suite of control surface deflections to be described as mode shapes; linear combinations of which have no effect on lift, pitching moment or rolling moment but are laterally asymmetric to induce a yawing moment on the wing. A summary of the whole method is shown in Fig. 5.3 and described thereafter.

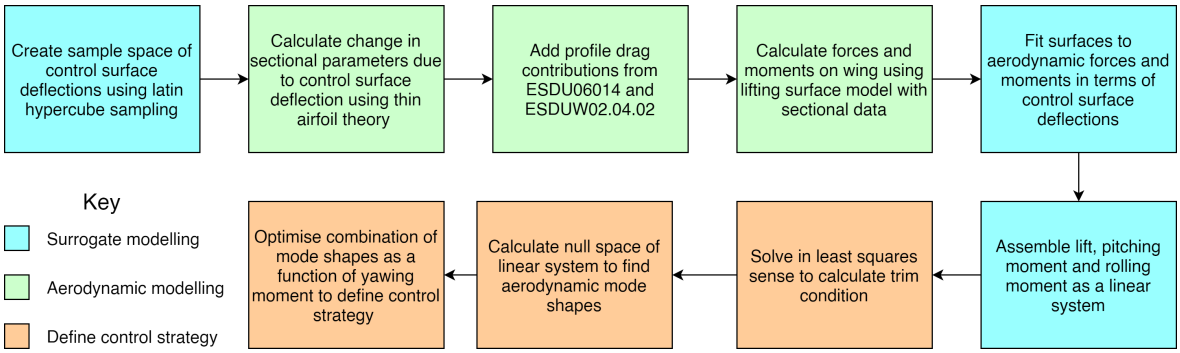

Figure 5.3. Process flow of control allocation method.

The first step in the process is to select a set of control surface deflections. Here we use Latin hypercube sampling as this sampling method ensures a well distributed set of control surface deflections are evaluated [154]. From these control surface deflections, the sectional lift and pitching moment coefficients can be calculated using thin aerofoil theory [155]. By using a fundamental theory such as thin aerofoil theory rather than experimental data, we ensure that the conclusions of this study are robust to an arbitrary aerofoil choice. However, as thin aerofoil theory makes an assumption of linear aerodynamics we must restrict the control surface deflections to the range -10° to 10°. Nevertheless, this restriction does not conflict with the overall aim to reduce the control surface deflection required for a given yawing moment. Furthermore, thin aerofoil theory is not able to capture any change in profile drag due to the control surface deflection. Therefore, a semi-empirical method from ESDU 06014 [151] is used to predict the change in profile drag. The planform profile drag is calculated using ESDUW02.04.02 [156], assuming a laminar flow for generality. This gives a profile drag coefficient, $C_{D0} = 0.002$ for all planforms investigated in Section 5.4.

Using the calculated sectional characteristics, the lifting surface model selected in Section 5.3.1 (see also selection process and discussion in Appendix B) is used to model the aerodynamic forces and moments on the 3D wing. A response function of the control surface deflections is then fit to the predicted force and moment coefficients using response surface methodology [157]. This allows for a more computationally efficient modelling of the aircraft response to control inputs whilst retaining the accuracy of the underlying models. These functions are calculated using least squares regression and take the form:

$$C_L = B_0 + \sum_{i=1}^{N} B_i \delta_i \tag{5.1}$$

$$C_m = C_0 + \sum_{i=1}^{N} C_i \delta_i \tag{5.2}$$

$$C_l = D_0 + \sum_{i=1}^{N} D_i \delta_i \tag{5.3}$$

$$C_D = E_0 + \sum_{i=1}^{N} E_i \delta_i + \sum_{i=1}^{N-1} \sum_{j=i+1}^{N} F_{i,j} \delta_i \delta_j + \sum_{i=1}^{N} G_i \delta_i^2 \tag{5.4}$$

$$C_n = S_0 + \sum_{i=1}^{N} S_i \delta_i + \sum_{i=1}^{N-1} \sum_{j=i+1}^{N} T_{i,j} \delta_i \delta_j + \sum_{i=1}^{N} U_i \delta_i^2 \tag{5.5}$$

These equations describe the lift (C_L), drag (C_D), pitching moment (C_m), rolling moment (C_l) and yawing moment (C_n) in terms of the control surface deflection (δ) and response function coefficients (B–G, S–U). In all cases, examined these fits have a coefficient of determination (r^2) of unity. Conveniently, the three quantities that must be maintained are a linear function of the control surface deflections (i.e., lift, pitch and roll). Taking the requirement that the aircraft must be in trim, Equations (5.1)–(5.3) may be written as the following linear system:

$$\begin{bmatrix} 0 \\ -C_0 \\ 0 \end{bmatrix} = \begin{bmatrix} B_1 & B_2 & \dots & B_N \\ C_1 & C_2 & \dots & C_N \\ D_1 & D_2 & \dots & D_N \end{bmatrix} \begin{bmatrix} \delta_1 \\ \delta_2 \\ \vdots \\ \delta_N \end{bmatrix} \tag{5.6}$$

$$\begin{bmatrix} 0 \\ -C_0 \\ 0 \end{bmatrix} = \mathbf{R}\delta \tag{5.7}$$

The left hand side of Eq. (5.7)) describes the trim state of the aircraft. On the right hand side, Row 1 specifies the change in lift, Row 2 specifies the change in pitching moment and Row 3 specifies the change in rolling moment, all with respect to control surface deflection. As for a stable aircraft with no control surface deflection, there will be a nose down pitching moment (C_0); this is included on the LHS to ensure the aircraft is longitudinally trimmed.

As this system is over-defined for all cases with two or more control surfaces on each semi-span, there are an infinite number of solutions to this system. As such, we here only consider the case of three control surfaces on each semi-span (six in total) as this provides a representative case for analysis.

To define a control strategy which allows the generation of a yawing moment we must first calculate the control surface deflection array, δ, for the trim state denoted as (δ_0). To find

this, Eq. (5.7) is solved in a least squares sense with the additional constraint that the control surface deflections are symmetric about the aircraft centreline ($y = 0$), as a symmetric lift distribution will produce symmetric induced drag.

To find the additional control surface deflection required to generate a yawing moment, we use the null space of the matrix, $\mathbf{R}$ (i.e., solutions of δ which satisfy $\mathbf{R}\delta = 0$). The number of null space vectors (unique solutions) is determined by the degree to which matrix $\mathbf{R}$ is rank deficient. Each of the null space vectors can be thought of as analogous to a mode shape (i.e., Eigen vector of the system). Any linear combination of these modes will ensure that the constraints of lift, pitching moment and rolling moment are satisfied but will produce an asymmetric load distribution. As an example, the modes of an untapered straight wing with three control surfaces on each semi-span are shown in Fig. 5.4 .

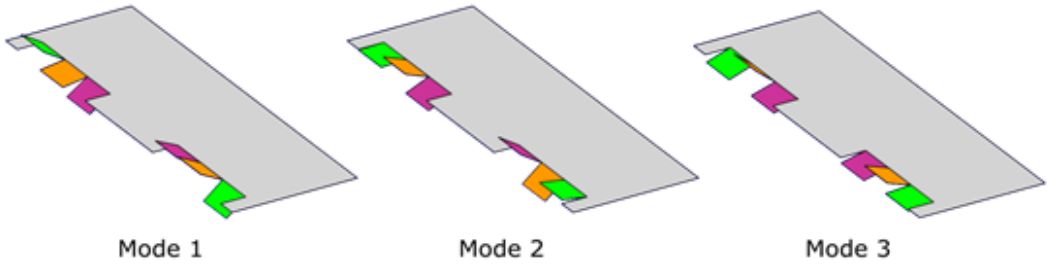

Figure 5.4. Visualisation of null space vectors for an untapered straight wing. Any linear combination of the three modes will ensure that the constraints on lift, pitching moment and rolling moment are satisfied whilst producing a yawing moment. Defections are exaggerated for clarity.

Next, the null space matrix, $\mathbf{n}$, is formed by assembling the null space vectors as the columns of $\mathbf{n}$. This can then be multiplied by a vector of gains ($\mathbf{k}$) such that the deflection can be written as a function of the gains:

$$\delta = \delta_0 + \mathbf{nk} \tag{5.8}$$

In doing this, the N unknown deflections are reduced to N-3 unknown gains, and the constraints on lift, pitching moment and rolling moment are implicitly satisfied. This is computationally significant as the size of the problem is reduced and trim conditions are always satisfied. For example, in the cases presented in this paper for three control surfaces on each semi-span, this reduces the number of unknowns from six to three.

Substituting Eq. (5.8) into Eq. (5.4) and Eq. (5.5) yields equations for the yawing moment and drag in terms of $\mathbf{k}$; however, unlike those for lift, pitching moment and rolling moment, the combination of modes is non-linear. These are quadratic equations with linear interactions

[1]Note that whilst these mode shapes would change with sideslip angle, they are defined here for only $\beta = 0$

between the modes.

As for all cases with more than two control surfaces on each wing, there is more than one unique solution of k to generate a given yawing moment. To select a control strategy, one must select a quantity to optimise. In this study, we consider two possible objectives relevant to the problem in hand; however, the method remains unchanged if other objective(s) are of greater significance to a designer .

The first objective is the aerodynamic efficiency of generating a yawing moment (denoted as X), and defined in Eq. (5.9) as the drag coefficient for a specific yawing moment. The second objective considered in this study is the area exposed in the normal plane by the control surface deflection (denoted as Y), and defined in Eq. (5.10) as the sum of the surface area of each control surface multiplied by the sine of its deflection angle [2].

$$X = C_D(\mathbf{k})|_{C_n} \tag{5.9}$$

$$Y = \sum_{i=1}^{N} A_i \sin\left(\delta_i(\mathbf{k})\right)|_{C_n} \tag{5.10}$$

The solution for **k** where X or Y is minimised for a given yawing moment is both analytically complex and specific to the metric selected, a theoretical solution is therefore not pursued. To find the optimum value of **k**, we evaluate $C_n(\mathbf{k})$, $C_D(\mathbf{k})$ and $\delta(\mathbf{k})$ across the range of gains (**k**) which produces control surface deflections of up to 10°.

To find the optimum strategy (i.e., the optimum **k** as a function of C_n), we first decompose the range of yawing moments required to trim between 0° and 10° of sideslip into M discrete values. It is then possible to represent the value of the gain k_1 in terms of the desired yawing moment and the remaining gains by rearranging the function $C_n(\mathbf{k})$ to $k_1 = f(C_n, k_{2\to N})$. We then decompose the remaining gains $k_{2\to N}$ into P discrete values which are evaluated to calculate k_1, X and Y. From this, the minima in X or Y is selected as the optimum gain. Note that this method requires the evaluation of MP^{N-4} points. As a reference of computational efficiency, evaluation for the case of N = 6, M = 500 and P = 1000 on a standard laptop with a 2.4 GHz core i5 processor takes 17 s.

As an example, the surfaces of constant yawing moment for a straight, untapered wing with three control surfaces on each semi-span are calculated and shown in Fig. 5.5. Over the range evaluated, in all cases, there is a single minima in the drag coefficient. For all geometries analysed throughout this work, there was only one minima.

There are two regions for each sideslip angle shown which correspond to the positive and

[2] This metric is used as a surrogate for observability.

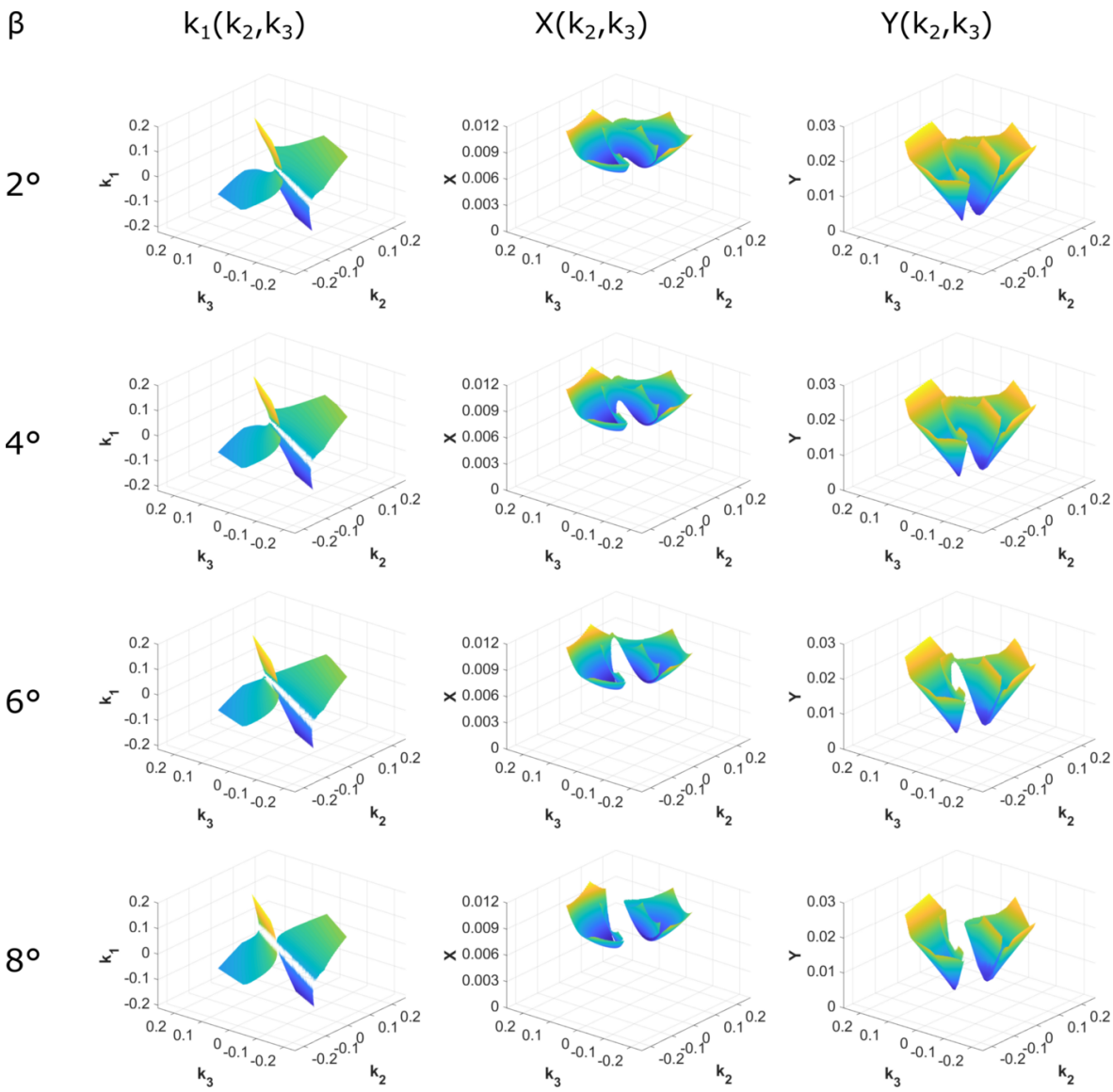

Figure 5.5. Iso-surfaces of constant yawing moment for an untapered straight wing. For each sideslip angle case presented. Left-hand plots show the values of **k** to attain the given sideslip angle and the centre and right-hand plots show the results of the optimisation functions X and Y, respectively.

negative solutions for k_1. The leftmost region (corresponding to the positive solution in this case) reduces in size as the required yawing moment increases and is less aerodynamically efficient. The rightmost region is both more aerodynamically efficient and stable in size as the yawing moment increases. The iso-surfaces do not change significantly with angle of attack but are specific to the planform geometry.

5.4 Results and Discussion

5.4.1 Wing Geometries

As the simplest case for which an optimum control strategy needs to be found, the results in this section are presented for three control surfaces on each semi-span. In addition to being the simplest, this setup of control surfaces is representative of that found on many tailless aircraft designs [158]. Control strategies are evaluated at yawing moments required to trim at a sideslip angle of 0° up to 10°, at an angle of attack of 4°, for wings with a quarter chord sweep of 0, 30 and 45 degrees with taper ratios of 0.2 and 1. In all cases analysed within this section the trim at sideslip is statically stable. In all cases, the longitudinal static margin is set to 5% of the mean aerodynamic chord, a typical value for flying wing configurations. This provides a representative range over which the proposed method could be comprehensively judged.

For all cases investigated below, all the control surfaces on each semi-span have a length of 10% span and are 20% of the local chord. Control surfaces are positioned at $\eta = 0.5$, 0.7 and 0.9 measured to the outboard edge. This is taken as a representation of typical arrangement of control surfaces on a tailless aircraft [158]. By fixing the size and location of the control surfaces, the problem size is restricted to allow reasonable investigation. Note that there is no limitation in the method to prevent analysis of less conventional geometries and control surface positions.

The optimum control strategy is calculated in terms of the aerodynamic efficiency (X) and aggregate control deflection (Y) as defined in Section 5.3.3. To provide a reference case for comparing the usefulness of the obtained results from the proposed method, each of the two metrics is compared to the same geometry where the outer control surface is replaced with a Split Drag Rudder (SDR) using a bias angle of 20° as defined by Qu et al. [141] [3]. To calculate the performance of the SDR, the LS model was adapted with the change in sectional lift and profile drag due to the SDR taken from ESDU 14004 [159] and 96026 [160], respectively. Note that ESDU 14004 (used for evaluation of lift and rolling moment due to the SDR) does not allow for small deflections below 12 degrees for this arrangement; therefore, the selection of the bias angle value of 20° fits within this applicability range. More importantly, it allows for a possible improvement in low speed performance due to reduced coupling shown by Qu et al. [141].

[3] The bias is added to the SDR implementation to prevent control coupling due to SDR deflection. This is not required for the mode shaping implementation as the coupling is not present.

5.4.2 Unswept Wing

The optimum control strategy for unswept wings is shown in Fig. 5.6. Fig. 5.6a,b shows results for optimising aerodynamic efficiency using X as an objective, whereas Fig. 5.6c,d shows results for optimising aggregate control deflection using Y as an objective. In all cases, the x-axis is represented in terms of a given sideslip angle which in turn implies a target yawing moment.

For the untapered wing, the control strategies are broadly similar; the starboard wing acts as a distributed SDR [141] with one control surface deflecting down and the others up. The difference between the two strategies is that for maximum aerodynamic efficiency the port wing is not actuated to reduce the change in drag, whereas the optimisation to minimise the exposed area makes more use of these surfaces.

For the tapered wing, the strategies for each optimisation function differ. For minimising the aggregate deflection the strategy is broadly similar to the untapered wing. However, for minimising the total drag, the outer control surface is deflected TEU. This is because the effectiveness of the outer control surface is reduced because of the reduced chord, therefore the optimiser uses the more effective centre control surface to reduce the total drag. Fig. 5.7 demonstrates that despite the total drag comprising 58% profile drag, the yawing moment is generated almost exclusively (greater than 99%) by induced drag.

Fig. 5.8 shows the result of each of the optimisation functions for each of the control strategies compared to a SDR. Several interesting observations can be made from this demonstration. First, it is clear that for both tapered and untapered planforms either optimisation strategy gives similar results for the aerodynamic efficiency ratio, X/X_{SDR}. This is to be expected as minimising the exposed area of the control surfaces will also minimise the profile drag contribution. Second, for the untapered planform only, both optimisations yield similar results in terms of the aggregate control deflection ratio (Y/Y_{SDR}); however, for the tapered case, the aggregate control deflection is marginally improved (i.e., decreased) by minimising Y. Finally, given that the y-axes are normalised with respect to the performance metric for the SDR, the performance impact of the proposed method can be directly assessed: Fig. 5.8a shows that this method uses approximately 30% less drag than a SDR to produce the same yawing moment for the untapered wing and 10% less for the tapered wing. Fig. 5.8b shows a clear performance benefit in terms of the reduction in the area exposed in the normal plane as this reduction varies between approximately 30% at high yawing moments up to around 80% at low yawing moments. This reduction suggests a favourable effect in aggregate control deflection.

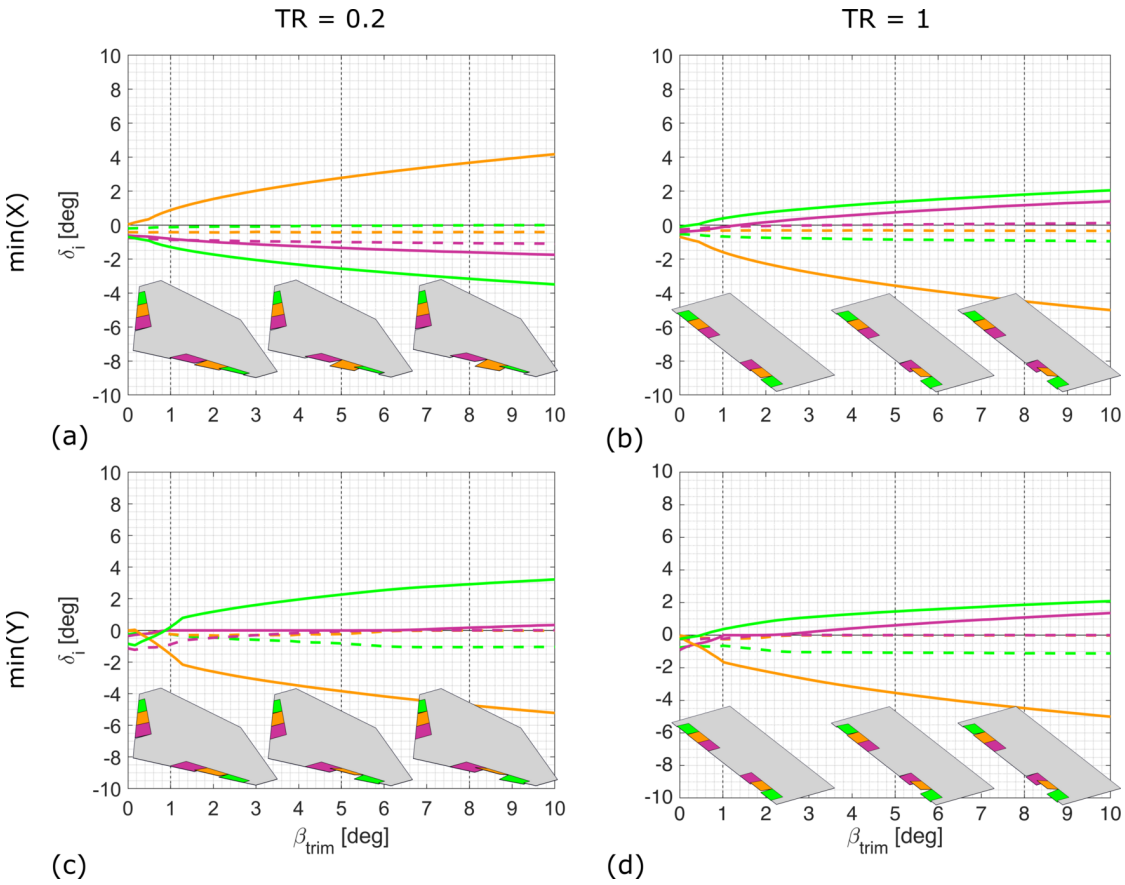

Figure 5.6. Deflection required to generate yawing moment to trim at a given sideslip angle, β_{trim}, for a straight wing with objectives of maximising aerodynamic efficiency (**a**,**b**) and minimising aggregate control deflection (**c**,**d**) for a taper ratio 0.2 (**a**,**c**) and 1 (**b**,**d**). Dashed lines represent port surfaces and solid lines are for starboard surfaces. Positive deflections are defined as trailing edge down. For visualisation purposes, insets show deflections required to trim at one, five and eight degrees of sideslip.

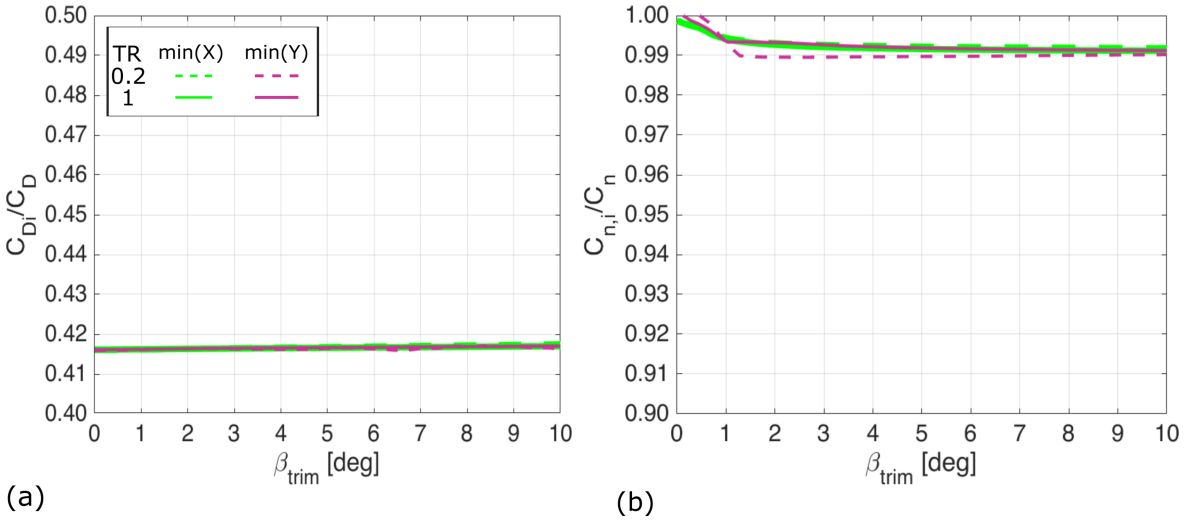

Figure 5.7. Relative contribution of the induced drag to the total drag (**a**) and the yawing moment (**b**) for unswept wing. In all cases, the induced drag is responsible for over 99% of the yawing moment produced by this method. This is despite the total drag comprising 58% profile drag.

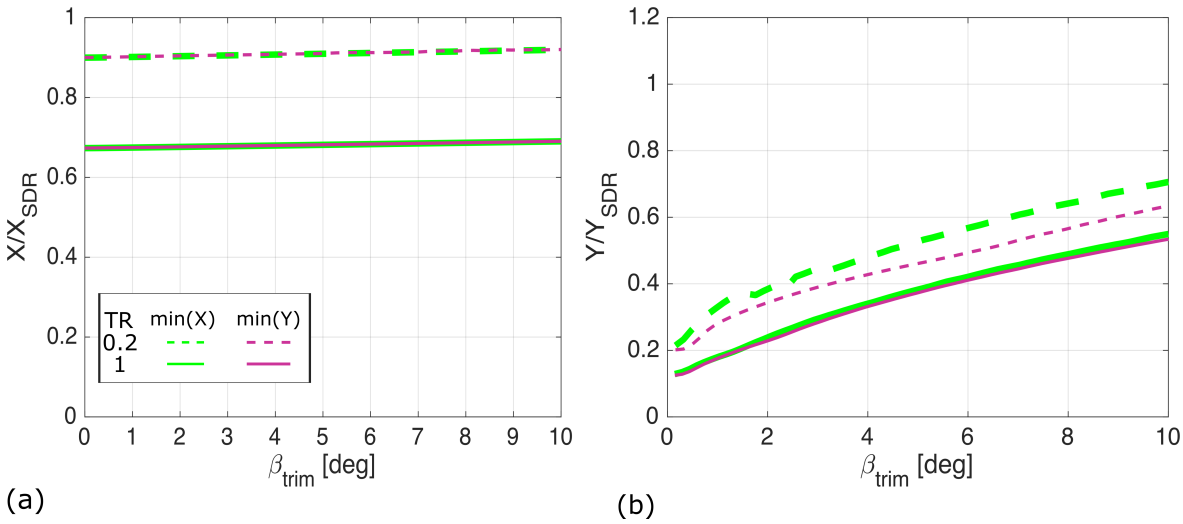

Figure 5.8. Optimisation functions aerodynamic efficiency (**a**) and aggregate control deflection (**b**) objectives for an unswept wing normalised by the same metrics for a SDR. Variations are shown up to a given sideslip trim angle of 10 degrees.

5.4.3 Thirty Degree Sweep

Increasing the quarter chord sweep to 30 degrees does not significantly change the control significantly for the untapered wing Fig. 5.9. For the tapered wing, the deflections required are reduced compared to the unswept wing. Examining the control strategy in any of the cases shown in Fig. 5.9, it can be seen that the yawing moment is primarily generated by the outboard two control surfaces on the starboard wing.

Similar to the finding for the zero sweep case, Fig. 5.10 shows that in all cases with 30 degree sweep the yawing moment is generated almost exclusively by induced drag. Note that, the induced drag contribution to the total drag within the case of untapered, unswept wing was still a major contribution but the introduction of sweep made this contribution even more significant. The change from the unswept wing is because of the increased load at the wingtips which improves the control surface effectiveness. This also explains the reduced benefit to the control strategy for the tapered wing, as the taper reduces the magnitude of the lift at the tips. However, in practice, it is undesirable to have such high loads at the wing tips and the introduction of twist may reduce this benefit. Interestingly despite the increase in the induced drag contribution to the total drag, the induced drag contribution to the yawing moment is roughly similar to that of the unswept case. This is because the profile drag contributions are small and almost symmetric about the aircraft centreline.

Fig. 5.11 shows the result of each of the optimisation functions for each of the control strategies when normalised to the SDR case. Again for (X/X_{SDR}), the SDR is approximately 40% less efficient for the same yawing moment for the untapered wing and 10% less efficient for the tapered wing. In the case of the 30 degree swept wing, the difference in aggregate

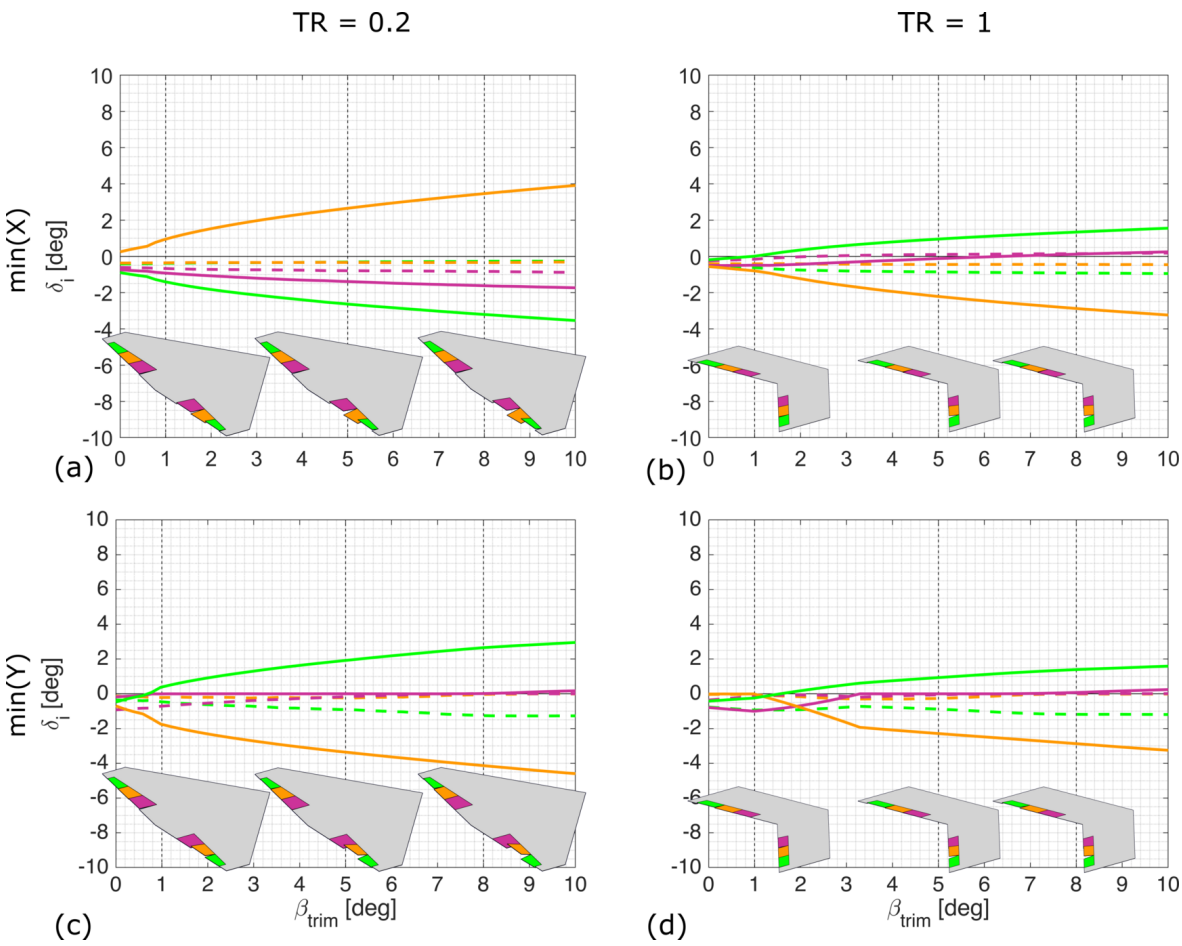

Figure 5.9. Deflection required to generate yawing moment to trim at sideslip for a 30 degree swept wing with objectives of maximising aerodynamic efficiency (**a**,**b**) and minimising aggregate control deflection (**c**,**d**) for a taper ratio 0.2 (**a**,**c**) and 1 (**b**,**d**). Dotted lines indicate port surfaces and solid lines are starboard surfaces, positive deflections trailing edge down. Inset shows deflections required to trim at one, five and eight degrees of sideslip.

control deflection (Y/Y_{SDR}) is small between the two optimisation methods but still shows a significant benefit compared to the SDR with improvements in aggregate control deflection of at least 40%. For the tapered wing when compared to the unswept case, there is now a small aggregate control deflection benefit at higher yawing moments as the deflections on the port wing are reduced. There is also a reduced aggregate control deflection for the untapered wing across the entire range of yawing moments analysed.

5.4.4 Forty-Five Degree Sweep

Further increasing the sweep from 30 degrees to 45 degrees has a large impact on the control strategies (Fig. 5.12). The most significant change in increasing the sweep is the increased deflections on the port wing; this is due to the increased coupling, particularly in pitch, due to the increased sweep.

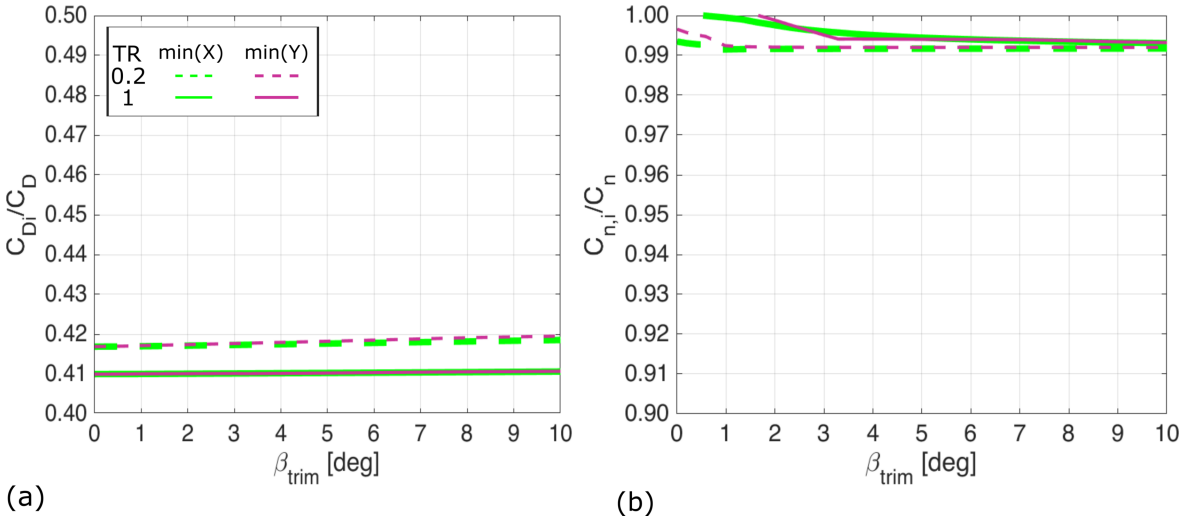

Figure 5.10. Relative contribution of the induced drag to the total drag (**a**) and the yawing moment (**b**) for the 30 degree swept wing. In all cases, the induced drag is responsible for over 99% of the yawing moment produced by this method and induced drag is responsible for approximately 42% of the total drag.

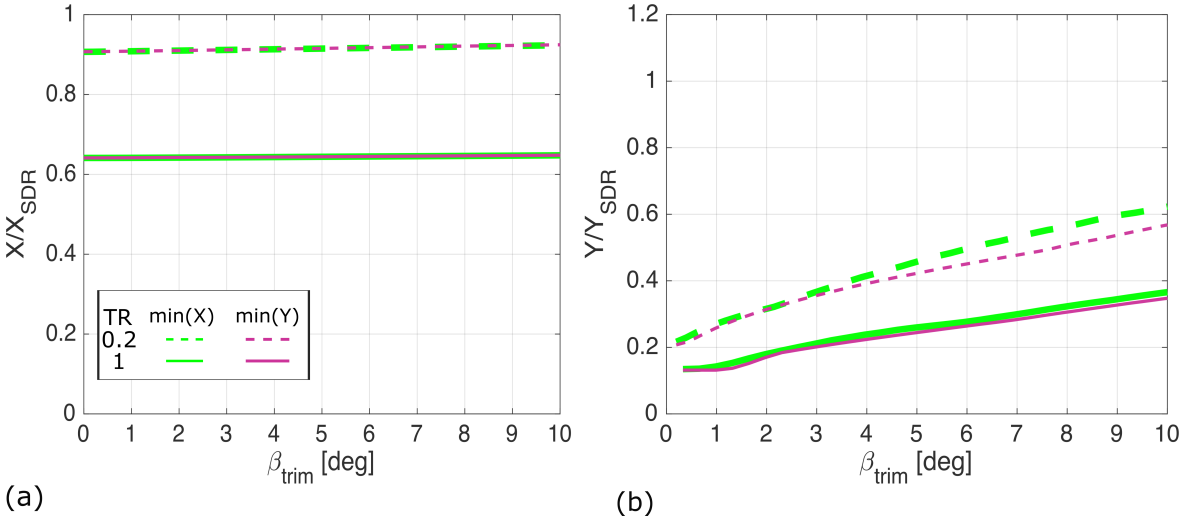

Figure 5.11. Optimisation functions aerodynamic efficiency (**a**) and aggregate control deflection (**b**) objectives for a 30 degree swept wing normalised by the same metrics for a SDR. Variations are shown up to a given sideslip trim angle of 10 degrees.

In all cases, in Fig. 5.12, the crux of the control strategy is to deflect the two outer control surfaces of the starboard wing in opposing directions to generate induced drag on the outer sections. Fig. 5.13 shows that, whilst induced drag remains a significant contributor to the yawing moment, the relative contribution of induced drag to the total drag is increased relative the cases of unswept and 30 degree swept wing. This is due to the port surface deflections required to maintain trim because of the increased coupling introduced by the greater sweep angle.

Fig. 5.14 shows the results of the optimisation functions for each control strategy and a comparison to the SDR. The result trends for the aerodynamic efficiency (X/X_{SDR}) are very similar to the unswept and 30 degree swept cases. Unlike the previous two cases (i.e., unswept

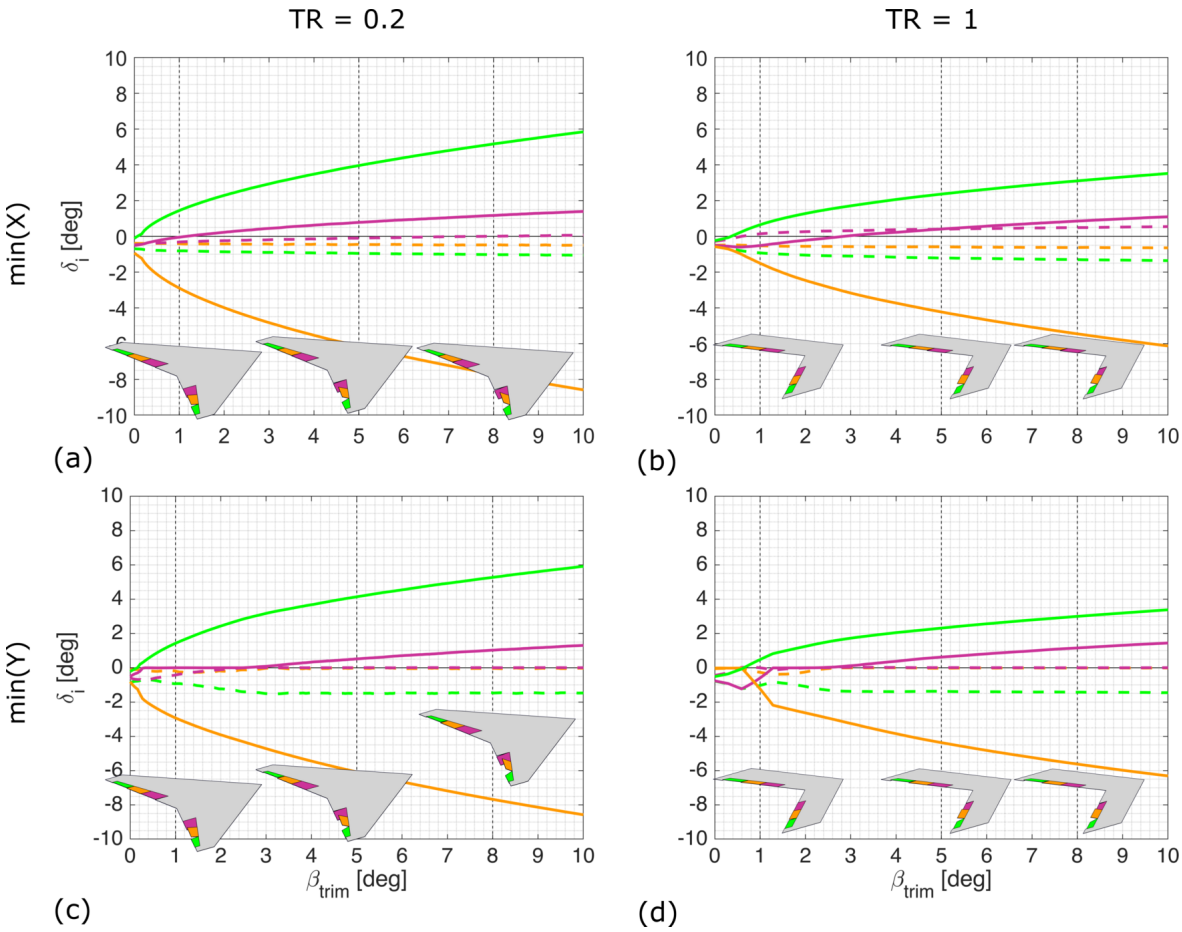

Figure 5.12. Deflection required to generate yawing moment to trim at sideslip for a 45 degree swept wing for objectives of maximising effectiveness (**a**,**b**) and minimising aggregate control deflection (**c**,**d**) with taper ratios 0.2 (**a**,**c**) and 1 (**b**,**d**). Dotted lines indicate port surfaces and solid lines are starboard surfaces, positive deflections trailing edge down. Inset shows deflections required to trim at one, five and eight degrees of sideslip.

and 30 degree sweep), there is only a marginal benefit in terms of aggregate control deflection (Y/Y_{SDR}) as the two methods (i.e., optimising aerodynamic efficiency or aggregate control deflection) produce very similar results. For small yawing moments, there is a large benefit in aggregate control deflection compared to the SDR, however this reduces as the yawing moment increases. For the wing planforms considered here, the SDR starts to show a benefit in terms of aggregate control deflection for sideslip angles to trim over around eight degrees.

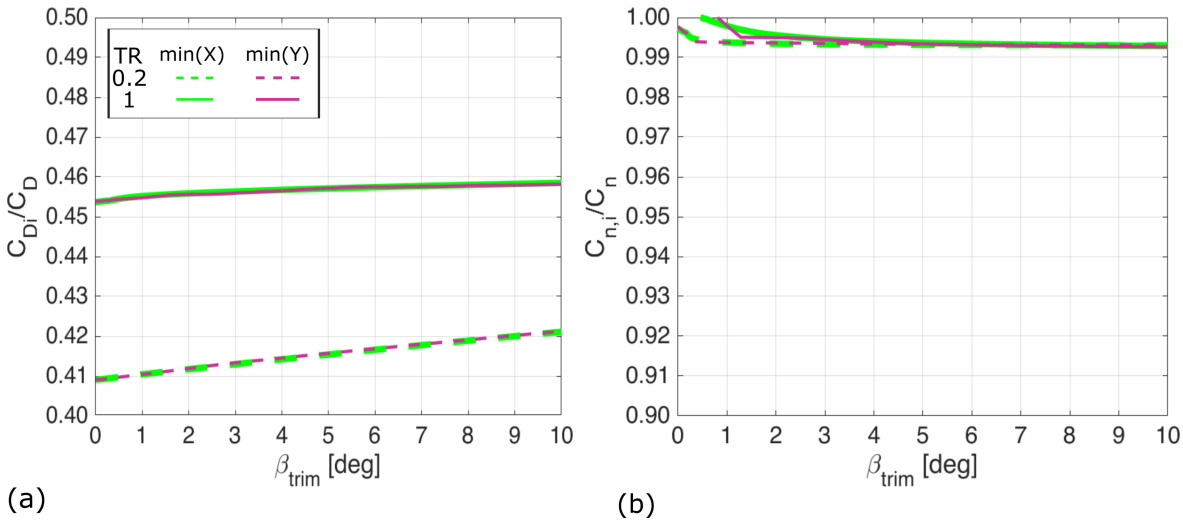

Figure 5.13. Relative contribution of the induced drag to the total drag (**a**) and the yawing moment (**b**) for the 45 degree swept wing. In all cases, the induced drag is responsible for over 99% of the yawing moment produced by this method. This is despite the total drag comprising over 50% profile drag.

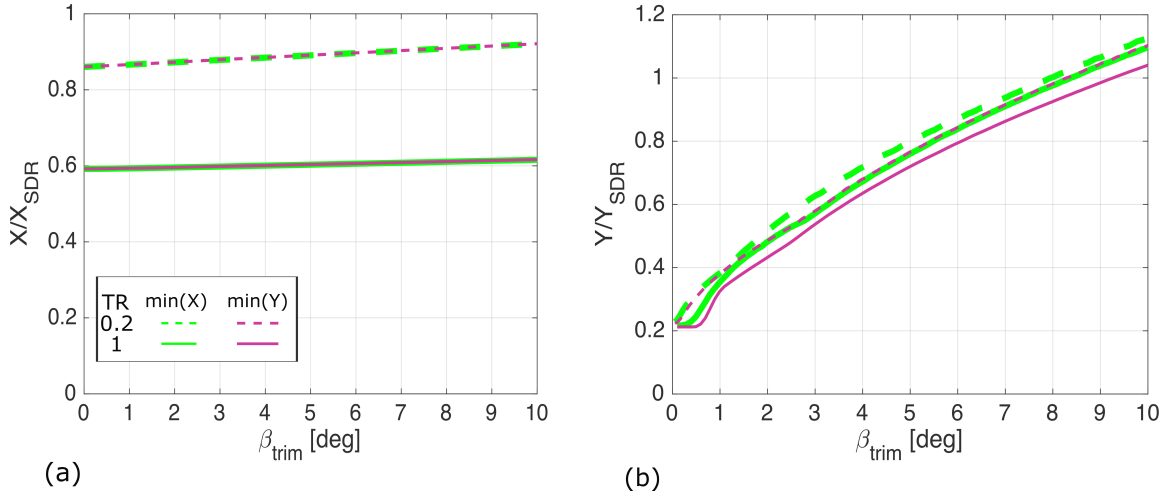

Figure 5.14. Optimisation functions aerodynamic efficiency (**a**) and aggregate control deflection (**b**) objectives for a 45 degree swept wing normalised by the same metrics for a SDR. Variations are shown up to a given sideslip trim angle of 10 degrees.

5.5 Conclusions

This work considers exploiting asymmetries in induced drag distribution on a wing as a primary mechanism by which a required yawing moment can be generated. The presented analysis shows that, for trapezoidal wings, it is possible to generate yawing moments to trim up to 10° of sideslip using only the conventional trailing edge controls. For all cases analysed, the maximum control deflection did not reach the limit of 10° suggesting that it is possible to achieve yawing moments in excess of this. This is achieved through a novel method that can define a control strategy to produce laterally asymmetric drag with no change in the overall lift, pitching moment and rolling moment. The proposed method identifies 'control allocation mode shapes' based upon the zero-sets of surrogate aerodynamic formulation that is originally

based on a range of aerodynamic tools to evaluate the required aerodynamic characteristics including thin aerofoil theory, lifting surface theory and ESDU data sheets. Combinations of these obtained control allocation mode shapes as a function of a required yawing moment could then be optimised against different objectives to define an adequate control strategy. In this work, we have shown that by using a linear combination of the aerodynamic mode shapes, complex control deflections can be defined as function of a small number of gain parameters. This would allow for simple control laws governing the optimum gains as a function of yawing moment to be implemented with little computational expense on the aircraft. This control authority in yaw is useful for designers to explore the removal of vertical stabilising surfaces. Furthermore there is a significant reduction in the aggregate control deflection impact when compared to the case of an SDR, showing the benefit of this proposed method over conventional solutions in terms of both control deflection and drag. This method of control allocation can be applied to any control effector, including fluidic devices, provided the force and moment response can be linearised with respect to the control variable.

The method developed herein was applied into a range of simple untwisted trapezoidal wing planforms. This includes unswept and moderately swept wings and taper ratios of 1 and 0.2. The planform which is best able to achieve the minimum aggregate control deflection and total drag was the wing with the quarter chord sweep of 30 degrees. This was due to a favourable tradeoff between the positive effects of sweep increasing the effectiveness of the outboard control surfaces and the negative effect of increasing the coupling between pitch and roll. For all cases analysed in this paper, introducing taper both improved the aerodynamic efficiency and reduced the aggregate control deflections when producing a yawing moment. As in practice low observable aircraft are generally designed to have moderately swept with a low taper ratio, this is favourable for low observable designs.

We proposed two optimisation objectives for control allocation, maximum aerodynamic efficiency defined in terms of minimising the total drag to achieve a given yawing moment and minimum aggregate control deflection defined in terms of minimising the total projected surface area to achieve a given yawing moment. Our analysis suggests that the most beneficial is to optimise for aggregate control deflection by reducing the exposed area in the normal plane. This is because both optimisation objectives proposed produced results with negligible differences in terms of aerodynamic efficiency. This is to be expected as reducing the area exposed will also reduce the contribution of profile drag. To better interpret our results, we normalised the obtained performances with respect to those of a SDR case. In all demonstrations considered herein, the aerodynamic efficiency of the SDR was inferior to the induced drag modulation method presented. However, the aggregate control deflection benefit is clear in that the aggregate area exposed in the normal plane can be reduced by up to a factor of eight by using the presented method.

Chapter 6

Paper 3: Yaw control of maneuvering tailless aircraft using induced drag – a control allocation method based on aerodynamic mode shapes

Summary

This chapter provides a demonstration of the method developed in Chapter 5 to the MAGMA aircraft. It was originally presented during the 2020 Scitech forum [161]. The contributions of each author are detailed in Table 6.1.

Much of the synthesis of the method is the same as in Chapter 5, however in this case the application to the MAGMA planform provides a reference for the effectiveness of the method on planforms representative of future tailless aircraft concepts. The main objective of this paper was to compare the effectiveness of the mode shaping solution to a more conventional control solution using profile drag based control surfaces.

It was found that for small control inputs, the total control deflection required to achieve a given yawing moment is reduced. This provides an opportunity to define a control allocation method which can be used during mission phases where a stealth requirement would outweigh agility. Typically, these mission phases would be during the cruise phase of flight where only small control inputs are required for course correction and disturbance rejection. Therefore, the developed control allocation method is well suited to this application.

Task	TRS	MRAN	WJC	CW
Funding Acquisition		x	x	x
Supervision		x	x	x
Project Administration		x	x	x
Conceptualisation	x	x	x	x
Methodology	x	x	x	x
Formal Analysis	x			
Investigation	x			
Software	x	x		
Validation	x			
Visualisation	x			
Writing - original draft	x			
Writing - review and editing		x	x	x

Table 6.1. Contributor Roles Taxonomy for Chapter 6

Abstract: *This paper proposes a novel method to achieve three-axis control of a tailless aircraft using conventional conformal trailing edge controls only. The method is based on the synthesis of control allocation modes which produce laterally asymmetric profile drag and induced drag at constant lift, pitching moment and rolling moment. Results are presented for a generic low aspect ratio swept wing planform at a range of trimmed sideslip angles up to 10 degrees, with control allocations optimized for either minimum drag or minimum aggregate control deflection. Obtained solutions have equivalent authority to conventional mid-chord spoilers with reduced overall drag and, at angles of trimmed sideslip less than 4 degrees, reduced aggregate control deflection. This presents designers with an option for directional control which reduces the need for non-conformal controls outside of the low speed flight regime.*

6.1 Introduction

Performance and operational requirements for low observable aircraft drive designs towards all flying wing configurations of moderate sweep ($\Lambda_{LE} = 45°$–$60°$) and low aspect ratio (AR=2-4). The relatively short moment arm of the fin presents challenges for directional stability and control, as relatively large vertical surfaces (fins) are typically required to achieve classical values for fin volume coefficient. As an alternative means of control, some designs utilize drag-based effectors positioned towards the wingtips to effect a yawing moment without the need for permanently deployed surfaces. Whilst these devices are effective, there is a significant increase in required design effort and system complexity due to the strong coupling of these controls between different axes [121]. Furthermore, deployment of non-conformal surfaces to produce drag may have a significant impact on the observability of the platform [122].

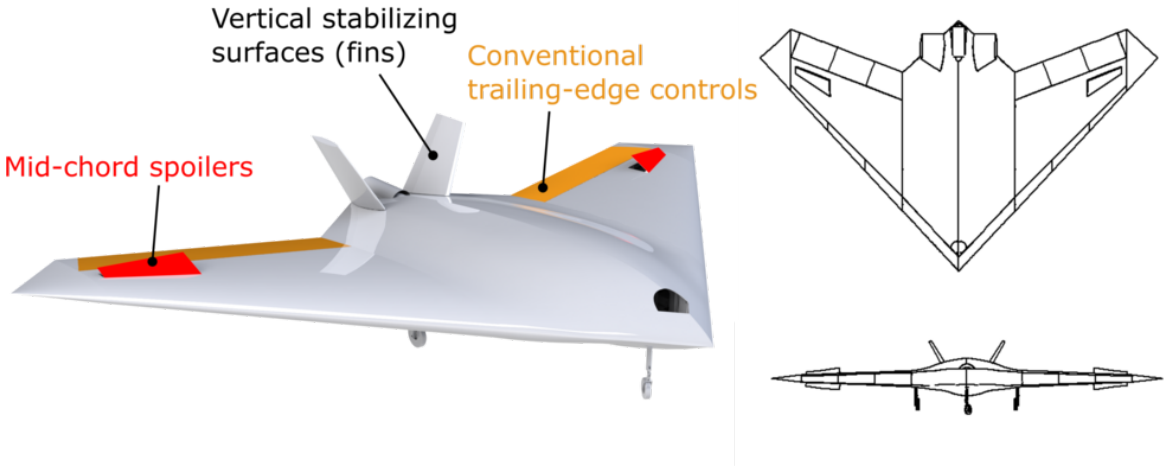

Figure 6.1. Control surface arrangement for the MAGMA aircraft

In this paper, we propose an alternative yaw control method which uses conventional trailing edge controls to generate yawing moments by inducing laterally asymmetric drag with negligible coupling with lift, pitch and roll. As the trailing edge controls are already necessarily present, this may lead to a reduction in control suite complexity. Furthermore, the observability impact of these controls may be mitigated more easily than non-conformal controls such as spoilers. The control allocation method proposed here is developed such that a given yawing moment demand can be achieved with no change in the overall lift, pitching moment or rolling moment. A novel contribution of the work lies in the development of appropriate low order aerodynamic modelling tools and mathematical techniques to identify control allocation modes that can be used to synthesise control inputs against different performance targets.

As a case study, we investigate the application of this method on the MAGMA aircraft, Fig. 6.1. This aircraft was developed at the University of Manchester as a low risk demonstrator for non-conventional flight controls [7]. To date the aircraft has demonstrated the effectiveness of Fluidic Thrust Vectoring (FTV) and Circulation Control (CC) technology. Although the method in this paper is developed for conventional trailing edge controls, we aim in the future to apply the same method for yaw control using CC devices. The aircraft has currently flown in the configuration with fins, providing directional stability but not directional control. Development work for a finless variant using mid-chord spoilers on the upper and lower surfaces has been completed but not yet flight tested. This paper will compare the effectiveness of using mid-chord spoilers and conventional trailing edge controls for directional control. The method is outlined in Section 6.2, results presented in Section 6.3 and conclusions drawn in Section 6.4 .

6.2 Method

6.2.1 Aerodynamic Model

As the method developed in this paper is intended to allow designers to assess control options during preliminary design stages, a computationally inexpensive method of computing the aerodynamic properties due to control surface deflection is required. To model the change in sectional lift and pitching moment coefficients, thin airfoil theory [162] was used to ensure the analysis is robust to an arbitrary airfoil selection.

For the 3D wing modeling, several methods were compared, including: Classical lifting line theory [79], an adapted lifting line theory to include sweep effects [102], Vortex Lattice Method [162] and Lifting Surface (LS) methodology [16]. From these, LS was selected as the most applicable as it best captured the aerodynamic outputs compared experimental reference cases. Moreover, it can be easily adapted for different control methods (e.g. conventional or fluidic controls) with little computational expense.

To validate the applicability of the LS model, model predictions were compared to experimental data from Stenfelt and Ringertz [75]. The experimental data provides information on the yawing moment due to opposing surface deflection on the same side of a tailless aircraft at zero degrees angle of attack. Whilst there is no imposed requirement to maintain trim on other axes, it provides a useful validation case.

The yawing moment generated by the surface deflections is shown in Fig. 6.2. A positive deflection is defined as the outer control surface Trailing Edge Up (TEU) and inner surface Trailing Edge Down (TED). The solid red line on the plot shows the sideslip trim angle whilst accounting for the total drag from deflecting the control surfaces. This total drag comprises the induced drag contribution from the LS model and the profile drag contribution modelled based on ESDU 06014 [151]. Note that, throughout this paper all yawing moments are represented as an equivalent sideslip angle of trim (i.e. $C_n/C_{n\beta}$). $C_{n\beta}$ is in this case evaluated using the LS model without the fins and is a function of angle of attack.

For positive deflections (outer surface TEU) the predicted total drag agrees well with the experimental data, following the lower bound of the experimental uncertainty. However, for negative deflections the model over predicts the yawing moment generated. This is because TED outer control surface deflections promote spanwise flow over the outer control surface, reducing the control effectiveness [142]. As the aim of the study is to minimize the control surface deflection required to generate a specific yawing moment, this is unlikely to limit the applicability of the model. However, results where the outer control surface is deflected greater than 5 degrees TED should be treated with caution.

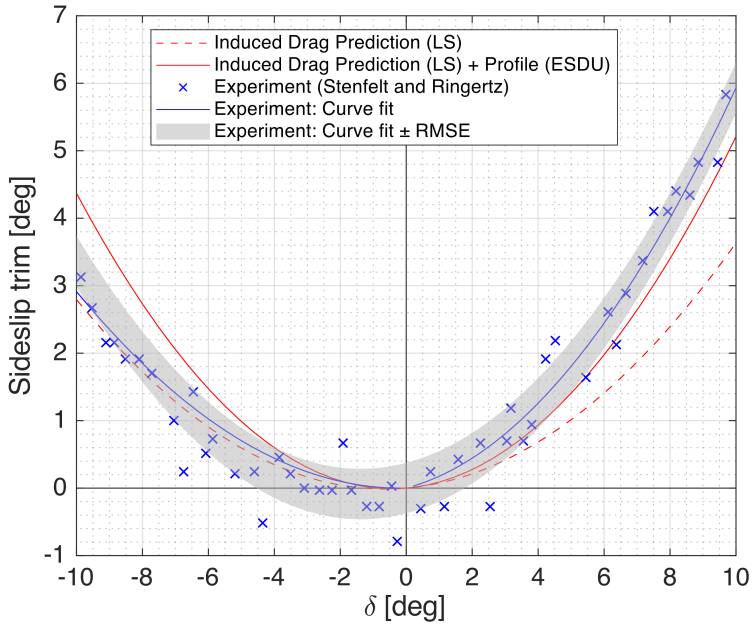

Figure 6.2. Comparison of predicted yawing moment against experimental results for opposing deflections of dual surfaces on the starboard wing. Positive deflection is outer control surface TEU and inner control surface TED. [1]

6.2.2 Control Allocation

The aim of the control allocation strategy developed within this section is to achieve a specific sideslip demand with no change in lift, pitching moment or rolling moment from the trim state. This objective has been previously attempted as a pure control allocation problem (i.e. using closed loop control [152]). However, here, this method is developed in the aerodynamics context through using a combination of aerodynamic mode shapes which ensure that these constraints are always implicitly satisfied. We define aerodynamic mode shapes as unique laterally asymmetric lift distributions which satisfy the requirements of no net change in lift, pitching moment or rolling moment. Control allocation mode shapes are defined as the control surface deflections which yield a lift distribution corresponding to an aerodynamic mode shape. Therefore, the two definitions of mode shape are highly related and are interchangeably referred to as modes shapes. To identify these mode shapes, a method is developed based upon the null space (or zero sets) of a control derivative matrix. This method is similar to methodology used in identifying stable PID gains within a known system (see for example [153]), but is extended such that the output of the method identifies control surface deflections based on aerodynamic inputs; in this case angle of attack and sideslip. This is a novel way of dealing with control surface effects through allowing a suite of control surface deflections to

[1] A correction factor applied to the LS result could capture the effect of spanwise flow on the yawing moment. However, the modeling of the effects of spanwise flow are planform specific beyond the scope of this work. Instead the uncorrected result from LS is used to demonstrate the control allocation strategy within this chapter and throughout the thesis. Future work may wish to include the non-linear effects of flow breakdown within the control allocation strategy.

be described as mode shapes; linear combinations of which have no effect on lift, pitching moment or rolling moment but are laterally asymmetric to induce a yawing moment. To establish the mode shapes for a given geometry, we must first construct a control derivative matrix. Using the aerodynamic models described in the previous section, we evaluate the aerodynamic forces and moments for a set of control surface deflections selected using Latin hypercube sampling [154]. Due to the linear assumptions within the models selected in the previous section, the lift, pitching moment and rolling moment responses to control surface deflection are constant with angle of attack. The response functions for the drag and yawing moment are quadratic and functions of angle of attack. Therefore, we must evaluate the forces and moments for each angle of attack we wish to analyze.

With the aerodynamic data being constructed, we fit a response function for the aerodynamic force and moment coefficients using response surface methodology [157]. This allows for further reductions in computational cost to evaluate the aerodynamic forces and moments, and allows for the calculation of the mode shapes. The response functions take the form:

$$C_L = B_0 + \sum_{i=1}^{N} B_i \delta_i \tag{6.1}$$

$$C_m = C_0 + \sum_{i=1}^{N} C_i \delta_i \tag{6.2}$$

$$C_l = D_0 + \sum_{i=1}^{N} D_i \delta_i \tag{6.3}$$

$$C_D = E_0 + \sum_{i=1}^{N} E_i \delta_i + \sum_{i=1}^{N-1} \sum_{j=i+1}^{N} F_{i,j} \delta_i \delta_j + \sum_{i=1}^{N} G_i \delta_i^2 \tag{6.4}$$

$$C_n = S_0 + \sum_{i=1}^{N} S_i \delta_i + \sum_{i=1}^{N-1} \sum_{j=i+1}^{N} T_{i,j} \delta_i \delta_j + \sum_{i=1}^{N} U_i \delta_i^2 \tag{6.5}$$

For all geometries analyzed by the authors, the functions in this form have a coefficient of determination (r^2) of unity. As Eq. (6.1) – Eq. (6.3) are linear, they can be written in the form of Eq. (6.6) given the constraint that the aircraft must maintain lift and trim in pitch and roll (i.e. $\Delta C_L = 0$,$C_m = 0$ and $C_l = 0$).

$$\begin{bmatrix} 0 \\ -C_0 \\ 0 \end{bmatrix} = \begin{bmatrix} B_1 & B_2 & \cdots & B_N \\ C_1 & C_2 & \cdots & C_N \\ D_1 & D_2 & \cdots & D_N \end{bmatrix} \begin{bmatrix} \delta_1 \\ \delta_2 \\ \vdots \\ \delta_N \end{bmatrix} = \bar{\bar{R}}\bar{\delta} \tag{6.6}$$

The left hand side of Eq. (6.6) describes the trim state of the aircraft. On the right hand side

row 1 specifies the change in lift, row 2 specifies the pitching moment, and row 3 specifies the rolling moment, all with respect to control surface deflection. As for a stable aircraft with no control surface deflection there will be a nose down pitching moment (C_0), this is included on the LHS to ensure the aircraft is longitudinally trimmed. Note that there is no equivalent on the LHS for rolling moment coefficient because for zero control surface deflection, a balanced aircraft should have no rolling moment.

As MAGMA has 6 control surfaces in total, Eq. (6.6) is rank deficient and thus there are infinitely many solutions. Any δ which satisfies this system will maintain lift and trim in pitch and roll, however is not necessarily laterally symmetric and therefore may produce a yawing moment. However, identifying the solution for a given yawing moment (Eq. (6.5)) is non-trivial, involving the solution of a second order function of 6 variables (i.e. the control deflection for each surface).

To reduce the complexity of the system, we take the null space of $\bar{\bar{R}}$ (i.e. solutions of $\bar{\delta}$ which satisfy $\bar{\bar{R}}\bar{\delta} = 0$). Each of the null space vectors can be thought of as analogous to a mode shape (i.e. Eigen vector of the system). Any combination of these modes will ensure that the constraints of lift, pitching moment and rolling moment are satisfied but are laterally asymmetric. The solutions of the mode shapes for the MAGMA planform are visualized in Fig. 6.3. Note that as each of the equations in $\bar{\bar{R}}$ are independent of angle of attack, these mode shapes do not change with angle of attack. However, the combination required to optimally achieve a required yawing moment will change with angle of attack.

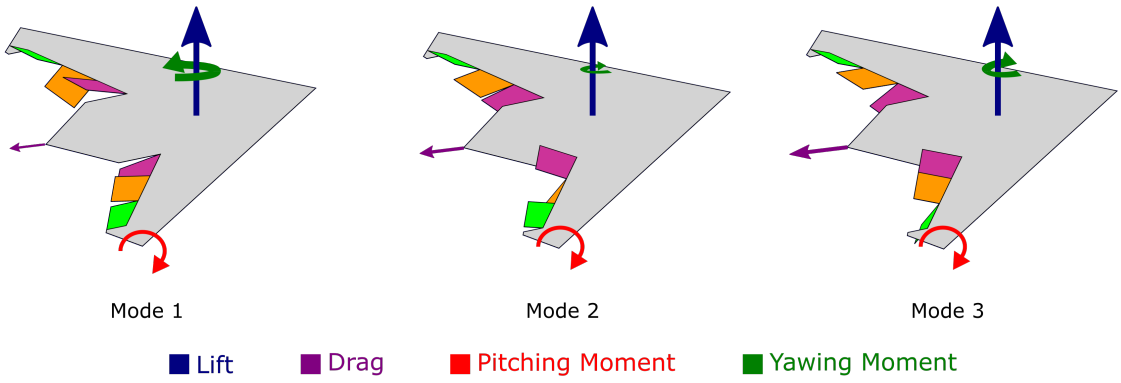

Figure 6.3. Control allocation mode shapes and aerodynamic forces and moments on the MAGMA planform. Rolling moment not shown as it is zero for all cases. For all three modes the lift and pitching moment are equal. The drag and yawing moment differs due to the asymmetric lift induced drag and profile drag.

The null space matrix, $\bar{\bar{n}}$, is next formed by assembling the null space vectors as the columns of $\bar{\bar{n}}$. This can then be multiplied by a vector of gains ($\bar{k}$) such that the deflection can be written as a function of the gains and control surface deflections required to trim (δ_0):

$$\bar{\delta} = \bar{\delta_0} + \bar{\bar{n}}\bar{k} \tag{6.7}$$

In doing this: the six unknown deflections are reduced to three unknown gains, and the constraints on lift, pitching moment, and rolling moment are implicitly satisfied. This is computationally significant, as the size of the problem is reduced and trim conditions are always satisfied. However, we still have three variables and only one objective (i.e. a target yawing moment/sideslip angle). Therefore to identify an optimal solution, the designer must select a further objective to optimise. In this study we present two examples: The first objective is to maximise aerodynamic efficiency of generating a yawing moment, measured in Eq. (6.8) as the drag coefficient for a given yawing moment, X. Thus the aerodynamic efficiency is maximised where X is minimised. The second objective considered in this study is to minimise the area exposed in the normal plane by the control surface deflection (denoted as Y), and defined in Eq. (6.9) as the sum of the surface area of each control surface multiplied by the sin of its deflection angle.

$$X = C_D(\bar{k})|_{C_n} \tag{6.8}$$

$$Y = \sum_{i=1}^{N} \left(A_i \sin(\delta_i(\bar{k})) \right|_{C_n} \tag{6.9}$$

These metrics serve as surrogates for performance and observability design drivers (X and Y respectively). It is expected that they will yield similar results as minimising the total surface deflections will reduce the profile drag due to control surface deflection. However, where the greatest design pressure is observability, designers will generally be willing to accept relatively large increases in drag (X) for improvements in observability (Y).

Although analytical solutions to these objectives are possible, they are both analytically complex and specific to the objective(s) selected. Therefore in this paper, a numerical optimizer is utilized. This computes the optimization functions over a range of $\bar{k}$ which yield the required yawing moment and selects the point which minimizes the objective function. Whilst computationally more expensive than optimization algorithms such as interior point, it is more numerically robust and requires computational times of less than 20s on a standard laptop per optimization.

6.3 Results

In this section, we compare the control effectiveness of spoilers and mode-shaping to trim the aircraft at a given sideslip angle. The effectiveness of the spoilers was modeled using semi-empirical methods taken from ESDU 96026 [160]. They are operated with a bias angle of 30° [121] to mitigate coupling effects [2]. The geometric and aerodynamic properties used in this section are summarized in Table 6.2 for the aircraft without a fin.

Property	Value	Comment
Wing span $[m]$	4.01	
Wing Aspect Ratio	3.4	
Spoiler Area $[m^2]$ (total)	0.16	
Wing lift curve slope $[rad^{-}1]$	3.09	Evaluate from LS model
Wing zero-lift drag coefficient (C_{d0})	0.0119	[149] - Empirical
Yawing moment due to sideslip (N_v)	$0.26C_L^2 - 0.0015$	[163] - Analytical

Table 6.2. Geometric and aerodynamic properties.

The maximum achievable sideslip angle as a function of angle of attack was evaluated, Fig. 6.4. The maximum yawing moment was limited by the maximum deflection of the control surface, this is 90° for the spoilers and 10° for the trailing edge control surfaces used for mode-shaping. The reason for limiting control surfaces to just 10° is to ensure that the assumption of linear aerodynamics in the underlying models is applicable. Fig. 6.4 suggests that both methods of control have a greater authority at lower angles of attack. This is because the aircraft becomes more directionally stable at higher angles of attack [163]. For both mode-shaping and spoilers the yawing moment generated is almost constant with angle of attack. Note that although it would appear mode-shaping reaches a plateau of effectiveness, this is because the maximum sideslip angle evaluated was 10 degrees not that the control is saturated. This constraint corresponds to a 10kt crosswind at landing (for MAGMA, the anticipated most onerous case).

As the technique is most effective at lower angles of attack (and equivalently low C_L), the following examples explore the effectiveness of the method at an angle of attack of 1°. Fig. 6.5, shows the control allocations required for minimizing aerodynamic drag (left) and aggregate control deflection (right). The control strategy is similar for both optimization objectives, with the port wing control surfaces deflecting in alternate directions to maximize the induced drag. The actuation of the starboard wing is subtly different although for both cases there is little movement of these control surfaces.

The metrics for each optimization are compared to those of the spoilers, Fig. 6.6. Both optimization function yield similar results for the aerodynamic drag (X), which is 16% of the drag produced by the spoilers. The aggregate control deflection for mode-shaping (including

[2]The bias is added to the SDR implementation to prevent control coupling due to SDR deflection. This is not required for the mode shaping implementation as the coupling is not present.

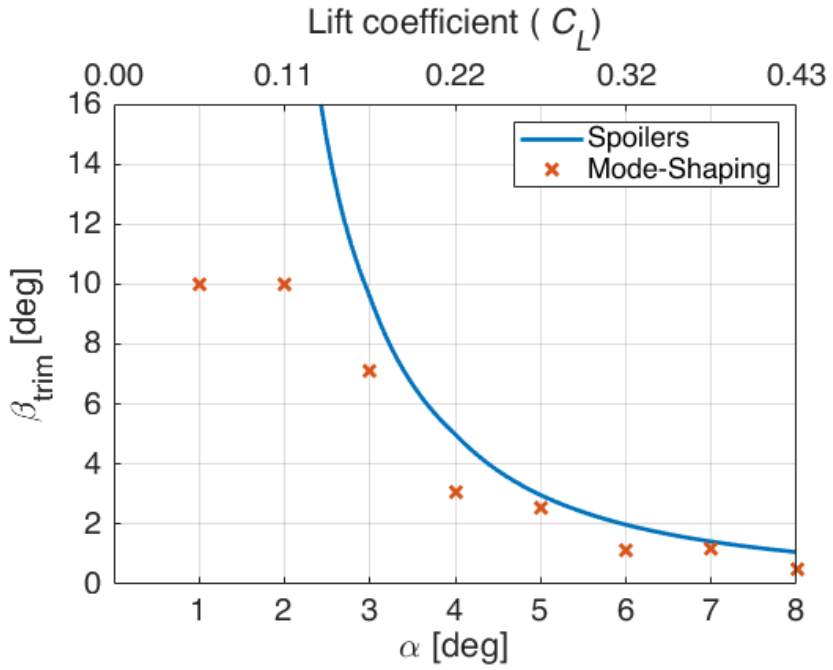

Figure 6.4. Maximum achievable sideslip trim using spoilers and mode-shaping. Note that for mode-shaping, the maximum sideslip angle evaluated was 10 degrees.

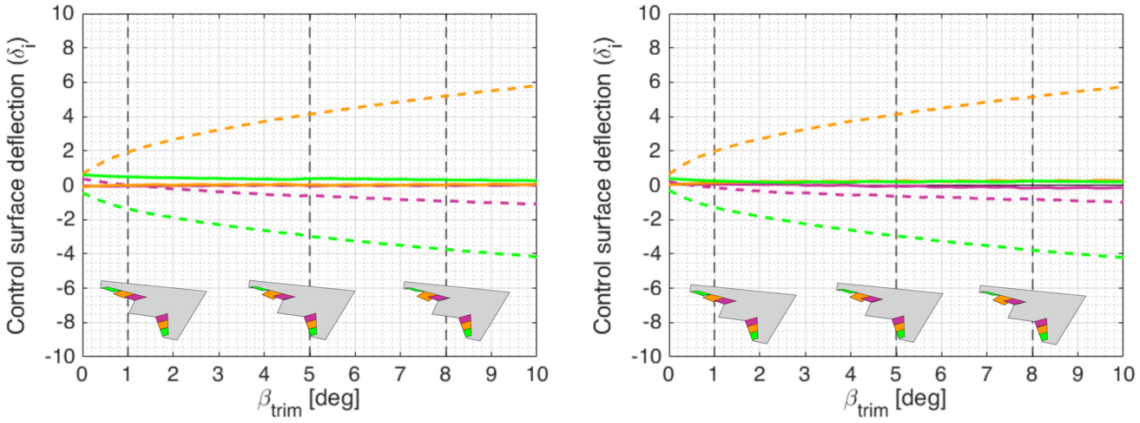

Figure 6.5. Control allocations for generating a yawing moment. Left shows solution for minimizing aerodynamic drag (X) and right for minimizing aggregate control deflection (Y). The overall strategy is similar in both cases.

both optimization objectives) is less than that of the spoiler for small sideslip angles ($\beta \leq 4$). Comparing the mode-shaping results for both objectives, setting the optimization objective to reduce the aggregate control deflection shows a marginal improvement compared to minimizing drag. This is not unexpected, as the control allocations shown in Fig. 6.5 also showed a consistent behavior.

Finally, to explore the mechanisms responsible for the yawing moment we examine the contribution of induced drag to the total drag and yawing moment, Fig. 6.7, for the mode-shaping case to achieve $min(Y)$. It can be seen here that although the induced drag comprises only less than 5% of the total drag, it is responsible for just over 50% of the total yawing

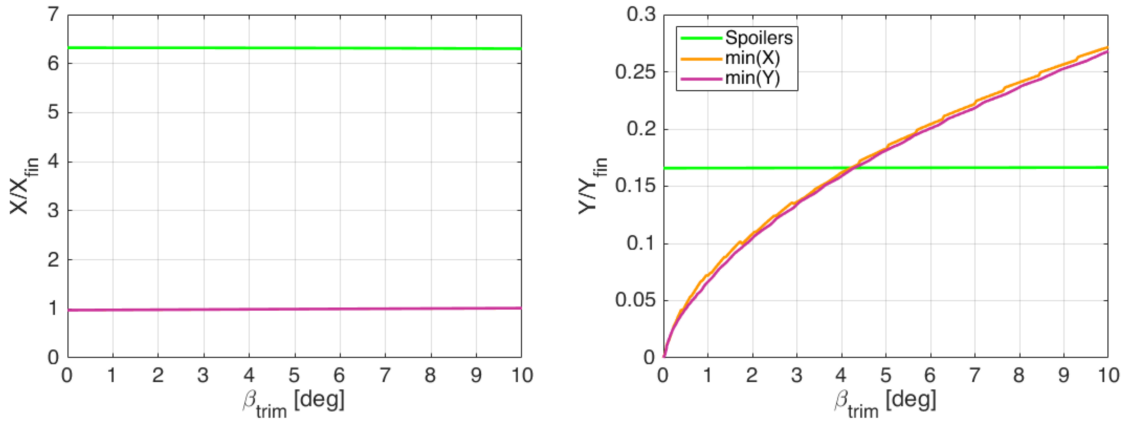

Figure 6.6. Optimization metrics for $\alpha = 1^\circ$ normalized by values for the fins. Mode-shaping produces 16% of the drag of spoilers and shows a reduction in aggregate control surface deflection for $\beta < 4^\circ$.

moment. From this, we can deduce that the alternating deflection on the port wing acts partly like a spoiler increasing the profile drag but also generates a roughly equal increase in induced drag which acts in the same sense, further increasing the yawing moment generated. The additional induced drag produced by this method means that the same yawing moment can be produced for a reduced total control surface deflection.

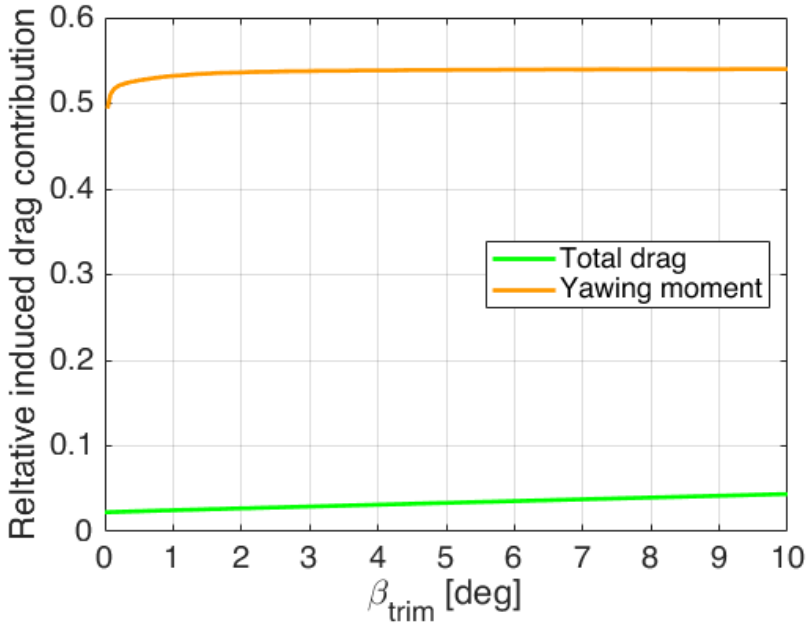

Figure 6.7. Induced drag contribution to total drag and yawing moment. Despite the induced drag being less than 5% of the total drag it contributes over 50% to the yawing moment.

6.4 Conclusion

The work presented shows that asymmetric control surface deflection can produce sufficient yawing moments by exploiting the asymmetries caused in both induced and profile drag. The method for assigning these deflections identifies mode shapes based upon the zero-sets of surrogate aerodynamic models. These models are based on a range of aerodynamic tools to evaluate the required aerodynamic characteristics including: thin aerofoil theory, lifting surface theory, and ESDU data sheets. Combinations of these obtained mode shapes, as a function of a required yawing moment, could then be optimized against different objectives to define an adequate control strategy. In this work, we have shown that by using a linear combination of the aerodynamic mode shapes, complex control deflections can be defined as function of a small number of gain parameters. This would allow for simple control laws governing the optimum gains as a function of yawing moment to be implemented with little computational expense on the aircraft. This control authority in yaw is useful for designers to explore the removal of vertical stabilizing surfaces. However, for terminal flight phases where high control authority is required, more conventional directional control solutions may still needed. This reduces some of the benefits compared to a pure mode shaping approach but nevertheless allows a space to explore in the trade-off between mission and performance requirements.

Comparisons with conventional drag based methods of directional control (i.e. spoilers) have shown that mode-shaping can achieve comparable directional control authority across all cases analyzed ($C_L < 0.43$). In the configuration analyzed, using a mode-shaping method has shown a reduction in drag six times that of using spoilers and furthermore a reduction in the aggregate control deflection required for $\beta < 4^\circ$. The reduction in aggregate control deflection is shown to be greater than 60% for $\beta < 1^\circ$.

The control authority of both spoilers and mode-shaping reduces as the angle of attack increases. In the configuration analyzed this results in a maximum sideslip trim angle at $\alpha = 8^\circ$ of $\sim 1^\circ$ ($C_L = 0.43$). This would not be sufficient for a crosswind approach and landing and therefore a more authoritative directional control method would be required for this case (for example larger spoilers/split elevons). However, mode-shaping provides sufficient control authority for stability augmentation and disturbance rejection meaning that large deflections of non-conformal controls would only be required for terminal phases of a flight. This is beneficial for both performance and observability requirements. Furthermore, if the method is applied to circulation control devices then this could provide a method for directional control without the need for external moving parts.

Chapter 7

Paper 4: Coordinated rolling manoeuvres using lift-based effectors

Summary

This chapter builds on the method described in Chapter 5 and Chapter 6 to extend the method from steady state to a control method used for the mitigation of adverse yaw during a rolling manoeuvre. The journal paper from which this chapter is taken is currently not published, but will be submit to IEEE Access. The contributions of each author are detailed in Table 7.1.

The work in this chapter develops a dynamic control allocation scheme which calculates the required control deflection to maintain the vertical component of lift and zero sideslip during a rolling manoeuvre. For the manoeuvre, the aircraft starts trimmed wings level and the aircraft flight paththe dynamics modeled from initiation until a bank angle of 45° is achieved. A dynamic inversion approach is used to calculate the required moment coefficients for a roll which is coordinated in all three axes. The control allocation is then performed using both a split drag rudder configuration and the mode shaping configuration to compare the effectiveness.

This work is applied to a generic trapezoidal planform to show the general applicability of this method. The planform is of low aspect ratio and moderate sweep to be representative of a typical tailless aircraft. The potential of the mode shaping approach to be used as part of a full 3-axis control solution is demonstrated. However, noting the limitations such an application would place on the agility the main use case is likely for course corrections and disturbance rejection during the cruise phase of a mission.

Task	TRS	MRAN	WJC	CW
Funding Acquisition		x	x	x
Supervision		x	x	x
Project Administration		x	x	x
Conceptualisation	x	x	x	x
Methodology	x	x	x	x
Formal Analysis	x			
Investigation	x			
Software	x	x		
Validation	x			
Visualisation	x			
Writing - original draft	x			
Writing - review and editing		x	x	x

Table 7.1. Contributor Roles Taxonomy for Chapter 7

Abstract: *The attitude control of tailless aircraft is typically achieved through a system of trailing edge flaps with combined effectiveness in both pitch and roll. However, these surfaces exhibit a degree of coupling in the yaw axis. This paper presents a novel control allocation method which allows for the trailing edge controls to generate yawing moments with no coupling. This is demonstrated through a typical rolling manoeuvre to negate the yaw coupling and provide the required control authority to complete the manoeuvre without the need for additional control surfaces. Analysis shows that for a typical tailless aircraft configuration, it is possible to perform a coordinated rolling manoeuvre using only the trailing edge controls with a reduction of at least 30% of the required control deflection compared to a typical profile drag based control solution.*

7.1 Introduction

In recent years, there has been an increased interest in tailless, all flying wing configurations. As a results, there have been many subscale tailless aircraft demonstrators for both civil [164]–[166] and military [6], [7], [48] concept testing. These configurations result in very small moment arms for the vertical fins resulting in larger surfaces to meet given stability and control requirements. For both civil and military aircraft there is a pressure to reduce the size of these fins due to the drag and, more so for the military concepts, the observability impact [167], [168]. However, if the fins are removed typically the aircraft will become directionally unstable; in this case the aircraft would be particularly susceptible to departure from controlled flight if sideslip were induced.

A manoeuvre which commonly induces sideslip is the aircraft roll manoeuvre. This manoeuvre will be necessary in any aircraft mission in order to effect a change in the aircraft's heading. This is typically affected by deflection of wing trailing edge controls to introduce

a lateral asymmetry in the spanwise lift distribution and hence rolling moment about the aircraft centre-line. However, the control inputs will also cause a change in spanwise drag distribution and this will introduce a secondary yawing moment, leading to some degree of roll-yaw coupling [17], [54], [112], [134], [169], [170]. For roll manoeuvres used to turn an aircraft, the roll-yaw coupling due to control surface deflection is adverse in the sense that it leads to an out of turn (uncoordinated) moment and hence sideslip.

The magnitude of adverse yaw generated during a rolling manoeuvre can be minimised by effective design of the wing trailing edge control surfaces and control allocation strategy. One such method of this is by tailoring the symmetric lift distribution (i.e. Cruise) such that deflecting the control surfaces generates a proverse yawing moment. This has been shown to be successful through analytical [112]–[114], [147], [170], [171], numerical [71], [113], [172] and experimental [145], [173] work. These methods work by using a Bell shaped distribution, developed by Prandtl [146], [174] and later Nickel [112] using different assumptions, along with strategic aileron placement such that the upgoing control surface generates a greater induced drag than the downgoing control surface. Although this method is succesfull in aleviating the impact of adverse yaw, it does not present a solution to the problem of directional control. This is because, for a directionally unstable aircraft, any sideslip perturbation will inherently grow until the aircraft departs. Therefore if any yawing moment is produced due to a roll input, whether that is adverse or proverse, a sideslip will be introduced. Without some other means of yaw control to counteract this, the aircraft will depart from controlled flight.

To provide yaw control, some studies have investigated continuous control of the spanwise load distribution by means of morphing [145], [147]. These solutions appear to provide control authority which is sufficient for full 3-axis control of an aircraft. However, the actuation systems are typically complex and require high torque output compare to conventional control surfaces [145]. A more typical solution would be to use Split Drag Rudders (SDRs), which, when deployed, produce laterally asymetric drag on the airframe and therefore a yawing moment [54], [132]. Through control allocation algorithms efforts have been made to reduce the observability impact of these control surfaces [122], however there is still a performance and observability penalty for use of this control method.

An alternative method of yaw control uses laterally asymetric induced drag created by actuating control surfaces on the same wing in opposing directions [75], [76], [134]. This method has the advantage of not introducing any additional control surfaces to the wing and the weight and additional complexity of the associated actuators. However, in the method proposed in these studies the inboard and outboard effectors are actuated by an equal magnitude in the opposing sense. Whilst this will produce a yawing moment, there will also be a secondary effect in both pitch and roll.

In this paper we propose an alternative yaw control approach which uses only the trailing edge controls. The control surfaces are deflected in such a way to induce laterally asymmetric induced drag, but whilst maintaining the required lift, pitching moment and rolling moment [53], [130], [161]. As these controls are already necessarily present for control purposes there is no increased complexity of adding extra actuation systems, and the observability impact will also be minimized. Previous works by the authors [130], [161] (Chapter 5 and Chapter 6) have shown the potential of this control method to trim an aircraft in steady sideslip where trailing edge controls can reduce both the drag (indicator for aerodynamic efficiency) and required control surface deflection (indicator for observability) when compared to wing-tip drag devices. This paper will build on these previous contributions and will extend them to demonstrate the potential of this novel control method for yaw control during a rolling manoeuvre.

7.2 Theory

Adverse yaw can be well understood using low order tools such as Prandtl's lifting line. Prandtl hypothesised that the induced drag on a wing section is a function of the lift on that section and the angle of attack induced at that section due to downwash. Both of these quantities are functions of the spanwise lift distribution: the lift on a section can be found directly from the lift distribution and the downwash (and therefore induced angle of attack) is a function of the derivative of the distribution. Therefore, we can think of induced drag at a section as proportional to the product of the magnitude and derivative of the spanwise lift distribution at that section (i.e. $C_{di}(\eta) \propto C_l(\eta)\frac{\partial C_l(\eta))}{\partial \eta}$ where $C_l(\eta)$ is the local lift coefficient).

By understanding the relationship between the lift distribution and induced drag, the explanation of adverse yaw is apparent. Consider an unswept, untwisted rectangular wing of aspect ratio 5 with control surfaces extrema at 90% and 60% span. If these control surfaces are deflected to induce a rolling moment to starboard wing (i.e. port wing trailing edge down, starboard wing trailing edge up) the lift distribution is modified as shown in Fig. 7.1. This leads to a large increase in drag on the starboard wing and a large decrease in drag on the port wing, generating the adverse yawing moment.

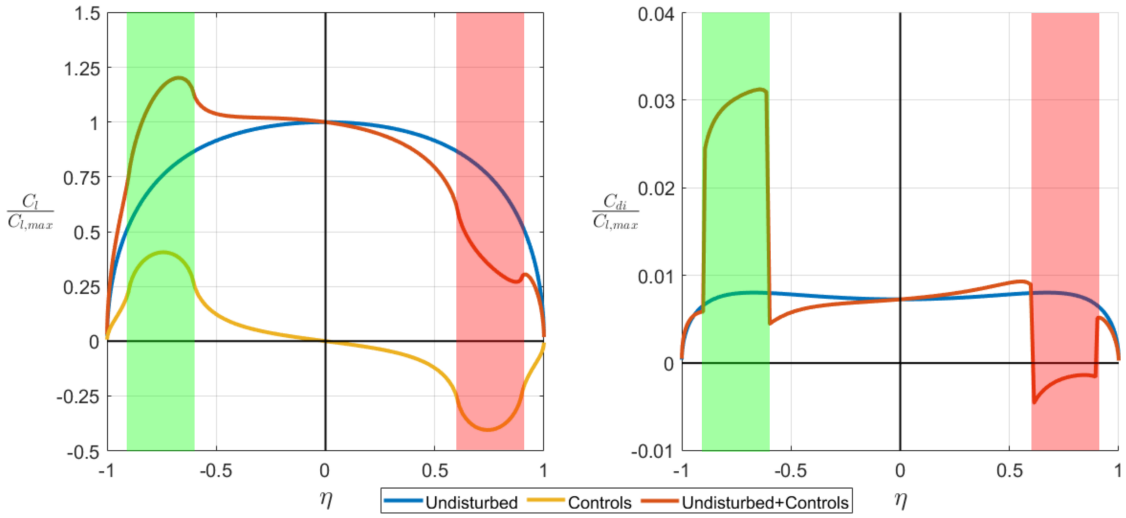

Figure 7.1. Lift and Induced drag distribution for an unswept, untwisted rectangular wing of aspect ratio 5. Green region has control surfaces deflected 3° downwards and red region has control surfaces deflected 3° upwards. The induced drag in the green region is greater than the red leading to a roll to the right, but out of turn yaw to the left.

7.3 Method

7.3.1 Case Study Aircraft

The aircraft selected to demonstrate the efficacy of our proposed method is taken to be representative a generic future, low observable UAV. It is therefore of low aspect ratio and moderately swept. The geometry and assumed inertia are described in Table 7.2, and the control surface layout is presented in Fig. 7.2. The sweep angle is selected so that the leading edge sweep is greater than 45 degrees but less than 60 degrees to avoid the formation of strong leading edge vortices [175]. The inertia of the aircraft is estimated by assuming a uniform mass distribution over the planfrom.

Parameter	**Quantity**
Aspect Ratio	3
Wing Span	$4m$
Taper ratio	0.2
Quater-chord sweep	45°
Leading edge sweep	51°
Mass	$100kg$
I_{xx}	$89kgm^2$
I_{yy}	$42kgm^2$
I_{zz}	$131kgm^2$

Table 7.2. Aircraft geometry and inertia.

The layout in Fig. 7.3 shows the two control surface arrangements considered in this work. The first is shown on the starboard wing with a layout in which the two most inboard control surfaces are used for pitch and roll control (i.e. in the conventional sense) and the outer control

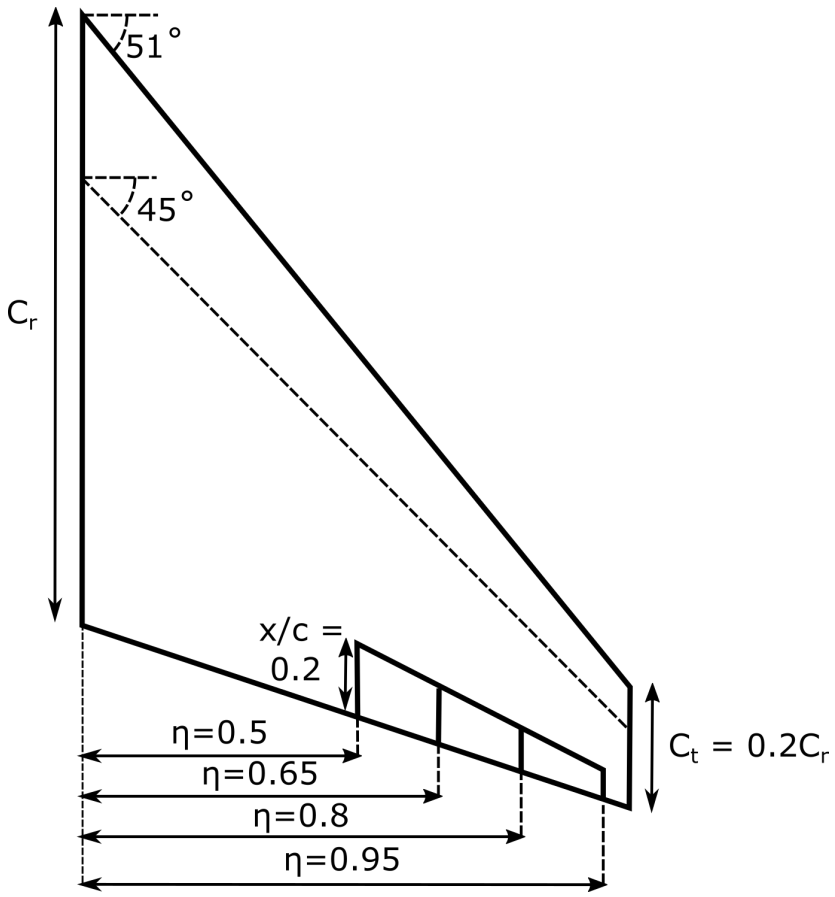

Figure 7.2. Geometry of the case study aircraft.

surface is replaced with a Split Drag Rudder (SDR). In this configuration the SDR is primarily used for yaw control of the aircraft although there are some secondary control effects in roll and pitch.

The second arrangement is shown on the port wing employing the mode shaping approach in which the control surfaces are deflected in such a way which induces asymmetric induced drag but does not otherwise affect the trim state of the aircraft. In this configuration, the pitch and roll of the aircraft are controlled by changing the symmetric and antisymmetric components of the control deflection (Fig. 7.4). This will have some secondary control effect in yaw, due to the adverse yaw effect discussed in Section 7.2. However, we can define an additional asymmetric component using the mode shaping technique. The control mode shape defined is laterally asymmetric however is designed such that the change in lift distribution produces no change in pitching moment, rolling moment or lift. Therefore, by this additional asymmetric component we can produce a yawing moment to counteract the adverse yaw due to the antisymmetric deflection and use the remaining control authority for yaw control which is independent of the symmetric and antisymmetric deflections.

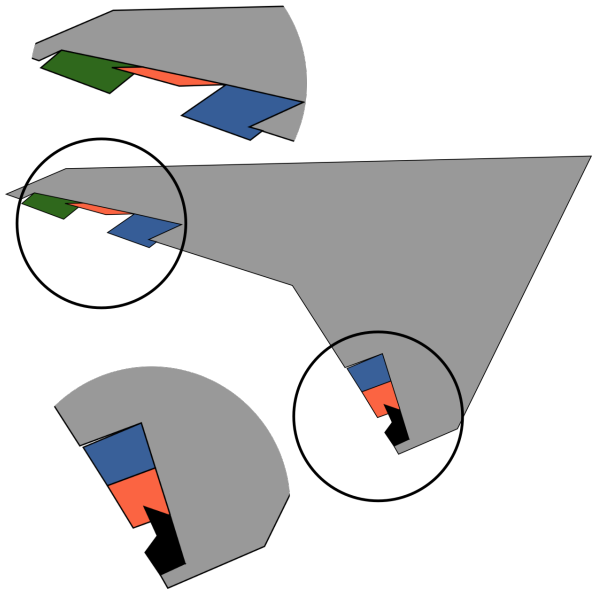

Figure 7.3. Control configurations tested. Port: asymmetric control deflection (mode shaping) to produce laterally asymmetric drag using only conventional control surfaces. Starboard: Typical Split Drag Rudder configuration.

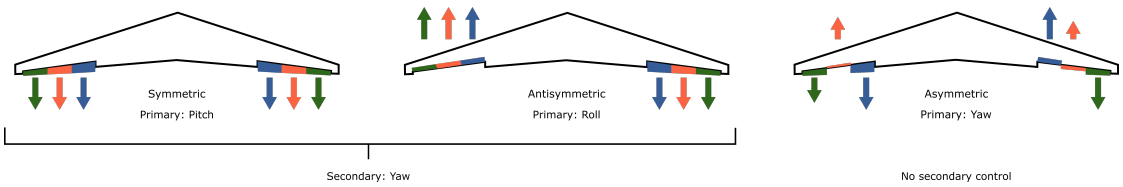

Figure 7.4. Symmetric, Antisymmetric and Asymmetric control components illustrated independently. The control input using only the trailing edge controls is produced by a combination of these three components.

7.3.2 Manoeuvre Modelling

In order to assess the effectiveness of each control surface arrangement specified in the previous section, the state of the aircraft must be modelled through a rolling manoeuvre. A summary of the process used to perform this is shown in Fig. 7.5. The section enclosed within the broken lines indicate the models used within this work to assess the efficacy. However, if this method were to be implemented in flight this would be replaced with the aircraft actuation systems and sensors to ascertain the aircraft state.

To begin the manoeuvre, the aircraft is initially trimmed wings level at a specified angle of attack. There is then a step antisymmetric control input to begin the roll, the magnitude of this input will be discussed in Section 7.3.4. The aircraft state and control input are then passed to the aerodynamic model to calculate the forces and moments. Depending on the implementation this block can be replaced with any model which takes the aircraft and control states and outputs forces and moments. In this work we use a modified lifting surface method described in Section 7.3.3. These forces and moments are then passed to a flight dynamics model. Again, when implementing this method any flight dynamics model could be used.

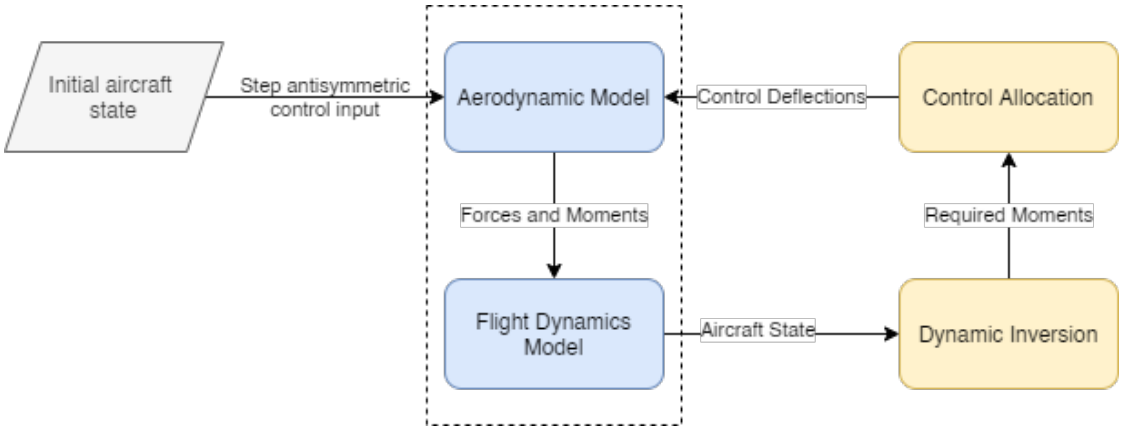

Figure 7.5. Process used to calculate model rolling manoeuvre. The blocks in broken lines would be substituted for control actuators and sensors to read the aircraft state if implemented in flight.

In this implementation, we assume that at all points during the rolling manoeuvre the turn is coordinated, and the vertical component of lift is maintained, reducing the complexity required.

The aircraft state is then passed to the dynamic inversion block which calculates the required pitching and yawing moment required to maintain the required angle of attack and zero sideslip. This process is detailed in Section 7.3.4. Finally, the controls are updated using the control allocation method described in Section 7.3.4 and 7.3.4 for the SDR and mode shape configurations respectively.

7.3.3 Aerodynamic Modelling

To allow for efficient computation of aerodynamic forces and moments within the manoeuvre modeling, a low order aerodynamic model was used to reduce the computational expense. The selection of the most appropriate low order model for this task, performed previously by the authors, can be found in [130], with the Lifting Surface (LS) model [16] identified as the preferred approach. It was selected as, of the methods considered, it best captured the aerodynamic outputs compared experimental reference cases and can be easily adapted for different control methods with little computational expense. The implementation of the lifting surface model, including the treatment of control surfaces, is fully discussed in [130], so details will not be repeated here, and only key considerations will be discussed in what follows. The aerodynamic modelling process is, also, summarized in Fig. 7.6.

The lifting surface model calculates the spanwise (γ) and chordwise (μ) load distributions for a given geometry through the solution of a linear system of Aerodynamic Influence Coefficients (AIC). The assembly and inversion of the AIC matrix is the most computationally expensive part of the model. As the AIC must be reconstructed and therefore inverted every time the sideslip angle changes, we use a process of linear superposition to remove this

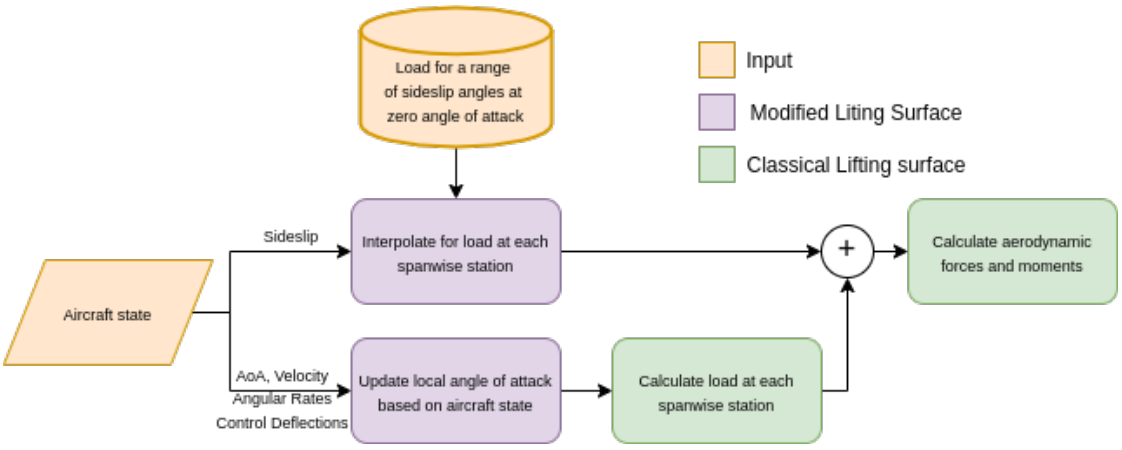

Figure 7.6. Modified lifting surface model.

reformation from the process (see Fig. 7.6). To acheive this, the spanwise and chordwise load distributions are calculated for a range of sideslip angles at zero angle of attack (i.e $\gamma(\beta)|_{\alpha=0^\circ}$ and $\mu(\beta)|_{\alpha=0^\circ}$); these distributions are then superimposed with the load distribution calculated at each time step from the state given by the flight dynamics model (i.e $\gamma(\alpha)|_{\beta=0^\circ}$ and $\mu(\alpha)|_{\beta=0^\circ}$)). In this way, LS evaluations are dramatically reduced allowing efficient execution.

To calculate the load distribution at zero angle of attack, the angular rates of the aircraft must be taken into account as these will modify the local angle of attack as a function of the spanwise location. An intermediate angle of attack is found as the sum of the geometric angle of attack and the change due to pitch and roll rate:

$$\Delta\alpha_0(\eta) = \alpha_g + \Delta\alpha_p + \Delta\alpha_q \tag{7.1}$$

Roll rate is accounted for by changing the local angle of attack at each section by:

$$\Delta\alpha_p(\eta) = \arctan\left(\frac{p\eta b}{2V_\infty}\right) \tag{7.2}$$

Similarly, for the pitch rate:

$$\Delta\alpha_q(\eta) = \arctan\left(\frac{q\,(0.5b\eta\tan\Lambda_{LE} + 0.25c(\eta) - x_{CG})}{V_\infty}\right) \tag{7.3}$$

Finally, the angle of attack is updated in response to yaw rate to represent the increased lift due to asymmetries in the oncoming flow. This leads to the final local angle of attack below, which is used by the lifting surface model to calculate the load:

$$\alpha(\eta) = \alpha_0(\eta) \left(\frac{V_\infty - 0.5 b \eta r}{V_\infty} \right)^2 \tag{7.4}$$

7.3.4 Control Allocation

Antisymmetric Deflection

Now we must find the magnitude of aileron input required for the manoeuvre based on these constraints. As a first step, we define the variable τ as the time taken to roll to 45°. We then consider the rolling aircraft as a one dimensional system in which the only moments acting on the aircraft are due to control input and roll damping from the wing:

$$I_{xx}\ddot{\phi} - L_p\dot{\phi} - L_\xi\xi \ = 0 \tag{7.5}$$

By solving Eq. (7.5) for $\phi(t)$ with a constant ξ, we find:

$$\phi(t) = L_\xi \xi \left(\frac{I_x x}{L_p^2} \left(e^{\frac{L_p}{I_{xx}} t} - 1 \right) - \frac{t}{L_p} \right) \tag{7.6}$$

Finally, to find the required control deflection we substitute $\phi(\tau) = 45^\circ \ (\frac{\pi}{4} rad)$ into Eq. (7.6):

$$\xi = \frac{\pi}{4 L_\xi \left(\frac{I_x x}{L_p^2} \left(e^{\frac{L_p}{I_{xx}} \tau} - 1 \right) - \frac{\tau}{L_p} \right)} \tag{7.7}$$

Required control moments – Dynamic inversion

To calculate the required moments for control of the aircraft, we first define a state vector (x) which describes the full state of the aircraft at some point in time. We define this as $x^T = \begin{bmatrix} \psi & \theta & \phi & p & q & r & \gamma & C_l \end{bmatrix}$.

At any timestep we can find the rate of change of the state variable using the state space equation:

$$\dot{x} = f(x) + g(x)u \tag{7.8}$$

We define this as a function of the aircraft state rather than the more conventional approach of a linear system as the function is non-linear. The utility of this will become clear later in

this section. The angular velocities of each of the Euler angles ($\dot{\psi}$, $\dot{\theta}$ and $\dot{\phi}$) are updated using the angular rates (p,q and r) which are defined in the stability axes. Therefore, by appropriate transformation the angular velocity of each of the Euler angles is readily obtained.

The angular rates are updated by calculating the moments on the aircraft, these are calculated in body axis using the matrix of aerodynamic derivatives in Eq. (7.9). The derivatives are evaluated using the LS model described in Section 7.3.3.

$$M_{SA} = \begin{bmatrix} L_p(\alpha) & 0 & L_r(\alpha) & 0 & L_\beta(\alpha) \\ 0 & M_q(\alpha) & 0 & M_\alpha & M_\beta(\alpha) \\ N_p(\alpha) & 0 & N_r(\alpha) & 0 & N_\beta(\alpha) \end{bmatrix} \begin{bmatrix} p \\ q \\ r \\ \alpha \\ \beta \end{bmatrix} \tag{7.9}$$

Using an appropriate transformation matrix these moments are transformed from stability axes to the body axes. The vector of moments is then divided by the aircraft inertia tensor to calculate the rate of change of the angular rates p, q and r. The change in flight path angle (γ) is readily obtained using the assumption that at all points during the manoeuvre the aircraft is in a coordinated turn. If this is the case, then the rate of change of the flight path angle must be:

$$\dot{\gamma} = \frac{g \tan \phi}{V_\infty} \tag{7.10}$$

Finally, the rate of change of the roll control input is zero as we have defined this in a previous step. We can then define the desired properties of the aircraft in the form:

$$y = h(x) \tag{7.11}$$

In this case y is a 2 element vector which maintains a constant vertical component of lift and zero side slip. To calculate the required moment, we then differentiate Eq. (7.11) to obtain:

$$\dot{y} = \nabla h \dot{x} \tag{7.12}$$

Substituting in Eq. (7.8):

$$\dot{y} = \nabla h(f(x) + g(x)u) \tag{7.13}$$

Simplified as:

$$\dot{y} = F(x) + G(x)u \tag{7.14}$$

However, in this case $G(x)$ (i.e. $\nabla hg(x)$) is zero. This is to be expected as the control inputs will change the angular rates but do not directly change the flight path or orientation of the aircraft. This means that equation Eq. (7.14) is non-invertible and therefore cannot be solved in this form for u. To overcome this, we differentiate again giving:

$$\ddot{y} = \nabla F\dot{x} \tag{7.15}$$

Again, substituting Eq. (7.8):

$$\ddot{y} = \nabla F(f(x) + g(x)u) \tag{7.16}$$

To linearise the output, we define an auxiliary input (v):

$$v = \nabla hg(x)u + \nabla f(x) - \dot{d} \tag{7.17}$$

Which we differentiate in time and substitute into Eq. (7.14) to yield:

$$\ddot{y} = \dot{v} + \ddot{d} \tag{7.18}$$

We then define an error vector (e) which describes the difference between our current and desired state:

$$e(t) = d(t) - y(t) \tag{7.19}$$

Substituting this into Eq. (7.18) gives an expression for the error dynamics as:

$$\ddot{e} = -\dot{v} \tag{7.20}$$

If we choose a simple PI controller to select an appropriate value for v, the error dynamics become a second order ODE:

$$\ddot{e} + K_p\dot{e} + K_I e = 0 \tag{7.21}$$

For this work, the proportional and integral gains were set at 20 and 800 respectively. This was found to provide a satisfactory performance in the cases analysed. Finally, we substitute Eq. (7.21) into Eq. (7.20) and the result into Eq. (7.18). The required moments are then calculated using Eq. (7.14):

$$u = G(x)^{-1}\left(K_p\dot{e} + K_I e + \ddot{d} - F(x)\right) \tag{7.22}$$

Split Drag Rudder

With the required moments calculated from the previous section, the required control surface deflections can be easily calculated for the SDR configuration. First, the inboard two control surfaces are deflected antisymmetrically by the angle ξ calculated in Section 7.3.4. Similarly, the symmetric part of the deflection is calculated using the pitch derivative and the required pitching moment:

$$\eta = \frac{C_m}{C_{m,\eta}} \tag{7.23}$$

The SDRs operate in a bias mode as defined in [121], with a bias angle of 20 degrees [1]. This achieves two things, firstly the roll-yaw and pitch-yaw coupling of the SDR and secondly it linearises the yaw response with respect to SDR angle. Therefore, the deflection required by the split drag rudders is:

$$\zeta = 20^\circ \pm \frac{C_n}{C_{n,\zeta}} \tag{7.24}$$

The resultant deflection angle of the two most inboard control surfaces on each semispan are therefore the sum of the antisymmetric (ξ) and symmetric (η) parts.

Trailing Edge Controls

The yaw response of the aircraft to trailing edge control deflection is a somewhat more complex problem. However, as we have defined the mode shapes in such a way that the pitching moment and rolling moment are held constant [130], we can define the trailing edge control deflection

[1] The bias is added to the SDR implementation to prevent control coupling due to SDR deflection. This is not required for the mode shaping implementation as the coupling is not present.

as three unique components: A symmetric part, which controls pitch; An antisymmetric part, which controls roll; and, an asymmetric part, which controls yaw.

The pitch and roll deflections are easily defined using the linear control derivatives and required control moments. Note however that the control derivatives will be different to the SDR configuration as we actuate all three trailing edge surfaces.

To define the asymmetric control surface deflection, we use the representation of yawing moment coefficient as a function of control surface deflection from [130]:

$$C_n = C_{n0} + \Sigma_{i=1}^{N} D_i \delta_i + \Sigma_{i=1}^{N} \Sigma_{j=}^{N} E_{ij} \delta_i \delta_j + \Sigma_{i=1}^{N} F_i \delta_i^2 \tag{7.25}$$

Where δ_i is the deflection of the ith control surface. This is made up of the symmetric and antisymmetric components for pitch and roll control (δ_s and δ_a) and the gains for each mode shape (k), which represent the asymmetric component:

$$\delta_i = \delta_{s,i} + \delta_{a,i} + k\mathbf{n}_{i*} \tag{7.26}$$

Where $\mathbf{n}_{i*}$ represents the ith row of the null space matrix $\mathbf{n}$.

The principle by which the asymmetric mode shapes induce a yawing moment is based upon introducing an asymmetry in the spanwise loading which introduces an imbalance in the induced drag. However, during a rolling manoeuvre there is an additional antisymmetric loading induced, the strength of which is proportional to the non-dimensional roll-rate ($\frac{pb}{V_\infty}$). This affects the value of C_{n0} and the matrix D, Eq. (7.25). The matrices E and F are unaffected by this as they represent the interaction between control surfaces and profile drag of the control surface respectively. We can therefore write Eq. (7.25) as:

$$\begin{aligned} C_n\left(\frac{pb}{V}, \delta\right) =& C_{n0}\left(\frac{pb}{V}\right) + \Sigma_{i=1}^{N} D_i\left(\frac{pb}{V}\right)\delta_i \\ &+ \Sigma_{i=1}^{N}\Sigma_{j=}^{N} E_{ij}\delta_i\delta_j + \Sigma_{i=1}^{N} F_i\delta_i^2 \end{aligned} \tag{7.27}$$

For this configuration with six control surfaces in total, there are three mode shapes and therefore Eq. (7.27) is under defined (one equation and three unknown gains). Therefore, to find a control deflection we use a Sequential Quadratic Programming optimizer which finds the mode shape gains which satisfy the yawing moment demand for the minimum total deflection and ensure all control surface deflections are less than ten degrees so that the assumption of linear aerodynamics remains valid. Additionally, the speed of the control surfaces is restricted to $30^\circ/s$ to represent a typical actuator. We can write this as the optimisation problem:

$$\begin{aligned} \text{Minimise:} \quad & J(k) = \Sigma_{i=1}^{N} (A_i \sin(\delta_i(k)))^2 \\ \text{Subject to:} \quad & -10^\circ \leq \delta_i(k) \leq 10^\circ \\ & -30^\circ \Delta t \leq \delta_{i,t} - \delta_{i,t-\Delta t} \leq 30^\circ \Delta t \\ & C_n \left(\frac{pb}{V}, \delta(k) \right) = C_{n,d} \end{aligned} \tag{7.28}$$

This optimisation may fail as it is not guaranteed a feasible region will exist (for example the yawing moment demand could exceed maximum authority of the trailing edge controls). If this is the case the optimisation is rerun to minimise the error in yawing moment whilst keeping the maximum deflection less than ten degrees:

$$\begin{aligned} \text{Minimise:} \quad & J(k) = \left(C_n \left(\frac{pb}{V}, \delta(k) \right) - C_{n,d} \right)^2 \\ \text{Subject to:} \quad & -10^\circ \leq \delta_i(k) \leq 10^\circ \\ & -30^\circ \Delta t \leq \delta_{i,t} - \delta_{i,t-\Delta t} \leq 30^\circ \Delta t \end{aligned} \tag{7.29}$$

With the optimal mode shape gains obtained through the optimization, the control surface positions can be updated using Eq. (7.26).

7.4 Results

To assess the efficacy of the proposed control allocation method, a rolling manoeuvre was simulated for each of the control configurations. The case study aircraft was initially at a trimmed, wings level flight condition at a specified angle of attack between 1 and 6 degrees. At t=0 there was a step asymmetric input sufficient to roll the aircraft to a bank angle of 45 degrees in τ seconds. τ was varied between 1.2 seconds and 8 seconds to show the efficacy of the control allocation methods for both aggressive and gentle manoeuvres.

First, we examine the performance of the SDR configuration throughout the manoeuvre, Fig. 7.7. The axes in Fig. 7.7 are set to be the same as Fig. 7.8 to simplify comparison. It can be seen that for even the most aggressive manoeuvres, the SDR comfortably maintains the desired angle of attack. To quantify this, an angle of attack excursion is defined as the difference between the current and desired angle of attack. This configuration also keeps the sideslip less than half a degree in all cases. Examining the case where $\tau = 1.4s$, the performance prescribed by relevant military specifications [2] (MIL-SPEC) [176], we see that

[2] Specifications are taken for a class II (tactical reconnaissance) aircraft in phase A (Up and away with normal pilot workload) flight.

the manoeuvre can be completed for all angles of attack examined within the limits defined in the MIL-SPEC of 2 degrees proverse and 5 degrees adverse sideslip.

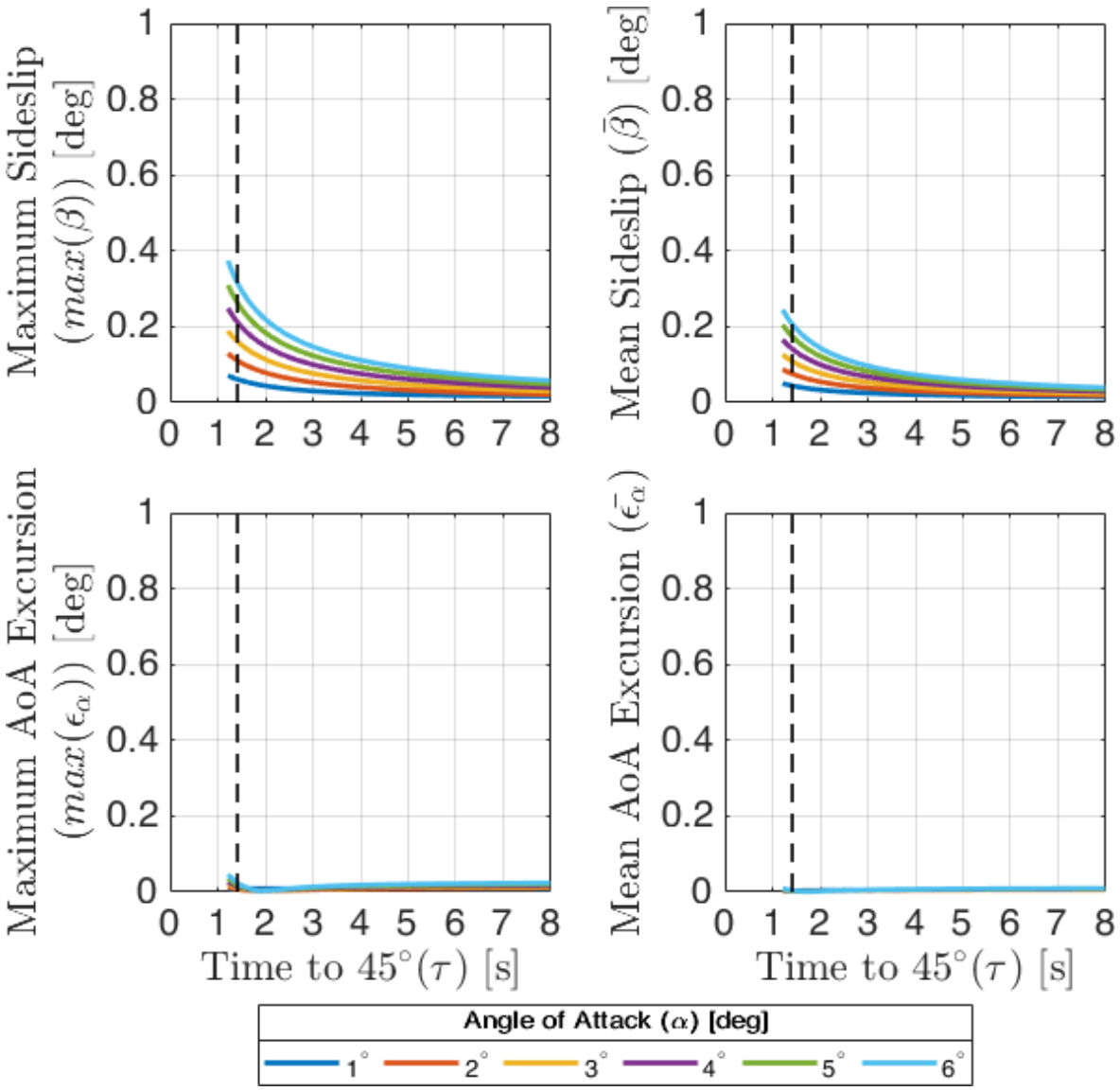

Figure 7.7. Aerodynamic angles during rolling manoeuvre for SDR configuration.

Next examining the performance of the aircraft through the manoeuvre in the trailing edge control configuration, Fig. 7.8. Cases where the manoeuvre fails, either because the error in angle of attack is greater than 10% or the sideslip exceeds the limits defined in [176], are represented with a broken line. The agility of the aircraft is clearly reduced compared to the SDR configuration and is only able to complete the manoeuvre in 1.4s as specified by MIL-F-8785C at an angle of attack of one degree.

However, examining the aerodynamic angles in Fig. 7.8 we see that in all cases the manoeuvre fails due to an error in the angle of attack, which has an excursion of greater than 10%, rather than sideslip, which is comfortably within the MIL-SPEC limits. This is because of coupling between the angle of attack and sideslip due to the roll rate and as the

yaw control is saturated (i.e. the yaw demand is greater than the control authority), the correct combined moment of pitch and yaw demanded by the dynamic inversion controller is not imparted to the aircraft. This results in this error in angle of attack.

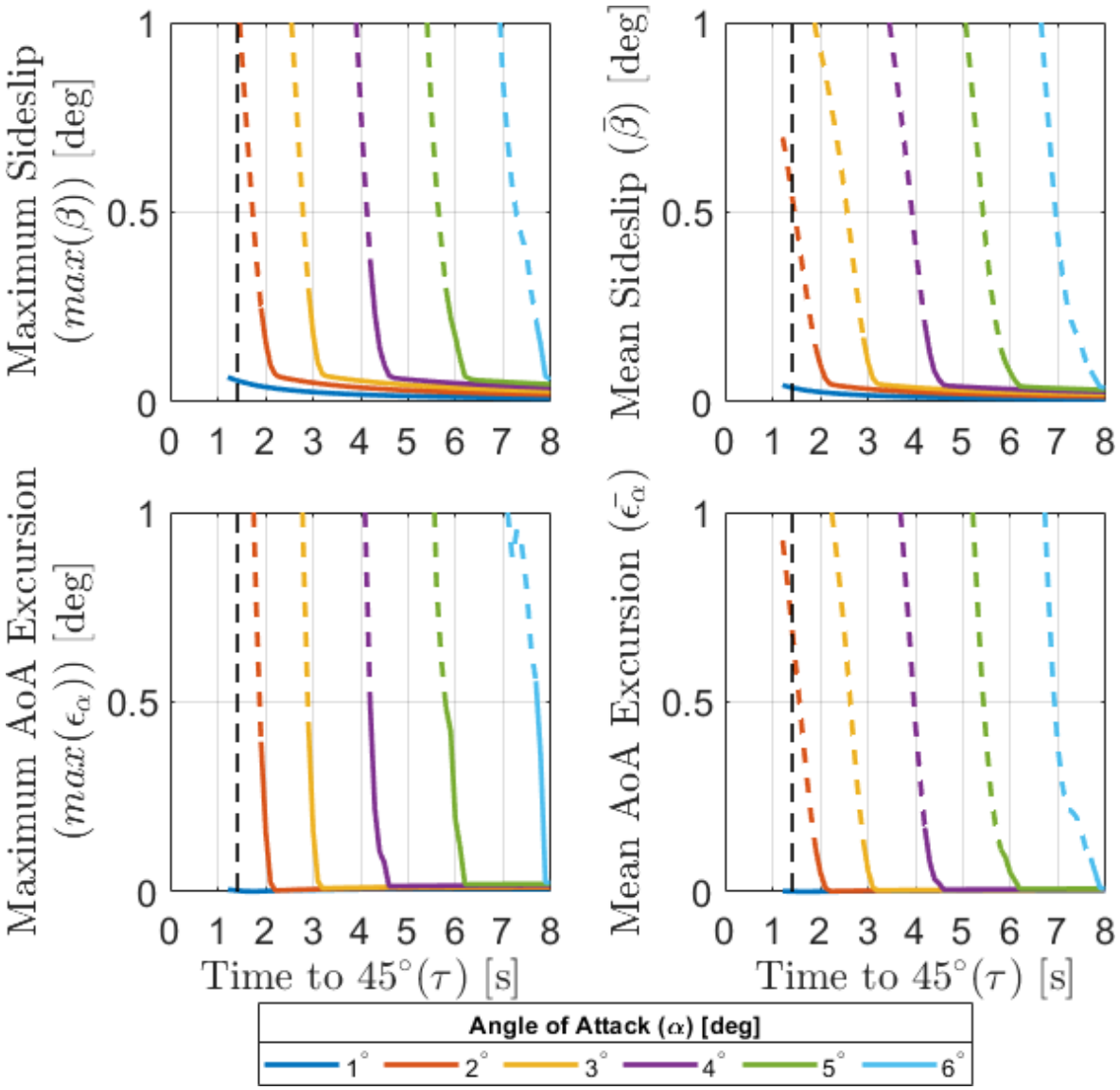

Figure 7.8. Aerodynamic angles during rolling manoeuvre for trailing edge control configuration.

However, the goal of the method using only trailing edge controls was not to achieve an improved agility but rather to reduce the control system complexity and aggregate deflection required to manoeuvre. We compare the mean and maximum control deflection throughout the manoeuvre, defined as the area presented in the normal plane of the aircraft, in Fig. 7.9. Examining the mean deflection we can see that in all cases examined in this work, the total deflection reduced to at least 40% of the SDR configuration by using the trailing edge controls only. Furthermore, we can see that for gentle manoeuvres at angles of attack of 4 degrees and below the reduction in deflection is greater than 70%.

Examining the maximum deflection of each configuration the pattern is less clear, although

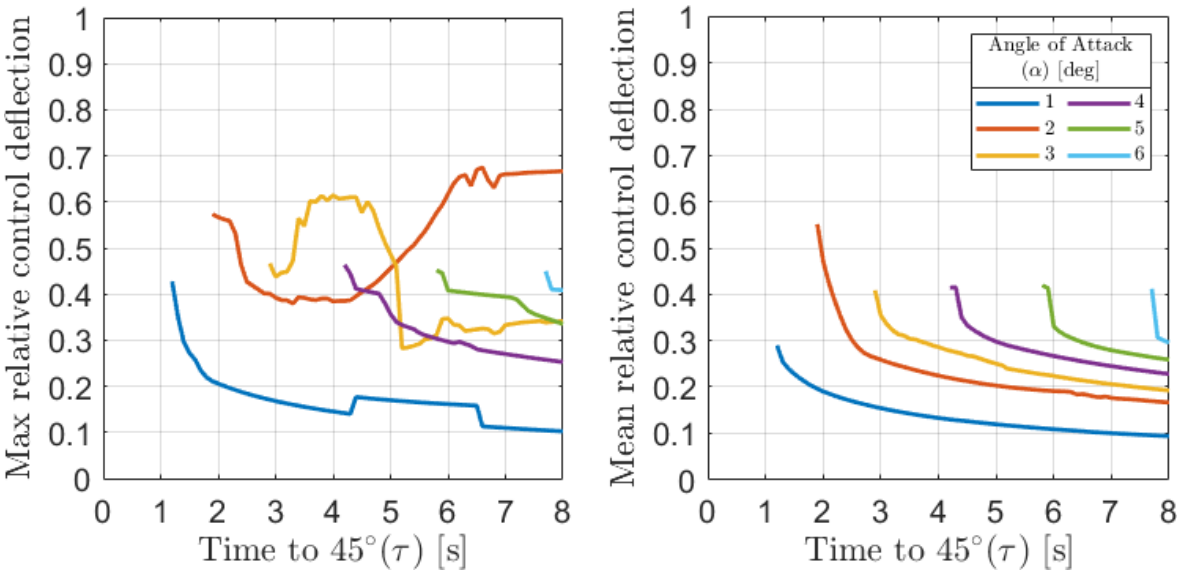

Figure 7.9. Relative control deflection during rolling manoeuvre. A value of less than unity indicates the total deflection of the mode shaping configuration is less than that of the SDR configuration.

it can be seen that again in all cases the maximum deflection is reduced by at least 30%. The reason for the behaviour shown in Fig. 7.9 is due to the fact that there is not one unique solution which satisfies the requirement on yawing moment. There is one solution in which the outermost control surface on the starboard wing is deflected upwards and one in which it is deflected downwards, this is shown in Fig. 7.10 where the roll at $\tau = 3s$ is shown for angles of attack of 1-3 degrees. In Fig. 7.10a, the outer control surface is deflected upwards and in Fig. 7.10c it is deflected downwards. Deflecting the trailing edge downwards gives a greater maximum yawing moment however the total deflection is increased. Once an initial direction is selected however, this solution becomes the only viable solution in the optimiser due to the constraint on the actuation speed of $30^\circ/s$. It is therefore thought that the maximum control deflection curve in Fig. 7.9 could be smoothed by imposing a specific search direction. For example, by imposing that the outer control surface on the downgoing wing must be deflected downwards.

Examining Fig. 7.10d we can see that using either control configuration has very little effect on the roll angle with time and Fig. 7.10e shows that both control methods also keep the angle of attack excursion less than 0.5%. In Fig. 7.10f, we see that for the one and two degree angle of attack cases there is very little difference between the mode shape and SDR configurations in terms of the sideslip angle. However, for the three degree case we see that the sideslip on the mode shape configuration overshoots that of the SDR before returning to the same level. This is because, as we can see in Fig. 7.10c, the control is briefly saturated at its maximum deflection of ten degrees as the required yawing moment exceeds the control authority. This is the reason why the actuation strategy at three degrees looks so different. Rather than meeting the control requirement for the minimum total deflection the optimiser

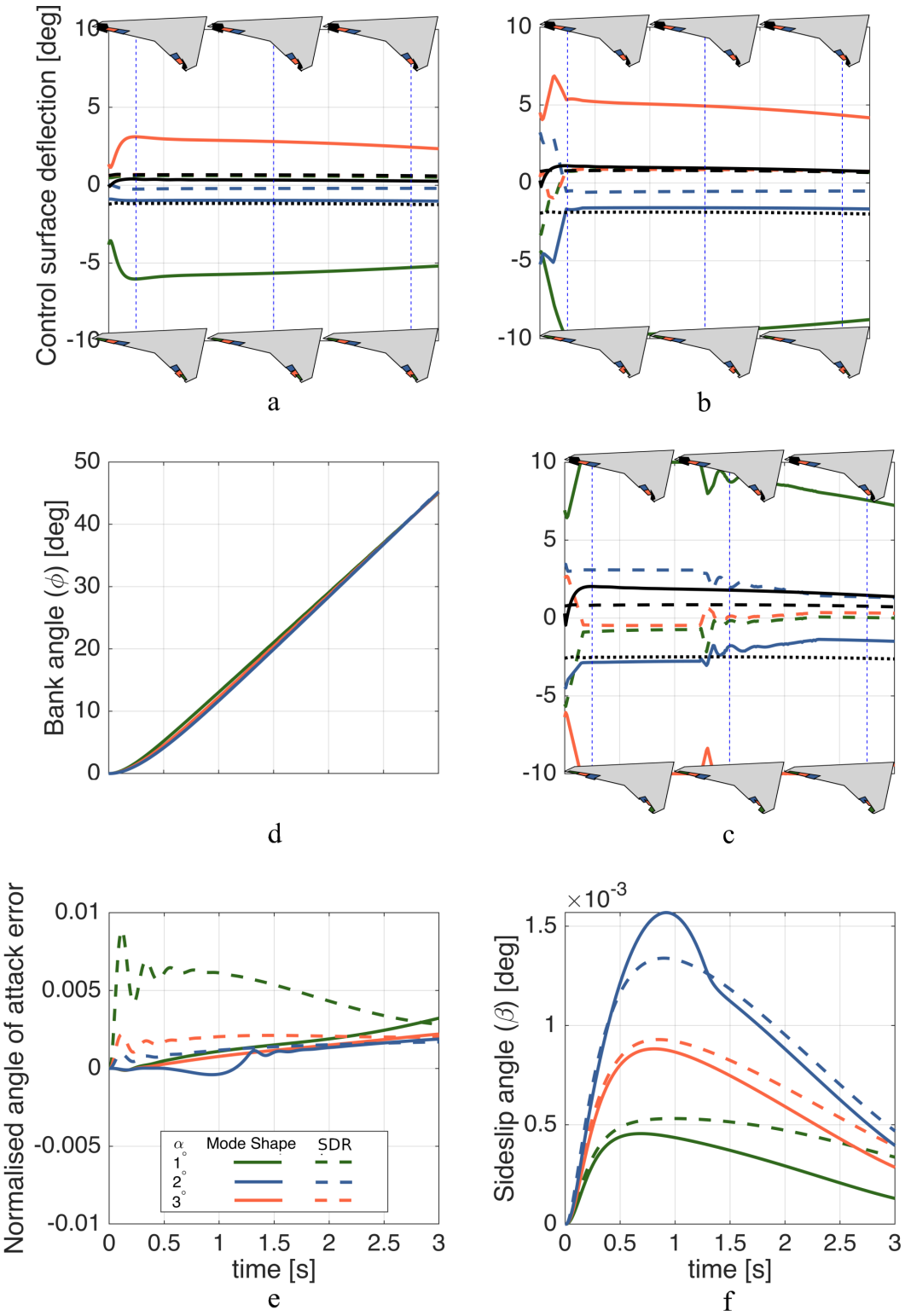

Figure 7.10. Control deflection through rolling manouvre with $\tau = 3s$ for angles of attack of 1° **(a)**, 2° **(b)** and 3° **(c)**. The progress through the manoeuvre is shown in **(d)** along with the angle of attack error normalised by the initial angle of attack **(e)** and sideslip angle **(f)**.

instead seeks to minimise the difference between the required and delivered control moment. To do this, it must deflect the outer control surface down to maximise the yawing moment.

7.5 Conclusion

The method presented in this paper demonstrates an opportunity to provide full three axis control solution using only the trailing edge controls. By utilising combinations of mode shapes an asymmetric control component can be defined which have no effect in pitch or roll but has sufficient control authority to overcome the secondary control effects from the trailing edge controls operating in a conventional sense, and to provide sufficient yaw control during a rolling manoeuvre.

For the example geometry analysed, taken to be representative of a typical future design, the control authority from the mode shaping approach is sufficient to perform a rolling manoeuvre within the limits specified by relevant standards for angles of attack up to one degree. For higher angles of attack there is a reduction in the agility of the aircraft which means it no longer meets the requirements of the standard. However, when comparing the total deflection of the mode shaping configuration to the typically used split drag rudder there is more than a 50% reduction. This reduction could impact on the observability of such an aircraft, improving its survivability in complex threat environments at the expense of agility. In addition, removing a SDR in favour of a standard trailing edge control would lead to a reduction in the weight and complexity of the actuation system. This provides designers an opportunity to trade-off agility and survivability at early design stages. However, it is thought that the control authority and therefore the agility of the aircraft using the mode shaping technique would be improved by extending the maximum control surface deflection beyond ten degrees. This would require additional analysis to ensure that the linear assumptions underpinning the method remain valid.

In implementing this method, designers may also find opportunities to configure an aircraft depending on its mission profile. It is conceivable of a configuration in which the outer control surface is operated as a conventional surface which can also split to act as a SDR. In this configuration, the control allocation on the aircraft could choose to implement a mode shaping or more conventional approach depending on whether observability or agility is the greatest concern at the time.

Chapter 8

Paper 5: A Control Allocation Method to Reduce Roll-Yaw coupling on Tailless Aircraft

Summary

This chapter provides a demonstration of the method developed in Chapter 7 to the MAGMA aircraft. It was originally presented during the 2021 AIAA Scitech forum [53]. The contributions of each author are detailed in Table 8.1.

Much of the methodology used in this paper is the same as Chapter 7, but applied to the MAGMA aircraft to give a reference case for planform representative of future tailless aircraft concepts. The effectiveness of the mode shaping approach is compared again to mid-chord spoilers (the same configuration as Chapter 6) over a range of lift coefficients and roll rates representing the operational envelope of the aircraft.

The results from this chapter show that for yaw control during a rolling manoeuvre at angles of attack less than five degrees, the mode shaping approach can achieve the same or greater agility than the spoiler configuration with a reduced aggregate control deflection. This represents the majority of the aircraft's operational envelope. The time the aircraft is at high angle of attack is likely to be during the terminal phases of the mission, where the environment is relatively low threat. Therefore, the mode shaping approach appears to be a viable control solution for the MAGMA aircraft for up and away flight conditions.

Task	TRS	MRAN	WJC	CW
Funding Acquisition		x	x	x
Supervision		x	x	x
Project Administration		x	x	x
Conceptualisation	x	x	x	x
Methodology	x	x	x	x
Formal Analysis	x			
Investigation	x			
Software	x	x		
Validation	x			
Visualisation	x			
Writing - original draft	x			
Writing - review and editing		x	x	x

Table 8.1. Contributor Roles Taxonomy for Chapter 8

Abstract: *This paper proposes a novel method to achieve three-axis control of a tailless aircraft using conventional trailing edge controls only during a rolling maneuver. The method is based on the synthesis of control allocation modes which produce laterally asymmetric drag at constant lift, pitching moment and rolling moment. Required control moments throughout a rolling maneuver are calculated using a dynamic inversion approach and control allocation performed by calculating the required combination of control modes. Results are presented for the MAGMA aircraft for roll rates which achieve a bank angle of 45 degrees in between 1.2s and 8s. Obtained solutions have equivalent or improved authority to conventional mid-chord spoilers for lift coefficients up to 0.3, representing a large part of the operational envelope of the aircraft.*

8.1 Introduction

An aircraft roll maneuver is typically effected by deflection of wing trailing edge controls to introduce a lateral asymmetry in the spanwise lift distribution and hence rolling moment about the aircraft centerline. However, the control inputs will also cause a change in spanwise drag distribution and this will introduce a secondary yawing moment, leading to some degree of roll-yaw coupling. For roll maneuvers used to turn an aircraft, the roll-yaw coupling due to control surface deflection is adverse in the sense that it leads to an out of turn (uncoordinated) moment [17], [54], [112], [134], [169], [170].

The magnitude of adverse yaw generated during a rolling maneuver can be minimized by effective design of wing trailing edge control surfaces and control allocation strategy [17], [54], [112], [134], [169], [170], [172]. However, typically some adverse yaw will still be present and requires input from other controls to mitigate [54]. This required yaw control is generally provided by the use of actuated fins at the rear of the aircraft or deployable drag

devices positioned towards the wing tips, and both of these methods can have a significant impact on the observability of the aircraft [122].

For aircraft designs where observability is of significant concern, the planform design generally converges to all flying wing configurations with leading edge sweep between 45 and 60 degrees and of moderate aspect ratios (3-6). These configurations result in very small moment arms for the vertical fins resulting in larger surfaces to meet given stability and control requirements. Yaw control from drag devices toward the wing tips can be used as part of an active control system for stability augmentation in finless designs [117]. These devices have the advantage of being stowed when not in use and therefore only have an impact when deployed and, the outboard wing location provides a favorable moment arm. However, use of such devices increases control system complexity and weight, and there is often significant coupling in both pitch and roll.

In this paper we propose an alternative yaw control approach which uses only the trailing edge controls. The control surfaces are deflected in such a way to induce laterally asymmetric induced drag, but whilst maintaining the required lift, pitching moment and rolling moment [130], [161]. As these controls are already necessarily present for control purposes there is no increased complexity of adding extra actuation systems, and the observability impact will also be minimized. Previous works by the authors [130], [161] have shown the potential of this control method to trim an aircraft in steady sideslip where trailing edge controls can reduce both the drag (indicator for aerodynamic efficiency) and required control surface deflection (indicator for observability) when compared to wing-tip drag devices. This paper will build on our previous contributions and will extend them to demonstrate the potential of this novel control method for yaw control during a rolling maneuver.

8.2 Method

8.2.1 Aircraft Geometry

In this work, we will evaluate the proposed control solution on the MAGMA aircraft [6], [7], Fig. 8.1. This aircraft was designed and manufactured at the University of Manchester in partnership with BAE Systems as a demonstrator for novel flight controls on a representative planform for a future military UAV application. However, the reader must note that the spoilers on MAGMA are slightly undersized and the wing loading is lower than for a full sized operational aircraft. This in turn means that the inertias would be reduced meaning control inputs required to achieve specific angular accelerations are also reduced; therefore, the impact of adverse yaw is reduced and a greater control authority is available in yaw. Nevertheless, the results from this study will show the potential of the proposed control allocation method

to this type of planform.

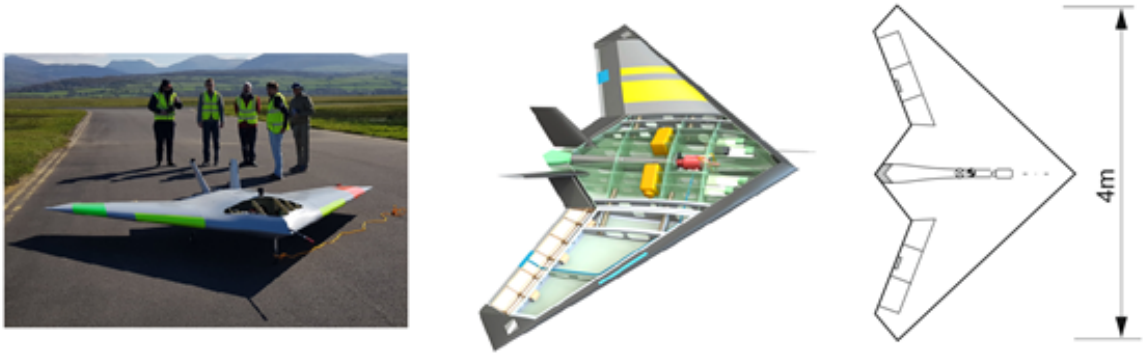

Figure 8.1. MAGMA aircraft

In MAGMA's conventional configuration, passive directional stability is provided by fixed fins. There is no provision for active yaw control. If these fins are removed a method of directional control is required as part of a stability augmentation system to prevent departure from controlled flight [163]. In this work we consider two aircraft configurations: firstly the main test case where the directional control is provided by trailing edge control only (orange surfaces, Fig. 8.2) and secondly a reference case where the directional control is provided by a mid-chord spoiler positioned close to the wing tips (red surfaces, Fig. 8.2).

For convenient application within the aerodynamic models developed in this work (Section 8.2.3), the control surface geometries are idealized to the solid outlines shown in Fig. 8.2 (original geometry shown as dashed lines). Furthermore, the aircraft profile is idealized to a flat plate – this is a reasonable assumption as the aerodynamic effects of interest to this study are dominated by planform rather than profile shape. A lifting surface model is used to derive the lateral and longitudinal derivatives (Section 8.2.3) for the flight dynamics model (Section 8.2.4) based on the input data in Table 8.2. The inertias in Table 8.2 are evaluated in the body axes of the aircraft assuming the off-diagonal terms are zero. When deployed the spoilers will strongly influence the flow over the outer control surface. Therefore, for the spoiler configuration, only the inboard and central control surfaces are used.

8.2.2 Maneuver Requirements

The maneuver considered in this study is a pure roll with requirements taken from relevant military standards [176]. For a representative tactical reconnaissance mission profile, the aircraft is required to roll to a bank angle of 45° in 1.4s. The manoeuvre starts with a step aileron input at t=0 and the input is held in this fashion until the required bank angle is achieved. Throughout the manoeuvre the sideslip angle should be maintained within the limits of 2° proverse and 5° adverse [176] and the aircraft should maintain level flight, i.e. the vertical

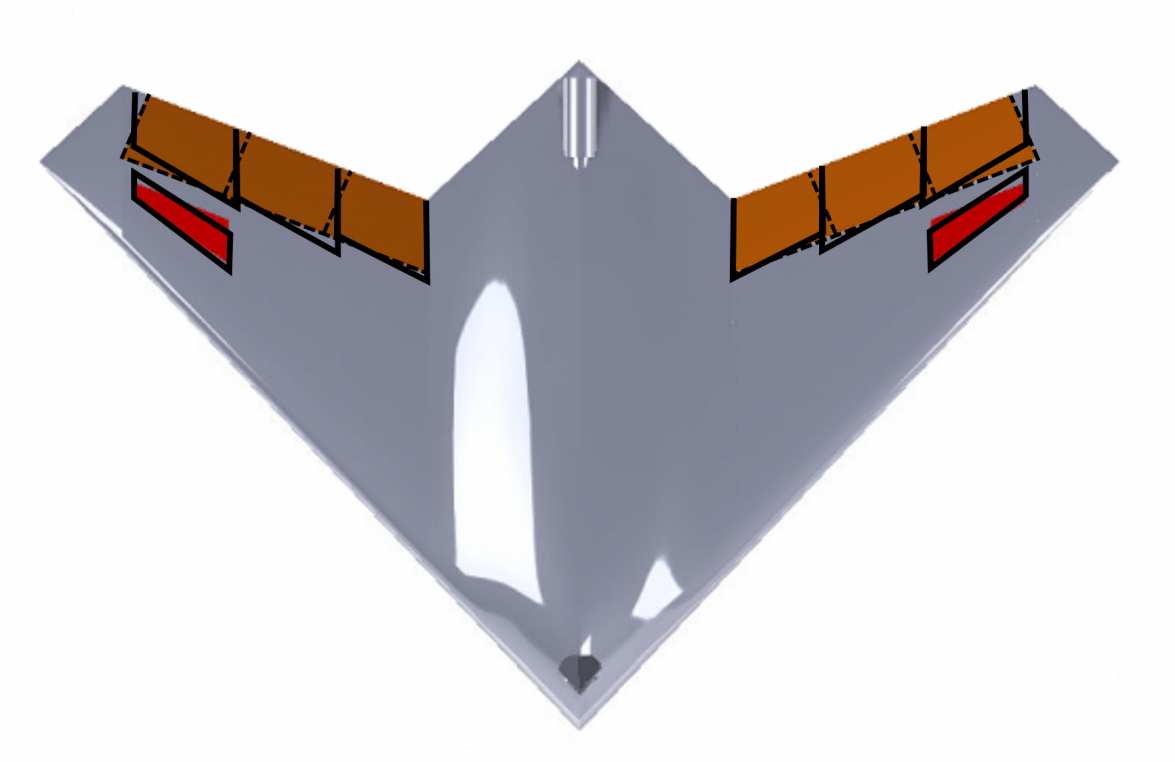

Figure 8.2. MAGMA control surface geometry. Original control surfaces shown by broken line and idealized by solid line.

Property	Value
Mass (I_{xx}) $[kg]$	40
Mass moment of inertia about x-axis (I_{xx}) $[kgm^2]$	18.6
Mass moment of inertia about y-axis (I_{yy}) $[kgm^2]$	18.9
Mass moment of inertia about z-axis (I_{zz}) $[kgm^2]$	24
Span $[m]$	4.01
Span wise location of crank $[m]$	0.565
Span wise location of tip section $[m]$	1.695
Leading edge sweep $[deg]$	47
Root Chord $[m]$	2.52
Chord at Crank $[m]$	1.4
Chord at tip section $[m]$	0.62
Width of inner control surface $[m]$	0.329
Width of center control surface $[m]$	0.377
Width of outer control surface $[m]$	0.377
Inner control surface length [% local chord]	22%
Inner control surface length [% local chord]	28%
Inner control surface length [% local chord]	32%
Outer position of spoiler $[m]$	1.65
Spoiler width $[m]$	0.35
Spoiler hinge line location [% local chord]	38%
Spoiler length [% local chord]	15%

Table 8.2. MAGMA idealized properties

component of lift is constant. Assuming a positive final bank angle, we can express these constraints as:

$$-2^\circ \leq \beta \leq 5^\circ \tag{8.1}$$

and:

$$C_L(t) = \frac{C_{L,t=0}}{\cos\left(\phi(t)\right)} \tag{8.2}$$

Now we must find the magnitude of aileron input required for the maneuver based on these constraints. As a first step, we define the variable τ as the time taken to roll to 45°. We then consider the rolling aircraft as a one dimensional system in which the only moments acting on the aircraft are due to control input and roll damping from the wing:

$$I_{xx}\ddot{\phi} - L_p\dot{\phi} - L_\xi\xi = 0 \tag{8.3}$$

By solving Eq. (8.3) for $\phi(t)$ with a constant ξ, we find:

$$\phi(t) = L_\xi\xi\left(\frac{I_{xx}}{L_p^2}\left(e^{\frac{L_p}{I_{xx}}t} - 1\right) - \frac{t}{L_p}\right) \tag{8.4}$$

Finally, to find the required control deflection we substitute $\phi(\tau) = 45^\circ\left(\frac{pi}{4}\right)$ into Eq. (8.4):

$$\xi = \frac{\pi}{4L_\xi\left(\frac{I_{xx}}{L_p^2}\left(e^{\frac{L_p}{I_{xx}}\tau} - 1\right) - \frac{\tau}{L_p}\right)} \tag{8.5}$$

8.2.3 Aerodynamic Modeling

To allow for efficient computation of aerodynamic forces and moments within the developed process, a low order aerodynamic model was used to reduce the computational expense. Details of the model selection process, performed previously by the authors, can be found in [130], with the Lifting Surface (LS) model [16] identified as the preferred approach. The implementation of the lifting surface model, including the treatment of control surfaces, is fully discussed in [130], so details will not be repeated here, and only key considerations will be discussed in what follows. The aerodynamic modelling process is, also, summarized in Fig. 8.3.

The lifting surface model calculates the spanwise (γ) and chordwise (μ) load distribution for a given geometry through the solution of a linear system of Aerodynamic Influence Coefficients (AIC). The assembly and inversion of the AIC matrix is the most computationally expensive

part of the model. As the AIC must be reconstructed when the sideslip angle changes, we use linear superposition to remove this step from the process (see Fig. 8.3): the spanwise and chordwise load distributions are calculated for a range of sideslip angles at zero angle of attack (i.e $\gamma(\beta)|_{\alpha=0^\circ}$ and $\mu(\beta)|_{\alpha=0^\circ}$); these distributions are then superimposed with the load distribution calculated at each time step from the state given by the flight dynamics model (i.e $\gamma(\alpha)|_{\beta=0^\circ}$ and $\mu(\alpha)|_{\beta=0^\circ}$)). In this way, LS evaluations are dramatically reduced allowing efficient execution.

Roll rate is accounted for by changing the local angle of attack at each section by:

$$\alpha_p(\eta) = \arctan\left(\frac{p\eta b}{2V}\right) \tag{8.6}$$

Similarly, for the pitch rate:

$$\alpha_q(\eta) = \arctan\left(\frac{q\left(y(\eta)\tan\Lambda_{LE} + 0.25c(\eta) - x_{CG}\right)}{V}\right) \tag{8.7}$$

Finally, the angle of attack is also updated in response to yaw rate to represent the increased lift due to asymmetries in the oncoming flow:

$$\Delta\alpha_r(\eta) = \alpha(\eta)\left(\left(\frac{V - 0.5b\eta r}{V}\right)^2 - 1\right) \tag{8.8}$$

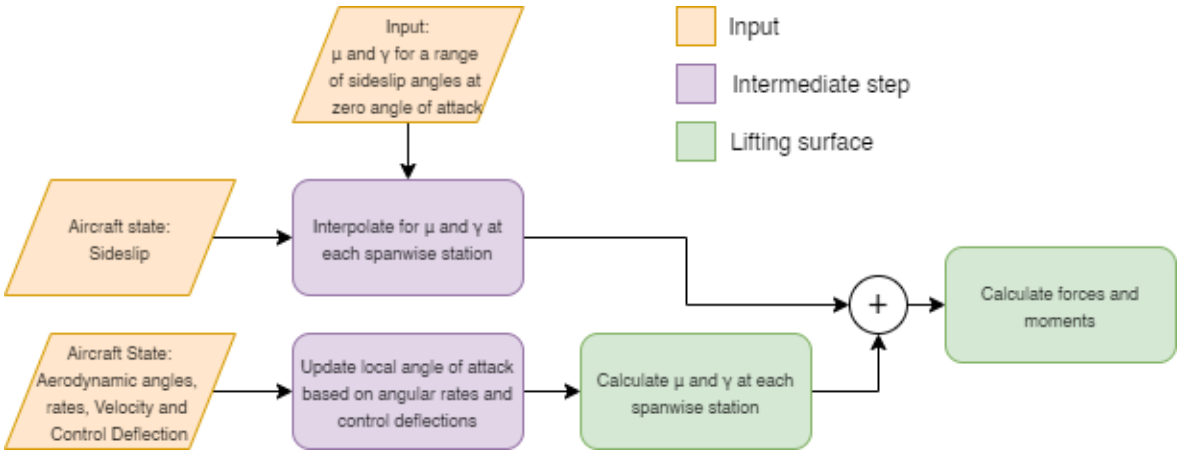

Figure 8.3. Lifting Surface Model

The aerodynamic forces and moments on the aircraft are calculated in the aerodynamic wind axes by the LS model. We designate the forces and moments calculated by the model as the vectors $\mathbf{F_w}$ and $\mathbf{M_w}$. These are subsequently used in the flight dynamics model in the body axes by appropriate transformation.

8.2.4 Flight Dynamics Modeling

The purpose of the flight dynamics model is to evaluate the flight path angle and orientation angles of the aircraft throughout the maneuver in response the forces and moments from the aerodynamic model. The flight dynamics model used in this work is first-order in time (i.e. $\mathbf{x_{t+\Delta t}} = \mathbf{x_t} + \dot{x}\Delta t$). Whilst this is a simple model it was found that with a suitable time step ($\Delta t = 20ms$) results can reach an accuracy level comparable to fourth order Runge-Kutta approaches whilst allowing a simpler implementation of the control allocation algorithm. The flight dynamics model is also simplified by assuming that at all times the lift coefficient is maintained as specified in 8.2 and that the velocity is unchanged from the initiation of the maneuver, meaning that the aircraft will always be in level flight. In this way, we can define the required angle of attack throughout the maneuver (α_{obj}) and assess the achievement of this constraint by defining an angle of attack excursion as the difference between the current angle of attack and required angle of attack and allow this to vary by 10% of the initial angle of attack ($\alpha_{t=0}$). We define the required angle of attack as:

$$\alpha_{obj}(\phi) = \frac{\alpha_{t=0}}{\cos\left(\phi(t)\right)} \tag{8.9}$$

Using these assumptions we can define our aircraft state as $\mathbf{x}^T = \begin{bmatrix}\psi & \theta & \phi & p & q & r & \gamma_y & C_{l\xi}\xi\end{bmatrix}$, where all the symbols take their usual meaning and for clarity γ_y is the flight path angle between the initial heading of the aircraft and the current direction of travel and $C_{l\xi}\xi$ is the rolling moment coefficient due to the aileron deflection. We further define a control input as $\mathbf{u}^T = [C_{m\sigma}\sigma, C_{n\zeta}\zeta]$ where $C_{m\sigma}\sigma$ and $C_{n\zeta}\zeta$ are the pitching and yawing moment coefficients due to relevant control deflections, respectively; these are the control moments we wish to define as will be discussed in Section 8.2.5. With the aircraft state and control input defined, we can write the equations of motion in a state space form as:

$$\dot{\mathbf{x}} = f(\mathbf{x}) + g(\mathbf{x})\mathbf{u} \tag{8.10}$$

Eq. (8.10) forms the basis of calculating the required control moments in the following section, however to model the flight path of the aircraft the lifting surface model described in the preceding section is implemented as shown in Fig. 8.4. The outputs of this model represent are the state of the aircraft and can therefore be used to update the aircraft state in the next time step.

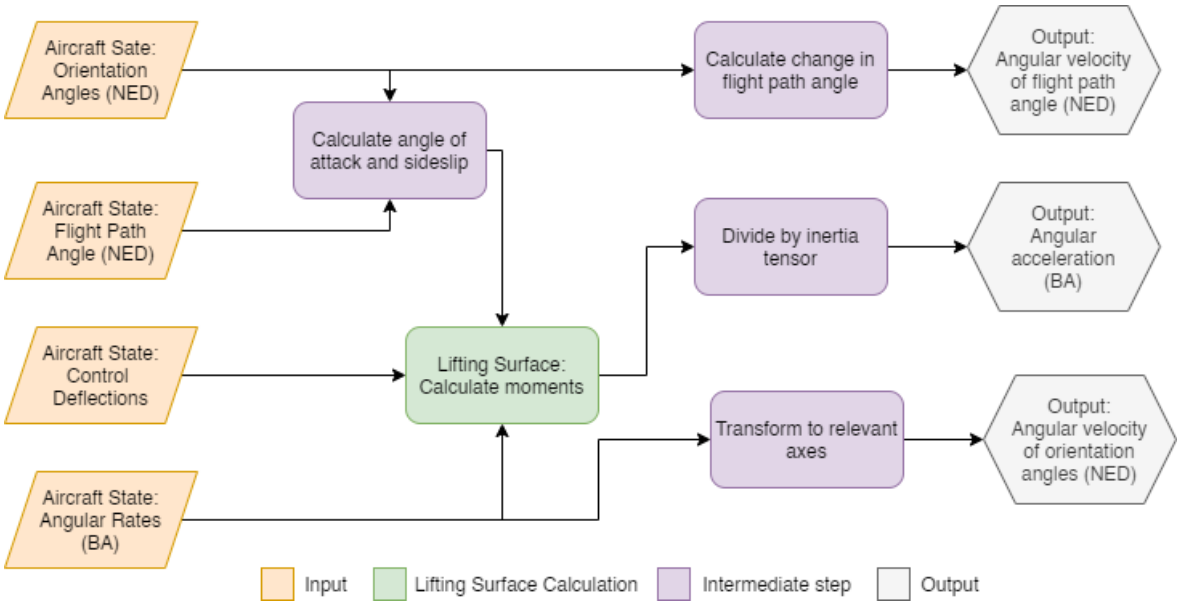

Figure 8.4. Lifting Surface Model

8.2.5 Required Control Moments - Dynamic Inversion

In order to define the required control moment coefficients, $C_{m\sigma}\sigma$ and $C_{n\zeta}\zeta$, a dynamic inversion approach is adopted [177]. In Section 8.2.2 we defined the requirements for the rolling maneuver to be: (1) maintaining the vertical component of lift (Eq. (8.2)), and (2) maintaining sideslip limits (Eq. (8.1)). As we have two moments to define we require two objective variables, therefore the lift coefficient and sideslip angle are obvious choices. We can then write our objective variables (y_{obj}) as:

$$y_{obj} = h(x) = \begin{bmatrix} \theta\cos\phi + (\psi - \gamma)\sin\phi \\ (\gamma - \psi)\cos\phi + \theta\sin\phi \end{bmatrix} = \begin{bmatrix} \alpha \\ \beta \end{bmatrix} \tag{8.11}$$

Note that, α is a now alternatively representing the lift coefficient. By differentiating Eq. (8.11). with respect to time, we introduce the control input (u):

$$\dot{y}_{obj} = \nabla h\dot{\mathbf{x}} = \nabla hf(x) + \nabla hg(x)\mathbf{u} \tag{8.12}$$

However, as $\nabla hg(x)$ is zero ($g(x)$ only influences the angular rate: p, q and r) this does not allow us to define the control inputs. Differentiating Eq. (8.12) again:

$$\ddot{y}_{obj} = \nabla\dot{h}\dot{\mathbf{x}} + \nabla h\ddot{\mathbf{x}} = F(\mathbf{x}) + G(\mathbf{x})\mathbf{u} \tag{8.13}$$

where $F(x) = \dot{\nabla h}f(x) + \nabla hf(\dot{x})$ and $G(x) = \dot{\nabla h}g(x) + \nabla hg(\dot{x})$. This, now allows us

to define the control input as a function of the objective variables. To linearize this relationship, we introduce the auxiliary input:

$$\mathbf{v} = \nabla hg(\mathbf{x})\mathbf{u} + \nabla hf(\mathbf{x}) - \dot{\mathbf{d}} \tag{8.14}$$

where d is the reference input (i.e. the desired value of the objective variables). However, as $\nabla hg(x)$ is zero we must again differentiate in time:

$$\dot{\mathbf{v}} = G(\mathbf{x})\mathbf{u} + F(\mathbf{x}) - \ddot{\mathbf{d}} \tag{8.15}$$

This allows us to define the control input in terms of our auxiliary input (v), reference input (d) and aircraft state (x):

$$\mathbf{u} = G^{-1}\left(\dot{\mathbf{v}} + \ddot{\mathbf{d}} - F(\mathbf{x})\right) \tag{8.16}$$

Finally, to define the control input we must define the auxiliary input and reference input. We define the reference input to maintain the required angle of attack and ensure sideslip is zero:

$$\mathbf{d} = \begin{bmatrix} \frac{\alpha_{t=0}}{\cos\phi} \\ 0 \end{bmatrix} \tag{8.17}$$

therefore:

$$\ddot{\mathbf{d}} = \begin{bmatrix} \frac{\alpha_{t=0}}{\cos\phi}\left(\phi^2\left(\tan\phi + \sec\phi\right)\ddot{\phi}\tan\phi\right) \\ 0 \end{bmatrix} \tag{8.18}$$

The auxiliary input is defined as:

$$\dot{v} = k_p(\mathbf{d} - \mathbf{y}) + k_d(\dot{\mathbf{d}} - \dot{\mathbf{y}}) \tag{8.19}$$

We find that for the MAGMA aircraft, $k_p = diag(800, 400)$ and $k_d = diag(20, 40)$ provides a suitable and stable response.

8.2.6 Control Allocation

Using the required moments calculated in the previous section the required control deflections can now be evaluated. For a given value of τ we can calculate the required aileron deflection using Eq. (8.5), this value is held constant throughout the maneuver. Using the required control moments calculated using Eq. (8.16), we can then calculate the required elevator deflection at each timestep as:

$$\sigma = \frac{C_{m,des}}{C_{m,\sigma}} \tag{8.20}$$

The process of calculating the required trailing edge control deflection to achieve a given yawing moment has been discussed previously [130], [161], therefore only a summary is provided here. We begin by considering the effect of the control surface deflection on lift, pitching moment and rolling moment as a linear system. By taking the null space of this system we define control mode shapes for the aircraft (Fig. 8.5). Any linear combination of these mode shapes will produce laterally asymmetric induced drag but gives no change in lift, pitching moment or rolling moment.

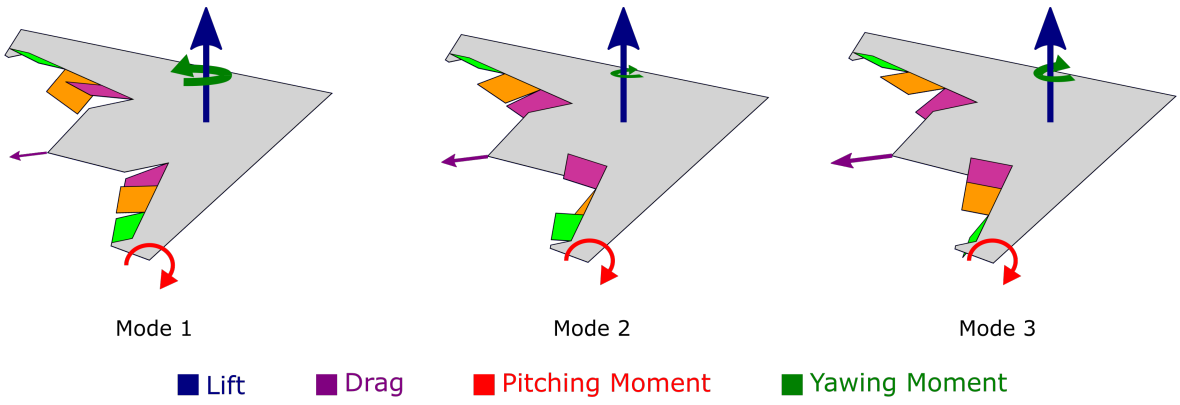

Figure 8.5. Illustration of three control mode shapes that give different yawing moments for the same lift and pitching moment

Using these mode shapes, represented in the column space of $\mathbf{n}$, we can write the control deflection as a function of the aileron input (ξ), elevator input (σ) and mode shape gains (k):

$$\boldsymbol{\delta}(\sigma, \xi, k) = \boldsymbol{\delta_0}(\sigma, \xi) + \mathbf{n}k \tag{8.21}$$

We then write the yawing moment coefficient as a function of control surface deflection:

$$C_n(\boldsymbol{\delta}) = S_0 + \Sigma_{i=1}^{N} S_i \delta_i + \Sigma_{i=1}^{N-1} \Sigma_{j=i}^{N} T_{i,j} \delta_i \delta_j + \Sigma_{i=1}^{N} U_i \delta_i^2 \tag{8.22}$$

The coefficients in Eq. (8.22) are found by evaluating a sample of control deflections and fitting a surface using least squares regression. The physical interpretation of this is that the control surface deflections perturb the lift distribution and therefore change the distribution of induced drag. However, it should be recalled that the roll rate of the aircraft will also have a large impact on the base distribution. By evaluating these coefficients S-U for a range of non-dimensional roll rates (pb/V), we find that T and U are constant with roll rate and only S varies in a linear fashion. This allows us to write the yawing moment coefficient provided by control surface deflection as a function of the control inputs, mode shape gains and roll rate:

$$\begin{aligned} C_n(\xi, \sigma, k, \frac{pb}{V}) =& S_0 + \Sigma_{i=1}^{N} S_i \left(\frac{pb}{V}\right) \delta_i(\sigma, \xi, k) \\ &+ \Sigma_{i=1}^{N-1} \Sigma_{j=i}^{N} T_{i,j} \delta_i(\sigma, \xi, k) \delta_j(\sigma, \xi, k) \\ &+ \Sigma_{i=1}^{N} U_i \delta_i^2(\sigma, \xi, k) \end{aligned} \tag{8.23}$$

For a given aircraft state and control input, we have already defined the aileron input (ξ) in Eq. (8.5) and elevator input (σ) in Eq. (8.20). We also know the value of pb/V and have defined the required yawing moment from the controls ($C_{n\xi}\xi$), therefore we are left to solve $C_n(k)|_{(\zeta,\sigma,p)} = C_{n\xi}\xi$ to evaluate the gains, k. For the configuration of MAGMA, this results in a single equation with three unknown gains. We therefore approach the solution to this as an optimization problem where we seek to minimize the total control deflection required to achieve a specific yawing moment which we define as the sum of the total area projected in the normal plane of the aircraft during control deflection. Furthermore we limit the maximum deflection of each control surface to 10 degrees, this ensures the response to the control surface is always linear. The optimization problem can, thus, be formulated as:

$$\begin{aligned} \min_{k} \quad & \Sigma_{i=1}^{N} A_i \sin\left(\delta_i(k)\right) \\ s.t. \quad & C_n(k) = C_{n,\xi}\xi \\ & -10^\circ \leq \delta_i \leq 10^\circ \end{aligned} \tag{8.24}$$

This optimization is completed using Sequential Quadratic Programming (SQP). If the optimization fails (i.e. the constraints cannot be satisfied), this indicates that the required yawing moment is outside of the feasible region, therefore, in such a case, we perform a different optimization as described below which will yield a result on the edge of the feasible region.

$$\begin{aligned} \min_{k} \quad & \left(C_n(k) - C_{n,\xi}\xi\right)^2 \\ s.t. \quad & -10^\circ \leq \delta_i \leq 10^\circ \end{aligned} \tag{8.25}$$

Once the vector of mode shape gains has been calculated, we can substitute this back into Eq. (8.19) to determine the deflection of each trailing edge control surface.

8.2.7 Reference Case – Spoilers

As stated previously, we include a control configuration in which the directional control is provided by spoilers positioned towards the wing-tips as a reference case. In this case, the outer control surface is not used as it is obscured by the spoilers (Fig. 8.2). Therefore, the inner and center control surfaces are operated in a laterally symmetric sense to provide pitch control and asymmetrically for roll control. Directional control is provided by the spoilers. Because of this, the values of $C_{m\sigma}$ and $C_{l\zeta}$ will be lower than the configuration which uses trailing edge controls only (i.e. a greater deflection angle will be required to achieve the same moment).

Similarly to the previous section, we first calculate the required aileron deflection using Eq. (8.5). The elevator deflection required at each timestep can then also be calculated using Eq. (8.20) by using the control moments defined from the dynamic inversion model.

Wing tip drag devices such as spoilers can show significant cross coupling with other axes and therefore require deflection of other control surfaces to counteract these secondary effects. To overcome this, the control implementation in this study uses the bias offset of 20° as proposed by Rajput et al. [121] [1]. This has two main benefits: Firstly it removes the cross-coupling in pitch and roll, and secondly it results in a linear response between the control input and yaw response. In this case, the yaw control input required to achieve the specified yawing moment is simply:

$$\xi = \frac{C_{n,\xi}\xi}{C_{n,\xi}} \tag{8.26}$$

Where $C_{n\xi}$ is evaluated at the initiation of the maneuver.

[1] The bias is added to the SDR implementation to prevent control coupling due to SDR deflection. This is not required for the mode shaping implementation as the coupling is not present.

8.3 Results

To assess the effectiveness of the spoilers and trailing edge controls for yaw control the rolling maneuver was assessed for a range of τ from 1.2s to 8s and for lift coefficients ranging from 0.05-0.4. These ranges cover the operational envelope of the aircraft in non-terminal flight phases ($C_{L,max} = 0.7$, $C_{L,maxRange} = 0.35$), provide the opportunity to assess the maneuvering limits and compare the actuation required for each control configuration.

First, we examine the performance of the trailing edge controls, Fig. 8.6. In this figure, solid lines represent test cases where the maneuver satisfies the constraints defined in Eq. (8.1) and Eq. (8.2) and dotted lines show where these constraints are not satisfied. The maximum values show the greatest excursion from the objective conditions during the maneuver (i.e. $\beta = 0$, $\alpha = \alpha_{obj}$) and the mean values show the time averaged excursion through the maneuver.

For all angles of attack up to and including 5°, the minimum τ (i.e. the greatest roll rate) is less than or equal 1.4s (shown by the dashed line) and therefore meets the requirements of MIL-F-8785C [176]. This suggests that using the proposed approach relying on trailing edge controls is a viable control option across the majority of the flight envelope for maximum sideslip angles of less than half a degree. Furthermore, the reduced maneuverability (i.e. greater value of the minimum τ at which both constraints are satisfied) corresponds to the very highest angles of attack in the flight envelope, typically only used during final approach where aggressive maneuvering would not be required. Therefore, trailing edge controls using the mode shaping approach proposed here represent a suitable solution for full three axis control.

Comparing the trailing edge controls to the approach using spoilers (Fig. 8.7), we see that the trend with angle of attack is reversed. The spoilers provide suitable control properties at high angles of attack but become less effective at lower angles of attack. However, this result should not be taken as completely indicative for a full-scale aircraft; this is because the spoilers on MAGMA were added retrospectively and due to structural constraints, are somewhat smaller than desired. Despite this, it can be seen that the spoiler provides adequate control to satisfy the maneuvering requirements at angles of attack of 2° and greater. For all angles of attack it can be seen that using this control method the sideslip angle is kept comfortably below half a degree and that the maneuver fails only due to the error in angle of attack (defined by Eq. (8.9)) being greater than 10%. During maneuvers lasting only a few seconds however, this error is unlikely to result in any meaningful stability or control issues.

Finally, we compare the penalty to the aircraft in terms of the area deflected during control actuation. This quantity is proportional to the change in profile drag and is assumed to be related to the change in observability during the maneuver [122]. Fig. 8.8 shows the relative aggregate area deflected defined as the aggregate deflection of the trailing edge control method

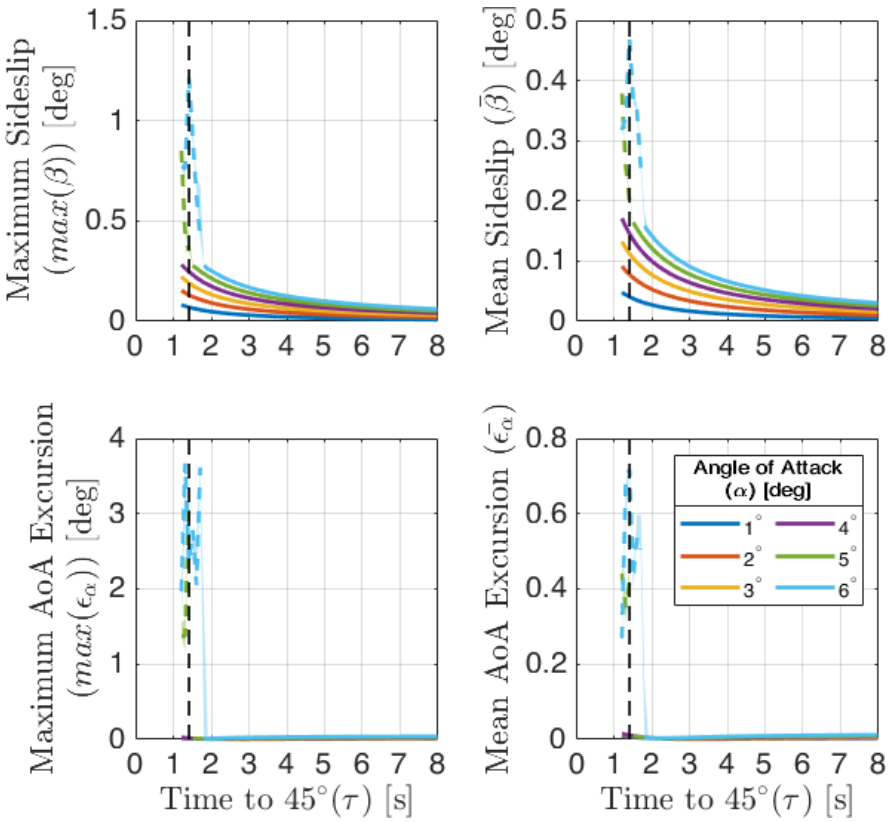

Figure 8.6. Maximum (left) and mean (right) Sideslip (Top) and error in angle of attack (bottom) for a rolling maneuver using only trailing edge controls. Dotted lines indicate maneuvers in which the error in angle of attack exceeded 10% of $\alpha_{t=0}$. Broken black line shows target performance of $\tau = 1.4s$

normalized by the aggregate deflection using spoilers. It can be seen that in all cases, both the maximum and mean control deflection is reduced by at least 20%. Most significantly for gentle maneuvering ($\tau \geq 4s$) the maximum aggregate deflection during the maneuver is reduced by at least 60%. When looking at the mean aggregate deflection throughout the maneuver (time averaged) even for the most aggressive maneuvers with angles of attack less than four degrees, representing the non-terminal flight phases of the aircraft, the improvement is in excess of 50% compared to the spoilers.

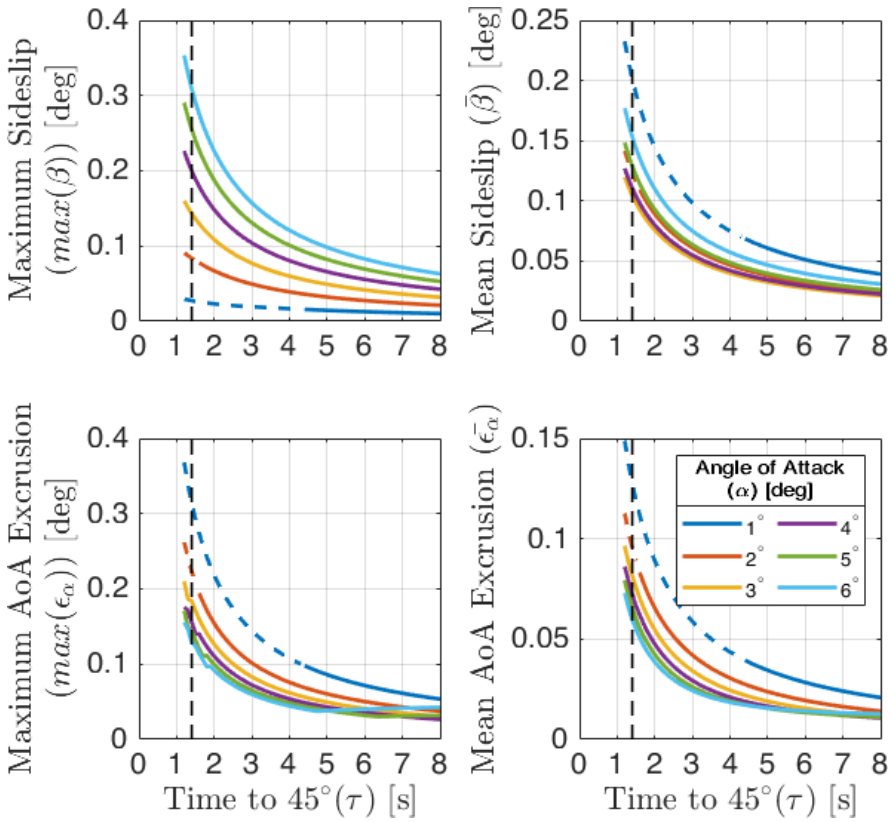

Figure 8.7. Maximum (left) and mean (right) Sideslip (Top) and error in angle of attack (bottom) for a rolling maneuver using spoilers for directional control. Dotted lines indicate maneuvers in which the error in angle of attack exceeded 10% of $\alpha_{t=0}$. Broken black line shows target performance of $\tau = 1.4s$

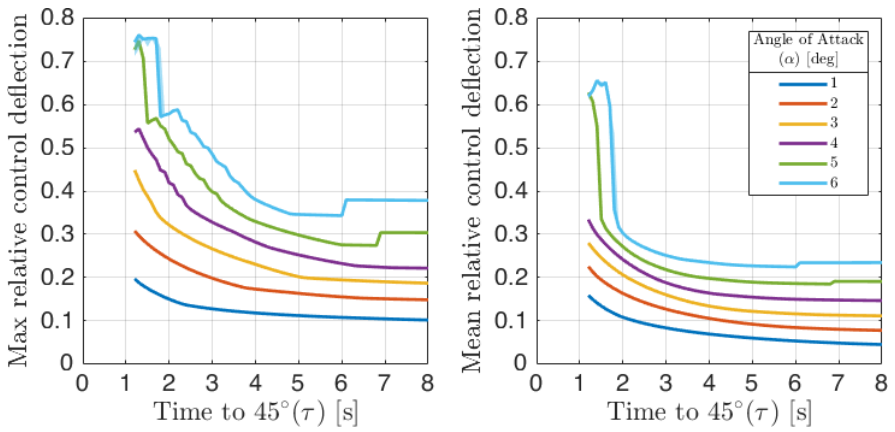

Figure 8.8. Maximum (left) and mean (right) relative aggregated control deflection during rolling maneuver. Values less than unity indicate that the total control surface area deflected using trailing edge controls is less than that using spoilers.

8.4 Concluding Remarks

This work has developed a control allocation method which can alleviate the effects of adverse yaw on tailless aircraft during roll maneuvers using only the conventional trailing edge controls. The allocation method uses combinations of mode shapes which are derived using surrogate models created from aerodynamic data from low-order tools. These mode shapes

ensure that there is theoretically no coupling between yaw and other axes. Analysis has shown that using the proposed control allocation method can yield turn performance comparable to using the spoiler solution for the MAGMA vehicle for the rolling manoeuvres analysed in this work. The spoilers show a benefit in maneuverability at angles of attack greater than five degrees however, at all other angles of attack the proposed solution using only trailing edge controls shows equivalent or improved maneuverability whilst reducing the required aggregate control deflection. It is anticipated that for planforms with a greater wing loading these benefits will still be present but in a reduced magnitude.

The benefits of using this control allocation method may also present themselves in the form of weight saving and reduced control system complexity. By using the conventional trailing edge controls the requirement for additional drag based control surfaces and their associated actuation systems is removed. This benefit, combined with the potential reduction in observability present possible opportunities for implementation on next generation reconnaissance aircraft where the trade-offs presented are favorable for the mission environment they will be operating in. However, for terminal flight phases where high control authority is required, more conventional directional control solutions may still needed. This reduces some of the benefits compared to a pure mode shaping approach but nevertheless allows a space to explore in the trade-off between mission and performance requirements.

Chapter 9

Paper 6: Three-axis control of tailless aircraft using fluidic actuators: MAGMA case study

Summary

The paper presented in this chapter investigates the potential for three-axis control of the MAGMA aircraft using only fluidic control effectors. A method is developed to assess the performance of a given control configuration in both mission performance and the required mass flow rate during a typical mission. This was originally presented at the 2021 AIAA Aviation forum [178]. The contributions of each author are detailed in Table 9.1.

This chapter examines four control configurations which use a combination of Circulation Control (CC), Fluidic Thrust Vectoring (FTV) and Wing-tip Reaction Jets (WRJs) to impart control moments. With pitch control provided by either FTV or CC; roll control by CC and yaw control using either FTV, WRJs or modeshaping with the CC devices.

The configuration of the modeshaping technique presented in this chapter differs from that presented in Chapter 4 – Chapter 8 in two key aspects. Firstly, the spanwise extent of the CC devices is less than that of a conventional flap due to the limited mass flow budget to supply these. Secondly, there are only two CC units on each wing as opposed to the three conventional control surfaces considered previously; this is due to the simplistic design philosophy used for the MAGMA aircraft. This configuration was chosen as it is reflective of the design constraints that are imposed on such a demonstrator aircraft.

Due to the limited control authority available from the circulation control units, the angular acceleration which could be produced in the roll axis was low.This necessitated the development of a path planning algorithm to generate a feasible roll command input. The resulting method of path planning has application to any fixed wing aircraft in which the roll authority is

Task	TRS	MRAN	WJC	CW
Funding Acquisition		x	x	x
Supervision		x	x	x
Project Administration		x	x	x
Conceptualisation	x	x	x	x
Methodology	x	x	x	x
Formal Analysis	x			
Investigation	x			
Software	x	x		
Validation	x			
Visualisation	x			
Writing - original draft	x			
Writing - review and editing	x	x	x	x

Table 9.1. Contributor Roles Taxonomy for Chapter 9

constrained.

Ultimately, the decision to implement the CC units in this way resulted in the yaw control authority from this method not meeting the requirements for directional control of the aircraft. However, this paper is still included here as the framework developed will allow the assessment of alternate configurations where these design constraints may become more relaxed.

The remaining configurations using FTV or WRJs for yaw control are analysed using a model predictive control approach to calculate the required control inputs based on the known performance of the fluidic effectors. The performance data in this case is derived from flight tests of the MAGMA airframe.

By examining these fluidic configurations, it can be seen that with fluidic devices manufactured using currently available techniques, it is possible to generate sufficient control authority for full 3-axis control of a tailless aircraft representative of future concepts with the fins removed over a typical mission profile.

Abstract: *This paper presents an assessment of the opportunity for full three-axis control of the MAGMA aircraft with the fins removed using a combination of Fluidic Thrust Vectoring, Circulation Control and Wingtip Reaction Jets.Effectiveness of the fluidic actuators is defined by values derived from previous flight test campaigns. Simulations are undertaken to assess the mass flow required to fly a typical mission for the aircraft. Results show that by using the circulation control devices for roll and pitch control, and the fluidic thrust vectoring for yaw, full control can be achieved using a mean value of 60% of the available mass flow from the engine.This result indicates that it would be possible to demonstrate full three-axis control of a sub-scale demonstrator aircraft within the limits of current manufacturing technology.*

9.1 Introduction

Recently, there has been an increased interest in the feasibility of active flow control solutions for control of aircraft; particularly, when applied to next generation military Unmanned Aircraft Systems (UAS) [44]. These novel control effectors remove the requirement to actuate external moving surfaces on an aircraft which subsequently allows improvements in both aerodynamic [179] and mission performance [122]. More importantly in this regard is removing the seams or gaps created by particular control configurations to improve the observability characteristics of the aircraft.

To demonstrate the feasibility of using novel fluidic effectors in flight, MAGMA, a demonstrator aircraft was designed and developed at the University of Manchester in partnership with BAE Systems, Fig. 9.1. Flight trials demonstrated the successful use of Fluidic Thrust Vectoring (FTV) and Circulation Control (CC), Fig. 9.2, for control of pitch and roll respectively [6], [7]. These flights were to demonstrate the use of an integrated propulsion unit, i.e. the compressed air required for the fluidic controls is taken from the compressor stage of the engine rather than carrying a separate air source. The control authority of these devices was sufficient to complete a full circuit at the test airfield without the need for any external moving surfaces. Nevertheless, MAGMA is still missing a method of fluidic control in the yaw axis.

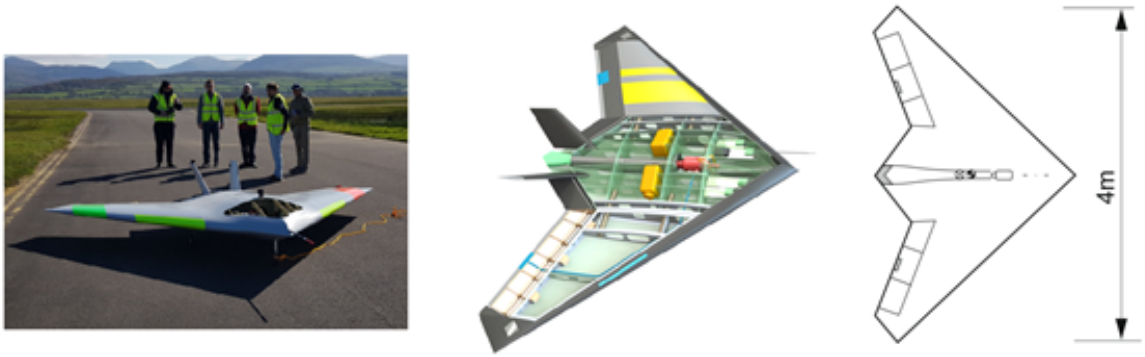

Figure 9.1. MAGMA demonstrator aircraft

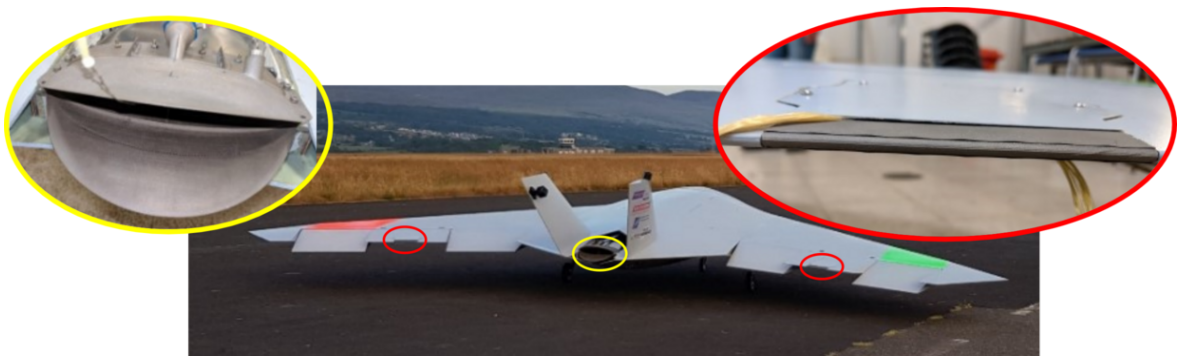

Figure 9.2. Existing fluidic control on MAGMA aircraft.

In the configurations shown in Fig. 9.1 and Fig. 9.2, there is no requirement for yaw control. This is because the aircraft is directionally stable due to the presence of the fins at the trailing edge. However, there is a design pressure to remove the fins on operational platforms for reasons of mission performance, namely reduced observably and fuel consumption. This would lead to marginal directional stability, or even instability dependent upon the angle of attack [163]. In this case, a method of directional control would be required for stability augmentation. Traditionally this control is provided by means of drag devices deployed towards the wing tips (i.e. spoilers or split drag rudders), however this introduces further external moving surfaces and is therefore undesirable.

In this paper, we will evaluate the potential fluidic control solutions that can satisfy a directional control requirement as part of a fluidic control suite. This objective has been undertaken before by the NATO AVT-239 task group [46], however this paper makes the following two novel contributions: Firstly, the operation of the CC units in a crow-mixing mode is considered, this means that a modeshaping approach can be used to create a lateral asymmetry in induced drag . Use of asymmetric induced drag for yaw control has been shown to be effective for conventional trailing edge controls [130], [161]; its application to fluidic control will explored here. Secondly, the analysis performed in this paper will use control performance data derived from fluidic control flight tests [6], [7]. This will demonstrate the control capabilities of fluidic devices manufactured at the limits of current capabilities.

9.2 Method

9.2.1 Fluidic Systems

The fluidic systems on the MAGMA aircraft are powered by bleed air from a modified Hawk 240R model aircraft engine [180]. The bleed supply is delivered at a maximum pressure of $4.2bar$ at a mass flow rate of $40g/s$ (approximately 9% of the core mass flow) at maximum thrust [7]. However, it is worth noting that to achieve this the engine must be run continuously at maximum thrust. The bleed air supply is taken from the compressor stage of the engine and therefore reduces the total available thrust, from $230N$ to $180N$. The layout of the engine and bleed system as installed, is shown in Fig. 9.3.

The fluidic devices shown in Fig. 9.2 are the Fluidic Thrust Vectoring (FTV) in yellow, and the Circulation Control (CC) devices in red. These have both been flight tested as part of the MAGMA flight test program and therefore their efficacy is known. The FTV efficacy is quantified by the change in thrust angle (i.e. the angle between the thrust line and the aircraft XY plane) per unit mass flow and is $\frac{\partial \theta}{\partial \dot{m}} - 0.007$ where θ is in radians and $\dot{m}$ is in g/s. In practice this means that with the full mass flow budget of $40g/s$ used by the FTV the thrust

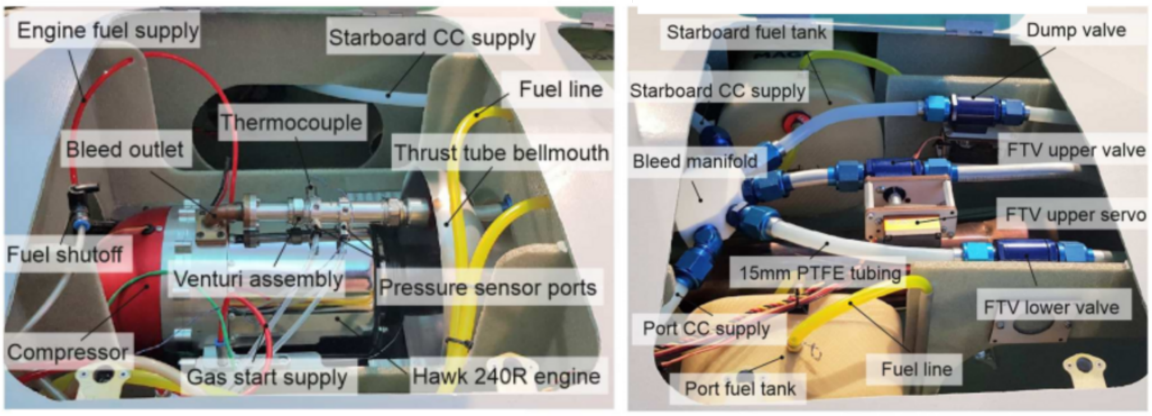

Figure 9.3. MAGMA engine (left) and bleed system (right) layout [6].

angle can be modified by up to 16 degrees. The CC efficacy is quantified by the change in local lift coefficient per unit 2D momentum coefficient (The ratio of the momentum of the fluid used to the free stream momentum, C_μ). From the flight trial data, this was calculated to be $\frac{\partial C_l}{\partial C_\mu} = 4.8$. The maximum 2D momentum coefficient measured in flight was 6.6% giving a maximum change in the local lift coefficient of 0.3.

In this work, we will also consider an additional method of control by placing nozzles at the wingtips as pure reaction jets. These Wingtip Reaction Jets (WRJs) are not geared controls in that they use the momentum from the bleed air to directly generate a force with no secondary effects (for example the CC generates a force by modifying the local lift coefficient on the wing). However, they will provide a suitable reference with which to compare the geared controls against.

9.2.2 Simulation Method

Simulations were implemented in MATLAB Simulink, Fig. 9.4 The flight dynamics are computed using the Body Euler Angles 6DoF block. From this the aircraft state is passed to the control allocation module, described in greater detail in Section 9.2.6, which calculates the required mass flow rates for each of the fluidic actuators. These mass flow rates are then used to calculate the effect from the fluidic actuators. For the CC units this is a change in local lift coefficient and for the Jets and FTV this is a force and moment output. The change in lift coefficient from the CC units is then used with the aircraft state to calculate the aerodynamic forces and moments using the lifting surface method [16]. Implementation of the lifting surface method as part of the current work is described in [53]. Finally, the force and moment outputs from the Aerodynamics module and fluidic devices are summed and returned to the flight dynamics module.

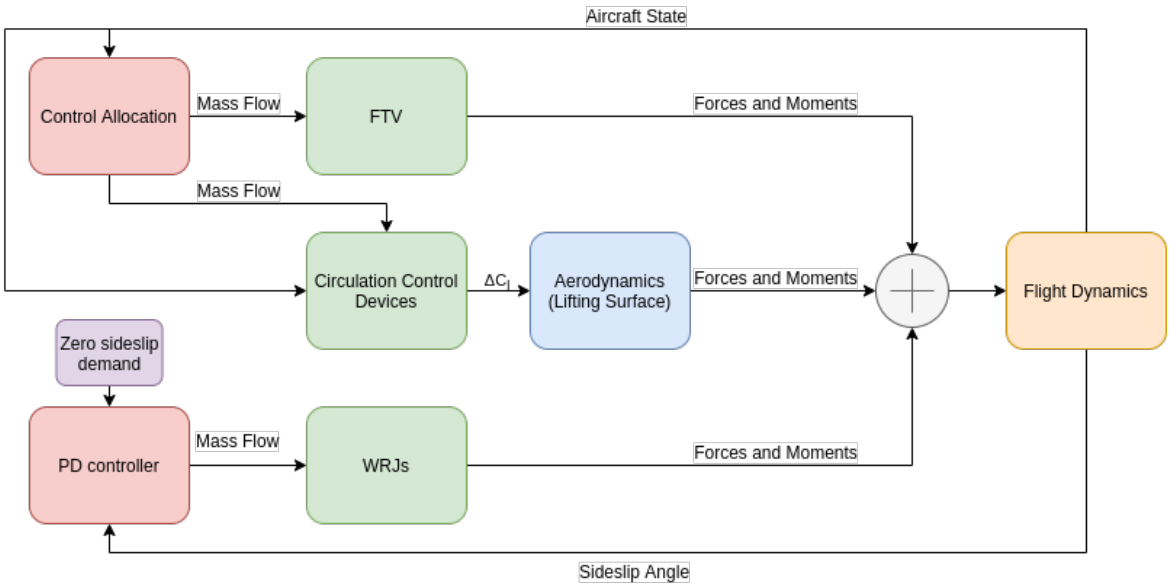

Figure 9.4. Simulink model data flow, example with yaw control by Wing-tip Reaction Jets (Configuration 4).

9.2.3 Mission

The mission profile chosen for this case study is based on a typical flight track used during testing of the aircraft at Snowdonia Aerospace Centre, Llanbedr, UK, Fig. 9.5 [6], [7]. The simulated mission is initialised with the aircraft at point A, with the aircraft trimmed longitudinally for straight and level flight at an altitude of $100m$ AGL. The aircraft then flies a left-hand circuit for a time of 90 seconds in still conditions [1].

The design point for the aircraft when operating in fluidic control mode requires the engine to be operating at high thrust to maximise availability of bleed. For the simulation, thrust was fixed at the maximum continuous value of $180N$ [7] and the zero-lift drag coefficient of the airframe (gear down) calibrated to match the airspeed recorded during flight trials of $\sim 40m/s$ [6], [7] under this thrust condition, giving a zero-lift drag coefficient $C_{D0} = 0.03$.

9.2.4 Control strategies

A number of control strategies are defined in order to explore different 3-axis control options, Fig. 9.6. The baseline aircraft is the same as that shown in Fig. 9.2, but with the fins removed.

Configurations 1 (CC) and 2 (PFTV) use a method of yaw control developed by the authors called mode shaping [53], [130]. In this method control effectors are used in such a way that the net change in lift pitching moment, rolling moment and lift is zero, but the combined sum of induced and profile drag is laterally asymmetric, which produces a yawing moment. The

[1] Although gust and turbulence response will play a role in the required control authorities, they are out of scope for the work presented here.

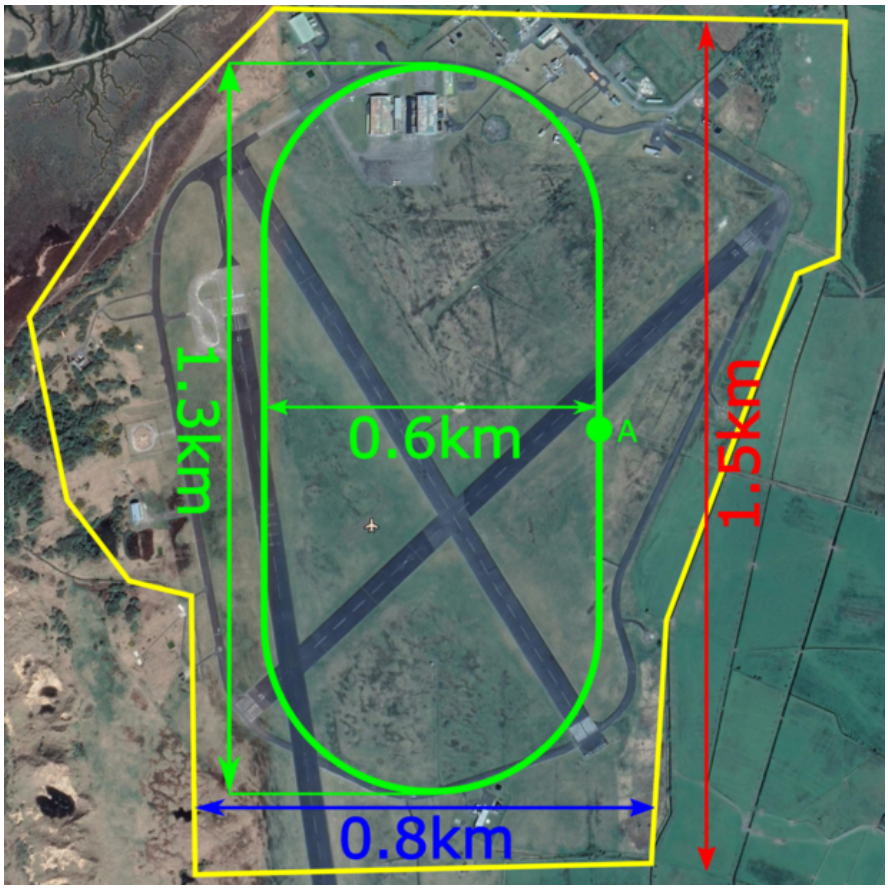

Figure 9.5. Useable flying area, Llanbedr - Wales, UK. Yellow outline shows limit of permitted flying area and green track is the proposed circuit. The mission is started trimmed, wings level at point A.

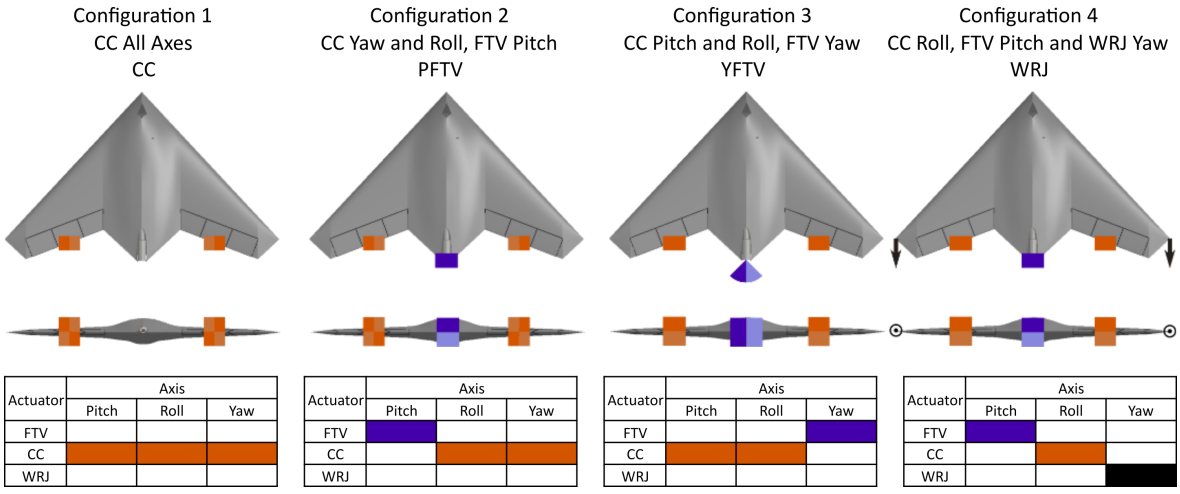

Figure 9.6. Aircraft fluidic control configurations.

number of mode shapes for any given aircraft is defined by the number of independent control effectors minus three. For configurations 1 (CC) and 2 (PFTV), two independent CC units are used on each wing to increase the number of available modes and allow yaw control to be a function of a single parameter (k). In configuration 1 the aircraft is controlled entirely using the CC devices whereas configuration 2 uses the CC for roll and yaw, and the FTV for pitch

control.

Configuration 3 (YFTV) is similar to the control configuration shown in Fig. 9.2, but using FTV for yaw, and CC for pitch and roll. Because the control demands on the CC is reduced compared to configurations 1 (CC) and 2 (PFTV), the number of CC units is reduced from 2 on each wing to 1 on each wing.

Finally, configuration 4 (WRJ) is included as a reference case to judge the benefits of using geared fluidic devices such as CC and FTV with unaugmented jet reaction control. It uses the same control configuration as the flight-tested aircraft with FTV for pitch and CC for roll, but with WRJs for yaw control.

9.2.5 Path Planning

In order for the control allocation to be successful a feasible roll command signal must be generated. To achieve this, an optimiser is used to plan the aircraft path as a piecewise series of circle arc segments which follow a desired path, Fig. 9.7. In this example, to demonstrate the robustness of the path planning, the aircraft is initialised 100m to the right of the desired path. The angular acceleration in roll was limited to 3 degrees/s^2 to reduce the impact of fluidic system saturation on path feasibility.

To generate the path, the angular acceleration in roll is defined by a series of updates (u):

$$\dot{p}(k+m|k) = \dot{p_k} + \sum_{j=k}^{k+m} u_j \tag{9.1}$$

Assuming $\dot{p}_k = 0$, then integrating to find the roll rate:

$$p(k+m|k) = p_k + \sum_{j=k}^{k+m} j u_j \Delta t \tag{9.2}$$

We can then integrate again to find the roll angle:

$$\phi(k+m|k) = \phi_k + m p_k \Delta t + 0.5 \sum_{j=k}^{k+m} u_j (j\Delta t)^2 \tag{9.3}$$

Assuming a coordinated turn, we can then find the turn radius by:

$$R(k) = \frac{V_\infty^2}{g \tan(\phi(k))} \tag{9.4}$$

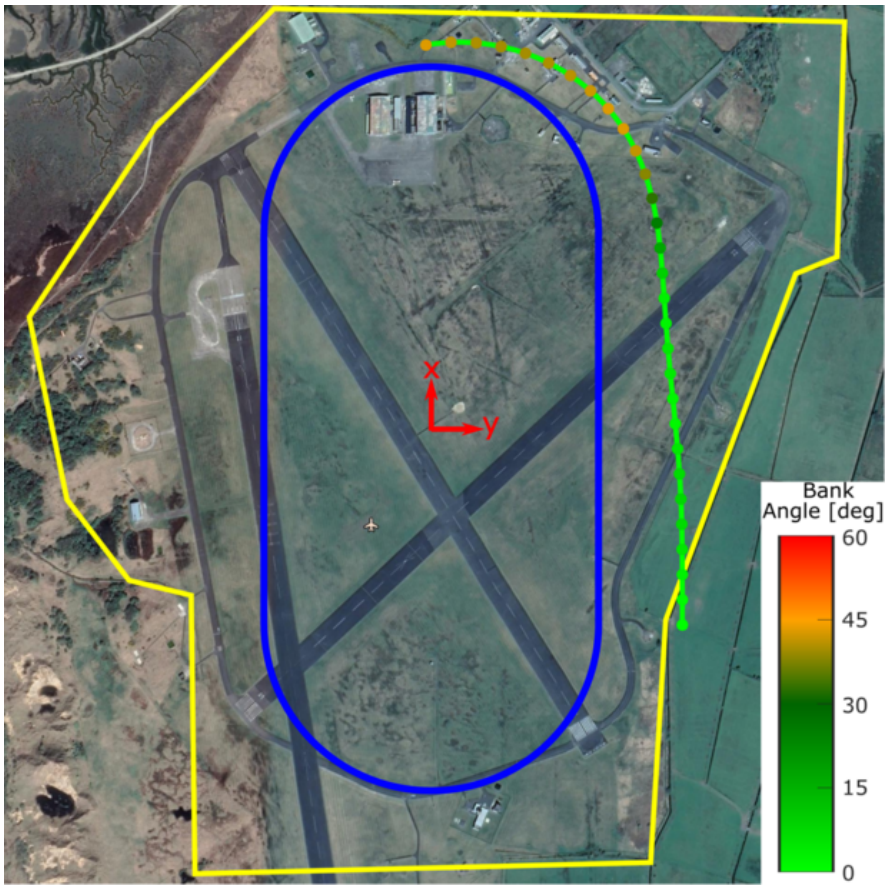

Figure 9.7. Output from path planning algorithm with the aircraft initialised wings level at the start of the right hand straight, 100m to the right of the desired path. Blue line is desired path and green line is output. The dots are at 1 second intervals along the output path and the colour represents the magnitude of the bank angle at that point. The axes shown are the reference axes system.

In a fixed timestep Δt, this sweeps out an arc:

$$\Delta\eta(k) = \frac{V_\infty \Delta t}{R(k)} \tag{9.5}$$

Using the arc angle, we can find the heading of the aircraft by:

$$\psi(k+i|k) = \psi + \sum_{j=k}^{k+i-1} \Delta\eta(j) \tag{9.6}$$

With the aircraft, heading we can define the aircraft velocity as:

$$V(k) = V_\infty e^{i\psi(k)} \tag{9.7}$$

Where the real part represents the X-velocity and the imaginary part the Y-velocity. Finally, the aircraft position is found by integrating the velocity:

$$X(k+m|k) = X_k - \sum_{j=k}^{k+m-1} (iR(j)e^{i\psi(j)}(e^{j\Delta\eta} - 1)) \tag{9.8}$$

Again, the X position is defined by the real part, and the Y position by the imaginary.

The path is then found by minimising the error between the desired path, shown in blue Fig. 9.7 and the output from Eq. (9.8). This minimization was performed by an interior-point solver. As the fluidic controls are relatively low authority, this optimization must be performed over a much longer time period than the control allocation. For this work, we used a horizon of 30 seconds. This was selected by defining a roll-time constant for the aircraft as the time taken to roll to 60 degrees, which is approximately 6 seconds. The horizon over which to optimize the path was then chosen to be 5 roll-time constants. Once the optimizer converges, the roll angle defined by Eq. (9.3) is used in the control allocation method defined in the following section.

9.2.6 Control Allocation

The control allocation must be able to account for the finite supply of bleed air from the engine, which can quickly lead to control saturation. For this reason, a simple PID control for the aircraft is unsatisfactory and a more sophisticated Generalised Predictive Control (GPC) method is used [181] instead.

The GPC algorithm is used to update the mass flow to the fluidic actuators at a rate of 10Hz with a control horizon of 1 second and a prediction horizon of 3 seconds. It was found that using a shorter prediction horizon than this would lead to unwanted oscillations in the control output. The update rate of 10Hz was used to limit the computational effort required at each control update as the GPC algorithm is much more computationally expensive than simpler feedback systems.

At low angles of attack, the aircraft is weakly directionally unstable. Because of this, a control system capable of reacting quickly to sideslip perturbations is required. To address this, a fast acting PD controller is use for the yaw axis with a preallocated mass flow budget of $5g/s$. The remaining $35g/s$ of mass flow from the engine is allocated by the GPC algorithm for pitch and roll control.

9.3 Results

9.3.1 Analysis of Yaw Control Gain and Maximum Effectiveness

Before performing the simulations, a basic analysis was performed to assess the different configurations in terms of gain (yawing moment coefficient per unit mass flow) and control authority (maximum yawing moment). This is important because the yaw control is allocated the most restricted mass flow budget, $5g/s$. Firstly, the gains for each configuration were calculated.

For configuration 1 (CC) and 2 (PFTV), yaw control is effected by actuating the CC units to effect asymmetric drag on the aircraft, a process called mode shaping. The derivatives used to calculate the control gain are shown in Table 9.2. The gain is found by first considering the mode shaping effectiveness (I), which is the yawing moment coefficient per unit control, and change in local lift coefficient per unit control (II). This can then be combined with the circulation control effectiveness (V) to find the change in control per unit mass flow. Finally, this is multiplied by mode shaping effectiveness to find the control gain.

Derivative	$\frac{\partial C_n}{\partial k}$ (I)	$\frac{\partial \lvert C_l \rvert}{\partial k}$ (II)	$\frac{\partial C_l}{\partial C_{\mu,2D}}$ (III)	$\frac{\partial C_{\mu,2D}}{\partial \dot{m}}$ (IV)	$\frac{\partial \lvert C_l \rvert}{\partial \dot{m}}$	$\frac{\partial k}{\partial \dot{m}}$ (VI)	$\frac{\partial C_n}{\partial \dot{m}}$ (VII)
Value	2.5×10^{-7}	3.49	4.8	0.0057	0.027	0.0078	1.9×10^{-9}
Source	Modeshape definition	Modeshape definition	Flight test data	Flight test data	(III)(IV)	(V)/(II)	(I)(VI)

Table 9.2. Mode shaping control gain.

In configuration 3 (YFTV), the FTV is used to produce a yawing moment. To calculate the control gain, shown in Table 9.3, the FTV effectiveness (I) is multiplied by the maximum thrust to calculate the change in side force (II). This is then multiplied by the distance from the centre of gravity and the thrust vectoring nozzle to find the yawing moment (III). Finally, this is normalized in the usual way to find the change in yawing moment coefficient (IV).

Derivative	$\frac{\partial \theta}{\partial \dot{m}}$ (I)	$\frac{\partial Y}{\partial \dot{m}}$ (II)	$\frac{\partial N}{\partial \dot{m}}$ (III)	$\frac{\partial C_n}{\partial \dot{m}}$ (IV)
Value	0.007	1.3	1.5	1.1×10^{-4}
Source	Flight test data	(I), Thrust data	(II), Aircraft Geometry	(III), Aircraft Geometry, Flight test data

Table 9.3. Fluidic Thrust Vectoring Control gain.

Finally, in configuration 4 (WRJ) the control gain is calculated by considering a pure reaction jet at the wing tips. By using the definition of C_μ it is apparent that the gain in terms of momentum coefficient is 0.5. The gain in terms of mass flow rate is then found by multiplying by the derivative (I) by (II) , Table 9.4.

A summary of the gains, both the absolute value and normalised by the gain for configuration 4, are shown in Table 9.5. Additionally, the maximum yawing moment coefficient, calculated

Derivative	$\frac{\partial C_n}{\partial C_\mu}$ (I)	$\frac{\partial C_\mu}{\partial \dot{m}}$ (II)	$\frac{\partial C_n}{\partial \dot{m}}$ (III)
Value	0.5	9.7×10^{-5}	4.8×10^{-5}
Source	Jet at wingtip	Flight test data	(I)(II)

Table 9.4. Wing-tip jet control gain.

by multiplying the gain by the maximum mass flow rate of $40g/s$, is shown and also normalized by the maximum expected yawing moment coefficient of 1.2×10^{-4} .

Control Method	Mode Shaping	Yaw FTV	Jet
Gain $\left(\frac{\partial C_n}{\partial \dot{m}}\right)$	1.9×10^{-9}	1.1×10^{-4}	4.8×10^{-5}
Normalized Gain	4.0×10^{-5}	2.2	1
Maximum Yawing Moment Coefficient	7.7×10^{-8}	4.3×10^{-3}	1.9×10^{-3}
Normalized Yawing Moment Coefficient $\left(\frac{C_n}{C_{n,max}}\right)$	6.4×10^{-4}	36	16

Table 9.5. Comparison of control gains and authority.

From Table 9.5, it can be seen that the methods using Mode shaping (i.e. Configuration 1 and 2), cannot generate a sufficient yawing moment to provide satisfactory directional control authority. In order to reach a satisfactory level of control an improvement of a factor of approximately 10^4 is required. With such a large improvement required, configurations 1 (CC) and 2 (PFTV) are not considered viable options beyond this point.

It is worth noting that the decision was made to place two CC devices on each semi-span in order to reduce the complexity of the system due to the design philosophy of MAGMA. This, in part, contributes to the low effectiveness of the mode shaping method. Increasing the number of degrees of freedom, that is increasing the number of actuators per wing, would increase the mode shaping effectiveness. Therefore, these mode shaping configurations may still be a viable solution on designs with different requirements which can better tolerate the increased complexity.

9.3.2 Mission Simulation

The output from the simulation of configurations 3 (YFTV) and 4 (WRJ) are shown in Fig. 9.8. The track for each of the configurations is shown as the multicoloured line with the colour at each point representing the ratio of the total mass flow budget used. It can be seen that both configurations follow the proposed circuit closely and that the greatest energy expenditure on control is on the entry and exit of the turn. The plots at the bottom of the figure show the breakdown of the mass flow used by each actuator and in total. For configuration 3 (YFTV), the mass flow used is dominated by the CC units for both pitch and roll control, with a very small amount used by the FTV for yaw control. Configuration 4 on the other hand uses a relatively steady 10-15g/s for the FTV to maintain longitudinal trim with the remainder of

the mass flow budget used mainly for roll control by the CC units with a small amount used for yaw control by the jets.

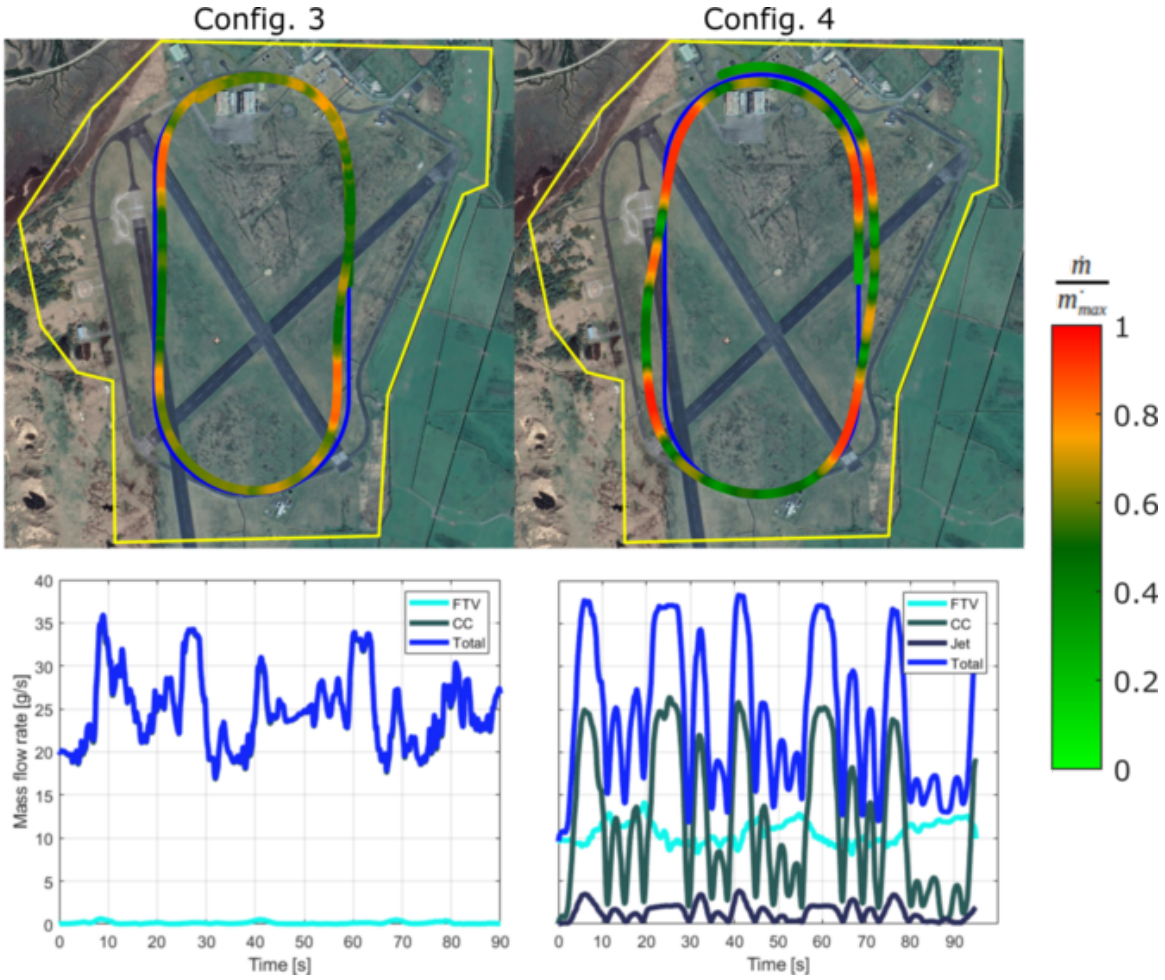

Figure 9.8. Mass flow used for flying proposed circuit at 100m AGL. Blue track is proposed circuit and the coloured line represents the mass flow used as a ratio to total budget.

A comparison of the mass flow used by each of the configurations is tabulated in Table 9.6 The mean mass flow used by configuration 3 is 3% of the total mass flow budget greater than configuration 4. However, the standard deviation of configuration 3 is 7% less meaning that the demand from the engine is more constant. Both configurations use the total mass flow budget during the manoeuvring. When considering the total mass flow used there is very little to separate the two configurations.

	Total Mass Flow			Yaw Mass Flow		
Configuration	Mean	Standard Deviation	Peak	Mean	Standard Deviation	Peak
3	62%	14%	100%	0.4%	0.4%	2.0%
4	59%	21%	98%	3.3%	2.4%	10%

Table 9.6. Comparison of mass flow for configuration 3(YFTV)and 4(WRJ),percentage of mass flow budget.

When considering the mass flow used by the yaw configurations however there is a much

more significant difference. It is clear from this that the FTV operating in yaw requires considerably less mass flow than the jets, both in terms of the mean and peak demand. This is important as it allows the aircraft more mass flow for pitch and roll control thereby increasing the agility of the aircraft.

Finally, in Fig. 9.9 we compare the ability of each of the configurations to maintain the setpoint of 100m AGL altitude and zero sideslip. Considering the altitude setpoint, we can see that both configurations maintain the setpoint to within $\pm 2m$ (2%). Configuration 4 (WRJ) keeps a better track of the setpoint due to the higher control authority in pitch of the FTV compared to the CC used in configuration 3 (YFTV). This is reversed when looking at the sideslip setpoint. The greater yaw authority of configuration 3 (YFTV) compared to the WRJ means that the sideslip is kept within $\pm 0.2^{\circ}$ compared to $\pm 0.9^{\circ}$, an improvement of approximately 75%.

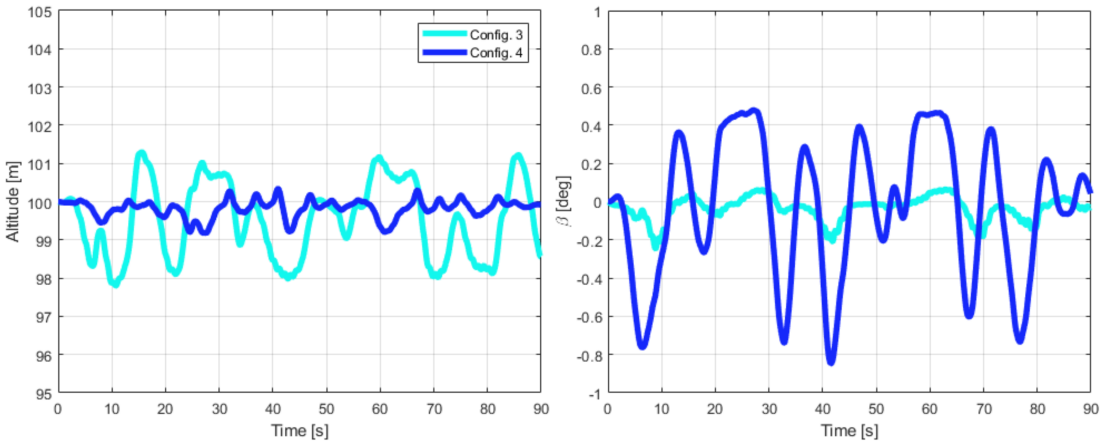

Figure 9.9. Altitude (Left) and Sideslip angle (Right) during the flight for configuration 3 (YFTV) and 4 (WRJ).

With little to separate the performance of configuration 3 (YFTV) and 4 (WRJ) this yaw authority could be the deciding factor. Whilst both configurations follow the proposed track closely using a similar mass flow budget, maintaining the condition of zero sideslip is important as perturbations (e.g. gusts/turbulence) in conditions where the aircraft is directionally unstable could lead to departure from controlled flight. Therefore, when considering a control option for full 3-axis control configuration 3 (YFTV) would be the preferred solution. However it is worth noting that for a YFTV configuration, changes to the engine thrust level will impact both the bleed air available and the magnitude of thrust which can be vectored. This could significantly impact the applicable range of a YFTV solution.

9.4 Conclusions

This work has developed a simulation tool to assess the suitability of various fluidic control configurations for full three axis control of the MAGMA aircraft. Four fluidic configurations have been assessed against a typical mission profile of a circuit with a width of 600m and length of 1.3km above Snowdonia Aerospace Centre, Llanbedr, UK. The effectiveness of each of the control actuators used is based upon data from flight tests, with the actuators manufactured at the limits of current 3D printing technology.

A preliminary analysis has shown that an approach based on asymmetric induced drag with two control actuators on each wing would not have sufficient control authority to maintain a setpoint of zero-sideslip during the rolling manoeuvres required in the circuit. Therefore, only the approaches which modify the thrust line to maintain a yawing moment (i.e. Yaw thrust vectoring and wingtip reaction jets) are considered for simulation. Simulations of the aircraft following the proposed circuits show both remaining configurations are able to follow the proposed circuit well, using similar mass flow budgets with a mean usage of approximately 60% of the available bleed air. The altitude setpoint is also maintained to within 2% by both configurations. The primary differentiator between these configurations is the ability to maintain zero sideslip. The superior yaw authority of the yaw FTV configuration means that this is the preferred option for full three axis control.

The results show that, with fluidic devices manufactured using current technology, it would be possible to implement a full three axis control on a sub-scale demonstrator aircraft with the fins completely removed. These controls will have sufficient authority to trim the aircraft and fly a full circuit without the need for any conventional control surfaces in still conditions and continuously at maximum thrust. Whilst these conditions may seem somewhat onerous, they do indicate that the maturity of fluidic controls is approaching the point where they can find practical application in more routine flight conditions. Further investigation is needed to validate these control solutions for gust and turbulence rejection in addition to terminal flight phases.

Chapter 10

Conclusions

10.1 Review of Contributions

The key contributions of the thesis are:

- Creation of a low order design method for identifying the most effective regions for AFC on an airframe to achieve yaw control without roll coupling.
- Creation of a control allocation method based on mode shaping to generate a yawing moment with no roll, pitch or lift coupling using asymmetric induced drag under steady flight conditions
- Extension of the control mode shaping method to allow yaw control during a rolling manoeuvre. This extension includes the anti-symmetric component of lift induced due to roll rate and its effect on induced drag.
- Application of the developed method to aircraft which control suites comprising both conventional control surfaces and fluidic circulation control actuators.
- Creation of a path planning algorithm to generate a feasible set of roll angle demands over a finite horizon given a constraint on the roll acceleration.
- A comparison of aircraft control suites comprising only fluidic actuators to affect three-axis control on a representative tailless aircraft for a typical mission. This involved the development of an analytical framework for evaluation of competing AFC solutions. The feasibility of full 3-axis control using only AFC was demonstrated for still conditions at maximum thrust.

10.2 Asymmetric Control Actuation

10.2.1 Control allocation

Through the work in this thesis a new method of defining an asymmetric control actuation has been developed, this has been named control mode shaping. It is so named as the premise of the method defines base asymmetric 'mode shapes' which can be either control deflections or changes in the local lift coefficient. The asymmetric control component can then be defined as a combination of these mode shapes. The analysis in this work has shown the feasability of using mode shapes to develop the required yaw control authority to trim at a steady sideslip and perform gentle manoeuvres. However, where greater yawing moments are required (i.e. terminal flight phases and spin recovery) an additional yaw control effector may be required to supplement the mode shaping. Nevertheless, mode shaping is shown to be a valid control option for cruise stages and gentle manoeuvring with a reduced impact on deployed area when compared to conventional, profile drag based control solutions. The key features of control mode shapes are:

1. **Mode shapes are defined from an aerodynamic analysis of the aircraft.**

   A control mode shape is defined as an actuation input which produces no change in the lift, pitching moment or rolling moment on the aircraft. By defining the asymmetric control input from these mode shapes, a yawing moment can be generated with no coupling to other axes. They are found by conducting a low order aerodynamic analysis of the forces and moments produced due to control actuation and assembling a linear system of this response in lift, pitching moment and rolling moment with respect to the control actuation. The mode shape is then defined by taking the null space of this system.

2. **The number of mode shapes is defined by the degree to which the aircraft is overactuated.**

   As the mode shapes are defined by the null space of a linear system, the number of null space vectors produced is by definition the degree to which the system is rank deficient. The number of inputs into the system is equal to the number of independent actuators and there are three unique functions (i.e. the lift, pitching moment and rolling moment) we seek to maintain. Therefore, the number of mode shapes generated is equal to the number of *independent* actuators minus three.

3. **When defining yaw control using mode shapes, there is no secondary control effect.**

In defining the mode shapes, a linear system defining the response in lift, pitching moment and rolling moment in response to a given actuation input is assembled. Therefore, defining mode shapes using null space of this system in theory guarantees that there is zero coupling with these forces and moments. Furthermore, any combination of mode shapes will generate no coupling effect.

4. **Mode shapes are unaffected by the state of the aircraft.**

   The assumption of linear aerodynamics for small control deflections and at low angles of attack is valid regardless of the method used to calculate the response of the aircraft to control inputs. Therefore, linearly superimposing the isolated effect of the control on the unactuated state on the aircraft is valid. We can therefore conclude that the mode shapes are invariant with changes in angle of attack or body angular rates.

5. **The yawing moment generated by the implementation of a mode shape *is* affected by the aircraft state.**

   The drag and yawing moment produced as a consequence of the asymmetries in the lift distribution do depend on the aircraft state. This is because the induced drag at any spanwise point is proportional to the product of the local lift and the spanwise rate of change of that lift. Because of this, any flight control system used on an aircraft must change the level of actuation as the aircraft manoeuvres in order to maintain a given yawing moment.

6. **Any method of actuation can be used to define a mode shape.**

   Provided that any actuator of interest modifies the local lift coefficient over a region of the wing the mode shaping methodology can be applied to it. There is one restriction that in the current form of the method, the change in local lift in response to some actuation parameter must be linear (or linearly mapped). If it is not then the method could still be applied, however rather than using the null space, the zero set of the system defining lift, pitching moment and rolling moment must be found. This would undoubtedly lead to a more complex control algorithm.

10.2.2 Case Studies

The simulated performance of the modeshaping technique has been compared to more conventional profile drag based controls for the MAGMA aircraft and a more generic swept trapezoidal planform. The control was implemented using a system of three trailing-edge camber flaps on each wing for both aircraft.

For the MAGMA aircraft, the control effectiveness was compared to mid-chord spoilers. At trim conditions (Chapter 6), it was found that both control options were able to produce yawing moment sufficient to trim up to a sideslip angle angle of 10°. Additionally, for small yawing moments (sideslip trim angles of up to 4°) the aggregate control deflection from the mode shaping technique is less than that of the more conventional spoiler solution. During a rolling manoeuvre (Chapter 8) the reduction in drag is not considered as a transient increase is unlikely to be of concern to designers. The reduction in control deflection is considered here as it has an impact on both survivablity and actuator sizing and is reduced by at least a factor of 2. Greater reductions of up to a factor of 10 for the least aggressive manoeuvres considered.

10.3 Fluidic Control

10.3.1 Low Angle of Attack AFC

1. **A moment due to AFC is produced by changing the surface pressure over an area removed from the centre of gravity.**

   If we are agnostic to the actuation method used to generate a moment, we can generalise the effect of an AFC actuator to changing the surface pressure over a given area which thereby generates a force normal to the area affected. The moment produced is then the cross product of the position of the area affected by the actuator relative to the centre of gravity and the force generated by the change in pressure. By generalising the effect of the actuator in this way, it is possible to identify the regions of the aircraft most suitable for generating a moment about any axis of interest.

2. **On a tailless with the fins removed, there are few areas which contribute to the yawing moment.**

   For an all-flying wing configuration, there is very little projected area when the aircraft is viewed from the front or the side. As this area is what will contribute to the yawing moment, there are limited opportunities for actuation.

3. **In order to achieve a pure yawing moment, a large change in surface pressure is required.**

   In the analysis performed in Chapter 4, only the lateral moments are considered. Even in this case, the changes in surface pressure required to ensure that the rolling moment is zero for a given yawing moment are relatively large. Large changes in surface pressure require AFC actuators with very high gains, a large amount of fluid for actuation or a combination

of both. Fluidic actuators utilised in flight will typically have a low mass flow budget and therefore it is unlikely that the required changes in surface pressure would be possible under this constraint without leveraging an instability in the flow to achieve a high gain. Typically, this is most effective at high angles of attack and would therefore not provide a useful yaw control solution for a large part of the flight envelope.

10.3.2 Case study: Three Axis Fluidic Control

Due to the limitations of directly modifying the surface pressure using AFC previously discussed the effectiveness of the mode shaping applied to circulation control is compared with alternate three axis control configurations (Chapter 9). The case study aircraft used is MAGMA and the control configurations used are in keeping with the simplistic design philosophy of the aircraft and effectiveness of the AFC actuators are taken from flight test data.

In this case study the mode shaping technique is successfully applied to a control suite which uses fluidic circulation control to modify the local lift coefficient on the wing rather than a conventional system of trailing edge flaps. This shows the generality of the mode shaping method developed in that it can be applied to any actuator which modifies the lift over a section of the wing. It is not restricted to moving control surfaces. Although the yawing moment generated by mode shaping within Chapter 9 is small, this is believed to be due to the simplistic configuration and small mass flow budget. More complex layouts involving multiple CC effectors on each wing are likely to show dramatic improvements in the yaw control authority.

In addition, a model predictive control method is developed to determine the optimum mass flow input for each of the actuators to fly a representative mission for the MAGMA aircraft. This provides a consistent approach to compare the configurations in defining the required control inputs. In developing the control algorithm for this work, it was clear that the conventional path planning techniques were not applicable to aircraft with the limitations on maneuverability as imposed by the limited mass flow budget. Therefore, a path planning algorithm was developed which was able to incorporate a restriction of the angular acceleration in the roll axis. Although it was developed as a solution in the context of fluidic controls, the usefulness of this algorithm extends to any fixed wing aircraft with low roll control authority.

Of the alternate control configurations examined, the two using thrust methods (i.e. FTV and reaction jets) for yaw control were able to meet the control demands of the aircraft within the available mass flow budget. This provides a demonstration that with currently available technology it is possible to achieve full three axis control of a tailless aircraft using only fluidic controls. Although it is worth noting that this does require the aircraft to remain at maximum

thrust in still conditions.

10.4 Recommendations for Future Work

1. Application of the mode shape technique to continuous changes in the lift distribution.

The work in this thesis has demonstrated the use of the mode shaping technique to generate yawing moments using actuators which modify the local lift coefficient over discrete sections of the wing. However it is also possible to modify the lift over the wing in a continuous way, for example in morphing wings. To generate yaw using morphing wings with no coupling is a particular challenge due to the large number of degrees of freedom present. It is thought that using a mode shaping technique to define mode shapes in terms of Fourier coefficients it would be possible to define a control strategy for three axis control by modifying the lift distribution in a continuous manner.

2. Extension of the mode shaping method to allow for larger control deflections.

The mode shaping method as presented in this thesis assumes that the response of the aircraft to control surface deflection is linear. To ensure this assumption remains valid the maximum control surface deflection is limited to 10°, somewhat limiting the available control authority. An investigation into the validity of the linear assumption at higher angles of attack and modifications to the method to account for significant non-linearities could lead to a greater control authority before saturation from the mode shaping technique.

3. Application of the developed methods to full scale flight vehicles.

A full scale operational UCAV have an all up mass exceeding 10 tonnes with a wingspan in the range $8 - 15m$. This means the mass moments of inertia in all three axes are increased meaning that a greater yawing moment must be generated to achieve the same value of yaw acceleration. This effect will require careful analysis to demonstrate over which mission phases mode shaping remains effective as the wing loading of the aircraft increases.

4. Development or application of an optimisation technique suitable for use in real time.

As the number of mode shapes increases, the optimisation problem (defined in Chapter 5) to find the combination of gains to achieve a given yawing moment with the least drag or aggregate deflection becomes increasingly expensive to solve. For a successful implementation in practice, this optimisation problem must be solved in real time at the update rate required to

maintain control of the aircraft. This update rate is determined by the inherent stability of the aircraft. Therefore, for tailless aircraft with marginal directional stability or instabilities this optimisation becomes very computationally expensive. Methods to determine the optimum combination of gains with reduced computational requirements or as a function of the flight condition such that they can be defined before flight makes control allocation in the way defined in this thesis more implementable.

5. **Development of integrated simulation models to capture hardware limitations and turbulence response.**

   In order to qualify a mode shaping approach for flight it will be necessary to show that such a control method does not introduce dynamic instabilities when interfaced with real hardware. Therefore a full simulation model which can incorporate both sensor and actuator delays will be required to demonstrate the flight conditions in which mode shaping is most useful. As part of this, it will also be possible to test the response of mode shaping to turbulence and gusts.

6. **Practical testing of mode shaping concepts.**

   The tools used within this work have been validated against existing experimental data. However, there has been no practical testing to date of the outcomes of this work. There is therefore an opportunity to demonstrate the generation of yawing moments using this method in ground based experiments (i.e. wind tunnels) and to demonstrate useful control inputs without coupling in flight test experiments.

7. **Application of the mode shaping technique for other purposes.**

   The methods developed within this work have focused on developing mode shapes which produce asymmetric induced drag. However, the methodology could be easily adapted to meet other objectives such as gust load alleviation and flutter suppression. This would require additional analysis to deal with such transient conditions but if developed in the early design stages could lead to a reduction in structural weight on any aircraft, not just flying wings.

References

[1] R. A. Bitzinger, *The modern defense industry: political, economic, and technological issues: political, economic, and technological issues*. ABC-CLIO, 2009.

[2] S. M. Hitzel, "Some lo-ucav directional control issues," in *2018 Applied Aerodynamics Conference*, 2018, p. 3330.

[3] J. R. Chambers and R. M. Hall, "Historical review of uncommanded lateral-directional motions at transonic conditions," *Journal of aircraft*, vol. 41, no. 3, pp. 436–447, 2004.

[4] R. Davidson, "Flight control design and test of the joint unmanned combat air system (j-ucas) x-45a," in *AIAA 3rd "Unmanned Unlimited" Technical Conference, Workshop and Exhibit*, 2004. DOI: 10.2514/6.2004-6557. eprint: https://arc.aiaa.org/doi/pdf/10.2514/6.2004-6557. [Online]. Available: https://arc.aiaa.org/doi/abs/10.2514/6.2004-6557.

[5] S. Woolvin, "Conceptual design studies of the 1303 configuration," in *24th AIAA Applied Aerodynamics Conference*, ser. Fluid Dynamics and Co-located Conferences, American Institute of Aeronautics and Astronautics, Jun. 2006. DOI: 10.2514/6.2006-2991. [Online]. Available: https://doi.org/10.2514/6.2006-2991.

[6] W. Crowther, I. Lunnon, T. Shearwood, *et al.*, "Flight demonstration of fluidic controls on a tailless flight vehicle – an overview of the magma programme fluidic technologies," in *RAES 2018 Applied Aerodynamics Conference*, 2018, pp. 24–26.

[7] C. Warsop, W. J. Crowther, and T. R. Shearwood, "Nato avt-239: Flight demonstration of fluidic flight controls on the magma subscale demonstrator aircraft nato avt-239 special session," in *AIAA Scitech 2019 Forum*, 2019, pp. 1–20, ISBN: 9781624105784. DOI: 10.2514/6.2019-0282.

[8] H. Babinsky, "How do wings work?" *Physics Education*, vol. 38, no. 6, pp. 497–503, 2003, ISSN: 13616552. DOI: 10.1088/0031-9120/38/6/001. [Online]. Available: www.iop.org/journals/physed.

[9] J. D. Anderson, *Fundamentals of aerodynamics*, 6th, ser. McGraw-Hill series in aeronautical and aerospace engineering. Boston, Mass: McGraw-Hill Higher Education, 2017, ISBN: 9781259129919.

[10] D. P. Raymer, *Aircraft design : a conceptual approach*, 5th ed., ser. AIAA education series. Reston, Va: American Institute of Aeronautics and Astronautics, 2012, ISBN: 9781600869112.

[11] L. Prandtl, "Königliche gesellschaft der wissenschaften zu göttingen," *ed. Tragflügeltheorie*, 1918.

[12] P. Saffman, *Vortex Dynamics*. Cambridge Univ. Press, 1992.

[13] H. Glauert, *The elements of aerofoil and airscrew theory*. Cambridge University Press, 1983.

[14] H. Multhopp and M. Schwabe, *Die Berechnung der Auftriebsverteilung von Tragflügeln*. 1938.

[15] A. Betz and L. Prandtl, "Schraubenpropeller mit geringstem Energieverlust," *Goett inger Ndchrichte*, 1919.

[16] H. Multhopp, "Methods for calculating the lift distribution of wings (subsonic lifting-surface theory)," Ministry of Supply, Tech. Rep., 1955. [Online]. Available: `http://naca.central.cranfield.ac.uk/reports/arc/rm/2884.pdf`.

[17] J. B. Russell, *Performance and stability of aircraft*. London : Arnold ; New York : Wiley, 1996, ISBN: 0340631708.

[18] G. S. Jones and R. D. Joslin, *Applications of circulation control technology*. American Institute of Aeronautics and Astronautics, May 2006. DOI: `10.2514/4.866838`.

[19] M. Forster, M. Biava, and R. Steijl, "Multipoint optimisation of coanda surfaces for transonic circulation control using the adjoint method," in *8th AIAA Flow Control Conference*, 2016, p. 3773.

[20] R. Harte, *Improvements in Means and Apparatus for Effecting Aerial Locomotion*, 1870.

[21] A. R. Weyl, "Tailless Aircraft and Flying Wings: A Study of Their Evolution and Their Problems," *Aircraft Engineering and Aerospace Technology*, vol. 16, no. 12, pp. 340–360, 1944, ISSN: 00022667. DOI: `10.1108/eb031199`.

[22] C. B. Smith, *Testing time. A study of man and machine in the test flying era.* 1961.

[23] S. Neumark, "Analysis of the Longitudinal Stability of Tailless and Tail-first Aircraft," RAE, Tech. Rep., 1944.

[24] K. G. Wilkinson, "The longitudinal response of tailless aircraft," RAE, Tech. Rep., 1945.

[25] A. W. Thorpe and M. F. Curtis, "Lateral stability of tailless aircraft," Aeronautical Research Council, Tech. Rep., 1943. [Online]. Available: https://reports.aerade.cranfield.ac.uk/handle/1826.2/3210.

[26] United States Air Force, "Trends of Development in Flying Wing and Tailless Aircraft," Tech. Rep., 1946.

[27] W. Bishop, "The Development of Tailless Aircraft and Flying Wings*," *The Aeronautical Journal*, vol. 65, no. 612, pp. 799–806, Dec. 1961, ISSN: 0368-3931. DOI: 10.1017/S0368393100075957. [Online]. Available: https://www.cambridge.org/core/journals/aeronautical-journal/article/abs/development-of-tailless-aircraft-and-flying-wings/F1DDD1D7E50ADC7CFE92028102D6DD87.

[28] G. H. Lee, "Tailless Aircraft Design Problems," *The Aeronautical Journal*, vol. 51, no. 434, pp. 109–131, Feb. 1947, ISSN: 0368-3931. DOI: 10.1017/S036839310011185X. [Online]. Available: https://www.cambridge.org/core/journals/aeronautical-journal/article/abs/tailless-aircraft-design-problems/4462ACDD4F04EA86433

[29] E. Schmidt, "Distinctive capabilities: Addressing the fighter gap with the silent eagle," Air University, Air Command and Staff College Maxwell Air Force Base United …, Tech. Rep., 2011.

[30] K. M. Dorsett and D. R. Mehl, "INNOVATIVE CONTROL EFFECTORS (ICE). WL-TR-96-3043," Wright Laboratory, Tech. Rep., 1996.

[31] C. Nieto-Wire and K. Sobel, "Reconfigurable delta operator eigenstructure assignment for a tailless aircraft," in *AIAA Guidance, Navigation, and Control Conference and Exhibit*, 2009, ISBN: 9781563479786. DOI: 10.2514/6.2009-6306. [Online]. Available: http://arc.aiaa.org.

[32] W. J. Gillard and K. M. Dorsett, "Directional control for tailless aircraft using all moving wing tips," in *22nd Atmospheric Flight Mechanics Conference*, 1997, pp. 51–58. DOI: 10.2514/6.1997-3487. [Online]. Available: http://arc.aiaa.org.

[33] S. R. Wells and R. A. Hess, "MIMO sliding mode control for a tailless fighter aircraft, an alternative to reconfigurable architectures," in *AIAA Guidance, Navigation, and Control Conference and Exhibit*, 2002, ISBN: 9781563479786. DOI: 10.2514/6.2002-4650. [Online]. Available: http://arc.aiaa.org.

[34] J. M. Barker and G. J. Balas, "Flight control of a tailless aircraft via linear parameter-varying techniques," in *1999 Guidance, Navigation, and Control Conference and Exhibit*, 1999, pp. 941–950. DOI: 10.2514/6.1999-4133. [Online]. Available: http://arc.aiaa.org.

[35] D. S. Grismer, J. H. Myatt, P. D. McKeehen, and J. M. Buffington, "Application of a nonlinear-indicial-response model to a tailless aircraft simulation," in *22nd Atmospheric Flight Mechanics Conference*, 1997, pp. 392–402. DOI: 10.2514/6.1997-3644. [Online]. Available: http://arc.aiaa.org.

[36] A. D. Ngo, W. C. Reigelsperger, S. S. Banda, and J. A. Bessolo, "Multivariable control law design for a tailless airplane," in *1996 Guidance, Navigation, and Control Conference and Exhibit*, AIAA, 1996, pp. 1–11. DOI: 10.2514/6.1996-3866. [Online]. Available: http://arc.aiaa.org.

[37] M. A. Niestroy, K. M. Dorsett, and K. Markstein, "A tailless fighter aircraft model for control-related research and development," in *AIAA Modeling and Simulation Technologies Conference, 2017*, 2017, ISBN: 9781624104510. DOI: 10.2514/6.2017-1757. [Online]. Available: http://arc.aiaa.org.

[38] A. G. Sparks, "Linear parameter varying control for a tailless aircraft," in *1997 Guidance, Navigation, and Control Conference*, 1997, pp. 1035–1043. DOI: 10.2514/6.1997-3636. [Online]. Available: http://arc.aiaa.org.

[39] A. D. Ngo, W. C. Reigelsperger, S. S. Banda, and J. A. Bessolo, "Tailless aircraft control law design using dynamic inversion & μ-synthesis," *IEEE Conference on Control Applications - Proceedings*, pp. 107–112, 1996. DOI: 10.1109/cca.1996.558615.

[40] C. Nieto-Wire and K. Sobel, "Eigenstructure assignment for a tailless aircraft," in *Collection of Technical Papers - AIAA Guidance, Navigation, and Control Conference 2007*, vol. 1, 2007, pp. 1053–1073, ISBN: 1563479044. DOI: 10.2514/6.2007-6417. [Online]. Available: http://arc.aiaa.org.

[41] J. M. Buffington, "Modular Control Law Design for the Innovative Control Aircraft Effectors (ICE) Tailless Fighter Configuration," Air Force Research Lab, Tech. Rep., Jun. 1999, p. 154. [Online]. Available: https://apps.dtic.mil/sti/citations/ADA374954.

[42] C. Warsop, D. R. Smith, and D. N. Miller, "NATO AVT-239: Innovative control effectors for manoeuvring of air vehicles-conclusions and next steps," in *AIAA Scitech 2019 Forum*, 2019, pp. 1–10, ISBN: 9781624105784. DOI: 10.2514/6.2019-0284.

[43] C. Warsop, M. Forster, and W. J. Crowther, "NATO AVT-239 task group: Supercritical coanda based circulation control and fluidic thrust vectoring NATO AVT-239 special session," in *AIAA Scitech 2019 Forum*, 2019, pp. 1–24, ISBN: 9781624105784. DOI: 10.2514/6.2019-0044.

[44] D. R. Smith and C. Warsop, "NATO AVT-239 Task Group: 'Innovative Control Effectors for Manoeuvring of Air Vehicles' – Introduction and Overview," in *AIAA Scitech 2019 Forum*. DOI: 10.2514/6.2019-0041. [Online]. Available: https://arc.aiaa.org/doi/abs/10.2514/6.2019-0041.

[45] M. A. Niestroy, D. R. Williams, and J. Seidel, "NATO AVT-239 task group: Active flow control simulation of the tailless ICE aircraft," in *AIAA Scitech 2019 Forum*, 2019, pp. 1–15, ISBN: 9781624105784. DOI: 10.2514/6.2019-0279.

[46] D. N. Miller, "NATO AVT-239 Task Group: An Assessment on the Prospects of Active Flow Control on a Future UAS," January, 2019, pp. 1–10. DOI: 10.2514/6.2019-0281.

[47] B. H. Maines and D. N. Miller, "NATO AVT-239 task group: Flow control system integration into the tailless ice aircraft," in *AIAA Scitech 2019 Forum*, 2019, pp. 1–8, ISBN: 9781624105784. DOI: 10.2514/6.2019-0046.

[48] S. S. Brandt, T. E. McLaughlin, D. R. Williams, B. H. Crawford, and J. A. Holmes, "Nato avt-239 task group: Flight test of compressed and bleed-air driven control effectors on the ice/saccon uas subscale aircraft," in *AIAA Scitech 2019 Forum*, 2019, ISBN: 9781624105784. DOI: 10.2514/6.2019-0283. [Online]. Available: http://arc.aiaa.org.

[49] D. N. Miller, D. R. Williams, C. Warsop, and D. R. Smith, "Nato avt-239 task group: Approach to assess prospects of active flow control on a next-gen tailless aircraft," *AIAA Scitech 2019 Forum*, no. January, pp. 1–8, 2019. DOI: 10.2514/6.2019-0042.

[50] A. Llopis-Pascual, "Supersonic Coanda Jets For Flight Control Effectors," Ph.D. dissertation, University of Manchester, Manchester, Dec. 2017. [Online]. Available: https://www.research.manchester.ac.uk/portal/en/theses/supersonic-coanda-jets-for-flight-control-effectors(0f6c2bba-aacd-4eca-8b62-d13208f2bb30).html.

[51] B. Robertson Welsh, "On the Influence of Nozzle Geometries on Supersonic Curved Wall Jets," Ph.D. dissertation, University of Manchester, Manchester, Aug. 2017. [Online]. Available: https://www.research.manchester.ac.uk/portal/en/theses/on-the-influence-of-nozzle-geometries-on-supersonic-curved-wall-jets(bc8817e4-c812-44bc-8dfb-f5d0fdf62a72).html.

[52] O. Afilaka, "Normal-Blowing Fluidic Thrust Vectoring for Supercritical Aft-deck Convergent-Divergent nozzles," Ph.D. dissertation, University of Manchester, 2019. [Online]. Available: https://www.research.manchester.ac.uk/portal/en/theses/normalblowing-fluidic-thrust-vectoring-for-supercritical-aftdeck-convergentdivergent-nozzles(c6a75bc7-3c0b-4fec-8720-9192a3246df6).html.

[53] T. R. Shearwood, M. R. A. Nabawy, W. J. Crowther, and C. Warsop, "A control allocation method to reduce roll-yaw coupling on tailless aircraft," in *AIAA Scitech 2021 Forum*, 2021. DOI: 10.2514/6.2021-1826. [Online]. Available: http://arc.aiaa.org.

[54] K. Nickel and M. Wohlfahrt, *Tailless aircraft in theory and practice*. Washington, DC : American Institute of Aeronautics and Astronautics ; London, England : E. Arnold, 1994, ISBN: 0340614021.

[55] D. Ciliberti, P. Della Vecchia, F. Nicolosi, and A. De Marco, "Aircraft directional stability and vertical tail design: A review of semi-empirical methods," *Progress in Aerospace Sciences*, vol. 95, pp. 140–172, 2017, ISSN: 0376-0421. DOI: https://doi.org/10.1016/j.paerosci.2017.11.001. [Online]. Available: https://www.sciencedirect.com/science/article/pii/S0376042117301598.

[56] R. C. Innis and W. E. Mc Neill, "The effect of yaw coupling in turning maneuvers of large transport aircraft," in *Conference on Aircraft Operating Problems*, 1965.

[57] R. A. DAVIS, "The Response of a Bisymmetric Aircraft to Small Combined Pitch, Yaw, and Roll Control Actions," *Journal of the Aeronautical Sciences*, vol. 24, no. 12,

pp. 905–910, 1957. DOI: 10.2514/8.3998. [Online]. Available: https://doi.org/10.2514/8.3998.

[58] J. Jones, "Simplified spectral analysis of the motion of an aircraft with a saturating yaw-damper," Tech. Rep., 1965. [Online]. Available: https://repository.tudelft.nl/islandora/object/uuid%3A4bc80e89-2bc1-4ec8-b710-b99a71487505.

[59] M. BERG, "Simultaneous control-law synthesis of an aircraft yaw-damper and modal suppression system using parameter optimization," 1991. DOI: 10.2514/6.1991-2630. [Online]. Available: http://arc.aiaa.org.

[60] W. H. Phillips, "GRAPHICAL SOLUTION OF SOME AUTOMATIC - CONTROL PROBLEMS INVOLVING SATURATION EFFECTS WITH APPLICATION TO YAW DAMPERS FOR AIRCRAFT," *National Advisory Committee for Aeronautics*, vol. OCtober, no. Technical Note 3034, p. 42, 1953.

[61] A. A. Schy and J. Gates, Ordway B., "A Theoretical Method of Analyzing the Effects of Yaw-Damper Dynamics on the Stability of an Aircraft Equipped With A Second-Order Yaw Damper," Tech. Rep., Dec. 1952. [Online]. Available: https://apps.dtic.mil/sti/citations/ADA377084.

[62] B. S. Esker and J. G. McArdle, "EXPERIMENTAL PERFORMANCE OF A VENTRAL NOZZLE WITH PITCH AND YAW VECTORING CAPABILITY FOR SSTOVL AIRCRAFT," *SAE Transactions*, vol. 102, pp. 353–363, 1993, ISSN: 0096736X, 25771531. [Online]. Available: http://www.jstor.org/stable/44739984.

[63] B. R. Taylor and S. Y. Yoo, "Engine yaw augmentation for hybrid-wing-body aircraft via optimal control allocation techniques," in *AIAA Guidance, Navigation, and Control Conference 2011*, 2011, ISBN: 9781600869525. DOI: 10.2514/6.2011-6253. [Online]. Available: http://arc.aiaa.org.

[64] S. P. Fears, "Low-speed wind-tunnel investigation of a porous forebody and nose strakes for yaw control of a multirole fighter aircraft," NASA, Tech. Rep. August 1995, 1995. [Online]. Available: https://ntrs.nasa.gov/search.jsp?R=19960001960.

[65] N. J. Wood and L. Roberts, "Experimental results of the control of a vortical flow by tangential blowing," NASA, Tech. Rep., 1986. [Online]. Available: https://ntrs.nasa.gov/citations/19860020622.

[66] K. P. Williams and S. P. Garry, "PNEUMATIC YAW CONTROL AT HIGH ANGLE OF ATTACK FOR LOW OBSERVABILITY COMBAT AIRCRAFT," in *21st ICAS Congress*, Melbourne: AIAA, 1998. [Online]. Available: http://icas.org/ICAS_ARCHIVE/ICAS1998/PAPERS/1103.PDF.

[67] N. J. Wood and W. J. Crowther, "Yaw control by tangential forebody blowing," *The Aeronautical Journal (1968)*, vol. 98, no. 974, pp. 147–154, 1994. DOI: 10.1017/S000192400004999X.

[68] W. J. Crowther, "Yaw control at high angles of attack by tangential forebody blowing," Ph.D. dissertation, University of Bath, 1994. [Online]. Available: https://researchportal.bath.ac.uk/en/studentTheses/yaw-control-at-high-angles-of-attack-by-tangential-forebody-blowi.

[69] N. Pedreiro, "Experiments in aircraft roll-yaw control using forebody tangential blowing," Ph.D. dissertation, Stanford University, 1998. [Online]. Available: https://www.proquest.com/docview/304455005.

[70] L. L. Gamble and D. J. Inman, "A tale of two tails: developing an avian inspired morphing actuator for yaw control and stability," *Bioinspiration & Biomimetics*, vol. 13, no. 2, p. 26 008, Feb. 2018. DOI: 10.1088/1748-3190/aaa51d. [Online]. Available: https://doi.org/10.1088/1748-3190/aaa51d.

[71] D. Keidel, U. Fasel, and P. Ermanni, "Control authority of a camber morphing flying wing," *Journal of Aircraft*, pp. 1–10, 2020, ISSN: 1533-3868. DOI: 10.2514/1.c035606.

[72] B. Obradovic and K. Subbarao, "Modeling of flight dynamics of morphing-wing aircraft," *Journal of Aircraft*, vol. 48, no. 2, pp. 391–402, 2011, ISSN: 15333868. DOI: 10.2514/1.C000269. [Online]. Available: http://arc.aiaa.org.

[73] A. C. Henry, G. Molinari, J. R. Rivas-Padilla, and A. F. Arrieta, "Smart morphing wing: Optimization of distributed piezoelectric actuation," *AIAA Journal*, vol. 57, no. 6, pp. 2384–2393, 2019, ISSN: 00011452. DOI: 10.2514/1.J057254. [Online]. Available: www.aiaa.org/randp..

[74] E. A. Zebedee, A. Mohammed, and M. S. Lawal, "Towards Morphing Wing Technology in Aircraft for Improved Flight Performance," in *2019 2nd International Conference of the IEEE Nigeria Computer Chapter (NigeriaComputConf)*, 2019, pp. 1–5. DOI: 10.1109/NigeriaComputConf45974.2019.8949627.

[75] G. Stenfelt and U. Ringertz, "Lateral stability and control of a tailless aircraft configuration," *Journal of Aircraft*, vol. 46, no. 6, pp. 2161–2164, 2009, ISSN: 0021-8669. DOI: 10.2514/1.41092. [Online]. Available: http://arc.aiaa.org.

[76] ——, "Yaw control of a tailless aircraft configuration," *Journal of Aircraft*, vol. 47, no. 5, pp. 1807–1811, 2010, ISSN: 0021-8669. DOI: 10.2514/1.C031017. [Online]. Available: http://arc.aiaa.org/doi/10.2514/1.C031017.

[77] ——, "Yaw departure and recovery of a tailless aircraft configuration," *Journal of Aircraft*, vol. 50, no. 1, pp. 311–314, 2013, ISSN: 15333868. DOI: 10.2514/1.C031868. [Online]. Available: http://arc.aiaa.org.

[78] F. W. Lanchester, *Aerodynamics : constituting the first volume of A complete work on aerial flight / by F.W. Lanchester*, English, 4th ed. Constable London, 1918, xvi, 442 p. :

[79] L. Prandtl, "Applications of modern hydrodynamics to aeronautics," NACA, Tech. Rep., 1923. [Online]. Available: https://ntrs.nasa.gov/citations/19930091180.

[80] G. Kennedy and J. R. Martins, "Parallel solution methods for aerostructural analysis and design optimization," in *13th AIAA/ISSMO multidisciplinary analysis optimization conference*, 2010, p. 9308.

[81] J. J. Alonso, P. LeGresley, and V. Pereyra, "Aircraft design optimization," *Mathematics and Computers in Simulation*, vol. 79, no. 6, pp. 1948–1958, 2009.

[82] H. Wang, Y. Wang, S. Wang, and F. Zhou, "Optimization strategy for performance improvement of a lift fan cowl lip based on panel method," *Journal of Mechanical Science and Technology*, pp. 1–10, 2021.

[83] Y. Jin, M. Olhofer, and B. Sendhoff, "Managing approximate models in evolutionary aerodynamic design optimization," in *Proceedings of the 2001 Congress on Evolutionary Computation (IEEE Cat. No.01TH8546)*, vol. 1, 2001, 592–599 vol. 1. DOI: 10.1109/CEC.2001.934445.

[84] R. Yondo, E. Andrés, and E. Valero, "A review on design of experiments and surrogate models in aircraft real-time and many-query aerodynamic analyses," *Progress in Aerospace Sciences*, vol. 96, pp. 23–61, 2018, ISSN: 0376-0421. DOI: https://doi.org/10.1016/j.paerosci.2017.11.003. [Online]. Available: https://www.sciencedirect.com/science/article/pii/S0376042117300611.

[85] A. Jungo, M. Zhang, J. B. Vos, and A. Rizzi, "Benchmarking new ceasiom with cpacs adoption for aerodynamic analysis and flight simulation," *Aircraft Engineering and Aerospace Technology*, 2018.

[86] M. Tyan, M. Kim, V. Pham, C. K. Choi, T. L. Nguyen, and J.-W. Lee, "Development of advanced aerodynamic data fusion techniques for flight simulation database construction," in *2018 Modeling and Simulation Technologies Conference*, 2018, p. 3581.

[87] C. Humphreys-Jennings, I. Lappas, and D. M. Sovar, "Conceptual design, flying, and handling qualities assessment of a blended wing body (bwb) aircraft by using an engineering flight simulator," *Aerospace*, vol. 7, no. 5, p. 51, 2020.

[88] V. M. Falkner, "The calculation of aerodynamic loading on surfaces of any shape," HM Stationery Office, Tech. Rep., 1943.

[89] E. Pistolesi, "Considerations on the mutual interference of airfoil systems," *LGL Report*, pp. 214–219, 1937.

[90] J. DeYoung, "Historical evolution of vortex-lattice methods," NASA., Tech. Rep., 1976. [Online]. Available: `https://ntrs.nasa.gov/citations/19760021076`.

[91] L. R. Miranda, R. D. Elliot, and W. M. Baker, "A generalized vortex lattice method for subsonic and supersonic flow applications," NASA, Tech. Rep., 1977. [Online]. Available: `https://ntrs.nasa.gov/citations/19780008059`.

[92] R. Ajaj, M. Friswell, E. Saavedra Flores, O. Little, and A. Isikveren, "Span morphing: A conceptual design study," in *53rd AIAA/ASME/ASCE/AHS/ASC Structures, Structural Dynamics and Materials Conference 20th AIAA/ASME/AHS Adaptive Structures Conference 14th AIAA*, 2012, p. 1510.

[93] D. Smith, M. Lowenberg, D. Jones, and M. Friswell, "Computational and experimental validation of the active morphing wing," *Journal of aircraft*, vol. 51, no. 3, pp. 925–937, 2014.

[94] T. Melin, A. Isikveren, and M. Friswell, "Induced-drag compressibility correction for three-dimensional vortex-lattice methods," *Journal of Aircraft*, vol. 47, no. 4, pp. 1458–1460, 2010.

[95] A. Septiyana, K. Hidayat, A. Rizaldi, *et al.*, "Analysis of aerodynamic characteristics using the vortex lattice method on twin tail boom unmanned aircraft," in *AIP Conference Proceedings*, AIP Publishing LLC, vol. 2226, 2020, p. 020 003.

[96] T. O. Milward, M. A. Bromfield, N. Horri, R. Ali, and S. Scott, "Multipoint angle of attack sensing for avoidance of loss of control in flight," in *AIAA Scitech 2019 Forum*, 2019, p. 1540.

[97] A. Baig, T. Cheema, Z. Aslam, Y. Khan, H. S. Dar, and S. Khaliq, "A new methodology for aerodynamic design and analysis of a small scale blended wing body," *J Aeronaut Aerospace Eng*, vol. 7, no. 206, p. 2, 2018.

[98] J. L. Hess and A. M. O. Smith, "Calculation of nonlifting potential flow about arbitrary three-dimensional bodies," *Journal of ship research*, vol. 8, no. 04, pp. 22–44, 1964.

[99] A. Koreanschi, O. Sugar-Gabor, and R. M. Botez, "Drag optimisation of a wing equipped with a morphing upper surface," *The Aeronautical Journal*, vol. 120, no. 1225, pp. 473–493, 2016.

[100] M. Saeedi, R. Wuchner, and K.-U. Bletzinger, "Multi-fidelity fluid-structure interaction analysis of a membrane wing," *International Journal of Aerospace and Mechanical Engineering*, vol. 9, no. 1, pp. 169–176, 2015.

[101] L. L. Erickson, "Panel methods: An introduction," NASA, Tech. Rep., 1990. [Online]. Available: https://ntrs.nasa.gov/citations/19910009745.

[102] W. F. Phillips and D. O. Snyder, "Modern adaptation of prandtl's classic lifting-line theory," *Journal of Aircraft*, vol. 37, no. 4, pp. 662–670, 2000. DOI: 10.2514/2.2649. [Online]. Available: https://doi.org/10.2514/2.2649.

[103] J. Reid, "A General Approach to Lifting-Line Theory, Applied to Wings with Sweep," Ph.D. dissertation, Utah State University, Aug. 2020. DOI: https://doi.org/10.26076/b992-3234. [Online]. Available: https://digitalcommons.usu.edu/etd/7842.

[104] C. D. Goates and D. F. Hunsaker, "Practical Implementation of a General Numerical Lifting-Line Method," in *AIAA Scitech 2021 Forum*, 2021. DOI: 10.2514/6.2021-0118. [Online]. Available: https://arc.aiaa.org/doi/abs/10.2514/6.2021-0118.

[105] J. N. Weber, G. G. Brebner, and D. Kuchemann, "Low-speed tests on 45.deg swept-back wings," Aeronautical Research Council, Tech. Rep., 1958. [Online]. Available: http://naca.central.cranfield.ac.uk/reports/arc/rm/2882.pdf.

[106] C. Bliamis, I. Zacharakis, P. Kaparos, and K. Yakinthos, "Aerodynamic and stability analysis of a VTOL flying wing UAV," *IOP Conference Series: Materials Science and Engineering*, vol. 1024, p. 12 039, Jan. 2021. DOI: 10.1088/1757-899x/1024/1/012039. [Online]. Available: https://doi.org/10.1088/1757-899x/1024/1/012039.

[107] T. S. Ganesh, M. C. Keerthi, S. Girish, S. Sreeja Kumar, and B. Mrunalini, "Control of Tailless Aircraft," in *Design and Development of Aerospace Vehicles and Propulsion Systems*, S. K. Kumar, I. Narayanaswamy, and V. Ramesh, Eds., Singapore: Springer Singapore, 2021, pp. 523–532, ISBN: 978-981-15-9601-8.

[108] T. M. Sherman, J. E. C. Tirona, Y. Haggag, *et al.*, "Manufacturing and Flight Testing of a Vertical Tailless Blended Wing-Body UAV Design," in *AIAA Scitech 2021 Forum*. 2021. DOI: 10.2514/6.2021-0819. [Online]. Available: https://arc.aiaa.org/doi/abs/10.2514/6.2021-0819.

[109] R. KARIMI KELAYEH and M. H. DJAVARESHKIAN, "Aerodynamic investigation of twist angle variation based on wing smarting for a flying wing," *Chinese Journal of Aeronautics*, vol. 34, no. 2, pp. 201–216, 2021, ISSN: 1000-9361. DOI: https://doi.org/10.1016/j.cja.2020.06.022. [Online]. Available: https://www.sciencedirect.com/science/article/pii/S1000936120303101.

[110] Z. Liu, L. Luo, and B. Zhang, "An Aerodynamic Design Method to Improve the High-Speed Performance of a Low-Aspect-Ratio Tailless Aircraft," *Applied Sciences*, vol. 11, no. 4, 2021, ISSN: 2076-3417. DOI: 10.3390/app11041555. [Online]. Available: https://www.mdpi.com/2076-3417/11/4/1555.

[111] F. Liu, Z. Wang, S. Zhang, and Z. Xiao, "Development of a Modularized Virtual Flight Simulator based on Multiple Discipline Coupled Method," *Journal of Physics: Conference Series*, vol. 2010, no. 1, p. 12 181, Sep. 2021. DOI: 10.1088/1742-6596/2010/1/012181. [Online]. Available: https://doi.org/10.1088/1742-6596/2010/1/012181.

[112] K. Nickel, "Minimal drag for wings with prescribed lift, roll moment and yaw moment," MRC, Tech. Rep., 1983.

[113] D. F. Hunsaker, Z. S. Montgomery, and J. J. Joo, "Adverse-yaw control during roll for a class of optimal lift distributions," *2909 AIAA JOURNAL*, vol. 58, no. 7, pp. 1–

12, May 2020, ISSN: 0001-1452. DOI: 10.2514/1.J059038. [Online]. Available: https://doi.org/10.2514/1.J059038.

[114] J. Richter, K. Hainline, and R. Agarwal, "Examination of proverse yaw in bell-shaped spanload aircraft," *Mechanical Engineering and Materials Science Independent Study*, 2019. [Online]. Available: https://openscholarship.wustl.edu/mems500/91.

[115] A. S. Hahn, "Vehicle sketch pad: A parametric geometry modeler for conceptual aircraft design," in *48th AIAA Aerospace Sciences Meeting Including the New Horizons Forum and Aerospace Exposition*, 2010, ISBN: 9781600867392. DOI: 10.2514/6.2010-657. [Online]. Available: http://arc.aiaa.org.

[116] S. J. Morris, "Integrated aerodynamics and control system design for tailless aircraft," in *Astrodynamics Conference, 1992*, 1992, pp. 1–10. DOI: 10.2514/6.1992-4604. [Online]. Available: http://arc.aiaa.org.

[117] J. Park, J. Y. Choi, Y. Jo, and S. Choi, "Stability and control of tailless aircraft using variable-fidelity aerodynamic analysis," *Journal of Aircraft*, vol. 54, no. 6, pp. 2148–2164, 2017, ISSN: 15333868. DOI: 10.2514/1.C034052.

[118] H. Kaya, H. Tiftikci, U. Kutluay, and E. Sakarya, "A multi-fidelity aerodynamic modelling approach for nato avt 251 ucav – muldicon," in *2018 Applied Aerodynamics Conference*, 2018. DOI: 10.2514/6.2018-3000. eprint: https://arc.aiaa.org/doi/pdf/10.2514/6.2018-3000. [Online]. Available: https://arc.aiaa.org/doi/abs/10.2514/6.2018-3000.

[119] R. M. Cummings, "Introduction: Saccon unihabited combat aerial vehicle experimental and numerical simulations," *Journal of Aircraft*, vol. 49, no. 6, p. 1541, Nov. 2012, ISSN: 0021-8669. DOI: 10.2514/1.c032134. [Online]. Available: https://doi.org/10.2514/1.C032134.

[120] P. Löchert, K. C. Huber, C. M. Liersch, and A. Schütte, "Control device studies for yaw control without vertical tail plane on a 53° swept flying wing configuration," in *2018 Applied Aerodynamics Conference*, American Institute of Aeronautics and Astronautics Inc, AIAA, 2018, ISBN: 9781624105593. DOI: 10.2514/6.2018-3329.

[121] J. Rajput, W. G. Zhang, and X. B. Qu, "A differential configuration of split drag-rudders with variable bias for directional control of flying-wing," in *Engineering Providing of Industrial Development*, ser. Applied Mechanics and Materials, vol. 643, Trans Tech Publications, 2014, pp. 54–59. DOI: 10.4028/www.scientific.net/AMM.643.54.

[122] Z. Li, C. Yong, and L. Duo, "Multi-effectors distribution of flying wing with stealthy optimization," in *2017 36th Chinese Control Conference (CCC)*, Jul. 2017, pp. 2864–2869. DOI: 10.23919/ChiCC.2017.8027800.

[123] R. W. Burnham, *Drectional control device for aircraft*, 1984. [Online]. Available: https://patentimages.storage.googleapis.com/25/90/d3/fc54039dc33f0a/US4466586.pdf.

[124] D. R. Williams and J. Seidel, "Crossed-actuation afc for lateral-directional control of an ice-101/saccon ucav," in *8th AIAA Flow Control Conference*, American Institute of Aeronautics and Astronautics Inc, AIAA, 2016, ISBN: 9781624104329. DOI: 10.2514/6.2016-3167.

[125] G. J. Balas, A. K. Packard, J. Renfrow, C. Mullaney, R. T. M', and Closkey, "Control of the f-14 aircraft lateral-directional axis during powered approach," *Journal of Guidance, Control, and Dynamics*, vol. 21, no. 6, pp. 899–908, Nov. 1998, ISSN: 0731-5090. DOI: 10.2514/2.4323. [Online]. Available: http://arc.aiaa.org/doi/10.2514/2.4323.

[126] C. Hord, "The provision of crosswind and tailwind information (amofsg/10-sn no. 14)," Icao, Montréal, Tech. Rep., 2013. [Online]. Available: http://www.nlr-atsi.nl/downloads/safety-aspects-of-aircraft-operations-in-cross.pdf.

[127] U. S. D. of Defence, "Mil-f-8785c: Flying qualities of piloted airplanes," 1980.

[128] U. L. Ly and Y. K. Chan, "Time-domain computation of aircraft gust covariance matrices," in *6th Atmospheric Flight Mechanics Conference*, Danvers, MA: Aiaa, 1980, pp. 482–491. DOI: 10.2514/6.1980-1615.

[129] U. S. D. of Defence, "Mil-hdbk-1797: Flying qualities of piloted aircraft," Tech. Rep., 1997.

[130] T. R. Shearwood, M. R. A. Nabawy, W. J. Crowther, and C. Warsop, "A novel control allocation method for yaw control of tailless aircraft," *Aerospace*, vol. 7, no. 10, pp. 1–21, 2020, ISSN: 22264310. DOI: 10.3390/aerospace7100150.

[131] P. Löchert, K. C. Huber, M. Ghoreyshi, and J. Allen, "Control device effectiveness studies of a 53° swept flying wing configuration . experimental , computational , and modeling considerations," *Aerospace Science and Technology*, vol. 1, p. 105 319, 2019, ISSN: 1270-9638. DOI: 10.1016/j.ast.2019.105319. [Online]. Available: https://doi.org/10.1016/j.ast.2019.105319.

[132] "B-2 aerodynamic design," in *'Aerospace Engineering Conference and Show'*, 1990. DOI: 10.2514/6.1990-1802. [Online]. Available: https://arc.aiaa.org/doi/abs/10.2514/6.1990-1802.

[133] V. Denisov, L. Shkadov, and S. Chernyshev, "The flying wing concept – the challenge for the future," no. July, pp. 1–11, 2003. DOI: 10.2514/6.2003-2887.

[134] M. Tomac and G. Stenfelt, "Predictions of stability and control for a flying wing," *Aerospace Science and Technology*, vol. 39, pp. 179–186, 2014, ISSN: 12709638. DOI: 10.1016/j.ast.2014.09.007. [Online]. Available: www.elsevier.com/locate/aescte.

[135] Z. J. Li and D. L. Ma, "Control characteristics analysis of split-drag-rudder," in *Applied Mechanics and Materials*, vol. 472, 2014, pp. 185–190, ISBN: 9783037859650. DOI: 10.4028/www.scientific.net/AMM.472.185.

[136] W. J. Hong and D. L. Ma, "Influence of control coupling effect on landing performance of flying wing aircraft," *Applied Mechanics and Materials*, vol. 829, pp. 110–117, 2016. DOI: 10.4028/www.scientific.net/amm.829.110.

[137] J. Paterson, "Overview of low observable technology and its effects on combat aircraft survivability," *JOURNAL OF AIRCRAFT*, vol. 36, no. 2, 1999. DOI: 10.2514/2.2468. [Online]. Available: http://arc.aiaa.org.

[138] O. Härkegård and S. T. Glad, "Resolving actuator redundancy - optimal control vs. control allocation," *Automatica*, vol. 41, no. 1, pp. 137–144, 2005, ISSN: 00051098. DOI: 10.1016/j.automatica.2004.09.007.

[139] N. Zhang, L. Wang, and F. Li, "Research on multi-task command allocation method for flying wing aircraft," eng, in *IOP conference series. Materials Science and Engineering*, vol. 892, IOP Publishing, 2020, pp. 12 039–.

[140] D. A. Handelman and R. F. Stengelj, "Combining expert system and analytical redundancy concepts for fault-tolerant flight control," *Journal of Guidance, Control and Dynamics*, vol. 12, no. 1, 1989. DOI: 10.2514/3.20366. [Online]. Available: http://arc.aiaa.org.

[141] X. Qu, W. Zhang, J. Shi, and Y. Lyu, "A novel yaw control method for flying-wing aircraft in low speed regime," *Aerospace Science and Technology*, vol. 69, pp. 636–649, 2017, ISSN: 12709638. DOI: 10.1016/j.ast.2017.07.036. [Online]. Available: http://dx.doi.org/10.1016/j.ast.2017.07.036.

[142] K. C. Huber, D. D. Vicroy, A. Schütte, and A. R. Hübner, "Ucav model design and static experimental investigations to estimate control device effectiveness and stability and control capabilities," in *32nd AIAA Applied Aerodynamics Conference*, 2014, pp. 1–20, ISBN: 9781624102882. DOI: 10.2514/6.2014-2002. [Online]. Available: http://arc.aiaa.org.

[143] T. Yue, X. Zhang, L. Wang, and J. Ai, "Flight dynamic modeling and control for a telescopic wing morphing aircraft via asymmetric wing morphing," *Aerospace Science and Technology*, vol. 70, pp. 328–338, 2017, ISSN: 12709638. DOI: 10.1016/j.ast.2017.08.013. [Online]. Available: http://dx.doi.org/10.1016/j.ast.2017.08.013.

[144] X. Xu and Z. Zhou, "Analytical study on the synthetic jet control of asymmetric flow field of flying wing unmanned aerial vehicle," *Aerospace Science and Technology*, vol. 56, pp. 90–99, 2016, ISSN: 12709638. DOI: 10.1016/j.ast.2016.07.007. [Online]. Available: http://dx.doi.org/10.1016/j.ast.2016.07.007.

[145] R. Guiler and W. Huebsch, "Wind tunnel analysis of a morphing swept wing tailless aircraft," *Collection of Technical Papers - AIAA Applied Aerodynamics Conference*, vol. 2, no. June, pp. 946–959, 2005, ISSN: 10485953. DOI: 10.2514/6.2005-4981.

[146] D. F. Hunsaker, Z. S. Montgomery, and J. J. Joo, "Control of adverse yaw during roll for a class of optimal lift distributions," no. January, pp. 1–24, 2020. DOI: 10.2514/6.2020-1264.

[147] Z. S. Montgomery, D. F. Hunsaker, and J. J. Joo, "A methodology for roll control of morphing aircraft." DOI: 10.2514/6.2019-2041. [Online]. Available: http://arc.aiaa.org.

[148] L. L. Gamble and D. J. Inman, "Yaw control of a smart morphing tailless aircraft concept," *Advances in Science and Technology*, vol. 101, pp. 127–132, 2016, ISSN: 1662-0356. DOI: 10.4028/www.scientific.net/ast.101.127.

[149] E. Phillips, M. Jentzsch, M. Menge, *et al.*, "Nato avt-239 task group: On the use of active flow control (afc) on tailless aircraft models to affect their trim and control," in *AIAA SciTech Forum*, San Diego, California, 2019. DOI: 10.2514/6.2019-0045. [Online]. Available: http://arc.aiaa.org.

[150] A. A. Cusher and A. Gopalarathnam, "Drag reduction on aircraft configurations with adaptive lifting surfaces," *Aerospace Science and Technology*, vol. 34, no. 1, pp. 35–44, 2014, ISSN: 12709638. DOI: 10.1016/j.ast.2014.01.012. [Online]. Available: http://dx.doi.org/10.1016/j.ast.2014.01.012.

[151] ESDU, *Zero-lift drag coefficient increment due to full-span plain flaps*. 2006, ISBN: 978 1 86246 590 9.

[152] M. W. Oppenheimer and D. B. Doman, "A method for including control effector interactions in the control allocation problem," in *Collection of Technical Papers - AIAA Guidance, Navigation, and Control Conference 2007*, vol. 1, 2007, pp. 1074–1083, ISBN: 1563479044. DOI: 10.2514/6.2007-6418.

[153] G. Fruchter, U. Srebro, and E. Zeheb, "On several variable zero sets and application to mimo robust feedback stabilization," *IEEE Transactions on Circuits and Systems*, vol. 34, no. 10, pp. 1208–1220, 1987, ISSN: 00984094. DOI: 10.1109/TCS.1987.1086056.

[154] M. Stein, "Large sample properties of simulations using latin hypercube sampling," *Technometrics*, vol. 29, no. 2, pp. 143–151, 1987, ISSN: 15372723. DOI: 10.1080/00401706.1987.10488205.

[155] A. Robinson and J. A. Laurmann, *Wing theory*, English, 1956.

[156] ESDU, *Drag of a smooth flat plate at zero incidence*. 2000, ISBN: 978 1 86246 450 6.

[157] R. H. Myers, *Response surface methodology : process and product optimization using designed experiments*, eng, Fourth edition., ser. Wiley Series in Probability and Statistics. Hoboken, New Jersey: Wiley, 2016, ISBN: 9781118916025.

[158] W. Lei and W. Lixin, "Reconfigurable flight control design for combat flying wing with multiple control surfaces," *Chinese Journal of Aeronautics*, vol. 25, pp. 493–499, 2012. DOI: 10.1016/S1000-9361(11)60412-3. [Online]. Available: www.elsevier.com/locate/cja.

[159] ESDU, *Lift and rolling moment due to spoilers on wings at subsonic speeds with trailing-edge flaps undeployed*. 2015, ISBN: 978 1 86246 751 4.

[160] ——, *Drag and yawing moment due to spoilers.* 2015, ISBN: 978 0 85679 990 7.

[161] T. R. Shearwood, M. R. A. Nabawy, W. J. Crowther, and C. Warsop, "Yaw control of maneuvering tailless aircraft using induced drag – a control allocation method based on aerodynamic mode shapes," in *AIAA Aviation 2020 Forum*, Reno, NV, 2020. DOI: 10.2514/6.2020-2677.

[162] J. Katz and A. Plotkin, *Low Speed Aerodynamics*, eng, ser. McGraw-Hill series in aeronautical and aerospace engineering February 2013. New York: McGraw-Hill, 1991, p. 351, ISBN: 0-07-050446-6. DOI: 10.1017/CBO9780511810329.

[163] T. R. Shearwood, M. R. A. Nabawy, W. J. Crowther, and C. Warsop, "Directional control of finless flying wing vehicles – an assessment of opportunities for fluidic actuation," in *AIAA Aviation 2019 Forum*, Dallas, TX: American Institute of Aeronautics and Astronautics, Jun. 2019, pp. 1–15, ISBN: 9781624105890. DOI: 10.2514/6.2019-3686. [Online]. Available: https://arc.aiaa.org/doi/10.2514/6.2019-3686.

[164] C. D. Regan, "In-flight stability analysis of the x-48b aircraft," in *AIAA Atmospheric Flight Mechanics Conference and Exhibit*, 2008, ISBN: 9781563479458. DOI: 10.2514/6.2008-6571. [Online]. Available: http://arc.aiaa.org.

[165] T. Risch, G. Cosentino, C. Regan, M. Kisska, and N. Princen, "X-48b flight test progress overview," in *47th AIAA Aerospace Sciences Meeting including The New Horizons Forum and Aerospace Exposition*. 2009. DOI: 10.2514/6.2009-934. [Online]. Available: https://arc.aiaa.org/doi/abs/10.2514/6.2009-934.

[166] S. V. Empelen and R. Vos, "Effect of engine integration on a 4.6%-scale flying-v subsonic transport," in *AIAA Scitech 2021 Forum*, 2021. DOI: 10.2514/6.2021-0939. [Online]. Available: https://arc.aiaa.org/doi/abs/10.2514/6.2021-0939.

[167] B. D. Steinberg and D. L. Carlson, "Experimental localized radar cross sections of aircraft," *Proceedings of the IEEE*, vol. 77, no. 5, pp. 663–669, 1989, ISSN: 15582256. DOI: 10.1109/5.32057.

[168] D. Jenn, "Radar and laser cross section engineering, second edition," 2005.

[169] L. F. Fehlner, "A study of the effect of adverse yawing moment on lateral maneuverability at a high lift coefficient," NACA, Tech. Rep., 1942. [Online]. Available: https://ntrs.nasa.gov/search.jsp?R=19930092512.

[170] M. R. Ahmed, M. M. Abdelrahman, G. M. ElBayoumi, and M. M. ElNomrossy, "Optimal wing twist distribution for roll control of mavs," *The Aeronautical Journal (1968)*, vol. 115, no. 1172, pp. 641–649, 2011. DOI: 10.1017/S0001924000006333.

[171] E. B. Aldana, A. Mendez, and M. Lone, "Closer look at the flight dynamics of wings with non-elliptic lift distributions," in *AIAA Scitech 2020 Forum*, vol. 1 PartF, 2020, pp. 1–13, ISBN: 9781624105951. DOI: 10.2514/6.2020-0284.

[172] M. R. A. Nabawy, M. M. ElNomrossy, M. M. Abdelrahman, and G. M. ElBayoumi, "Aerodynamic shape optimisation, wind tunnel measurements and cfd analysis of a mav wing," *The Aeronautical Journal (1968)*, vol. 116, no. 1181, pp. 685–708, 2012. DOI: 10.1017/S000192400000717X.

[173] A. H. Bowers, O. J. Murillo, R. R. Jensen, B. Eslinger, and C. Gelzer, "On wings of the minimum induced drag: Spanload implications for aircraft and birds," *Nasa/Tp–2016–219072*, no. March, pp. 1–22, 2016. [Online]. Available: http://www.sti.nasa.gov.

[174] L. Prandtl, "Über Tragflügel kleinsten induzierten Widerstandes," *Zeitschrift für Flugtechnik und Motorluftschiffahrt*, vol. 24, no. 11, pp. 305–306, 1933.

[175] M. V. Ol and M. Gharib, "Leading-edge vortex structure of nonslender delta wings at low reynolds number," *AIAA Journal*, vol. 41, no. 1, pp. 16–26, 2003, ISSN: 00011452. DOI: 10.2514/2.1930.

[176] U. S. D. of Defense, "Mil-f-8785c: Flying qualities of piloted airplanes," 1980.

[177] B. Stevens, F. Lewis, and E. Johnson, *Aircraft Control and Simulation: Dynamics, Controls Design, and Autonomous Systems, Third Edition*. 2015, ISBN: 9781119174882. DOI: 10.1002/9781119174882.

[178] T. R. Shearwood, M. R. A. Nabawy, W. J. Crowther, and C. Warsop, "Three-axis control of tailless aircraft using fluidic actuators: MAGMA case study," in *AIAA Aviation 2021 Forum*, Virtual Event: American Institute of Aeronautics and Astronautics (AIAA), Aug. 2021, pp. 1–12. DOI: 10.2514/6.2021-2530.

[179] R. Englar, "Circulation control pneumatic aerodynamics: blown force and moment augmentation and modification - Past, present and future," in *Fluids 2000 Conference and Exhibit*, 2000. DOI: 10.2514/6.2000-2541. [Online]. Available: https://arc.aiaa.org/doi/abs/10.2514/6.2000-2541.

[180] Hawk Turbine, *Hawk Turbine 240R*, 2021. [Online]. Available: http://www.hawkturbine.com/Technicalspecxxx.htm (visited on 06/18/2021).

[181] E. F. Camacho and C. B. Alba, *Model predictive control*. Springer science & business media, 2013.

[182] I. Gursul, Z. Wang, and E. Vardaki, "Review of flow control mechanisms of leading-edge vortices," *Progress in Aerospace Sciences*, vol. 43, pp. 246–270, 2007. DOI: 10.1016/j.paerosci.2007.08.001. [Online]. Available: https://ac.els-cdn.com/S0376042107000644/1-s2.0-S0376042107000644-main.pdf?%7B%5C_%7Dtid=dee38aaf-9c40-49f9-926c-d332339ff710%7B%5C&%7Dacdnat=1529052568%7B%5C_%7D4ca56b1180e7a1b451c43f6b564c97da.

[183] E. C. Polhamus and K. Aeb, "APPLICATION OF THE LEADING-EDGE-SUCTION ANALOGY OF VORTEX LIFT TO THE DRAG DUE TO LIFT OF SHARP-EDGE DELTA WINGS," NASA, Tech. Rep., 1968. [Online]. Available: https://ntrs.nasa.gov/archive/nasa/casi.ntrs.nasa.gov/19680022518.pdf.

[184] H. Werle, "On Vortex Bursting," Tech. Rep., 1984. [Online]. Available: https://ntrs.nasa.gov/archive/nasa/casi.ntrs.nasa.gov/19850001701.pdf.

[185] R. G. Bradley, W. O. Wrayf, A. C, and C. L. Cm, "A Conceptual Study of Leading-Edge-Vortex Enhancement by Blowing," *AIAA Journal Rept. P-1031C Journal of Spacecraft and Rockets Journal of Aircraft JANUARY J. AIRCRAFT*, vol. 2, no. 1, pp. 64–35, 1964. DOI: 10.2514/3.60318. [Online]. Available: https://arc.aiaa.org/doi/pdf/10.2514/3.60318.

[186] R. G. Bradley, W. O. Wray, and C. W. Smith, "AN EXPERIMENTAL INVESTIGATION OF LEADING-EDGE VORTEX AUGMENTATION BY BLOWING," NASA, Tech. Rep., 1974. [Online]. Available: https://ntrs.nasa.gov/archive/nasa/casi.ntrs.nasa.gov/19740011530.pdf.

[187] J. F. Campbell, "Augmentation of Vortex Lift by Spanwise Blowing," DOI: 10.2514/3.58703. [Online]. Available: https://arc.aiaa.org/doi/pdf/10.2514/3.58703.

[188] S. Guillot, E. Gutmark, and T. Garrison, "Delay of vortex breakdown over a delta wing via near-core blowing," in *36th AIAA Aerospace Sciences Meeting and Exhibit*, ser. Aerospace Sciences Meetings, American Institute of Aeronautics and Astronautics, Jan. 1998. DOI: doi:10.2514/6.1998-315. [Online]. Available: https://doi.org/10.2514/6.1998-315.

[189] A. M. Mitchell, D. Barberis, P. Molton, and J. Délery, "Oscillation of Vortex Breakdown Location and Blowing Control of Time-Averaged Location," *AIAA JOURNAL*, vol. 38,

no. 5, 2000. DOI: 10.2514/2.1059. [Online]. Available: https://arc.aiaa.org/doi/pdf/10.2514/2.1059.

[190] Q. Deng, I. Gursul, Q. Deng, and I. Gursul, "Effect of oscillating leading-edge flaps on vortices over a delta wing," in *4th Shear Flow Control Conference*, ser. Shear Flow Conference, American Institute of Aeronautics and Astronautics, Jun. 1997. DOI: doi:10.2514/6.1997-1972. [Online]. Available: https://doi.org/10.2514/6.1997-1972.

[191] N. J. Wood and L. Robertst, "Control of Vortical Lift on Delta Wings by Tangential Leading-Edge Blowing," *J. AIRCRAFT*, vol. 25, no. 3, DOI: 10.2514/3.45583. [Online]. Available: https://arc.aiaa.org/doi/pdfplus/10.2514/3.45583.

[192] D. Findlay and S. Kern, "of Blowing on High Angle of Attack Flow Over Delta Wings AlAA 22nd Fluid Dynamics , Plasma Dynamics & Lasers Conference," 1991. DOI: 10.2514/6.1991-1809.

[193] W. Gu, O. Robinson, and D. Rockwellf, "Control of Vortices on a Delta Wing by Leading-Edge Injection," *AIAA JOURNAL*, vol. 31, no. 7, 1993. DOI: 10.2514/3.11749. [Online]. Available: https://arc.aiaa.org/doi/pdfplus/10.2514/3.11749.

[194] H. Johari, D. J. Olinger, and K. C. Fitzpatrickt, "Delta Wing Vortex Control via Recessed Angled Spanwise Blowing," *JOURNAL OF AIRCRAFT*, vol. 32, no. 4, DOI: 10.2514/3.46794. [Online]. Available: https://arc.aiaa.org/doi/pdfplus/10.2514/3.46794.

[195] S. Mccormick and I. Gursulf, "Effect of Shear-Layer Control on Leading-Edge Vortices," *JOURNAL OF AIRCRAFT*, vol. 33, no. 6, DOI: 10.2514/3.47061. [Online]. Available: https://arc.aiaa.org/doi/pdf/10.2514/3.47061.

[196] N. M. Williams, Z. Wang, and I. Gursul, "Active Flow Control on a Nonslender Delta Wing," *Journal of Aircraft*, vol. 45, no. 6, 2008, ISSN: 0021-8669. DOI: 10.2514/1.37486. [Online]. Available: http://opus.bath.ac.uk/15950/.

[197] Z. Celik and L. Roberts, "Vortical flow control on a delta wing by lateral blowing," in *32nd Aerospace Sciences Meeting and Exhibit*, ser. Aerospace Sciences Meetings, American Institute of Aeronautics and Astronautics, Jan. 1994. DOI: doi:10.2514/6.1994-509. [Online]. Available: https://doi.org/10.2514/6.1994-509.

[198] J. S. Hong, Z. Z. Celik, and L. Roberts, "Effects of Leading-Edge Lateral Blowing on Delta Wing Aerodynamics," *AIAA JOURNAL*, vol. 34, no. 12, 1996. DOI: 10.2514/3.13426. [Online]. Available: https://arc.aiaa.org/doi/pdfplus/10.2514/3.13426.

[199] H. E. Helin and C. W. Watryt, "Effects of Trailing-Edge Jet Entrainment on Delta Wing Vortices," *AIAA JOURNAL*, vol. 32, no. 4, 1994. DOI: 10.2514/3.12056. [Online]. Available: https://arc.aiaa.org/doi/pdf/10.2514/3.12056.

[200] C. Shih and Z. Ding, "Trailing-Edge Jet Control of Leading-Edge Vortices of a Delta Wing," *AIAA JOURNAL*, vol. 34, no. 7, 1996. DOI: 10.2514/3.13252. [Online]. Available: https://arc.aiaa.org/doi/pdf/10.2514/3.13252.

[201] A. M. Mitchell, D. Barberis, P. Molton, and J. Délery, "Control of Leading-Edge Vortex Breakdown by Trailing Edge Injection," *JOURNAL OF AIRCRAFT*, vol. 39, no. 2, DOI: 10.2514/2.2942. [Online]. Available: https://arc.aiaa.org/doi/pdf/10.2514/2.2942.

[202] Z.-J. Wang, P. Jiang, and I. Gursul, "Effect of Thrust-Vectoring Jets on Delta Wing Aerodynamics," DOI: 10.2514/1.30568. [Online]. Available: https://arc.aiaa.org/doi/pdfplus/10.2514/1.30568.

[203] D. Greenblatt and I. J. Wygnanski, "The Control of Flow Separation by Periodic Excitation Vertical Axis Wind Turbine Active Flow Control View project Dynamic Stall and Massive Dynamic Stall Control View project The control of #ow separation by periodic excitation," vol. 36, pp. 487–545, 2000. DOI: 10.1016/S0376-0421(00)00008-7. [Online]. Available: https://www.researchgate.net/publication/239374129.

[204] A. W., "G. V. Lachmann, Boundary Layer and Flow Control. Its Principles and Application. Volume 1," *ZAMM - Journal of Applied Mathematics and Mechanics / Zeitschrift für Angewandte Mathematik und Mechanik*, vol. 42, no. 6, pp. 264–265, DOI: 10.1002/zamm.19620420616. [Online]. Available: https://onlinelibrary.wiley.com/doi/abs/10.1002/zamm.19620420616.

[205] P. Scholz, J. Ortmanns, C. Kahler, and R. Radespiel, "Leading Edge Separation Control by Means of Pulsed Jet Actuators," *3rd AIAA Flow Control Conference*, no. January 2015, 2006. DOI: 10.2514/6.2006-2850. [Online]. Available: http://arc.aiaa.org/doi/10.2514/6.2006-2850.

[206] D. Greenblatt and I. Wygnanski, "Effect of Leading-Edge Curvature on Airfoil Separation Control," *Journal of Aircraft*, vol. 40, no. 3, pp. 473–481, 2003, ISSN: 0021-8669. DOI: 10.2514/2.3142. [Online]. Available: http://arc.aiaa.org/doi/10.2514/2.3142.

[207] M. Koklu and L. R. Owens, "Comparison of Sweeping Jet Actuators with Different Flow-Control Techniques for Flow-Separation Control," DOI: 10.2514/1.J055286. [Online]. Available: https://arc.aiaa.org/doi/pdf/10.2514/1.J055286.

[208] R. Woszidlo, "PARAMETERS GOVERNING SEPARATION CONTROL WITH SWEEPING JET ACTUATORS Item Type text; Electronic Dissertation," Ph.D. dissertation, University of Arizona, 2011. [Online]. Available: http://hdl.handle.net/10150/203475.

[209] M. Jentzsch, L. Taubert, and I. Wygnanski, "On the Use of Sweeping Jets to Trim and Control a Tailless Aircraft Model," 2017. DOI: 10.2514/6.2017-3042. [Online]. Available: https://arc.aiaa.org/doi/pdf/10.2514/6.2017-3042.

[210] H. Schlichting, *Aerodynamics of the airplane*, eng. New York ; McGraw-Hill, 1979, ISBN: 0070553416.

[211] M. R. A. Nabawy and W. J. Crowther, "A quasi-steady lifting line theory for insect-like hovering flight," *PLOS ONE*, vol. 10, no. 8, pp. 1–18, 2015. DOI: 10.1371/journal.pone.0134972. [Online]. Available: https://doi.org/10.1371/journal.pone.0134972.

Appendices

Appendix A

Flow control of Vortex Dominated Flows

A.1 Steady and Pulsed Blowing

Blowing to increase the maximum attainable lift on swept planforms has been extensively covered within the literature, the location and direction of blowing can be subdivided into four main categories:

- Spanwise blowing, from the fuselage or wing surface;
- Lateral blowing, normal to the chord and in the plane of the wing from the fuselage or leading edge;
- Tangential blowing, tangential to the wing surface from the leading edge; and
- Trailing edge blowing, stream wise blowing from a location at or near the trailing edge of the wing.

All of the methods listed above are concerned with delaying the position of the leading edge vortex breakdown (i.e. moving it downstream, aft of the trailing edge) and increasing the strength of the vortex in order to increase the amount of non-linear vortex lift.

Before beginning the review of the different methods of blowing it is important to note the metric by which the amount of blowing applied is measured, defined as the momentum coefficient (C_μ). This is defined as the ratio of the injected momentum to the free stream momentum, however several different mathematical definitions have been used throughout the literature. To aid comparison between studies and methods, unless otherwise stated the momentum coefficient is quoted as the widely accepted definition of $C_\mu = \frac{\dot{m}V_j}{qS}$. Where, $\dot{m}$ is the total mass flow supplied, V_j is the jet exit velocity, q is the free stream dynamic pressure and S is the wing reference area.

To understand how the momentum coefficient scales from wind tunnel to flight scale, assuming the jet is of the same density as the free stream, the momentum coefficient can be

expressed as:

$$C_\mu = 2\left(\frac{V_j}{V_\infty}\right)^2\left(\frac{A}{S}\right) \tag{A.1}$$

From this it can easily be seen that the momentum coefficient scales with the ratio of the exit area to the wing area and with the square of the ratio of the jet velocity to the free stream velocity. Therefore, when scaling the systems it is important to bear in mind that the mass flow rate required to achieve the same level of control scales linearly with wing area for a given velocity ratio.

The greater challenge in scaling is for cases where the nozzle exit is choked and the free stream velocity is less than that required for flight conditions. In this case the mass flow rate used in the experiments scales with the square of the free stream velocity which may limit the practical applicability of the blowing techniques.

A.1.1 Spanwise Blowing

In a review into methods of controlling leading edge vortices Gursul [182] concluded that spanwise, 'along-the-core' blowing was the most effective method of delaying vortex breakdown. The relative efficacy of the methods was judged as shown in figure A.1, where Δx_{bd} is the change in breakdown location and c is the root chord. This metric is important as the vortex is responsible for increased lift on the aircraft [183] and therefore delaying this breakdown will delay the onset of both stall and the pitch instabilities associated with breakdown.

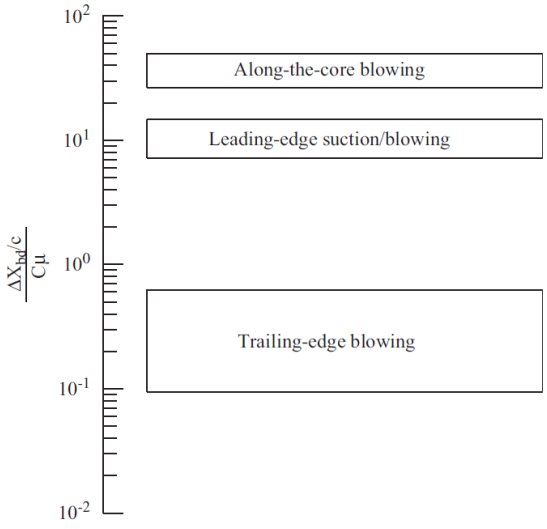

Figure A.1. Effectiveness of various methods of flow control [182].

The idea of using a jet to re-enforce the leading edge vortex core was first proposed by Werle, 1960 [184]. He subsequently noted that emitting a turbulent jet downstream of the

breakdown location without blowing was able to significantly displace the breakdown location of the vortex, figure A.2. However, the blowing rate here is 50% for a slender delta wing with a chord of 150 mm in a free stream velocity of $\sim 12ms^{-1}$ with a sonic jet. At flight scale the mass flow requirement for this jet would not be practically achievable, for example for an aircraft the size of the Eurofighter typhoon this level of blowing would require a mass flow of $\sim 465\%$ of the peak engine core flow at take-off speed.

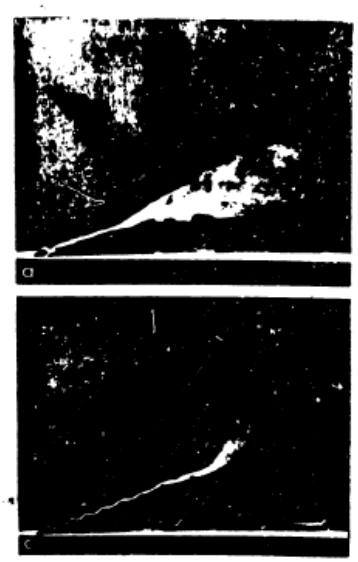

Figure A.2.
Flow visualisation of upper surface of delta wing without (top) and with (bottom) blowing [184]. Blowing from wing surface into vortex core.
Blowing moves the breakdown location (transition from thin to expanding vortex core) significantly rearwards.
$C_\mu = 0.5, V_\infty \approx 12ms^{-1}, \frac{V_j}{V_\infty} \approx 30.$

Bradley [185] conducted a similar experiment on a half-span delta wing of sweep 45° with along the core blowing from a location on the fuselage but for much reduced values of C_μ not exceeding 7.2%; this is still however 67% of the core flow for the example Eurofighter typhoon at take-off speed. The results of this study are of significant interest as it is one of the few flow control studies to explore the effects of blowing on a non-slender wings. This study did not include any measure in the change in breakdown location, however the changes in lift are taken as analogous to the change in breakdown location.

Figure A.3 shows the change in the Lift, Drag and Pitching moment with changing momentum coefficient. It can be clearly seen that the lift is increased with momentum coefficient at high angles of attack where the leading edge vortex may otherwise begin to breakdown. This type of blowing also has very little effect on the pitching moment coefficient (shown on the right, figure A.3) for low lift, however near stall for the unblown wing an increase in stability is observed with blowing as the flow stays attached at the trailing edge due to the reduced vortex size. This is validated by the smoke traces shown in figure A.4 which show the leading edge vortex being pulled much tighter into the surface of the wing, which

will increase the suction at the leading edge and also allows the flow to reattach on the wings surface before the trailing edge. For the increase in lift and stability there is a penalty in drag, however as in this case the increase in available lift is not a benefit for cruise the increased drag is not a significant trade off.

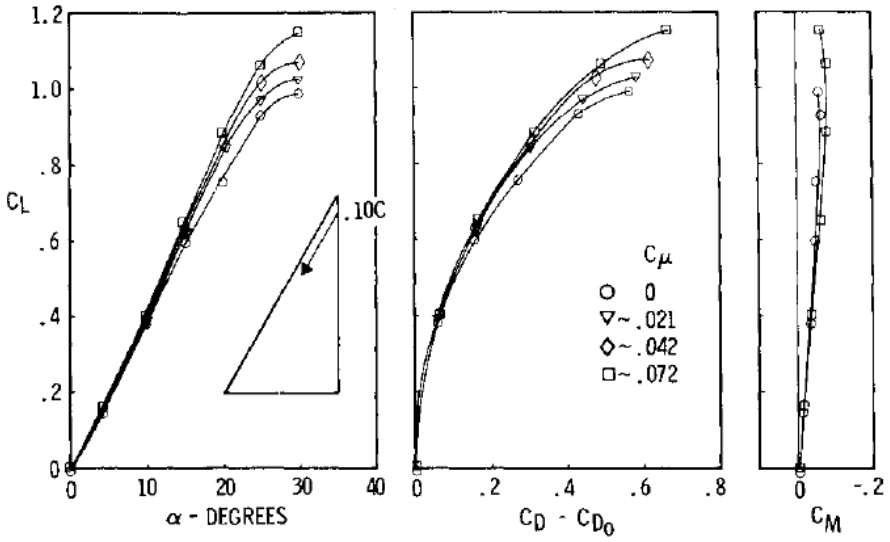

Figure A.3. Coefficient of lift, induced drag and pitching moment coefficient for varying momentum coefficient [185]. Blowing increases the strength of the leading edge vortex at higher angles of attack thereby increasing lift and drag. The longitudinal stability is improved by a delay in vortex breakdown.

By blowing along the core with a momentum coefficient of 7%, the amount of lift on the wing is increased to the full vortex lift predicted by Polhamus [183], as shown in figure A.5. This is significant as the leading edge vortex associated with the increased vortex lift does not usually form so strongly on non-slender wings. However, it is worth noting that the required mass flow rate for this type of blowing would either add a very significant thrust penalty if taken as bleed flow, or weight penalty if an independent air source is used.

The study also included a review of the effect of blowing on other moderately swept (40° - 60°) planforms and showed similarly positive results in increasing the amount of available lift. The results are not discussed here as the mechanisms behind the improvement and the blowing rates used are similar to what has been discussed above.

Further experiments by Bradley [186], at higher levels of C_μ were completed 10 years after this original study. The changes in lift and pitching moment are shown in figures A.6 and A.7 respectively. For Angles of Attack less than $\sim 8^\circ$ all levels of blowing do not significantly change the lift or pitching moment. However, for higher angles of attack, increasing the level of blowing moves the lift curve closer to the linear theoretical prediction.

The change in pitching moment for increasing momentum coefficient is similar to that of the lift. For the unblown case, a slight pitch break can be seen at $\sim 8^\circ$; the magnitude of the pitch break, but not its position, is reduced for all levels of blowing $< 20\%$ C_μ. For higher

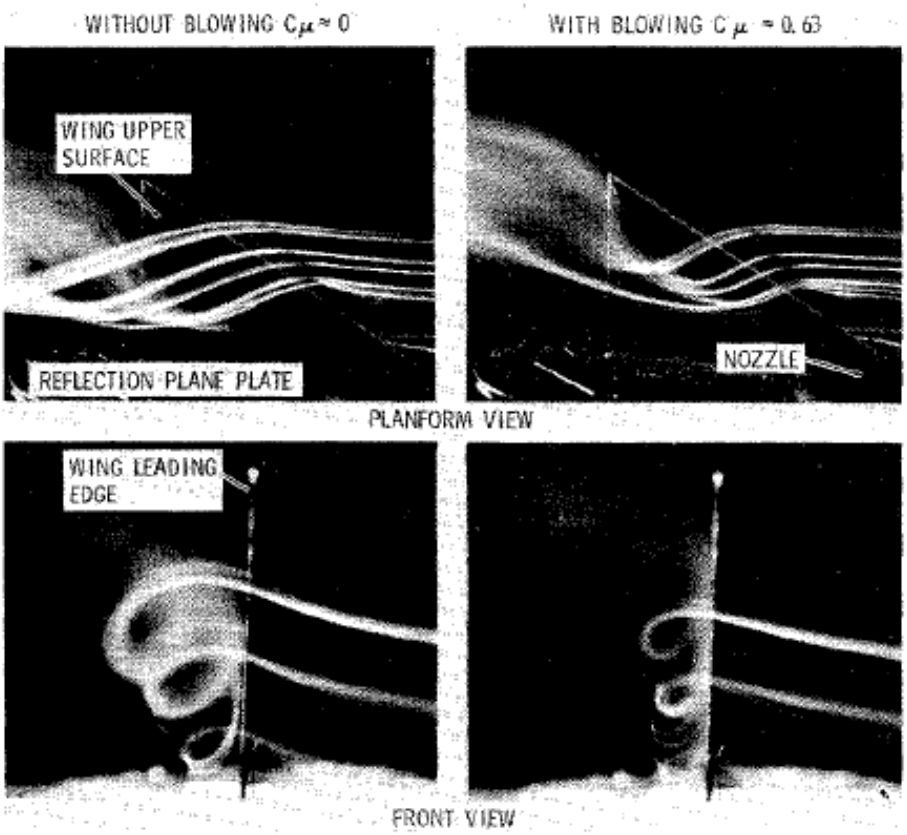

Figure A.4. Streamlines showing the shape of the leading edge vortex system at 25° angle of attack with and without blowing [185]. Without blowing the leading edge vortex is positioned high and inboard, meaning that the streamlines for the outboard section to not reattach to the upper surface. With blowing the vortex is pulled closer to the surface outboard, strengthening the vortex and its influence on the wing

levels of blowing, the position of the pitch break is delayed to a maximum of $\sim 20^\circ$. However, where the pitch break is delayed the severity of it is increased. Furthermore, it is worth noting that for the levels of blowing required to delay pitch break, at least 186% of the core flow for the reference eurofighter configuration is required so is not practical to implement in flight.

Further study using the same configuration was performed by Campbell [187]. He noted it was significant to improve the stability of the Leading Edge vortex for more moderately swept aircraft as the vortex will break down at lower angles of attack. Again, Campbell found that increasing the level of blowing does increase the lift on the wing up to the maximum predicted by Polhamous.

Campbell also made a comparison of the change in lift for each level of blowing to the amount of equivalent thrust in the direction of lift acheivable by vectoring the same nozzle directly downwards rather than along the vortex core; this is shown in figure A.8. Interestingly, low levels of blowing are more efficient at all angles of attack, although the merit of blowing at these low values is questionable in the pitch break region. It is also worth noting that the 'low' value of C_μ is 4%, no reference is made to a lower bound at which blowing ceases to be effective.

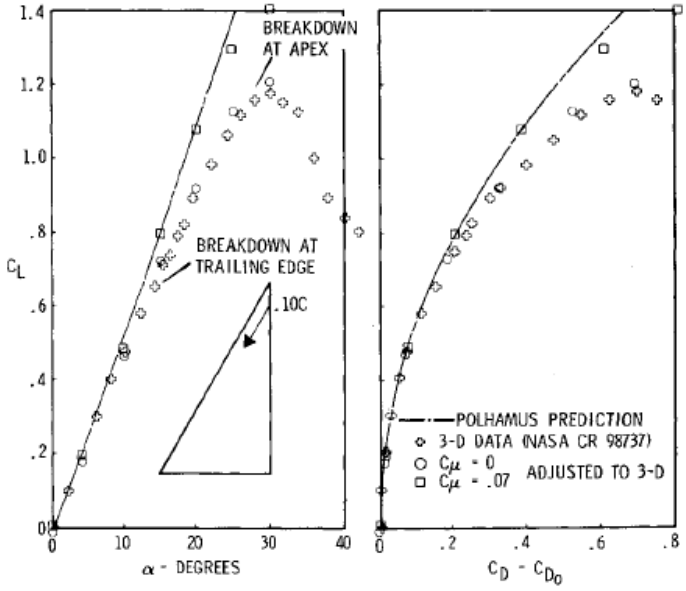

Figure A.5. Comparison of lift and drag with and without blowing to full vortex lift theory [185]. Blowing with a momentum coefficient of 7% is able to achieve full vortex lift.

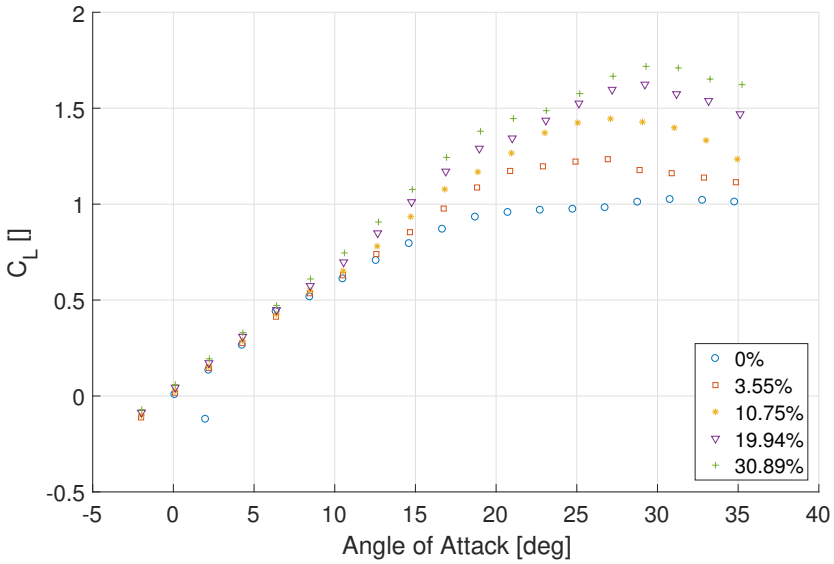

Figure A.6. Lift coefficient for high momentum coefficients [186]. Blowing extends the linear region of the lift curve slope and allows a higher lift coefficient to be attained.

A further analysis is made using a simple engine thrust degradation model to study the Specific Excess Power (SEP) available to a reference aircraft. The results of this, shown in figure A.9 show that manoeuvring performance is improved as for all load factors greater than one, the SEP is improved by blowing.

Whilst this analysis provides an interesting comparison, a major issue in one of the assumptions used to construct it render the results unreliable. The thrust model assumes that the offtake used for blowing is taken after the turbine exit where the air is already at high

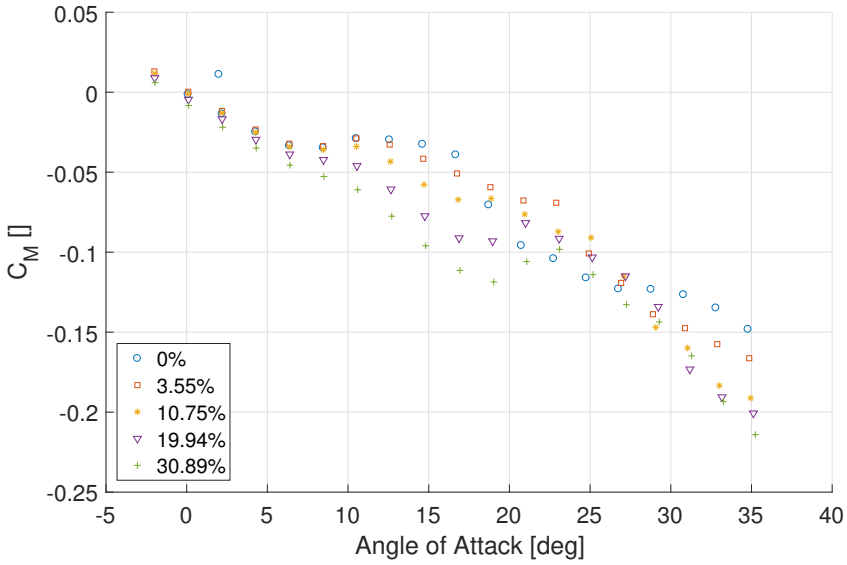

Figure A.7. Pitching moment coefficient for high momentum coefficients [186]. Blowing extends the linear region, simplifying control and delaying the pitch break effect.

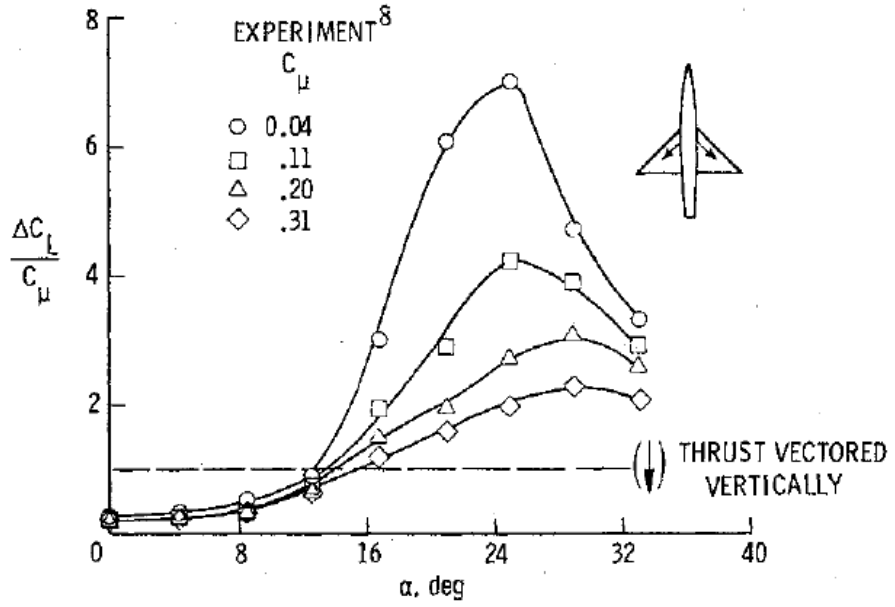

Figure A.8. Efficiency of increasing levels of spanwise blowing at varying angle of attack for a 45° delta wing [187]. Although higher levels of blowing are able to achieve a greater lift coefficient lower values of injected momentum are more efficient at increasing the lift at all angles of attack.

momentum. However, in common engine systems the bleed offtake is from the compressor. As the assumed engine is similar to a single engine used in the reference eurofighter typhoon we can assume that in the 4% C_μ case this corresponds to an offtake of 14% of the mass flow through the engine and the 31% C_μ case is more than total core flow.

Clearly then the 31% C_μ case is not possible from an engine design point of view, a 23% bleed would make significantly more of a difference to the thrust than the missing momentum from the exit. This is due to the reduced mass flow through the combustion chamber and extra

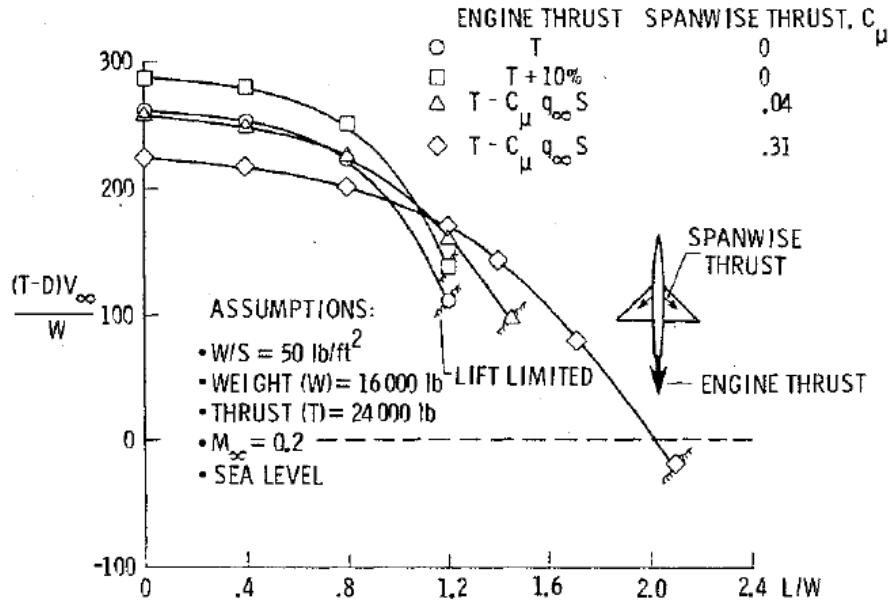

Figure A.9. Specific excess power available for a representative aircraft during a manoeuvre with a given load factor [187]. Although there is a thrust penalty at low load factors, spanwise blowing expands the manoeuvring envelope of the aircraft. The thrust loss due to blowing is assumed to be only due to the momentum deficit in the exhaust and the thrust component of spanwise blowing is recovered.

work required per unit mass through the turbine. However, some thrust is recovered through the streamwise component of the spanwise blowing leading to a drop in SEP much less than would otherwise be expected.

In 1997 Guillot [188] performed a series of tests on slender delta wings with much lower momentum coefficients of less than 1.5%. Importantly, Guillot found that when blowing from the surface of the wing, the delay in vortex breakdown location is very sensitive to the orientation of the jet; this is shown in figure A.10 which shows the vortex breakdown location with changing orientation of the jet measured anti-clockwise where 0° is blowing against the free stream.

One would expect that the orientation for the greatest change in vortex breakdown location would be blowing directly along the vortex core (i.e. $\sim 158^\circ$). However, as can be seen from figure A.10 the maximum change in breakdown location is for $\sim 170^\circ$. The reason for this is as the jet is emitted from the wing surface, the large swirl velocity of the vortex causes the jet to follow a curved path towards the leading edge of the wing. Therefore a jet initially along the axis of the core is deflected away from the core, whereas one directed slightly inboard of the core is directed such that the entire jet momentum is injected in the direction of the core.

It is worth noting however that as the angle of attack changes, the strength of the leading edge vortex and therefore the swirl velocity will change. The change in swirl velocity means the jet deflection will change, therefore the optimum jet angle is a function of angle of attack.

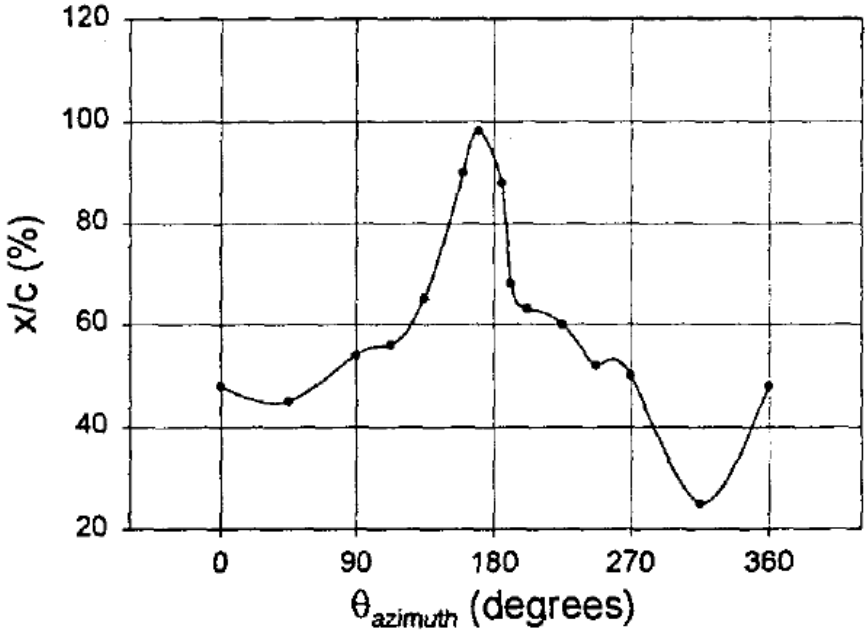

Figure A.10. Vortex breakdown location with varying blowing direction with $C_\mu = 1\%$ at 15° angle of attack. $\theta_{azimuth}$ is 0 blowing against the free stream, parallel to the fuselage and measured anticlockwise. The greatest change in breakdown location is achieved when blowing slightly inboard of the vortex core path.

As can be seen in figure A.11 at the optimum angle of blowing the improvement in vortex breakdown location saturates at $C_\mu \approx 1\%$, significantly lower values of blowing than used in previous studies. This level of blowing would take $\sim 9\%$ of the core mass flow for the reference case of the eurofighter typhoon at take off speed.

On the subject of experimental techniques, Guilliot also found that the breakdown location changed dependant upon whether it was measured by means of smoke visualisation or Laser Doppler Velocimetry (LDV). It is expected that this is because the Leading Edge Vortex is extremely sensitive to any disturbance. Therefore, as the LDV method is non-intrusive the measurement of the breakdown by this method is less likely to influence the measurement result.

Mitchell [189] performed a study on a 70° swept wing with low $C_\mu < 0.9\%$, which is approaching a value which could be practically implemented in flight. Unlike previous studies, Mitchel captured unsteady flow data and used this to present the time-averaged and rms values of the unsteady component. This allowed the analysis of the displacement of the vortex breakdown and the stability of the displacement.

Figure A.12 shows the time-averaged and RMS vortex breakdown location for varying free stream speed and angle of attack. It can be seen that for 27° as the speed of the flow is increased the time-averaged location of breakdown moves aft. However, this apparent increase in the stability of the vortex comes at the expense of an increased RMS value of the unsteady component. As the instability in the breakdown location generally does not occur in phase,

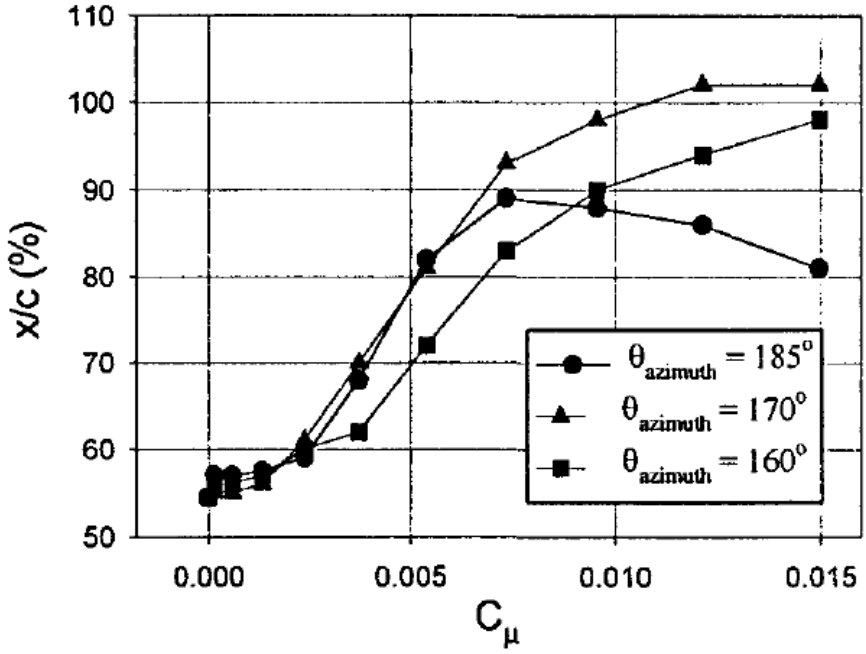

Figure A.11. Change in vortex breakdown location with increasing blowing with various blowing directions at 15° angle of attack [188]. For all levels of blowing, blowing inboard of the core was best able to delay the vortex breakdown.

this is likely to contribute to the 'wing rock' phenomenon common on slender wings. This pattern is not replicated when the angle of attack is increased to 30°. The breakdown location moves forward by $\sim 0.25\%$ of the chord from 27°, however at this higher angle of attack the breakdown location becomes much more stable.

From the time-averaged breakdown location shown in figure A.12 it is also worth noting that the breakdown location is not laterally symmetric. This is of concern as it can introduce large yawing and pitching moments at high angles of attack, potentially leading to departure from controlled flight.

With a low amount of blowing the breakdown location for an Angle of Attack of 27° can be displaced to the trailing edge for $C_\mu < 0.9\%$, as shown in figure A.13. The requirement for the momentum coefficient to displace the breakdown location is reduced as the freestream velocity is increased. It is also worth noting that as the momentum coefficient is increased, the stability of the breakdown location increases as shown by the RMS value decreasing. It is even possible with enough blowing ($C_\mu = 3\%, U = 15$) to fix the breakdown location with respect to time.

From figure A.13 it can also be seen that it is possible to independently control the breakdown location of each leading edge vortex. This gives rise to the possibility of using the spanwise blowing for lateral control of the aircraft by asymmetric control of the breakdown location.

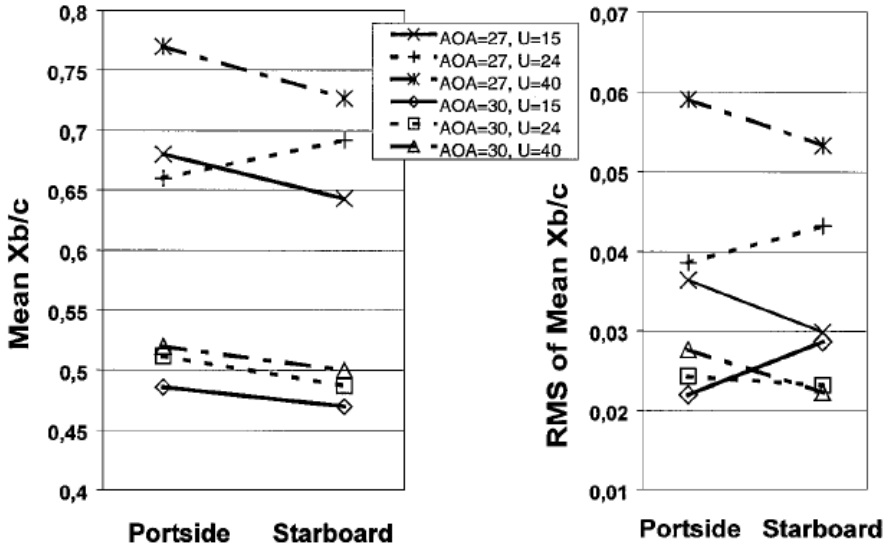

Figure A.12. Time averaged breakdown location (Left) and RMS of fluctuating component (Right) for varying angle of attack and speed [189]. Increasing the free stream speed has little effect on the vortex breakdown location, however the increasing speed reduces the fluctuating component. As would be expected, increasing the angle of attack causes the breakdown location to move forward.

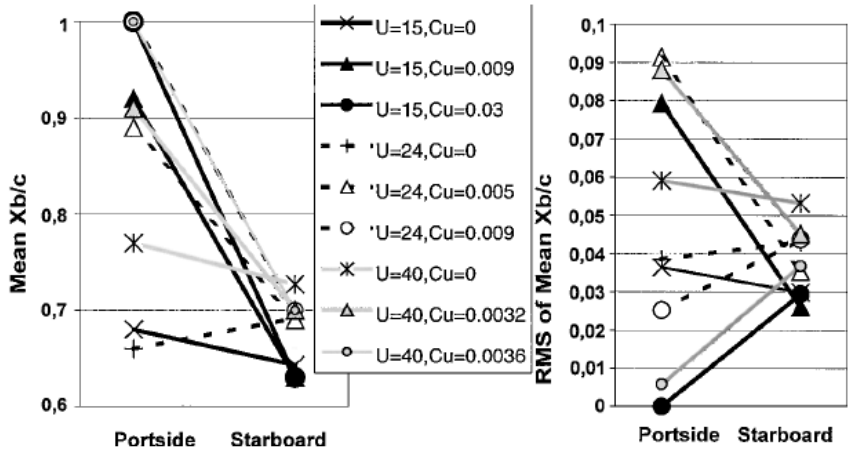

Figure A.13. Time averaged breakdown location (Left) and RMS of fluctuating component (Right) for varying momentum coefficient and speed at 27° angle of attack [189]. Blowing is applied on the port side of the aircraft. Actuation on the port side delays the vortex breakdown on the port side, however it encourages earlier breakdown on the starboard side. Low levels of blowing are required to displace the breakdown location, however additional momentum injection is required to stabilise the fluctuating component.

It was also noted by Mitchell that the surface pressure measurements were not capable of identifying the breakdown location alone. Therefore, some method of characterising the off body flow is required in order to identify the breakdown location.

A.1.2 Tangential Blowing

Tangential blowing is a fluidic method of adding energy to the sheer layer shed from the leading edge of a wing. Before considering fluidic injection, a method for achieving this is using

oscillating flaps on the leading edge [190]. In the study by Deng [190] he used phase-averaged flow visualisation data to show the effect of the oscillating flaps. He concluded that the flap adds energy to the vortex core and increases the ratio of axial to swirl velocity. This can generate a leading edge vortex at low angles of attack where one would not normally form or strengthen an existing vortex at higher angles.

Wood [191] conducted an experimental study on a 60° sweep delta wing with a tapered leading edge slot, as shown in figure A.14 in order to preserve conical flow. Modest momentum coefficients of no greater than 6% were used in this study with a definition of C_{μ} which at first glance is difference to the standard, however on inspection is equivalent.

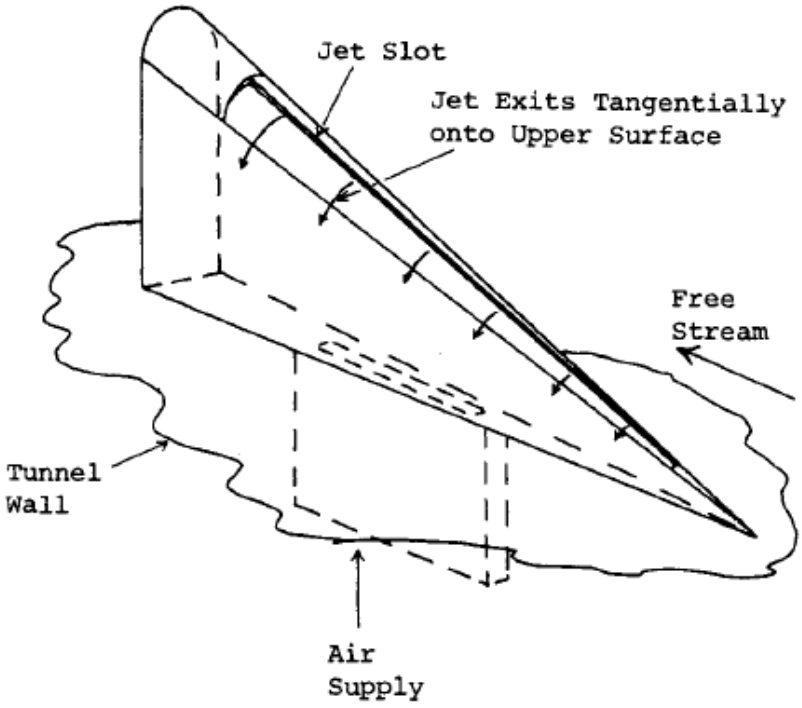

Figure A.14. Experimental setup used by Wood [191]. The tangential blowing slot at the leading edge tapers linearly with the chord in order to enforce flow conicality.

The left of figure A.15 shows the change in the normal load coefficient with increasing blowing. Much like the spanwise blowing techniques discussed previously the blowing does not have a large effect at low angles of attack, but rather extends the linear region of the lift curve slope. If the flow was conical as suggested by Wood then the normal coefficient would change uniformly with chord length. However, as shown in the right of figure A.15 the force is increased more on the forward sections of the wing than the aft; this would reduce the static stability of the aircraft and worsen the pitch-break effect, but no discussion or presentation of the pitching moment is made by the authors.

An interesting finding from [191] is that for any angle of attack it is possible to obtain fully attached flow over the wing. The amount of blowing predicted to achieve this is shown in figure

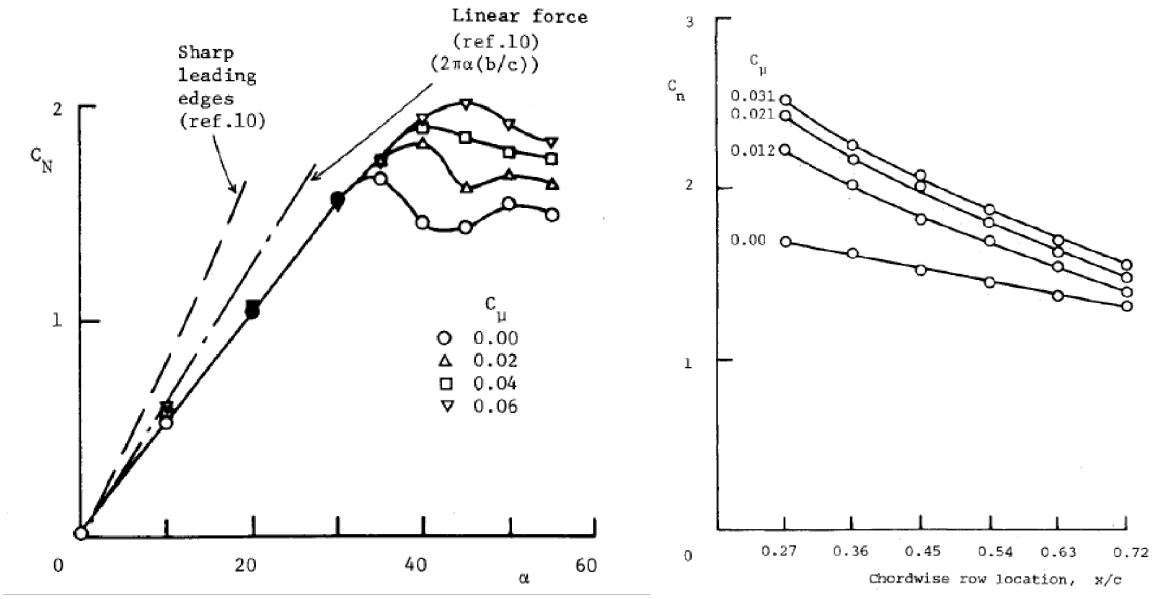

Figure A.15. Change in normal force coefficient for changing C_μ (left) and change in normal force coefficient with spanwise location for an angle of attack of 40° [191]. Blowing is able to delay stall and extend the linear region of the lift curve slope. Although there is a gain in the normal force, the right figure suggests that blowing increases the force on the front of the wing more than the aft. Therefore causing an increasing pitch up moment with increasing blowing.

A.16. It is worth noting however that this is inferred from the analysis of the experimental data and has not been tested empirically as part of this study. The level of blowing required however do appear achievable in low-speed flight for angles of attack less than 15°.

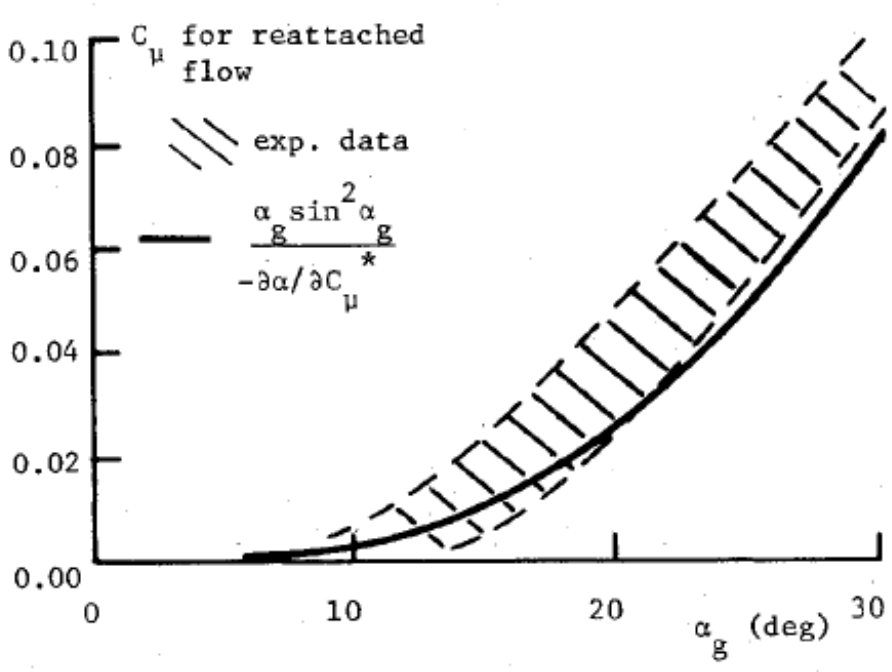

Figure A.16. Theoretical momentum coefficient requirement to obtain reattached flow on a 60° sweep delta wing [191]. The experimental data presented agrees closely with the theoretical requirement.

Findlay [192], conducted a numerical study of a 70° sweep delta wing with the aim of

modifying the path of the vortex core to avoid interaction with the fins to reduce buffet. The results of this numerical study showed that for 10° Angle of Attack blowing was able to increase the lift and increase the nose down pitching moment of the aircraft, shown in figure A.17. As the pitching moment for the unblown case is not shown and the change in pitching moment is only provided at one angle of attack, it is not possible to say whether blowing has effected the static stability of the aircraft.

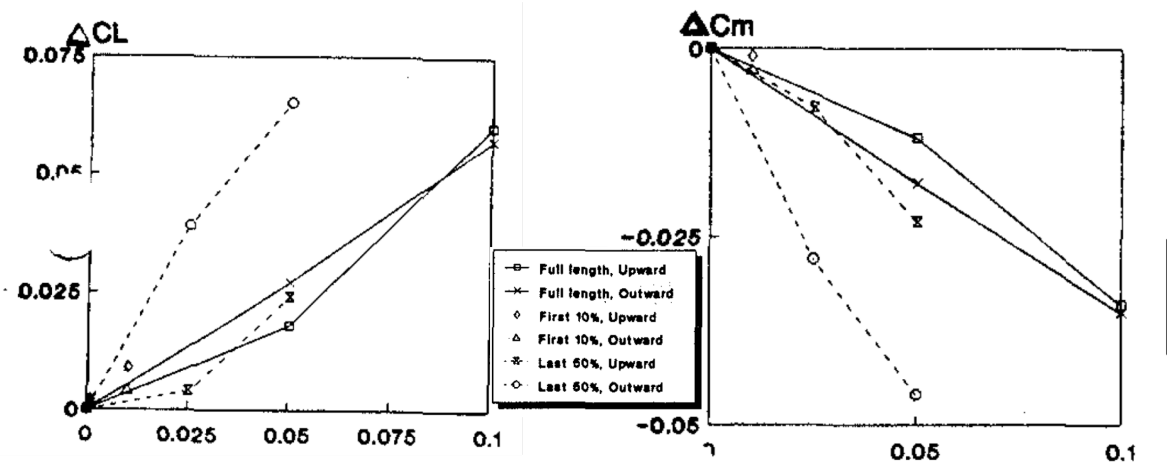

Figure A.17. Change in lift and pitching moment for a 70° swept wing with varying C_{μ} for an angle of attack of 10° [192]. Blowing in all cases shown here appears to increase lift and increase the pitch down moment of the aircraft for all levels of blowing below 1% C_{μ}.

For an increased angle of attack of 30° blowing reduces the lift on the wing, as shown in figure A.18. The pitching moment data for this higher angle of attack case is not shown therefore it is not possible to comment on the stability of the aircraft.

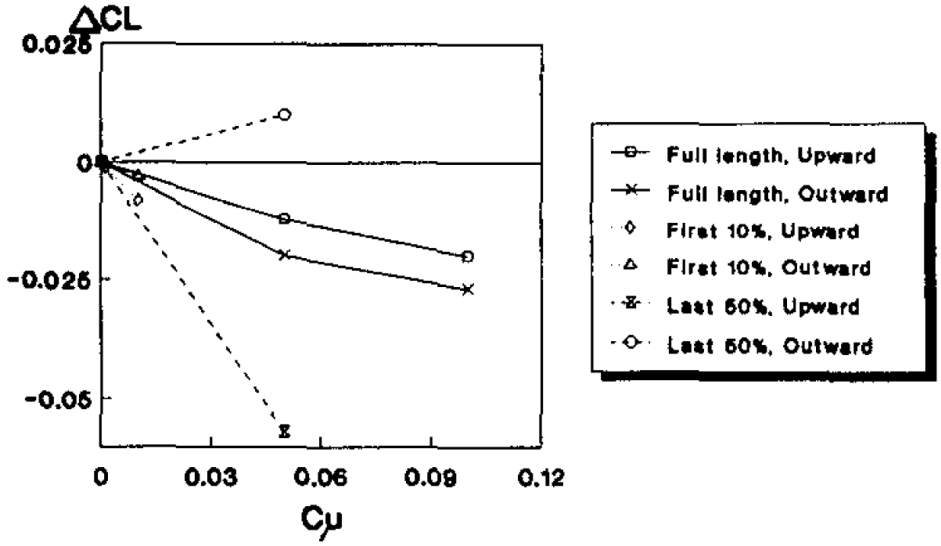

Figure A.18. Change in lift for a 70° swept wing with varying C_{μ} for an angle of attack of 30° [192]. Only lateral blowing on the outboard section of the wing is able to increase the lift, in all other cases the lift coefficient is reduced.

Gu [193], conducted an experiment in a water tunnel for a 75° sweep delta wing. Die was

injected at the apex of the wing in order to visualise the leading edge vortex and measure its breakdown location. The wing was held at 54° angle of attack in order to force breakdown near the apex, whilst this is much greater than any flight condition it is useful to observe the effect of the leading edge blowing. One significant difference from the studies in spanwise blowing is that the wing incorporates a rounded leading edge to house the blowing nozzle.

Figures A.19, A.20 and A.21 show how the burst location is displaced for blowing, suction and alternate blowing and suction with $C_{\mu} = 3.6\%$ respectivley. The alternate blowing and suction is 77% of a convective timestep as this was empirically found to be the most efficient frequency of alternation.

Clearly pure suction has a greater efficacy than pure blowing as the vortex breakdown is displaced by $\sim 10\%$ of the root chord further downstream. However, suction is practically much more difficult to achieve in flight which limits its application outside of static studies such as this.

Using alternate blowing and suction further displaces by an additional 8% of the root chord. This method of control could be achieved with no need for offtake from an engine as the net mass flow as zero, so is more likely to be possible in a flight environment. Whilst this sounds as the most attractive method for control, it was noted by Mitchell that alternate blowing and suction moves the position of the vortex core in time. This movement is likely to change the suction peak under the vortex and therefore also the lift and pitching moment. In the absence of force and moment data for this experiment it is not possible to infer the dynamic response of the aircraft. Therefore, further research is required in this area.

Johari [194] conducted a study of tangential leading edge blowing on a 60° sweep delta wing with a blowing coefficient of up to 10%. This method is slightly different from the others discussed in this section in that it blows from a line inboard of the leading edge but still in a direction tangent to the leading edge, as shown in figure A.22.

Using this method of Recessed Angled Spanwise Blowing (RASB), he found that the vortex breakdown location was improved by blowing downstream of the vortex breakdown location the breakdown location could be displaced up to 15% of the root chord for a C_{μ} of 10%. However, contrary to the findings of the other studies reviewed thus far, blowing upstream of the vortex breakdown location causes premature breakdown. The change in breakdown location is shown in figure A.23.

The figure on the right shows that RASB is most effective at 22° angle of attack, with an improvement in vortex breakdown location of 15% root chord. However, this is a clear outlier from the rest of the data points which indicate a relatively small improvement (<5%) for a large C_{μ} of 10%. It can also be seen in this figure that blowing from the most downstream port has the greatest positive effect on the vortex breakdown location.

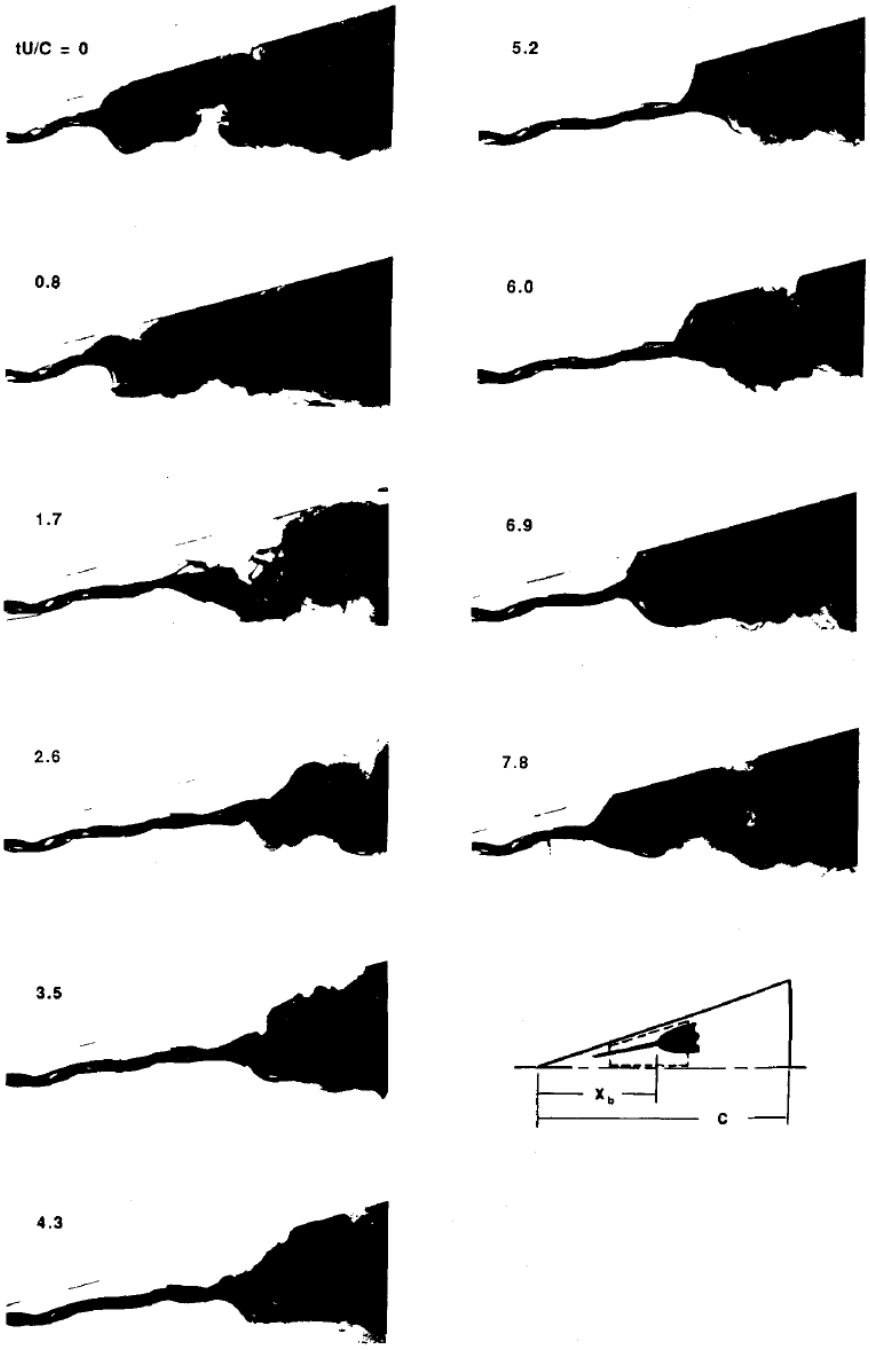

Figure A.19. Die trace of vortex core for a 75° sweep delta wing at 54° angle of attack [193]. Blowing with a momentum coefficient of 3.6% is initiated at tU/c = 0 and applied until tU/C = 3.5 where it is terminated. Blowing is able to significantly delay the vortex breakdown location and appears to prevent an oscillation in its position once the new location is established.

The figure on the left shows the vortex breakdown location for blowing from all three ports simultaneously. Interestingly, the breakdown location for 22° is coincident with port 1; this leads to a 10% change in breakdown location for a relatively low C_μ of 2%. However, further increases in C_μ have a much less significant effect on the breakdown location. Much like single port blowing, for all other angles of attack only very small improvements are made in

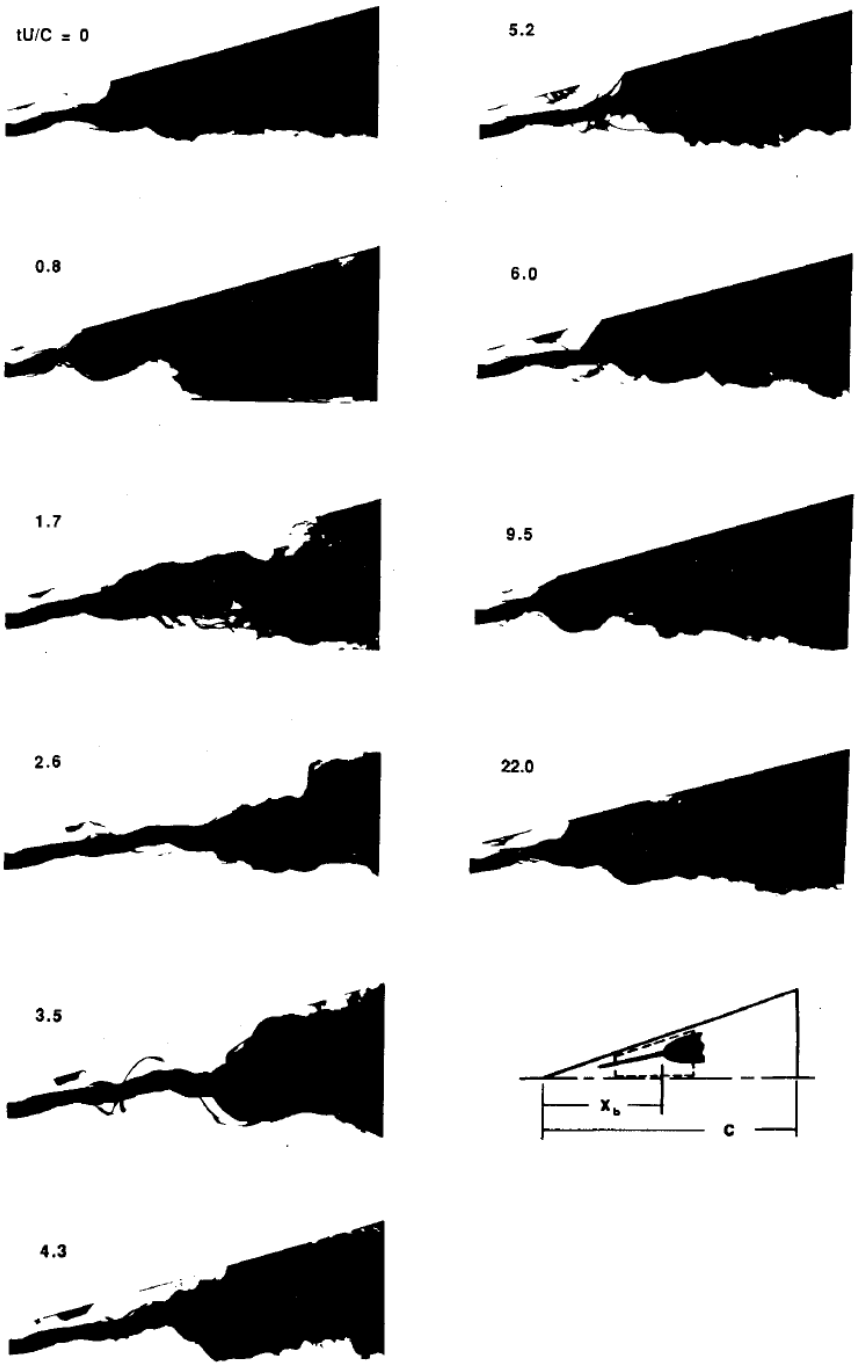

Figure A.20. Die trace of vortex core for a 75° sweep delta wing at 54° angle of attack [193]. Suction with a momentum coefficient of 3.6% is initiated at tU/c = 0 and applied until tU/C = 3.5 where it is terminated. Suction is able to significantly delay the vortex breakdown location although a small oscillation in its position is apparent.

the vortex breakdown location. Therefore, even if forgetting the demand a C_μ of 10% would place on the aircraft systems one would not select RASB as the blowing method over other methods discussed within this section.

McCormick [195] completed a study of tangential control using pure steady suction on a 70° sweep delta wing in a water tunnel. Two different models were used: one with the suction

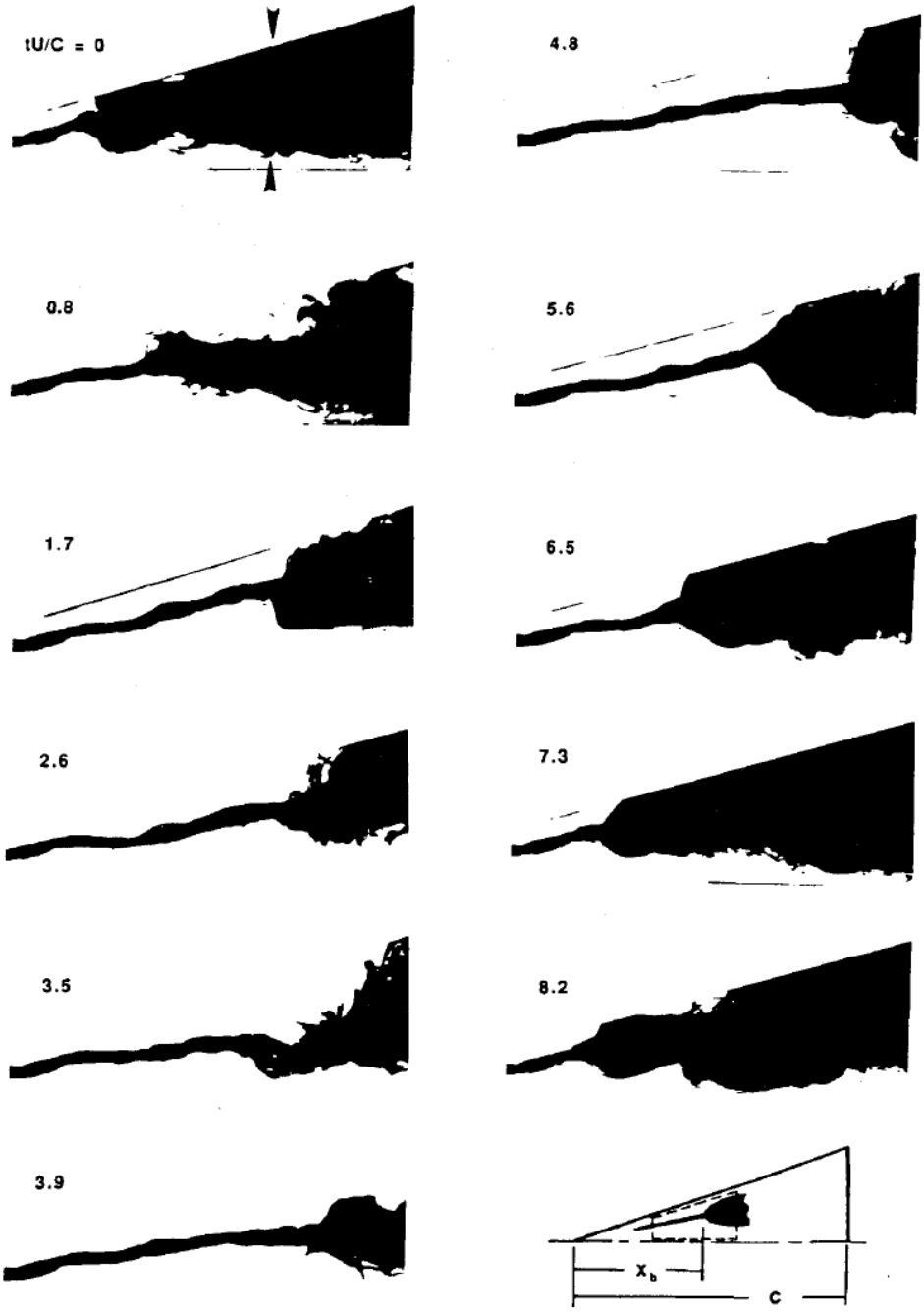

Figure A.21. Die trace of vortex core for a 75° sweep delta wing at 54° angle of attack [193]. Alternate blowing and suction with a momentum coefficient of 3.6% is initiated at tU/c = 0 and applied until tU/C = 3.9 where it is terminated. Actuation is able to delay the vortex breakdown location to a greater extent than pure blowing or suction although an oscillation in its position is apparent.

slot at the leading edge and the other with the suction slot parallel to but inboard of the leading edge, as shown in A.24. Both models used a momentum coefficient of up to 7%, however as this study uses suction it is difficult to compare with the blowing momentum coefficient as suction is more difficult to achieve in flight.

Figure A.25 shows the change in vortex breakdown location with increasing momentum

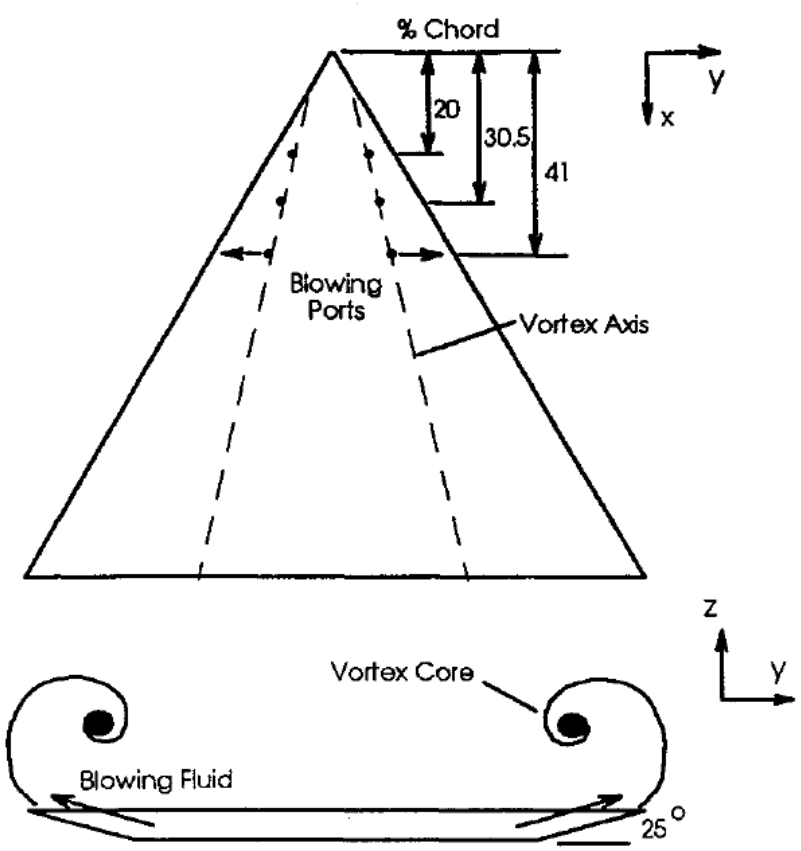

Figure A.22. Blowing location direction and orifice locations used by Johari [194]. The flow exits from under the vortex axis in a driection tangent to the leading edge to feed into the vortex core.

coefficient. An improvement in vortex breakdown location can be seen for low values of suction for the slot at the leading edge at moderate angles of attack, shown in the top figure. For very high angles of attack the suction has no effect on the vortex breakdown location, no explanation for this is presented by the author. For conditions in which suction was able to improve the vortex breakdown location it was found that there was improvement up to a point with increasing C_μ, the maximum being 2.4%. After this, the breakdown location 'saturated' and any further increase in C_μ lead to no change in the breakdown location; again no explanation for this behaviour is presented.

For the inboard suction slot, similar to the results of Johari [194] for blowing, McCormick found that actuation caused a premature breakdown of the vortex by as much as 60% of the root chord. The reason for this is as the vortex rolls up over the leading edge, the free sheer layer is already established by the time it encounters the jet so not vorticity is removed. However, its path is vectored by the suction leading to an increase in swirl velocity but no change in axial velocity. This leads to an increase in the swirl angle and therefore promotes vortex breakdown [195].

This effect is illustrated in figure A.26 which shows the RMS of the unsteady velocity component, analogous to the vorticity, at a cross flow plane of x/c = 0.6. It can be seen that

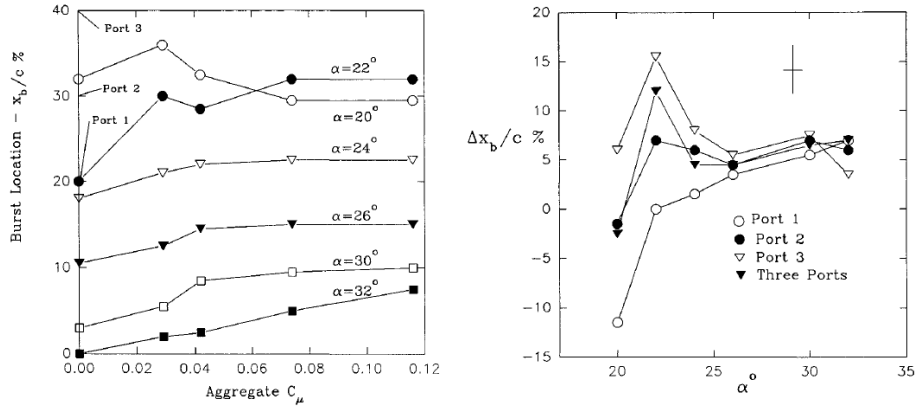

Figure A.23. Vortex breakdown location for changing angle of attack, momentum coefficient and blowing location (left) and blowing location only with a fixed $C_\mu = 10\%$ (right) [194]. Blowing at or aft of the breakdown location provides an improvement in the breakdown location, with the most significant improvement where blowing is applied at the breakdown location (left). Blowing only downstream of the breakdown location is able to provide a greater increase than blowing from all three ports.

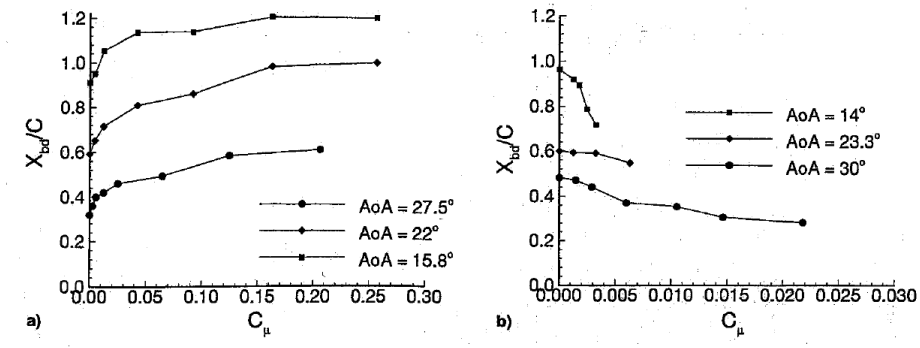

Figure A.24. Change in vortex breakdown location for suction from leading edge slot (left) and inboard slot (right) [195]. Suction from the leading edge slot improves the vortex breakdown location for all angles of attack shown, however, the improvement is saturated above $C_\mu \approx 5\%$. For the recessed slot suction has a deleterious effect on the vortex breakdown for all angles of attack at all levels of blowing.

suction on the leading edge (left) removes vorticity at that location and also causes the vortex to roll up tighter and closer to the wings surface, potentially leading to an increase in vortex lift. This method of suction has the effect of reducing the swirl angle and therefore increases the stability of the vortex. It was also found that there was no pairing between the leading edge vortices giving potential for this method to be used as roll control.

The images on the right of figure A.26 show the change in vorticity for suction at the inboard location. It can be seen that there is no significant removal of vorticity near the suction slot. However, the change in path of the region of high RMS velocity can be seen to be vectored further inboard as discussed previously.

Williams [196] experimented on a non-slender delta wing with a sweep of 50° in the poststall region using unsteady excitation to promote reattachment of the flow. Previous studies, including that of Gu [193] have shown that there is an optimum reduced frequency

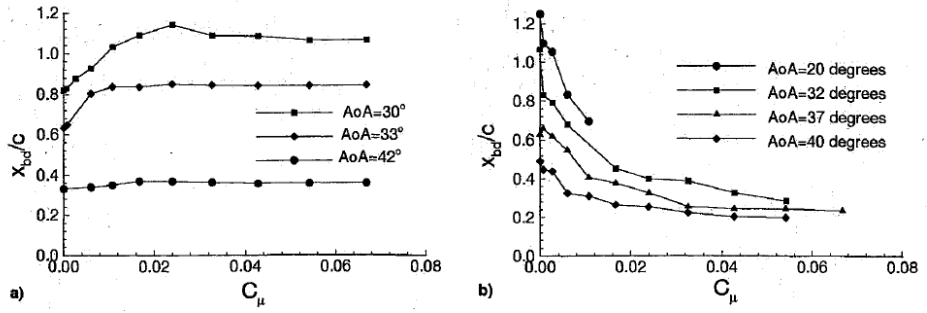

Figure A.25. Change in vortex breakdown location for suction from leading edge slot (left) and inboard slot (right) at high angle of attack. Suction from the leading edge slot improves the vortex breakdown location for all angles of attack shown, however, the improvement is saturated above $C_\mu \approx 5\%$ [195]. For the recessed slot suction has a deleterious effect on the vortex breakdown for all angles of attack at all levels of blowing.

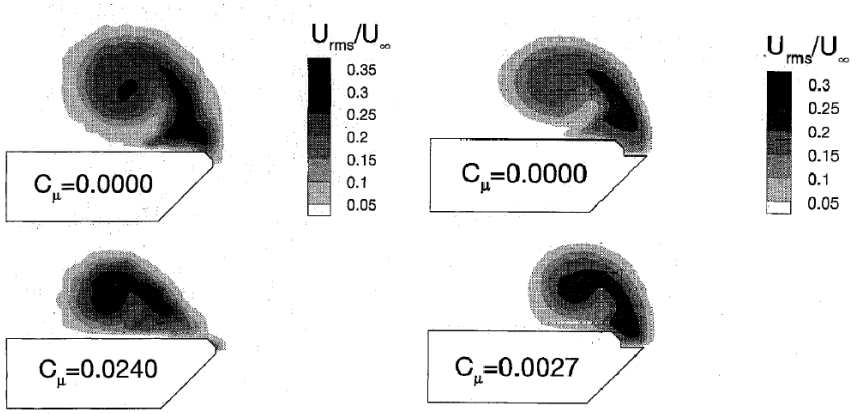

Figure A.26. Unsteady velocity component, representing vorticity, shown for a crossflow plane at 60% chord [195]. The leading edge slot (left) removes vorticity from the core, improving stability and causing roll up closer to the surface. The recessed slot does not remove a significant amount of vorticity but rather redirects the flow closer to the surface.

($\frac{fc}{U}$) of 1 - 2 at which pulsed blowing is most effective. Therefore, the experiments in this study were conducted at a reduced frequency of 1.5. As the pulsed blowing does not require a constant flow to the actuator, the momentum coefficient in this study is averaged over each blowing period. This leads to blowing coefficients no greater than 0.8%. The breakdown location is not discussed throughout this work, however comparisons can be made on the efficacy of blowing by use of the suction force coefficient.

Figure A.27 shows the efficacy and efficiency of increasing levels of C_μ for a reduced frequency of 1.5. As with other studies reviewed, increasing the blowing coefficient has little effect at low angles of attack but extends the linear region of the lift curve slope. Unlike the material reviewed thus far, significant delay in stall can be achieved for very low values of $C_\mu (< 0.05\%)$, which is possible to achieve in flight. A reason suggested for the reduced momentum coefficient during unsteady blowing is due to the excitation of the helical mode instability which plays an important role in vortex breakdown [182].

The right of figure A.27, like other material reviewed, shows the efficiency of blowing

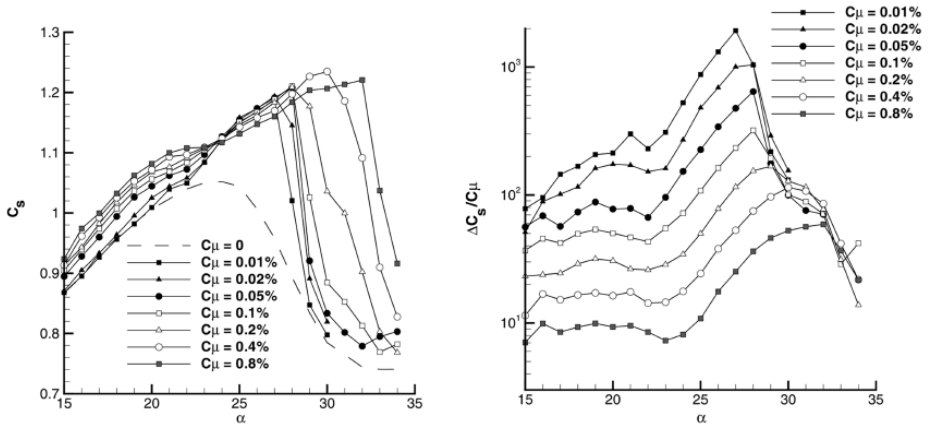

Figure A.27. Efficacy (left) and efficiency (right) of pulsed leading edge blowing on a 50° swept delta wing with a reduced frequency of $F^+ = 1.5$ [196]. Blowing is able to extend the linear region of the force coefficient and delay the onset of stall. Although higher levels of blowing are able to delay stall to the greatest extent, the lower levels of blowing are able to provide the increase in lift more efficiently.

defined as the ratio of change in suction coefficient to momentum coefficient is greatest for low blowing coefficients. Therefore for extending the useful range of angle of attack it is most useful to use low levels of blowing.

Williams [196] also tested blowing for partial slots along sections of the leading edge, shown in figure A.28. At 30° angle of attack blowing from the foremost sections of the wing, but not at the apex, provides the greatest change in suction coefficient for low amounts of blowing, dissagreeing with the results of Johari [194] highlighting the sensitivity of effects of blowing to the blowing location. No further analysis was presented at different angles of attack so no conclusion can be drawn on the merits of partial blowing. However, if this trend is repeated across other angles of attack it could provide a method of further reducing the momentum coefficient demand and further strengthen the case for this method of blowing to be implemented in flight.

With this said, no reference is made to the effect of this unsteady blowing on the pitching moment of the aircraft. Therefore, before this method is implemented in flight more research would be required into the changes in forces and moments experienced by the aircraft and how that would effect the flight dynamics.

A.1.3 Lateral Blowing

The numerical study by Findlay [192] also studied the effect of blowing laterally from the leading edge, i.e. in the streamwise direction against the flow. Referring back to figure A.17, it can be seen that for blowing at 10° angle of attack blowing laterally (outward) is more effective at increasing the lift coefficient than blowing tangentially (upward). It is also worthy of note that much like the tangential blowing results of Johari [194], blowing from the aft sections of

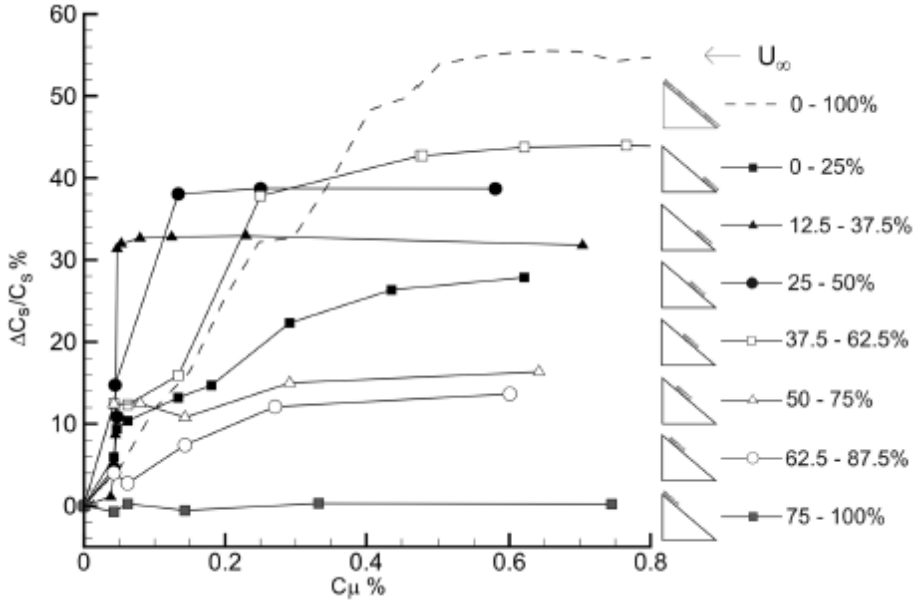

Figure A.28. Effect of actuation location on the normal force coefficient at 30° angle of attack [196]. For low momentum coefficients, blowing from the forward sections of the wing but offset from the apex proves more effective than full slot blowing.

the wing produces a greater change in lift coefficient than from the entire length of the leading edge. This is significant as it has the potential of improving the performance of the aircraft for a reduced momentum coefficient. The nose down moment of the aircraft is also increased with momentum coefficient, it is not possible to comment on the change in stability however as the pitching moment data is only provided as a change from the unblown case at one angle of attack.

Furthermore, it was found that blowing laterally from the aftmost section of the leading edge was the only method of flow control considered which was able to increase the lift coefficient at 30° angle of attack. This is shown in figure A.18. The pitching moment data for this angle of attack is not shown, therefore it is not possible to comment on the change in stability due to blowing. In all cases however, the momentum coefficient is too great to be able to achieve this method of control in a flight environment.

Celik [197], conducted an experimental study on a full span 60° sweep delta wing using lateral blowing from the leading edge. The direction however differs from that of Findlay in that Celik blows normal to the leading edge rather than in the streamwise direction. Pressure and 3-axis normal force and pitching and rolling moment data were measured allowing study of the interaction between vortices due to asymmetric blowing as a potential for lateral control.

Figure A.29 shows the change in normal force coefficient with changing angle of attack and momentum coefficient. At low angles of attack the normal force coefficient is reduced with blowing, however the reason for this is addressed in [197]; The angle of attack was defined

relative to the bottom surface of the model, if the zero lift line was used then the angle of attack is reduced by $\sim 7.5^{\circ}$. If this definition is used then the normal force coefficient is decreased for negative and increased for positive angles of attack. This suggests that lateral blowing increases the strength of the vortex regardless of which side of the wing it forms.

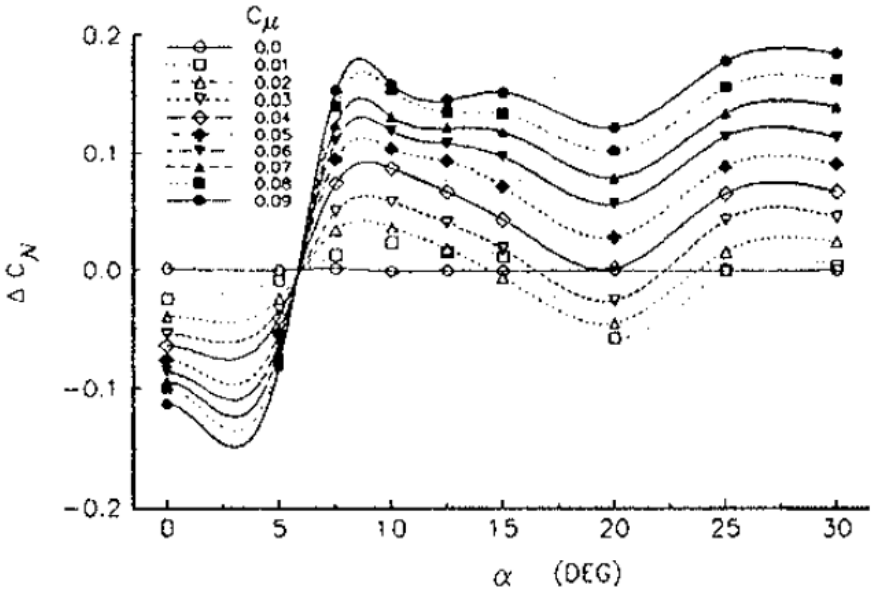

Figure A.29. Change in normal force coefficient for varying momentum coefficient and angle of attack [197]. Due to the definition of angle of attack used, the effective angle of attack is $\sim 7.5^{\circ}$ less than the angle of attack displayed. Blowing above $C_\mu = 4\%$ improves the lift at all angles of attack studied. However, for less than 4% the lift is reduced in the region between 15° and 20°.

At higher angles of attack for low blowing coefficient the normal force coefficient is also reduced. This suggests that for blowing rates less than 4%, the vortex strength is reduced in the region of 12° angle of attack ($\sim 20^{\circ}$ from bottom surface). Therefore, as high momentum coefficients are required this method of blowing is not possible for use as lift augmentation.

Asymmetric blowing has the potential to control the aircraft in roll, this technique has potential because blowing from only one of the leading edges should reduce the requirement on the momentum coefficient. The change in rolling moment coefficient is shown in figure A.30 for varying angle of attack and momentum coefficient. It can be seen that whilst it is possible to change the rolling moment by blowing, this method of control would be difficult to accomplish in flight.

Unless blowing is applied at a momentum coefficient of 6% or greater at angles of attack of around 20° the change in rolling moment changes sign. Whilst operating in this region of 'control reversal' would bring greater efficiencies, its effect is highly dependant upon angle of attack and is therefore not robust enough to be used as a flight control method. Furthermore, the momentum coefficient required to deliver the control far exceeds what would be practically possible in flight.

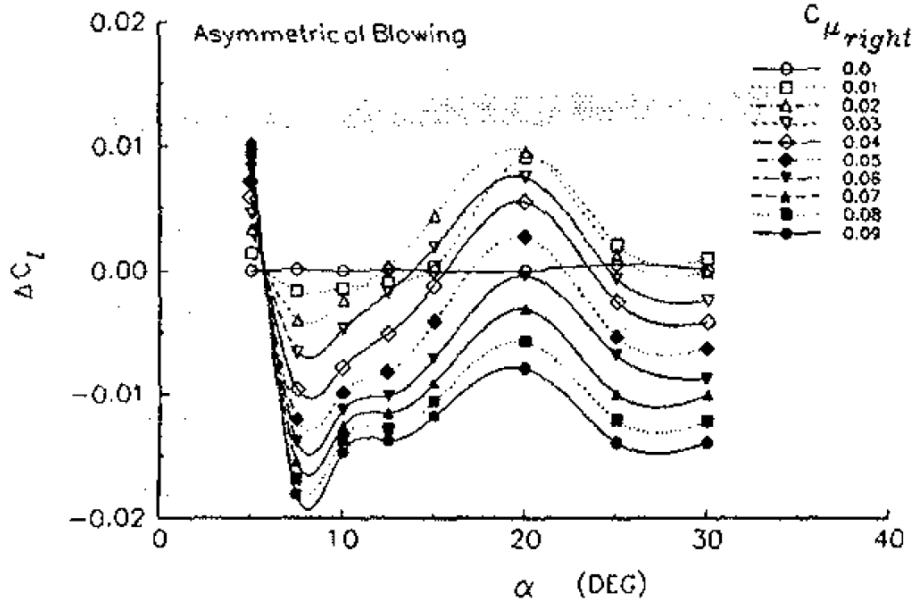

Figure A.30. Change in rolling moment for blowing on one side only [197]. 'Control reversal' is apparent for blowing coefficients less than 6%.

Although Celik stated that the experimental setup was able to measure pitching moment, this data is not presented so unfortunately no comment can be made on the effect of blowing on the static longitudinal stability of the aircraft. Although no data is presented, a numerical study of Celik's experiment performed by Hong [198] allows one to infer the pitching moment behaviour of the aircraft. Although Hong's study does not include pitching moment data, it does include surface pressure distributions at various chordwise locations for 10°, 20° and 30° angle of attack as shown in figures A.31, A.32 and A.33 respectively.

At 10° (figure A.31), the change in the pattern of the pressure coefficient is broadly similar indicating that there would be very little change in the pitching moment.

At 20° (figure A.32) however, it can be clearly seen that whilst blowing increases the suction at the forward positions, blowing at the aft positions reduces the suction. This will increase the nose up pitching moment at this point. As no reference unblown data is provided and the magnitude of the nose up moment is unknown it is not possible to comment on how this change in stability will effect the behaviour. However, due to the angle of attack at which this is occuring one would assume this behaviour would worsen the pitch break behaviour.

At 30° (figure A.33) the effect of blowing on the pitching moment is much less clear. There does not appear to be a significant change in the surface pressure with blowing therefore it is unlikely that there would be a large change in the pitching moment. It is worth noting in this figure that the distinct suction peak due to the vortex suction cannot be seen for the aft two pressure distributions suggesting that lateral blowing is not able to prevent the leading edge breakdown at this angle of attack.

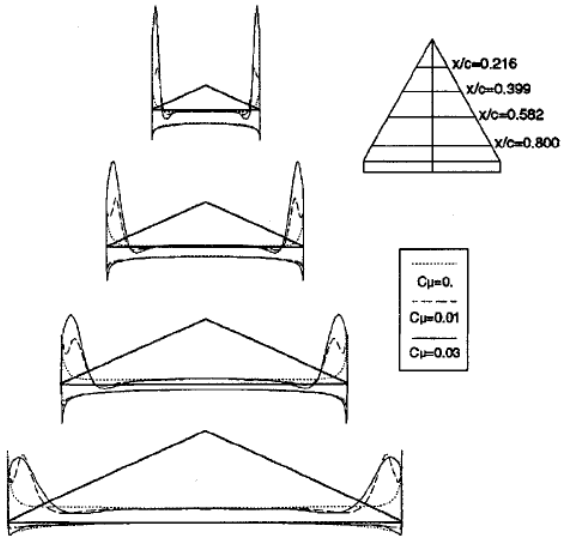

Figure A.31. Spanwise pressure distributions for various chordwise stations at 10° angle of attack [198]. The change in pressure distribution is relatively similar at all stations, therefore no significant change in pitching moment would be expected.

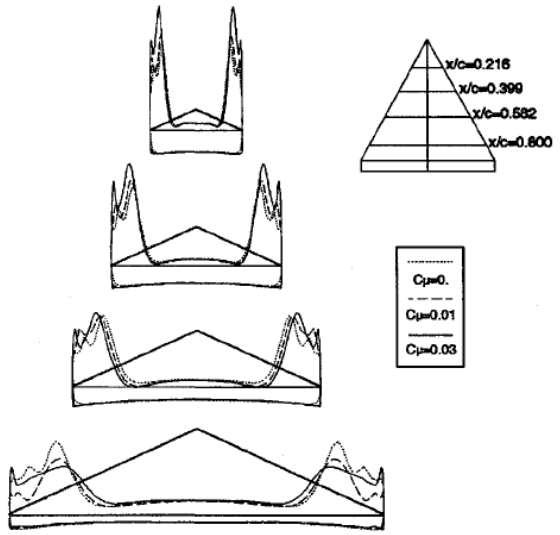

Figure A.32. Spanwise pressure distributions for various chordwise stations at 20° angle of attack [198]. The change increase in suction appears most prevalent at foremost stations, this would lead to a pitch up change in the pitching moment.

A.1.4 Trailing Edge Blowing

Helin [199] performed an water tunnel experiment on a 60° delta wing where flow was injected from rectangular ports on the trailing edge parallel to the free steam. The momentum coefficient in these experiments ranged from 1-154%. At first glance it would appear the higher levels of blowing should be discounted as not physically implementable, however as injection is from the trailing edge the actuation could come from the main aircraft thrust. The analysis of this study is limited to the vortex breakdown location and does not include any force or moment

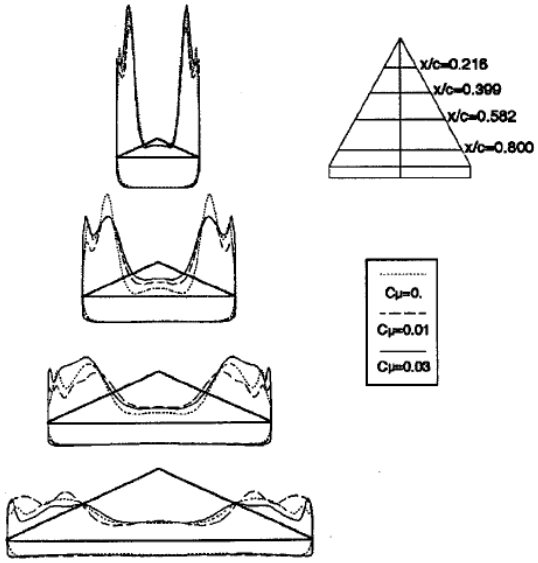

Figure A.33. Spanwise pressure distributions for various chordwise stations at 30° angle of attack [198]. The suction peak at the aft stations is not present at this high angle of attack, suggesting the vortex breakdown location is between 40% and 58% chord.

data.

It was found that if the vortex breakdown location is aft of the trailing edge then no effect is observed as a result of blowing from the trailing edge. However at higher angles of attack where the vortex breakdown location is over the wing, increasing the level of blowing is able to delay the breakdown location by up to 18% of the chord. Furthermore, where there is significant interaction and asymmetry in the breakdown location blowing is able to stabilise and reduce the asymmetry in the location. This will increase the lateral stability of the aircraft at high angles of attack and reduce the dynamic 'wing rock' problem encountered on highly swept wings.

Shih [200], performed a similar experiment again in a water tunnel but this time for the case of vectored thrust. When reviewing these results it is worth keeping in mind that the scenario in which these are gathered is completely unphysical. For the static case where the nozzle is vectored large pitching moments would be introduced and therefore a static analysis is inherently limited. Furthermore, for the dynamic pitching experiments the model is pitched up whilst the thrust is vectored downwards; this is physically incorrect and thus the results are not applicable to any flight case. Therefore, the dynamic experiments are not discussed here.

Nevertheless the change in vortex breakdown location for a C_μ of 111% and changing angle of attack and thrust vectoring angle are presented in figure A.34. From this it can be seen that in all cases except the upward blowing, the vortex breakdown location is improved by trailing edge injection and increasing the downwards angle at which the injected momentum is vectored further increases the breakdown location. The upward vectored jet shows a slight

improvement in breakdown location for the 10° angle of attack case but in all others shows no change in the vortex breakdown location. No explanation is provided for this by the authors.

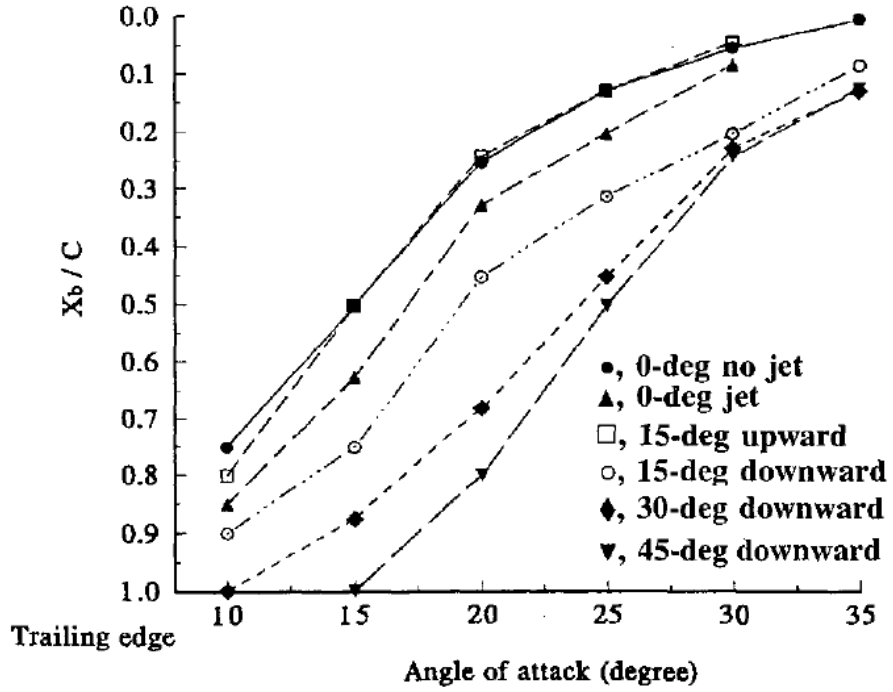

Figure A.34. Effect of the thrust vectoring direction on vortex breakdown location [200]. All cases apart from the upward blowing are able to delay the vortex breakdown location, increasing the downward deflection improves the vortex breakdown location.

Mitchell [201] conducted water tunnel experiments of a 75° sweep delta wing at high angles of attack in a water tunnel for injection parallel to the chord line and with momentum coefficients ranging from 14%-250%. Figure A.35 shows the change in vortex breakdown location for asymmetric injection. This method of control is unlikely to be achievable in flight as it would introduce large yawing moments due to the outboard positions of the trailing-edge nozzles. It is reviewed here as the coupling between asymmetric thrust and vortex position control provides a possible method of lateral control.

Low levels of injection (Velocity ratio = 5, $C_{\mu} = 14\%$) area able to improve the vortex breakdown location on the side of the injection by $\sim 8\%$ root chord and have an unfavourable effect on the opposite vortex by $\sim 15\%$. This has the effect of rolling the aircraft in a sense that causes the wing from which the injection to move up; therefore the yaw induced and the rolling moment turn the aircraft in the same sense, providing an opportunity for lateral control.

At a velocity ratio of 10 ($C_{\mu} = 56\%$), compared to the unblown case with port blowing there is a deleterious effect on the vortex breakdown location on the side of blowing and the unfavourable effect on the opposing vortex is lessened such that the change in breakdown location is roughly equal for both sides. This leads to a potential pitch up moment coupled

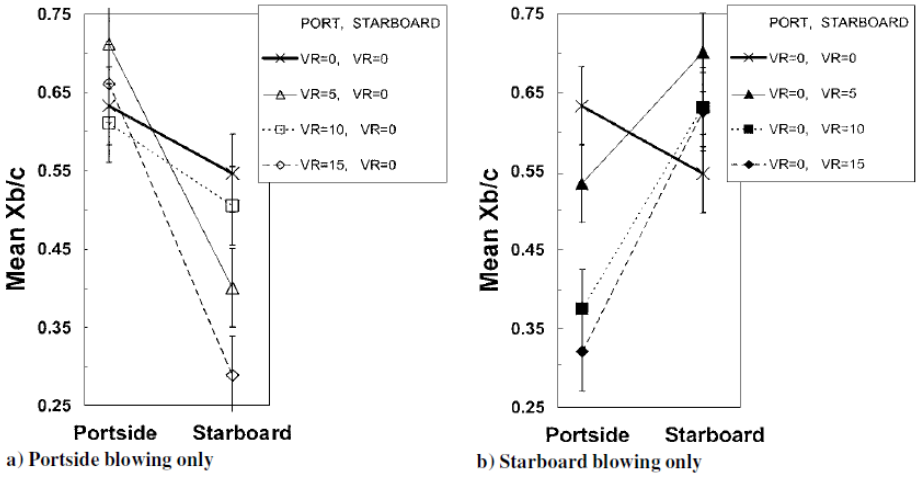

Figure A.35. Effect of asymmetric trailing edge blowing in the plane of the wing [201]. Velocity ratios of 5, 10, 15 correspond to a C_μ of 14%, 56% and 126% respectively. Low levels of blowing give the greatest change in differential breakdown location and therefore most effective for lateral control.

with a strong yawing moment, clearly this is an undesirable control input. With starboard blowing there is no significant change from the velocity ratio of 5 case, therefore there is not sufficient robustness in this method for use as a control method.

Increasing the velocity ratio further to 15 ($C_\mu = 112\%$) leads to an improvement in the vortex breakdown location on the blowing side in both cases, although the improvement is greater for starboard blowing. However, the improvement in vortex breakdown location is not as great as for a velocity ratio of 5. The vortex breakdown location on the unblown side moves further forward than in any other case for this increased level of blowing, thereby increasing the rolling moment. However, as the yawing moment imparted by this thrust asymmetry would be so large, this is not a practical method of controlling the aircraft.

Therefore, this method may find application as a possible lateral control system for low levels of blowing. In order to further reduce the effect of the asymmetry in thrust as a yaw input, the effect on the vortex breakdown location, or more directly the rolling moment, should be investigated with lower values of momentum input.

Figure A.36 shows the effect of symmetric momentum injection on the breakdown location for velocity ratios of 5, 10 and 15 which correspond to a momentum coefficient of 28%, 113% and 254% respectively. Similarly to asymmetric blowing, blowing at the lowest velocity ratio was able to improve the vortex breakdown location, however higher levels of blowing had a negative effect on the breakdown location. As the effect of symmetric blowing cannot be decoupled from thrust, rather than a method of control this effect is a consideration when trimming the aircraft.

Wang [202] performed a wind tunnel experiment on a slender 50° sweep delta wing with vectored trailing edge jets. The experiments were performed with the jets orientated parallel

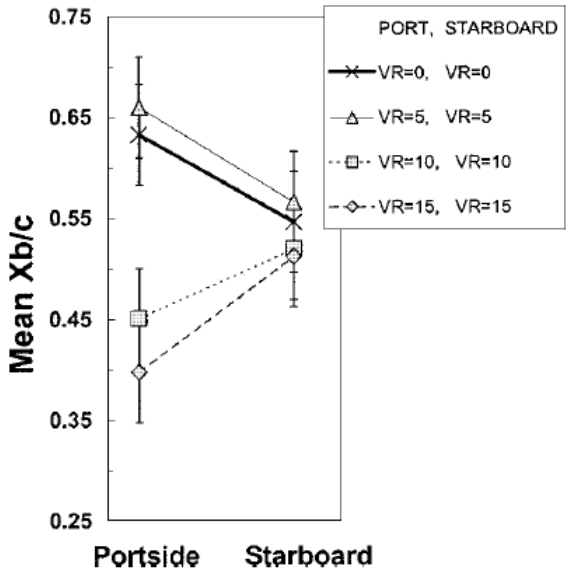

Figure A.36. Change in vortex breakdown location with symmetric momentum injection [201]. 5, 10 and 15 which correspond to a C_μ of 28%, 113% and 254% respectively. C_μ of 28% is able to delay the vortex breakdown location, higher levels of blowing promote premature vortex breakdown.

to the model and at a 30° downward deflection for static cases only. Aerodynamic forces and moments were measured by means of a six component internal balance, however within the analysis only the lift coefficient and change in vortex breakdown location is presented. A single thrust vectoring jet was placed on a rail behind the wing allowing its spanwise position to be altered; this means that unless blowing is applied along the model centreline the data presented is for asymmetric blowing.

The change in lift coefficient for blowing with a momentum coefficient of 24% is shown in figure A.37. For all angles of attack except a small region 26° - $28\circ$ angle of attack, blowing from the centreline of the model with a downward deflected jet had a negative effect on the lift coefficient. In a flight scenario this would not be noticed and would most likely be overcome by the effect of the component of thrust directed along the same direction as lift.

When the jet was located at 60% of the semispan it can be seen that there was an increase in the lift coefficient with blowing for all angles of attack. Furthermore, contrary to the results of Mitchell [201] the change in lift coefficient for the unvectored and downward vectored thrust is negligible.

Whilst other aerodynamic forces and moments were reported to be captured by the study, they are not presented or discussed by the author. The only reference given is that the *Variation of pitching moment is very similar to that of the lift coefficient'*. It is unclear whether this means the pitching moment is increased (i.e. nose up) or improved (i.e. nose down moment increased with angle of attack). If the former then this method of control is of no use unless the pitch up moment is overcome by downward vectored jets, if the latter than this method

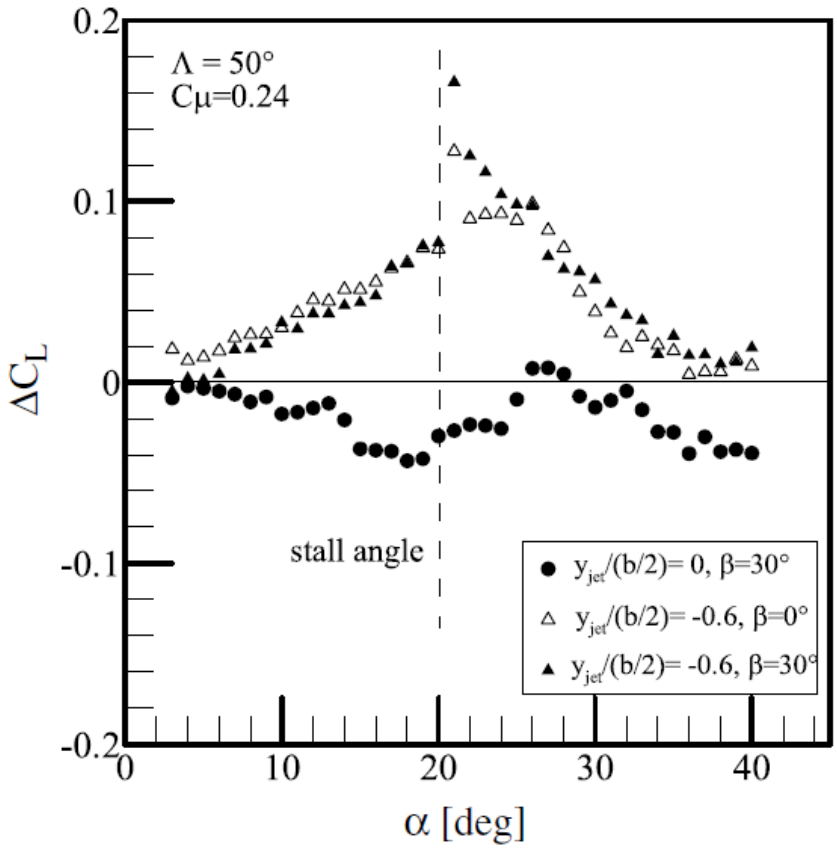

Figure A.37. Change in lift coefficient for changing jet deflection angle β (positive downwards) and jet location for a C_μ of 24% [202]. Blowing from under the vortex axis is able to improve the lift coefficient by the same amount regardless of the deflection angle.

will both improve the lift and pitch stability of the aircraft. However, it would not be possible to decouple the effects of control from thrust; as the driver to fly at high angles of attack is low speed performance, a large component of thrust as a 'side effect' of improved high angle of attack performance is not desirable.

A.2 Separation Control

Flow separation occurs when the fluid flow detaches from a solid surface, generally for flow over wings this is caused by an inability of the flow to overcome an adverse pressure gradient . It was shown by Prandtl as early as 1904 that the delay of separation was possible by removal of the low momentum flow within the boundary layer by suction through a slot on the surface [203]. Further research into the area over the following decades showed that it was possible to gain enhancement in lift and reduction in drag by means of blowing and suction as a means of boundary layer control [204].

Later experiments which utilised periodic addition of momentum found that the same authority in separation control was maintained for a greatly reduced momentum input [203].

This is due to the periodic perturbations causing a transition to turbulent flow, which is inherently less likely to separate due to the mixing between the high and low momentum layers of the boundary layer [205]. Therefore, due to the pressure to reduce the amount of flow required to improve flight performance in real flight cases the review here is limited to unsteady momentum injection for separation control.

Greenblatt [206] performed a comparison of the effect of leading edge curvature on the ability of leading edge alternate blowing and suction to delay stall. The actuation location has not held constant for both airfoils therefore rendering direct comparison of the two invalid. However, as the interest to this project is for small leading edge radius, the effects of blowing on the performance parameters of the NACA 0012 are of interest.

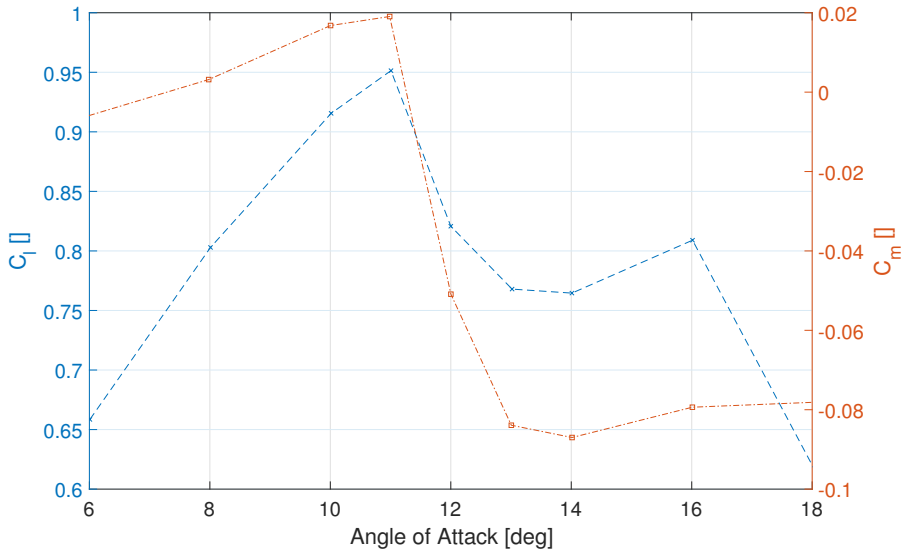

Figure A.38. Reference (unblown) lift and pitching moment coefficient for a NACA 0012 airfoil (data from [206]). A sharp leading edge stall can be seen at 11° angle of attack where there is a dramatic reduction in lift and nose down pitching moment.

Figure A.38 shows the lift and pitching moment coefficients for the unblown case. For the case of NACA 0012, a clear leading edge stall can be seen at $\sim 11^\circ$ marked by a sharp drop in lift coefficient and a rapid pitch down moment. Due to the absence of sweep this is a much different behaviour to the pitch break problem addressed in the previous section.

The mechanism by which the improvement in the onset of stall is effected can be seen in figure A.39. The higher frequency actuation is more able to perform the pressure recovery and can therefore support a greater suction peak before the leading edge bubble bursts and causes separation.

The change in pressure distribution can be seen to delay the onset of stall by up to 3° (measured by the change in pitching moment) with a C_μ of 1.8%, as shown in figure A.40. Clearly higher levels of blowing are more able to not only delay the onset of stall but reduce

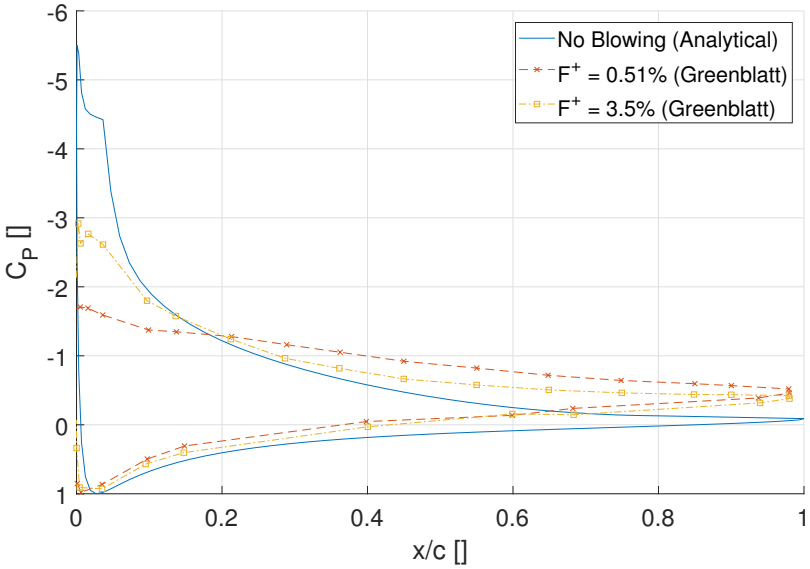

Figure A.39. Comparison of surface pressure coefficient for the flow with alternate blowing and suction [206] with analytical, attached flow solution. Higher frequency of actuation is better able to support the leading edge suction peak and pressure recovery on the upper surface of the airfoil.

the severity of the change in pitching moment when it does occur. Although the momentum coefficients seem unpractically high, the application of alternate blowing and suction means that the net mass flux required is zero and is therefore plausible.

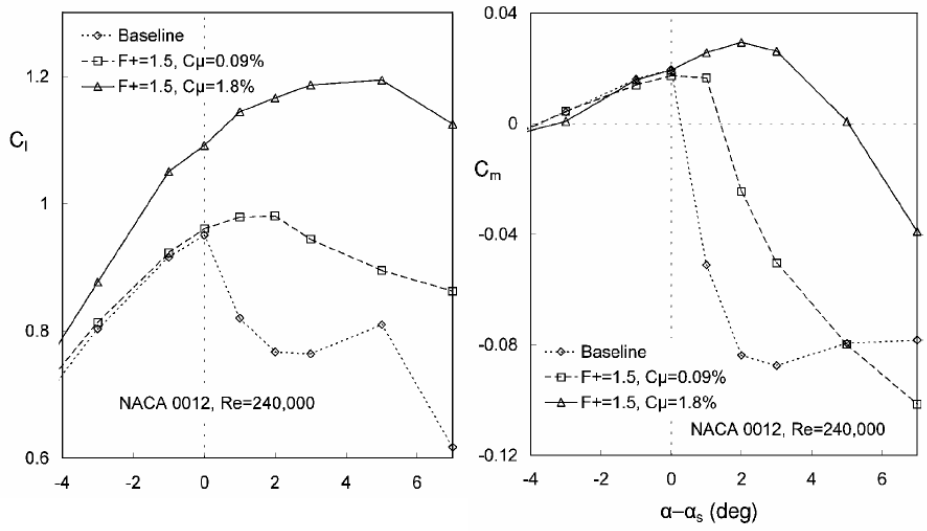

Figure A.40. Lift and pitching moment for actuation at F^+ of 1.5 and varying C_μ compared to the unblown case [206]. Higher levels of blowing increase the lift for any angle of attack and extend the linear region of the lift and pitching moment curve.

Scholz [205] performed a study to explore the effects of pulsed blowing from the leading edge to prevent separation due to the burst of a leading edge bubble on a thin airfoil. The injected momentum was able to provide a C_μ of up to 2.5%, however as the blowing is pulsed, the momentum coefficient will scale with the duty cycle. This is significant because as shown

in figure A.41, reducing the duty cycle is able to achieve greater increases in the normal force coefficient; for the 12% duty cycle this leads to a time averaged momentum coefficient of 0.3%. This is in the realm of possibility for flight implementation as it would require 3% of the core flow of a Eurofighter Typhoon to implement.

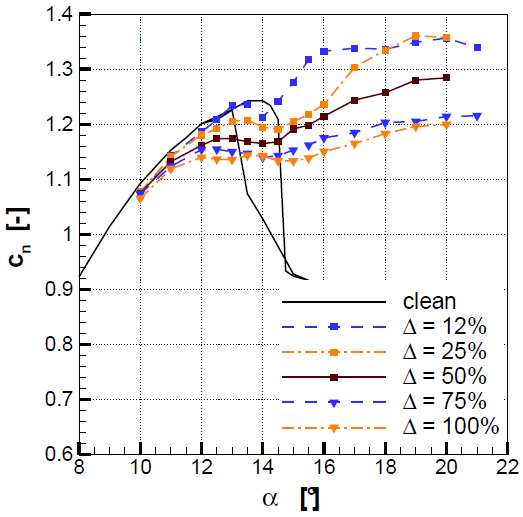

Figure A.41. Change in normal force coefficient for changing duty cycle of unsteady blowing for a fixed C_μ of $\sim 1.5\%$ and f of $75Hz$ [205].

From figure A.41, it can also be seen that any blowing from the leading edge has the effect of removing the hysteresis loop from the normal force coefficient. This will simplify the design of any flight control system by extending the linear area of operation. Whilst these improvements seem significant given the low C_μ and ease of implementation compared to alternate blowing/suction, it is worth noting that Scholz has not presented the change in pitching moment as part of his study; As seen in the work of Greenblatt [206], with actuation applied the effect of stall is apparent at lower angles of attack in the pitching moment than lift. Therefore, in order to compare directly the effect of periodic blowing to alternate blowing/suction further work is required.

Koklu [207] provided a comparison of different techniques of flow control to provide control of separation over a ramp. A particular focus of this study was the Sweeping Jet Actuator (SJA) which is able to provide an oscillatory output for a steady flow input. The main features of the SJA are shown in figure A.42. The flow enters through the main flow channel where it will attach to one of the Coanda surfaces, following this surface causes the jet to exit at a skewed angle. As the flow passes the feedback loop it causes a secondary flow which travels back to the where the main flow enters the actuator and causes the flow to detach from the Coanda surface and attach on the other side. The process then repeats causing a spatially oscillating output at the exit.

In this study Koklu showed that pulsed blowing was better able to prevent separation than

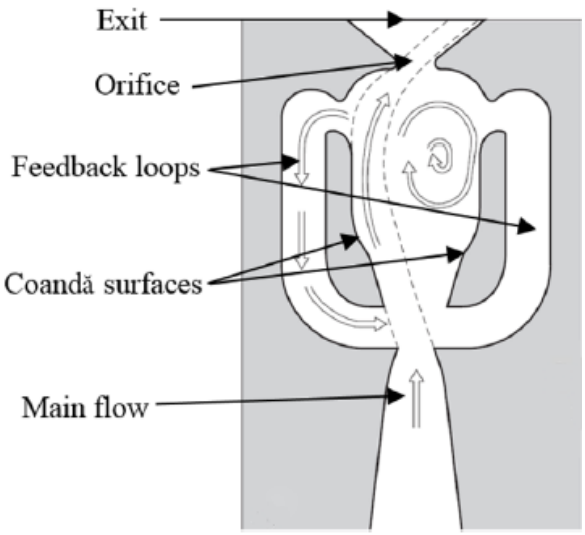

Figure A.42. Concept of a sweeping jet actuator [207]. The main flow enters and attaches to one of the Coanda surfaces. A feedback flow is setup through the feedback loop causing the flow to detach and subsequently attack to the opposite surface. This process repeats causing the output to oscilate spatialy.

steady blowing, agreeing with the results of Greenblatt [206]. He was also able to show that the SJA was better able to prevent separation than steady blowing. However, no comparison is made between the effectiveness of pulsed blowing and SJAs.

Data digitized from the plots provided by Koklu [207] show the change in the ramp centreline pressure distribution for pulsed blowing and SJAs are shown in figure A.43. Clearly both are able to provide an increase in the suction peak and keep the flow attached along the ramp. However, the pulsed case provides a greater suction peak with no separation during the pressure recovery suggesting a superior performance to SJAs.

Koklu states in this paper that the SJAs have not been optimised and the 2D flow assumption used in the data reduction (only centreline Cp distribution shown as a representative distribution) may artificially elevate the performance of the circular jets used for pulsed blowing. With this in mind, the mechanical simplicity and therefore flight reliability of the SJA may lead one to select this as a preferred method of separation control for a flight case.

Work by Woszildo [208] into the performance of SJAs provided insight into the parameters to be considered when applying SJAs to an aircraft. He showed that it is possible to use this method of actuation to improve the performance of flight control surfaces deflected to high angles, thereby increasing there effectiveness. This was limited to downwards deflections of the flap only and is therefore only applicable to the trim of aircraft with a tail or nose-down manoeuvres of any aircraft. Furthermore, the momentum coefficients used by Woszildo range from 1% - 6% which, from previous discussion, is clearly too large to find flight applications.

Further work by Jentzsch [209] applied SJAs to a swept lambda planform in an effort to

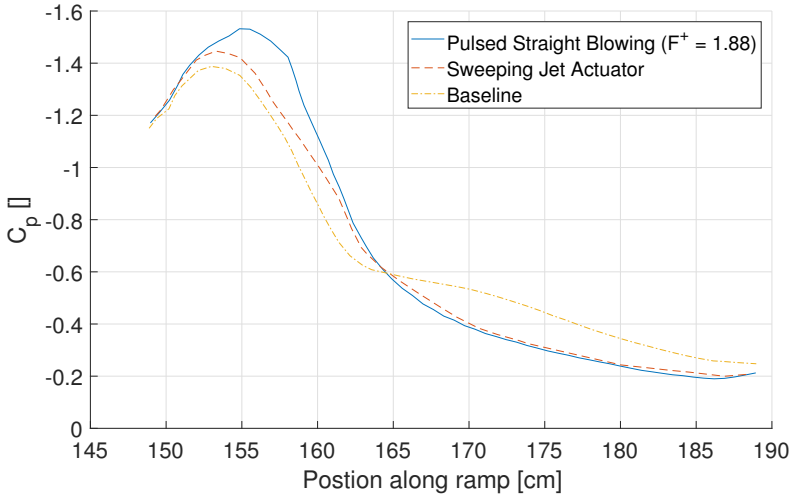

Figure A.43. Pressure coefficient along the ramp used by Koklu [207]. For the same momentum input the pulsed blowing appears to better increase the suction peak and pressure recovery. Both methods of actuation are able to increase the suction peak and keep the flow attached along the length of the ramp.

improve pitch stability and reduce elevator angle to trim. Whilst the aim of this work was fulfilled, the method has negative implications if removed from the wind tunnel and taken to a flight environment.

Figure A.44 shows how the pitching moment changes with respect to lift coefficient and angle of attack. Clearly for the baseline case the Moment Reference Point (MRP) has been selected to require a nose down pitching moment to trim; thereby causing a need for downward elevator deflection and allowing the method proposed by Woszildo [208] to be implemented. However, this means that the MRP selected is aft of the Aerodynamic Centre (AC) of the model giving an unstable (Positive slope) variation in the pitching moment until stall at $\sim 11^{\circ}$.

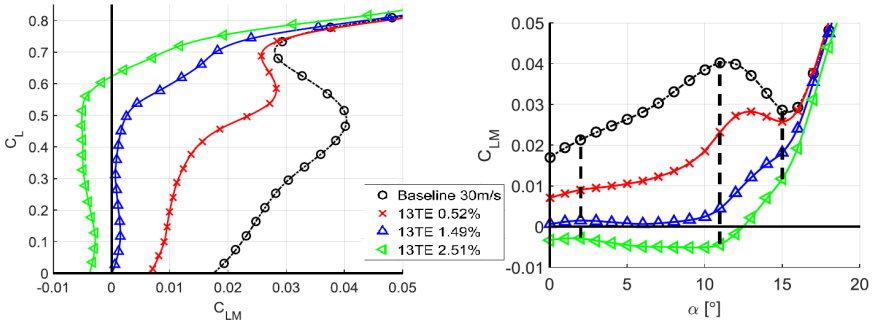

Figure A.44. Pitching moment curves for different levels of blowing from 13 trailing edge sweeping jet actuators [209]. Actuation appears to have the effect of moving the aerodynamic centre of the airfoil aft, however the severity of pitch break is increased with increasing momentum input.

Increasing the level of blowing successively moves the aerodynamic centre aft, thereby improving the stability of the aircraft and reducing the elevator angle to trim. For low angles of attack it can be seen that this is no different to moving the centre of gravity (in this case MRP) forward. For higher angles of attack however, increasing the level of blowing changes

the stall response of the aircraft from nose down (stable) to nose up (unstable) which is clearly undesirable. Furthermore, in the event of failure of the actuation system the AC will move forward to its original (baseline) configuration resulting in instability of the airframe.

Appendix B

Model Selection

B.1 Overview

Three models were selected for assessment: A Lifting Line Theory (LLT) modified for sweep effects [102], Vortex Lattice Method (VLM) [162] and Multhopp's Lifting Surface (LS) [16]. To assess the applicability of these models to the geometries studied within this paper the lift distribution, lift magnitude and induced drag magnitude predictions were selected as metrics for assessment. This is because, if the lift distribution is correct and the model is predicting the correct induced drag, then the moments, which are integral functions of the distribution, will also be correct.

We consider cases of both straight and swept wings. For the straight wing, the three models are compared against predictions from classical lifting line theory [79] as it provides the most convenient analytical solution for such wing geometry (no sweep and the aspect ratio is above three [170], [172], [210], [211]). For the swept wing case, the models were compared against available experimental data from a 45 degree swept wing of aspect ratio 5 [105]. It is expected that all models will perform well for the straight wing. For the swept wing, it is expected that the surface methods (i.e., VLM and lifting surface) will outperform the LLT methods.

B.2 Straight Rectangular Wing

The lift distribution and lift curve slope predictions of each of the three models are compared against those from the classical LLT (Figure B.1). The classical LLT solution adopted here is based on Glauert's method which adopts a Fourier series solution. As expected all models predict both the distribution and magnitude of lift well. It is worth noting that both surface methods under predict the lift cure slope compared to the classical LLT; however, this under-prediction is well noted within the literature (see, for example, [155]). Note that the lift distribution in this demonstration is evaluated at an angle of attack of 4.2° for consistency with the swept wing case in the following section where experimental data were available at

this angle of attack value. However, same conclusions will be obtained if any other angle of attack value is used.

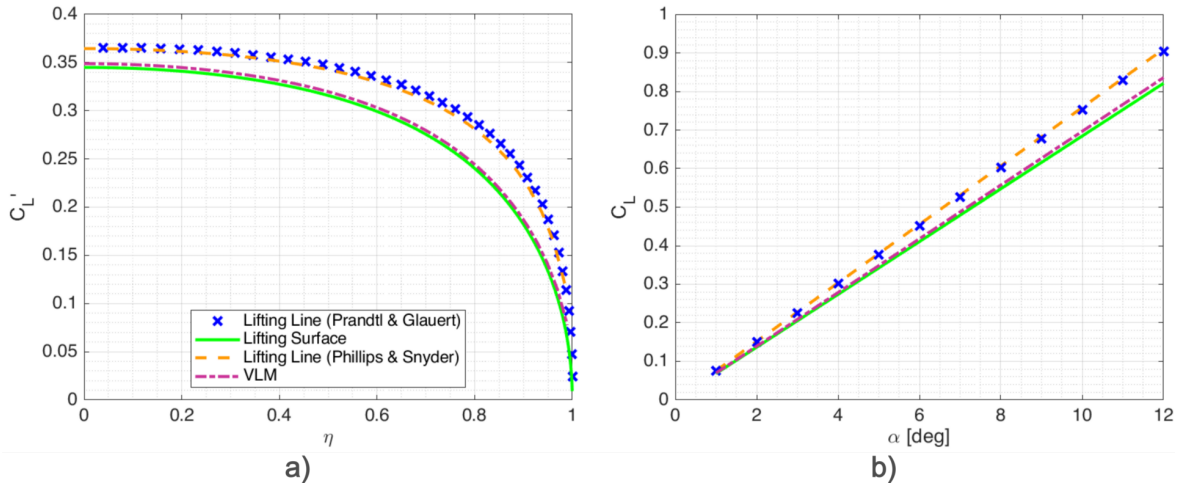

Figure B.1. (**a**) Lift distribution prediction at $\alpha = 4.2°$ and (**b**) lift curve slope for AR5 straight wing. All methods considered predict the shape of the lift distribution well, however both lifting surface and VLM predict a slightly lower lift curve slope.

The quantity of greatest importance to this method is the prediction of induced drag shown in Figure B.2. The modified LLT model by Phillips and Snyder [102] matches the classical LLT in terms of induced drag coefficient as a function of both angle of attack and lift. The VLM and LS methods both also predict the induced drag well as a function of the lift coefficient. Therefore, for an unswept wing, any of the models considered would be suitable.

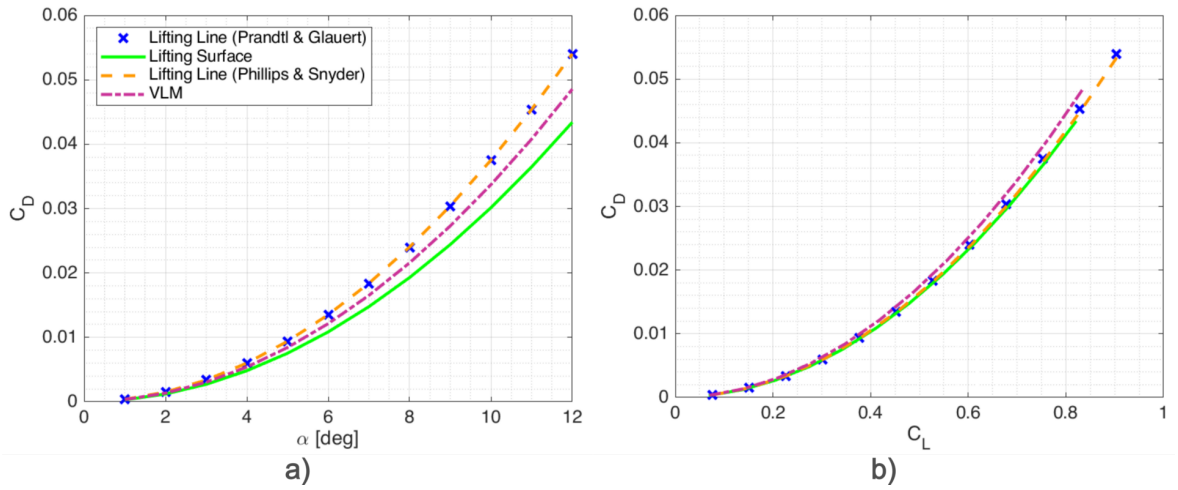

Figure B.2. Induced drag coefficient as a function of angle of attack (**a**) and lift coefficient (**b**). The results of the modified LLT match those from the classical LLT, as would be expected. Whilst the induced drag predictions for the LS and VLM appear to under predict the induced drag as a function of angle of attack, it can be seen that this is due to the lower lift prediction shown in Figure B.1. As a function of lift coefficient, the induced drag coefficient prediction from the LS model agrees well with the LLT prediction, whilst VLM slightly over predicts the induced drag coefficient.

B.3 Forty-Five Degree Swept, Untapered Wing

The classical LLT is known to fail in accurate prediction of the lift distribution for wings swept above 30 degrees [155]. As such, here we compare the three selected models against available experimental data [105] for spanwise distribution and the integral quantities of lift and drag for an untapered wing with 45 degree sweep and an aspect ratio of 5.

Figure B.3 shows the spanwise lift distribution and lift curve slope for each of the models compared with the experimental data. The modified lifting line model predicts the overall lift coefficient well, however the distribution is significantly shifted to the outboard sections. When combined with control surface deflections this distribution will lead to significant errors in the aerodynamic moments, therefore the modified lifting line is not suitable for the aims of our present study. Both surface methods agree well with the experimental data in both the lift distribution and lift curve slope.

When comparing the drag predicted by each of the models in Figure B.4 it can be seen that both surface models under predict the drag. This is expected as all these models are inviscid. However, when adding the profile drag contribution of the RAE101 aerofoil section used for the experiment a good agreement with the experimental results is found for the lifting surface model with the VLM slightly over predicting the total drag. The greater accuracy and reduced dependency on the discretisation of the geometry of the lifting surface method makes it our favourable model choice for use in this study.

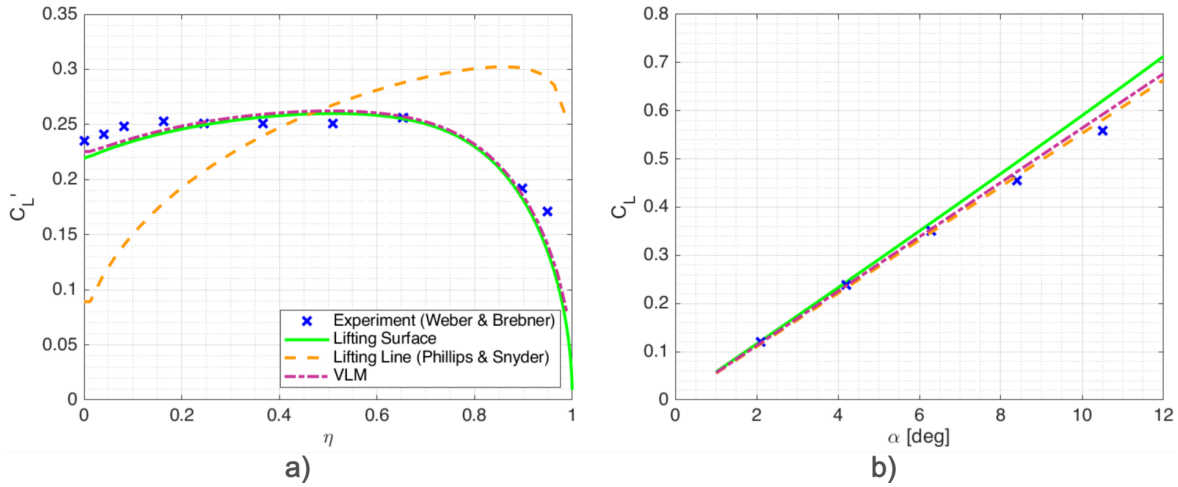

Figure B.3. (**a**) Spanwise lift distribution at 4.2 degrees and (**b**) lift curve slope for the low order methods considered. All methods predict the lift curve slope well enough, however the modified lifting line model skews the lift to the outboard sections of the wing. For our analysis purposes, this would lead to large errors in the predicted induced drag and aerodynamic moments.

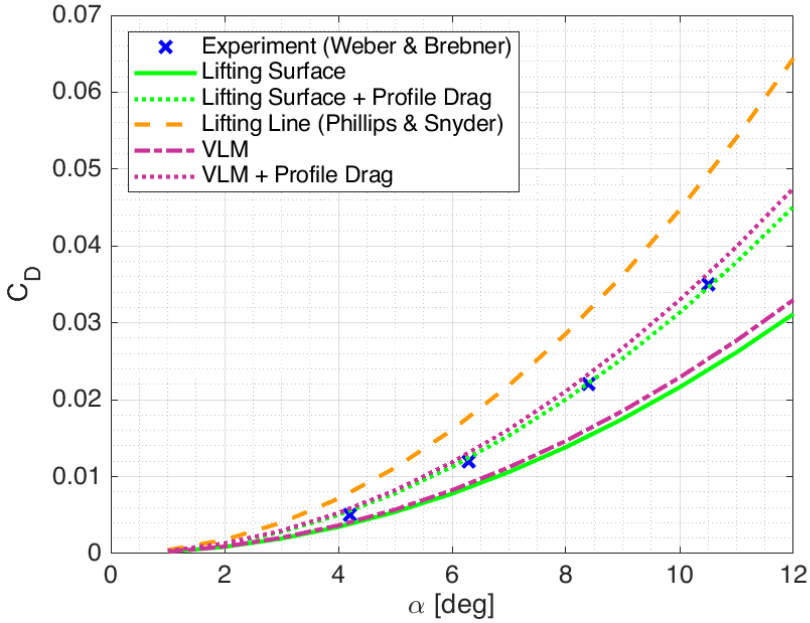

Figure B.4. Drag prediction comparison. Compared to the experimental data, the modified LLT predicts higher induced drag than the total drag measured in the experiment. The LS and VLM models appear to under predict the total drag compared to the experiment. This is expected as they only evaluate the induced drag component. As such, when adding the profile drag contribution of the RAE101 aerofoil used for the experiment, the predicted drag coefficient is in good agreement for the LS model, and is slightly over predicted for the VLM model.